Latently-reactive conjugated polymer-coated single-walled carbon nanotubes

Latently-reactive conjugated polymer-coated single-walled carbon nanotubes

By Darryl Fong, B.Sc.

A Thesis Submitted to the School of Graduate Studies in the Partial Fulfillment of the Requirements for the Degree of PhD in Chemistry

© Copyright by Darryl Fong, April 26, 2019
All Rights Reserved

McMaster University

PhD in Chemistry (2019)

Hamilton, Ontario (Department of Chemistry and Chemical Biology)

TITLE: Latently-reactive conjugated polymer-coated single-walled carbon nanotubes

AUTHOR: Darryl Fong (McMaster University)

SUPERVISOR: Dr. Alex Adronov

NUMBER OF PAGES: xxv, 312

Abstract

Single-walled carbon nanotubes (SWNTs) are intensely investigated nanomaterials that exhibit intriguing physical and optoelectronic properties. Although SWNTs are highly regarded in terms of their potential societal impact, commercialization of SWNT applications has been dampened by the difficulty in SWNT processability and purification. Current commercially viable carbon nanotube syntheses produce complex mixtures of metallic and semiconducting SWNTs, as well as amorphous carbon and metal catalyst particles. Furthermore, the ability to decorate carbon nanotube surfaces to modulate their properties is non-trivial, especially if concurrent preservation of optoelectronic properties is desired. To date, the issues of SWNT solubilization, sorting, and functionalization have been approached in a piecemeal fashion. Conjugated polymers, which are macromolecules that possess extended π-systems, have the potential to address all of these issues simultaneously. In my Thesis, I explore conjugated polymer structures to investigate (i) factors that influence dispersion selectivity, and (ii) the decoration of polymer-SWNT complexes by incorporating reactive moieties into the polymer structure.

The work presented in this Thesis begins by examining the ability of conjugated polymers to sort SWNTs. To date, the selective dispersion of metallic SWNTs is unrealized. In Chapter 2, I examine the effect of the electronic nature of the conjugated backbone on the selective dispersion of SWNTs by preparing SWNT dispersions pre- and post-methylation of a pyridine-containing conjugated polymer. In doing so, I prepare a series of polymers with identical degrees of polymerization and dispersity (to minimize extraneous selectivity factors) and find that electron rich π-systems disperse only semiconducting SWNTs, while electron poor

π-systems disperse relatively more metallic SWNTs. In Chapter 3, I challenge the conventional wisdom that complete backbone conjugation is required to selectively disperse semiconducting SWNTs by introducing non-conjugated linkers into the polymer backbone and demonstrating that nanotube sorting is still possible.

I next examine conjugated polymers as tools that can simultaneously sort SWNTs and impart reactivity to the polymer-SWNT complex, while preserving SWNT optoelectronic properties. In Chapter 4, I incorporate azides into polyfluorene side chains and perform solution-phase Strain-Promoted Azide-Alkyne Cycloaddition (SPAAC). I show that the polymer-SWNT complex can be rapidly decorated with strained cyclooctyne derivatives, and that only pre-clicked polymer enables for sorting of semiconducting SWNTs. The sorted SWNT population can then be made water soluble post-SPAAC, enabling for the study of SWNT emission in solvents with very different polarity. In Chapter 5, I examine the reactivity of azide-containing polymer-SWNT thin films and show that thin film properties can be drastically altered. Interfacial chemistry enables for the spatially-resolved patterning of a Janus polymer-SWNT thin film containing both hydrophilic and hydrophobic regions. In Chapter 6, I devise a system to perform aqueous solution-phase chemistry on the polymer-SWNT complex. The water soluble polymer-SWNT complex allows for functionalization of the hydrophobic SWNT scaffold with polar and charged molecules. Clicking an acidochromic switch onto the polymer-SWNT surface enables for control over the SWNT emission properties.

Lastly, in Chapter 7 I develop a conjugated polymer whose backbone can be functionalized using visible light. The visible-light mediated photoclick coupling of a conjugated polymer backbone enables for rapid polymer modification and is the first example of spatially-resolved conjugated polymer backbone functionalization.

Acknowledgements

At this milestone in my life, I would be remiss if I didn't highlight the people who've made getting to this point possible. First and foremost, I'd like to thank my supervisor, Prof. Alex Adronov, for providing a fantastic research environment. The unwarranted freedom to pursue ideas was unusual, and for that I am eternally thankful. I am grateful to my supervisory committee, Profs. Michael A. Brook and Jose M. Moran-Mirabal, for their insights throughout this process. Prof. Brook, the lessons in organic chemistry will remain timeless – and Prof. Moran-Mirabal, you were literally like a surrogate supervisor at times. I thank my high school teacher, Mr. Martin Stevens, and my elementary school teacher, Ms. Jan Penton, for being such constructive influences during my formative education.

Next, I would like to thank my loving – and at times unorthodox – family. I am grateful to my parents who have given me a firm moral compass and life lessons that I will take into the distant future. Mom, without you our family would not know that variety is the spice of life – and Dad, without you our family would not know the value in little things. I thank my siblings Darren, who would cry for us in protest when we would not; Jessica, who donated Peter to the cause; and Michael, who let me lecture him about my endless nonsense.

After traversing through the marathon that is a doctoral degree, the good times are what will ultimately be reminisced. Thank you to past and present group members, including Dr. Ryan C. Chadwick (valuable lesson in reading blog comments), Dr. Nicole A. Rice (sangria and bunnies!), Kelvin Li (my gambling friend), Christina Shamshoom (smiggles), William James "Jimmy" "Jimbo" "Jimbus" Bodnaryk (extra thanks for teaching me all about the horticulture of squash,

the fruit), Stuart A. McNelles (MacGyver and graph-man), Vladimir Kardelis (you're truly a special soul...), Dr. Eric Meischner (it's okay, not okay, I don't know!), Leonora Abdullahu, Victoria Marando, Alan Mo, Julia Pantaleo, Giancarlo Da-Ré, Naomi Wong, Maria Denk, Bram, and Rachael Wang (okay, maybe not quite the last one...) You guys were an awesome bunch. To Sheilan Sinjari, thanks for all the uplifting conversations. I am grateful for the honour of supervising some talented undergraduate students – Jason Yeung (sleep immune), Grace Andrews (Worcestershire sauce is still hard to pronounce), and Alice Lang (sleep deprived). I wish you the all the best. Special thanks to Scott Laengert for being my cover artist – you brought my scientific work to life.

Outside of the lab, I can't forget to shout-out the squash partners who've entertained me for hours (despite my badness) – Jimmy, Marcel Goguen, Ryan Munroe, Kevin de France, Benjamin Davis-Purcell, Zafar Syed, Dr. Scott Nash, Trevor Ho (those endless court sprints...), Brad Bergin, and the Mac squash team.

To my friends since the early days – Drs. Aatif "Tiffles" Qureshi, Kevin Gitau, and Brandon Tang – it was a wild train/car ride. One day we'll be reunited under one timezone. Shoutout to my Nexus 6P for teaching me that phones aren't bad and for taking a lot of publication quality photos. RIP Blackberry.

Last, but certainly not least, Michelle. You literally brought warmth and light into my life. Before I met you, I would sit in my cold basement room with the lights off after coming home. I don't know why I was so anathema to light. I didn't have a heater at the time, so I would wear my winter jacket to stay warm. After we met, the lights would never turn off again and the new heater would continue to churn out heat. Grateful wouldn't really do justice for how I feel about you. Here's to looking forward to a future full of laughter, lamb sauce, and date nights!!!

Contents

Abstract iii

Acknowledgements v

Acronyms xxii

1 Carbon Nanotube Sorting and Functionalization 1
- 1.1 Introduction . . . 2
  - 1.1.1 Enrichment of Single-Walled Carbon Nanotubes . . . 2
  - 1.1.2 General Considerations for Dispersion Preparation . . . 9
  - 1.1.3 Functional Polymer-Nanotube Complexes . . . 14
- 1.2 Reaction Kinetics . . . 19
  - 1.2.1 Reaction Order and Half-Lives . . . 20
- 1.3 Click Chemistry . . . 23
  - 1.3.1 Copper-Catalyzed Azide-Alkyne Cycloaddition . . . 25
  - 1.3.2 Initial Exploration Beyond CuAAC . . . 28
  - 1.3.3 Carbonyl Chemistry . . . 30
  - 1.3.4 Inverse-Electron Demand Diels-Alder Cycloaddition . . . 32
  - 1.3.5 Light-Controlled Click Chemistry . . . 34
- 1.4 Summary . . . 37
- 1.5 References . . . 38

2 Influence of Polymer Electronics on Selective Dispersion of Single-Walled Carbon Nanotubes 50
- 2.1 Introduction . . . 52
- 2.2 Results and Discussion . . . 54
- 2.3 Conclusions . . . 65
- 2.4 Supporting Information . . . 65
  - 2.4.1 General . . . 65
  - 2.4.2 Synthetic Procedures . . . 67
- 2.5 References . . . 107

3 Investigation of Hybrid Conjugated/Nonconjugated Polymers for Sorting of Single-Walled Carbon Nanotubes 112
3.1 Introduction . . . 114
3.2 Results and Discussion . . . 116
3.3 Conclusions . . . 129
3.4 Supporting Information . . . 130
3.4.1 General . . . 130
3.4.2 Synthetic Procedures . . . 132
3.5 References . . . 148

4 Decoration of Polyfluorene-Wrapped Carbon Nanotubes via Strain-Promoted Azide–Alkyne Cycloaddition 154
4.1 Introduction . . . 156
4.2 Results and Discussion . . . 158
4.3 Conclusions . . . 170
4.4 Supporting Information . . . 171
4.4.1 General . . . 171
4.4.2 Synthetic Procedures . . . 173
4.5 References . . . 183

5 Decoration of Polyfluorene-wrapped Carbon Nanotube Thin Films via Strain-Promoted Azide–Alkyne Cycloaddition 189
5.1 Introduction . . . 191
5.2 Results and Discussion . . . 193
5.3 Conclusions . . . 206
5.4 Supporting Information . . . 206
5.4.1 General . . . 206
5.4.2 Synthetic Procedures . . . 209
5.5 References . . . 218

6 Reactive, Aqueous-Dispersible Polyfluorene-Wrapped Carbon Nanotubes Modulated with an Acidochromic Switch via Azide-Alkyne Cycloaddition 226
6.1 Introduction . . . 228
6.2 Results and Discussion . . . 229
6.3 Conclusions . . . 240
6.4 Supporting Information . . . 241
6.4.1 General . . . 241
6.4.2 Synthetic Procedures . . . 242
6.5 References . . . 261

7 Visible Light-Mediated Photoclick Functionalization of a Conjugated Polymer Backbone **266**
7.1 Introduction . . . 268
7.2 Results and Discussion . . . 270
7.3 Conclusions . . . 280
7.4 Supporting Information . . . 281
7.4.1 General . . . 281
7.4.2 Synthetic Procedures . . . 284
7.5 References . . . 296

8 Concluding Remarks **300**
8.1 Scientific Conclusions . . . 300
8.2 General Remarks . . . 306
8.3 Recommendations for Future Work . . . 308
8.4 Cover Art Gallery . . . 310

List of Tables

1.1 Summary of click chemistries and their second-order rate constants (k_2). PBS = phosphate-buffered saline; LED = light-emitting diode. [a]CuAAC rate is highly dependent on [Cu(I)] and ligand identity. . . 36

3.1 Summary of PFdOMB-Cα-β Attributes, Including % NCL (by ^{1}H NMR Integration), M_n, and Dispersity 119

4.1 [a]$\Delta[\lambda_{em}]$ was calculated as $\lambda_{em}[D_2O]$ – λ_{em}[toluene]. 169
4.2 Emission Wavelengths of sc-SWNT Chiralities Dispersed by **PF-N$_3$** in Toluene and Toluene with mPEG$_{5000}$-OH 182

5.1 Atomic %s of C, N, and O for **PF-N$_3$**-SWNT Thin Film Pre- and Post-SPAAC With mPEG$_{5000}$-DIBAC or DIBAC-C$_{16}$ 216
5.2 Atomic %s of C, N, and O for Janus Polymer-SWNT Thin Film Functionalized With mPEG$_{5000}$-DIBAC or DIBAC-C$_{16}$ 217

6.1 Fluorescence intensities of sc-SWNT species coated with **PF-mPEG$_{5000}$-IDX** before and after the addition of 1.5 eq of *p*-TSA and 2.0 eq of Et_3N. *Δ[Intensity] was calculated as: $1-\frac{Intensity\ (no\ p-TSA)}{Intensity\ (Experimental\ Condition)\times 100\%}$. 255
6.2 Fluorescence Intensities of sc-SWNT Species Coated with **PF-N$_3$**-mPEG$_{5000}$ Before and After the Addition of 1.5 eq of *p*-TSA or 1.5 eq of *p*-TSA and IDX **10**. *Δ[Intensity] was calculated as: $1-\frac{Intensity\ (no\ p-TSA)}{Intensity\ (Experimental\ Condition)\times 100\%}$. 257

7.1 Data used to calculate second order rate constants in toluene. . . . 292
7.2 Fluorescence emission peaks of **PF-PAQ-mPEG$_{5000}$** in various solvents 293

List of Figures

1.1 Methodologies for the selective enrichment of SWNTs, including (a) DGU,[47] (b) agarose gel electrophoresis,[48] and (c) SEC.[38] Reproduced with permission. Copyright Springer Nature Publishing Group (2010), IOP Publishing Ltd. (2008), Springer Nature Publishing Group (2011), respectively. 4
1.2 Chemical structures of homopolymers derived from fluorene, thiophene, and carbazole monomers, as well as copolymers of fluorene with benzothiadiazole (BT) or binaphthol (BINAP) units. Reproduced with permission.[61] Copyright Royal Society of Chemistry, 2017. 5
1.3 First example of the selective dispersion of SWNTs using conjugated polymers. (a) PL and (b) graphene sheet maps of PFO-SWNT dispersions in toluene. (c) PL and (d) graphene sheet maps of PFO-BT-SWNT dispersions in toluene. Graphene sheet maps use normalized PL map intensities and compare the relative fluorescence intensities of different SWNT species present in the SWNT dispersion. Reproduced with permission.[56] Copyright 2007, Nature Publishing Group. 6
1.4 General overview of the SWNT dispersion protocol. Soluble conjugated polymer is sonicated with insoluble SWNT powder, and then SWNT bundles are removed by mild centrifugation. The variables involved in dispersion selectivity are categorized, where polymer features are labelled in blue and preparation conditions are labelled in red. Reproduced with permission.[61] Copyright Royal Society of Chemistry, 2017. 9
1.5 Selective dispersion and release of sc-SWNTs using PFO-BPy followed by metal complexation with a Re metal centre. Reproduced with permission.[102] Copyright 2015, American Chemical Society. . . 17
1.6 Chemical structures of monomers used for the enrichment and release of sc-SWNTs, as well as the PDDF-imine derivative. Reproduced with permission.[61] Copyright Royal Society of Chemistry, 2017. 18

1.7 Plot showing reaction conversion vs number of elapsed half-lives. The shaded yellow region indicates 97% conversion while the shaded blue region indicates 99% conversion. 23
1.8 Second-order reaction simulations plotting reaction conversion (%) vs time (h). (a) Reaction conversion at 100 μM reactant concentrations for both reagents A and B at various k_2 values (0.01 to 100 $M^{-1} \cdot s^{-1}$), and (b) reaction conversion for $k_2 = 1\ M^{-1} \cdot s^{-1}$ at various concentrations of substrate (10 μM to 100 mM). The horizontal black dashed lines indicate 50% conversion (i.e., the point of intersection with each simulated curve indicates the reaction half-life, $t_{1/2}$). 24
1.9 Proposed mechanism for CuAAC. (a) Reprinted with permission.[107] Copyright American Association for the Advancement of Science, 2013. 26
1.10 *In vivo* imaging during early zebrafish embryogenesis with fucosylated glycans containing guanine diphosphate fucose (GDP-fuc) with (GDP-fucAl) or without (control) alkyne functionalization. Embryos were dechorionated and reacted with Alexa Fluor 488-N_3 at 2.5 or 10 h post-fertilization (hpf) using CuAAC. Reproduced with permission.[110] Copyright American Chemical Society, 2010. . . 28
1.11 Second-order rate constants of various strained cyclooctyne derivatives with benzyl azide. Reproduced with permission.[112] Copyright Royal Society of Chemistry, 2013. 30
1.12 Pictet-Spengler ligation used by Bertozzi and co-workers. (a) Cannonical Pictet-Spengler reaction between an indole with pendant alkylamine and an aldehyde. (b) Proposed Pictet-Spengler ligation. Reproduced with permission.[125] Copyright Proceedings of the National Academy of Sciences of the United States of America, 2013. . 31
1.13 (a) Mechanism of IEDDA and (b) molecular orbital rationale for reactivity. Reproduced with permission.[118] Copyright Royal Society of Chemistry, 2017. 34
1.14 Visible light-mediated photoclick chemistry. (a) Structures of the vinyl ether (VE) and 9,10-phenanthrenequinone (PQ) coupling partners as well as the product phenanthrodioxine (PDO). (b) Absorption spectra of PQ and PDO. (c) Photographs before and after the click reaction, with the bottom photographs taken while irradiated with a handheld UV lamp at 365 nm. Reproduced with permission.[149] Copyright American Chemical Society, 2018. 36

2.1 Electron density maps of trimers for (A) **P1** and (B) fully methylated **P2**. Red denotes electron-rich regions, green denotes less electron-rich regions, and blue denotes electron-poor regions. 57
2.2 UV/Vis-NIR absorption spectra for **P1**-SWNT (red) and **P2**-SWNT (blue) in THF. 59
2.3 RBM regions of the Raman spectra using (A) 514 nm, (B) 633 nm, and (C) 785 nm excitation wavelengths. The yellow boxes denote the locations of signals arising from sc-SWNTs, while the blue boxes represent the locations of signals arising from m-SWNTs. The inset in (A) shows the G-band region, located at ~1590 cm^{-1}, upon excitation at 514 nm. 61
2.4 PL maps (A) and (B) correspond to **P1**-SWNT and **P2**-SWNT at a similar concentration and plotted on the same scale. (C) is the same **P2**-SWNT dispersion as (B) with an adjusted intensity scale. 63
2.5 ^{1}H NMR overlay for (A) **P2** and (B) **P1**. 72
2.6 Crude ^{1}H NMR spectra for **P2** after a reaction time of (A) 12 h (blue) and (B) 36 h (purple). If fully methylated, an integration of 9:3 aromatic:Py-CH_3 protons is expected; however, the aromatic region integrates to about twice this, which indicates that **P2** is ~50% methylated. 72
2.7 Electron density maps of trimers for partially methylated **P2**: (A) mono-methylation in the 1 position, (B) mono-methylation in the 2 position, (C) di-methylation in the 1 and 2 positions, and (D) di-methylation in the 1 and 3 positions. Red denotes electron-rich regions, green denotes less electron-rich regions, and blue denotes electron-poor regions. 73
2.8 UV/Vis-NIR absorption spectra (no normalization) for (A) **P1**-SWNT and (B) **P2**-SWNT in THF at varying polymer:SWNT ratios. 73
2.9 Photograph of **P1**, **P1**-SWNT, **P2**, and **P2**-SWNT (left to right) in THF solution. 73
2.10 Full Raman spectra of **P1**-SWNT (red), **P2**-SWNT (blue), and SWNT material (black) obtained at (A) 514 nm, (B) 633 nm, and (C) 785 nm excitation wavelengths. 74
2.11 Representative AFM images and corresponding height profiles of (A) **P1** and (B) **P2** with HiPCO SWNTs. The dashed white line is the location height trace, and the black scale bar represents 500 nm. 74
2.12 UV/Vis-NIR absorption spectra for **P1**-SWNT (red) and **P2**-SWNT (blue) in THF used for PL mapping. 75
2.13 UV/Vis-NIR absorption spectra for SDBS-SWNT in D_2O. 75
2.14 PL map of SDBS-SWNT dispersion in D_2O. 75

3.1 UV/vis–NIR spectra for polymer–SWNT dispersions produced in THF for the (a) PFdOMB-C3 series, (b) PFdOMB-C6 series, and (c) PFdOMB-C12 series. Photographs of the polymer–SWNT dispersions are color-coded with the appropriately colored dot above each dispersion. Note that the spectrum for the PFdOMB-C3-10–SWNT dispersion (red trace) was divided by a factor of 4. 122
3.2 RBM regions of the Raman spectra using (a) 514, (b) 633, and (c) 785 nm excitation wavelengths. The yellow boxes denote the locations of signals arising from sc-SWNTs, while the blue boxes represent the locations of signals arising from m-SWNTs. The inset in (a) shows the G-band region, located at ∼1590 cm^{-1}, upon excitation at 514 nm. 125
3.3 PL maps in THF corresponding to (a) PFdOMB-C6-25–SWNT and (b) PFdOMB-C6-50–SWNT. 125
3.4 UV/vis–NIR absorption spectra for PFdOMB-C6-50–SWNT dispersions prepared using plasma torch SWNTs in (a) THF and (b) toluene. Photographs of the polymer–SWNT dispersions are color-coded with the appropriately colored dot above each dispersion. The sample prepared in toluene with a polymer:SWNT mass ratio of 0.25:1 did not produce a stable SWNT dispersion, and the photograph is labeled with a black circle. The yellow boxes highlight the absorption regions corresponding to sc-SWNT chiralities, while the blue boxes highlight the regions corresponding to m-SWNT chiralities. 129
3.5 ^{1}H NMR data for (a) PFdOMB-C6-100 and (b) PFdOMB-C6-50 in $CDCl_3$. 143
3.6 UV/Vis-NIR spectra for polymer-SWNT dispersions produced in toluene. (a) PFdOMB-C3 series, (b), PFdOMB-C6 series, and (c) PFdOMB-C12 series. 143
3.7 Full Raman spectra using (a) 514 nm, (b) 633 nm, and (c) 785 nm excitation wavelengths. 144
3.8 UV/Vis-NIR spectra of polymer-HiPCO dispersions in THF used for PL mapping. 144
3.9 ^{1}H NMR spectrum of **5a** in $CDCl_3$. 144
3.10 DEPTq spectrum of **5a** in $CDCl_3$. 145
3.11 HPLC trace of **5a** at 254 nm. 145
3.12 ^{1}H NMR spectrum of **5b** in $CDCl_3$. 146
3.13 DEPTq spectrum of **5b** in $CDCl_3$. 146
3.14 HPLC trace of **5b** at 254 nm. 146
3.15 ^{1}H NMR spectrum of **5c** in $CDCl_3$. 147
3.16 DEPTq spectrum of **5c** in $CDCl_3$. 147
3.17 HPLC trace of **5c** at 254 nm. 147

4.1 FT-IR overlay of the **PF-N$_3$**–SWNT dispersion before (green) and 30 min after the addition of DIBAC-COOH (purple). 161
4.2 SPAAC of **PF-N$_3$**–SWNT complex with mPEG$_{5000}$–DIBAC. UV/Vis–NIR spectra of **PF-N$_3$**-coated plasma torch SWNTs pre-SPAAC (green) and post-SPAAC (purple) in (a) THF and (b) D_2O brine. (c) Photograph of organic/aqueous partitions pre- and post-SPAAC for **PF-N$_3$**-coated plasma torch SWNTs. UV/Vis–NIR spectra of **PF-N$_3$**-coated HiPCO SWNTs pre-SPAAC (green) and post-SPAAC (purple) in (d) THF and (e) D_2O brine. (f) Photograph of organic/aqueous partitions pre- and post-SPAAC for **PF-N$_3$**-coated HiPCO SWNTs. The photographs show the biphasic mixtures pre- and post-SPAAC under ambient conditions. 164
4.3 Raman spectra of **PF-N$_3$**–HiPCO dispersions pre- and post-SPAAC with mPEG$_{5000}$–DIBAC in toluene or D_2O at (a) 514, (b) 633, and (c) 785 nm. The yellow boxes denote the locations of signals arising from sc-SWNTs, while the gray boxes represent the locations of signals arising from m-SWNTs. 166
4.4 Photoluminescence maps of **PF-N$_3$**–HiPCO dispersions in (a) toluene (pre-SPAAC) and (b) D_2O (post-SPAAC with mPEG$_{5000}$–DIBAC). 168
4.5 Relative I_{PL} values for **PF-N$_3$**–mPEG$_{5000}$-coated sc-SWNTs dispersed in toluene (blue) or D_2O (orange). ***I_{PL} values in a given solvent are normalized to the IPL of the (7,6) species for that solvent. 168
4.6 Synthesis of monomers **3** and **4**. 173
4.7 ^{1}H NMR overlay of (a) **PF-Br** (blue) and (b) **PF-N$_3$** (red). 179
4.8 FT-IR overlay of (a) **PF-Br** (orange) and (b) **PF-N$_3$** (blue). 179
4.9 ^{1}H NMR spectrum of **mPEG$_{5000}$-DIBAC**. 179
4.10 Raman spectra collected at 785 nm of **PF-N$_3$**-SWNT dispersions (a) pre- (green) and (b) post-SPAAC (purple) with DIBAC-COOH. Spectra were normalized to the G-band at ~1590 cm^{-1} and offset for clarity. 180
4.11 FT-IR overlay of the SPAAC reaction between **PF-N$_3$**-SWNT and **mPEG$_{5000}$-DIBAC** (a) pre- (dark red) and (b) post-SPAAC (light blue). The post-SPAAC spectrum was obtained after 30 min. 180
4.12 UV/Vis-NIR spectra of **PF-N$_3$**-SWNT dispersions in 50/50 THF:D_2O with (i) nothing, (ii) two equivalents of mPEG$_{5000}$-OH (containing no DIBAC), or (iii) two equivalents of **mPEG$_{5000}$-DIBAC**. Photographs of the filtered dispersions are colour-coded accordingly with coloured dots above. 181

4.13 UV/Vis-NIR spectra of **PF-N$_3$**-HiPCO dispersions pre-SPAAC (toluene, dark yellow trace) and post-SPAAC with **mPEG$_{5000}$-DIBAC** (D_2O, blue trace). Spectra are offset for clarity. The photograph shows the pre-SPAAC polymer-SWNT dispersion in toluene. 181
4.14 UV/Vis-NIR spectra of **PF-N$_3$**-HiPCO dispersions diluted for PL mapping. 182
4.15 PL maps of **PF-N$_3$**-HiPCO in (a) toluene and (b) toluene mixed with 2.05 eq of mPEG$_{5000}$-OH. 182
4.16 UV/Vis-NIR spectrum of **PF-N$_3$**-mPEG$_{5000}$ used to disperse HiPCO SWNTs in toluene. Note that the spectrum was obtained by diluting the as-produced dispersion by a factor of 16 in toluene. The photograph shows the as-produced polymer-SWNT dispersion (undiluted). 183

5.1 FT-IR overlay of the **PF-N$_3$**–SWNT thin film after soaking in a 0.5 mg mL^{-1} solution of DIBAC–COOH in various solvents. (a) The pristine thin film (black) was soaked in a solution of DIBAC–COOH dissolved in (i) THF (green), (ii) CH_2Cl_2 (orange), (iii) acetone (purple), or (iv) EtOH (blue). (b) Pristine thin film either soaked (red) or vacuum filtered (light blue) with DIBAC–COOH dissolved in an alkaline aqueous solution. 196
5.2 TGA data showing mass loss upon heating under an argon atmosphere of (i) **PF-N$_3$** (blue), (ii) **PF-N$_3$**–SWNT (green), and (iii) **PF-N$_3$**–SWNT post-SPAAC with DIBAC–COOH (purple). . . 199
5.3 Modification of **PF-N$_3$**–SWNT thin film hydrophilicity using strained cyclooctyne derivatization. Photograph of a representative water droplet on the **PF-N$_3$**–SWNT thin film functionalized with (a) nothing (pristine), (b) mPEG$_{5000}$–DIBAC, or (c) DIBAC–C_{16}. The contact angles are 117 ± 1°, 73 ± 2°, and 107 ± 3°, respectively. . . 201
5.4 Raman spectra (λ_{ex} = 633 nm) of **PF-N$_3$**–SWNT dispersions pre-SPAAC (green) and post-SPAAC (purple) with DIBAC–COOH. Spectra were normalized to the G-band at ∼1590 cm^{-1} and offset for clarity. 203

5.5 Preparation of a Janus polymer–SWNT thin film using sequential strained cyclooctyne derivatization. (a) Cartoon representation of Janus thin film functionalization in a biphasic mixture. (b) Photograph (side view) of 5 μL water droplets on the SWNT thin film functionalized with DIBAC–C_{16} (left) and PEG_{5000}–DIBAC (right). The contact angles are 94 ± 3° and 63 ± 2°, respectively. The red dashed line indicates the boundary between hydrophilic (right) and hydrophobic (left) regions. Images (c) and (d) are close-up photographs of representative water droplets on the **PF-N_3**–SWNT thin film functionalized with DIBAC–C_{16} (c) or $mPEG_{5000}$–DIBAC (d). 205
5.6 Photograph of the **PF-N_3**-SWNT functionalization process. A 1 cm^2 **PF-N_3**-SWNT thin film is soaked in a solution of strained cyclooctyne. 215
5.7 FT-IR overlay of the **PF-N_3**-SWNT thin film soaked in a 0.5 mg·mL^{-1} solution of **mPEG$_{5000}$-DIBAC** in THF (orange) or H_2O (blue). . 215
5.8 UV/Vis-NIR spectra of **PF-N_3**-SWNT samples in THF used for PL mapping (i) prior to any functionalization (black), (ii) functionalized with **mPEG$_{5000}$-DIBAC** (orange). The samples were prepared by sonicating the corresponding thin film in THF for 1 h and then filtering the resulting dispersion through a cotton plug. 216
5.9 PL maps of **PF-N_3**-SWNT samples in THF (a) prior to any functionalization, (b) functionalized with **mPEG$_{5000}$-DIBAC**. The samples were prepared by sonicating the corresponding thin film in THF for 1 h and then filtering the resulting dispersion through a cotton plug. 216
5.10 Bar chart of sheet resistance measurements for (i) pristine, (ii) C_{16}-functionalized, and (iii) $mPEG_{5000}$-functionalized polymer-SWNT thin films. 217
5.11 Idealized cartoon showing the location of XPS measurements made on the Janus polymer-SWNT thin film. 217
5.12 ^{1}H NMR spectrum of DIBAC-C_{16} in $CDCl_3$. 218
5.13 uDEFT spectrum of DIBAC-C_{16} in $CDCl_3$. 218

6.1 ^{1}H NMR overlay of $mPEG_{5000}$-alkyne (red), **PF-N_3** homopolymer (green), and **PF-N_3-mPEG$_{5000}$** (blue) in $CDCl_3$. 231
6.2 Functionalization of the **PF-N_3**-$mPEG_{5000}$-SWNT complex (black) using CuAAC to couple 4-pentynoic acid (red), D-mannose-alkyne (green), $PDMS_{5000}$-alkyne (blue), and sulfobetaine-alkyne (purple). 234

6.3 UV/Vis-NIR spectra in THF of (a) IDX (100 μM) titrated with 0 – 1.6 eq of *p*-TSA (in 0.2 eq increments); and (b) the pristine **PF-PEG$_{5000}$-IDX**-SWNT dispersion (blue trace) followed by the addition of 1.5 eq of *p*-TSA (orange trace) and then the addition of 2.0 eq of Et_3N (purple trace). Polymer-SWNT dispersion photographs are colour-coded accordingly. 237
6.4 Photoluminescence maps of the **PF-PEG$_{5000}$-IDX**-SWNT dispersion in THF with (a) no *p*-TSA and (b) 1.5 eq of *p*-TSA. Maps are plotted on the same intensity scale. 239
6.5 Graphical representation of non-uniform fluorescence intensity changes for different sc-SWNTs. The experimental condition that includes "clicked" IDX with 1.5 eq *p*-TSA (blue) is compared to the control experiments where only 1.5 eq *p*-TSA is added (orange) and where 1.5 eq *p*-TSA and unbound IDX are added to the polymer-SWNT dispersion (purple). Intensity changes for the control experimental conditions are shown as the absolute value of change. Error bars represent the standard deviation for triplicate measurements (n = 3). 239
6.6 ^{1}H NMR overlay of **PF-Br** (red) and **PF-N$_3$** (blue) homopolymers in $CDCl_3$. 252
6.7 FT-IR spectra of **PF-Br** homopolymer (red), **PF-N$_3$** homopolymer (blue), and **PF-N$_3$**-mPEG$_{5000}$ (green). 252
6.8 UV/Vis-NIR spectra of **PF-N$_3$-mPEG$_{5000}$**-SWNT dispersion in THF (red) or D_2O (blue). The pristine THF dispersion was diluted two-fold to match the concentration of the D_2O dispersion. 253
6.9 FT-IR spectra of control experiments where $CuSO_4$ (green), (+)-sodium L-ascorbate (orange), or alkyne, i.e., 4-pentynoic acid (blue) were omitted from the reaction mixture. The control samples were stirred at RT for 16 h prior to obtaining the above IR spectra. The control experiments are juxtaposed with the pristine **PF-N$_3$-mPEG$_{5000}$**-SWNT dispersion (black) and the IR spectrum when the reaction mixture contains all reaction components (purple). . . 253
6.10 Photograph of a representative water droplet on the polymer-SWNT thin film functionalized with (a) nothing (pristine), (b) PDMS$_{5000}$-alkyne, (c) D-mannose-alkyne, or (d) zwitterionic sulfobetaine. The contact angles are 74 ± 3°, 80 ± 5°, 50 ± 1°, and 40 ± 4°, respectively. 253
6.11 Raman spectra (λ_{ex} = 633 nm) of **PF-N$_3$-mPEG$_{5000}$**-SWNT dispersions pre- (purple) and post-CuAAC (red) with 4-pentynoic acid. Spectra were normalized to the G-band at ~1590 cm^{-1} and offset for clarity. 254

6.12 FT-IR overlay of the CuAAC reaction between **PF-N$_3$-mPEG$_{5000}$**-SWNT and IDX pre- (black) and post-CuAAC (teal). The post-CuAAC IR spectrum was obtained after a reaction time of 30 min. 254
6.13 UV/Vis-NIR spectra of **PF-N$_3$-mPEG$_{5000}$**-SWNT dispersions in THF used for photoluminescence mapping in the control experiment where IDX was not linked to the SWNT surface. Spectra correspond to pristine dispersion (orange trace), dispersion with 1.5 eq *p*-TSA added (blue trace), and dispersion with both 1.5 eq *p*-TSA and 1 eq IDX added (purple trace). 255
6.14 Photoluminescence maps of control experiment with **PF-N$_3$-mPEG$_{5000}$**-SWNT dispersion in THF with (a) no *p*-TSA, (b) 1.5 eq of *p*-TSA, and (c) 1.5 eq of *p*-TSA and 1 eq of IDX (unbound). Maps are plotted on the same intensity scale. 256
6.15 Photoluminescence maps of the **PF-PEG$_{5000}$-IDX**-SWNT dispersion in THF with (a) no *p*-TSA, (b) 1.5 eq of *p*-TSA, and (c) 1.5 eq of *p*-TSA and 2.0 eq of Et_3N. Maps are plotted on the same intensity scale. 256
6.16 Graphical representation of fluorescence intensity changes for different sc-SWNTs. The experimental conditions include pristine **PF-PEG$_{5000}$-IDX**-SWNT conjugate (red) followed by the addition of 1.5 eq *p*-TSA (green) and the subsequent addition of 2.0 eq of Et_3N (blue). 256
6.17 ^{1}H NMR spectrum of mPEG$_{5000}$-alkyne in $CDCl_3$. 257
6.18 DEPTq spectrum of mPEG$_{5000}$-alkyne in $CDCl_3$. 258
6.19 ^{1}H NMR spectrum of PDMS$_{5000}$-alkyne in $CDCl_3$. 258
6.20 uDEFT spectrum of PDMS$_{5000}$-alkyne in $CDCl_3$. 259
6.21 ^{1}H NMR spectrum of sulfobetaine **6** in D_2O. 259
6.22 uDEFT spectrum of sulfobetaine **6** in D_2O. 259
6.23 ^{1}H NMR spectrum of IDX **10** in $CDCl_3$. 260
6.24 DEPTq spectrum of IDX **10** in $CDCl_3$. 260

7.1 HPLC data for the crude reaction mixtures for the photoclick reaction between PAQ and butyl vinyl ether in various organic solvents. The bottom chromatograms correspond to PAQ starting material (black) and the isolated photoclick product PAQ-BVE (red). 272

7.2 Photophysical properties in toluene of (a) the small molecule PAQ and its photoclick product, PAQ-BVE, and (b) the polymer **PF-PAQ** and its photoclick product, **PF-PAQ-BVE**. PAQ and PAQ-BVE were excited at λ_{ex} = 350 nm, while **PF-PAQ** and **PF-PAQ-BVE** were excited at λ_{ex} = 360 nm. Solid lines correspond to absorption spectra while dashed lines correspond to emission spectra. Photographs of each compound in toluene are shown prior to and during irradiation with a handheld UV lamp (λ_{ex} = 365 nm). Solutions are colour-coded with the appropriately coloured dot above. 275
7.3 UV-Vis absorption and fluorescence spectra in water of (a) **PF-PAQ**-mPEG$_{5000}$ (purple), **PF-PAQ** (orange), mPEG$_{5000}$-VE (blue), and **PF-PAQ** in the presence of mPEG$_{5000}$-OH after sonication in water. UV-Vis absorption and fluorescence spectra of **PF-PAQ**-mPEG$_{5000}$ in solvents of varying polarity in (b) and (c). Solid lines correspond to absorption spectra while dashed lines correspond to emission spectra. Photographs of each solution are shown with and without irradiation at λ_{ex} = 365 nm using a handheld UV lamp. Solutions are colour-coded with the appropriately coloured dot above. 278
7.4 Cartoon representation of **PF-PAQ-silicone** photopatterning process. (b) A representative confocal fluorescence microscope image of **PF-PAQ-silicone** after soaking the sample in a BVE/toluene solution for 2 min and illuminating with white LEDs while covering with a 3D printed mask. 280
7.5 Photograph of the photochemical reaction setup (reaction sample not shown). The lamp was adjusted accordingly for the specific experiment, and was positioned parallel to the sample during irradiation. A Kessil A160WE Blue Tuna saltwater aquarium light is used to irradiate the sample and an AC Infinity AXIAL 1238 muffin fan is used to keep the reaction mixture from overheating. 289
7.6 ^{1}H NMR spectrum of PAQ-BVE. 289
7.7 IR spectra of PAQ (teal) and PAQ-BVE (purple). 290
7.8 HPLC traces of the crude reaction mixtures for the photoclick reaction between PAQ and BVE in various solvents. The bottom traces correspond to PAQ starting material (black) and the isolated photoclick product PAQ-BVE (red), respectively. 290
7.9 ^{1}H NMR spectra of **PF-PAQ-BVE** (blue) and PAQ-BVE (red). . 291
7.10 IR spectra of **PF-PAQ** and **PF-PAQ-BVE**. 291
7.11 Plots of absorbance vs concentration (M) in toluene for (a) PAQ and (b) **PF-PAQ**. 292
7.12 Plots of $\ln\frac{[PAQ]_0}{[PAQ]}$ or $\ln\frac{[\mathbf{PF-PAQ}]_0}{[\mathbf{PF-PAQ}]}$ vs time (s) for (a) PAQ and (b) **PF-PAQ** (n = 3). 292

7.13 Photographs of **PF-PAQ-silicone** (a) pre-irradiation and post-irradiation with white LEDs (b) in the absence of BVE and (c) in the presence of BVE. (d) Photograph of the samples used for microscopy post-irradiation with white LEDs (i) without or (ii) with BVE present. Representative (e) brightfield image and (f) confocal fluorescence image of **PF-PAQ-silicone** post-irradiation. 294
7.14 ^{13}C DEPTq spectrum of PAQ-BVE in $CDCl_3$. 294
7.15 ^{1}H NMR spectrum of $mPEG_{5000}$-VE in $CDCl_3$. 295
7.16 ^{13}C DEPTq spectrum of $mPEG_{5000}$-VE in $CDCl_3$. 295
7.17 ^{1}H NMR spectrum of **PF-PAQ** in $CDCl_3$. 296

8.1 **Fong, D.**; Bodnaryk, W. J.; Rice, N. A.; Saem, S.; Moran-Mirabal, J. M.; Adronov, A. *Chem. - A Eur. J.* **2016**, *22*, 14560–14566. . . . 310
8.2 **Fong, D.**; Adronov. A. *Chem. Sci.* **2017**, *8*, 7292-7305. 311
8.3 **Fong, D.**; Andrews, G.; Adronov, A. *Polym. Chem.* **2018**, *9*, 2873–2879. 311
8.4 **Fong, D.**; Andrews, G. M.; McNelles, S. A.; Adronov, A. *Polym. Chem.* **2018**, *9*, 4460–4467. 312

List of Abbreviations

E_a	Activation Energy
M_n	Number-Average Molecular Weight
M_w	Weight-Average Molecular Weight
AFM	Atomic Force Microscopy
AuNP	Gold Nanoparticle
BPy	Bipyridyl
BT	Benzothiadiazole
BVE	Butyl Vinyl Ether
BWF	Breit-Wigner-Fano
CuAAC	Copper-Catalyzed Azide-Alkyne Cycloaddition
CV	Column Volume
CVD	Chemical Vapor Deposition
DEPT	Distortionless Enhancement by Polarization Transfer
DFT	Density Functional Theory
DGU	Density Gradient Ultracentrifugation
DIBAC	Dibenzoazacyclooctyne
DMAP	4-Dimethylaminopyridine
DMF	Dimethylformamide
DP	Degree of Polymerization
EtOAc	Ethyl Acetate
EtOH	Ethanol
FET	Field Effect Transistor
FT-IR	Fourier Transform Infrared

GPC	Gel Permeation Chromatography
HiPCO	High-Pressure Carbon Monoxide
HOMO	Highest Occupied Molecular Orbital
HPLC	High Performance Liquid Chromatography
HRMS	High-Resolution Mass Spectrometry
IDX	Indolinooxazolidine
IEDDA	Inverse-Electron Demand Diels-Alder Cycloaddition
KOAc	Potassium Acetate
KOH	Potassium Hydroxide
LED	Light-Emitting Diode
LUMO	Lowest Unoccupied Molecular Orbital
MeCN	Acetonitrile
MeOH	Methanol
m-SWNT	Metallic Single-Walled Carbon Nanotube
MWNT	Multiwalled Carbon Nanotube
NBS	*N*-Bromosuccinimide
NCL	Non-Conjugated Linker
NIR	Near Infrared
NMP	*N*-Methylpyrrolidone
NMR	Nuclear Magnetic Resonance
OPV	Organic Photovoltaic
PAQ	9,10-Phenanthrenequinone
PBS	Phosphate-Buffered Saline
PDMS	Polydimethylsiloxane
PDO	Phenanthrodioxine

PEG	Polyethylene Glycol
PEGMA	Polyethylene Glycol Methylacrylate
PF	Polyfluorene
PFO	Poly(9,9-di-*n*-octylfluorene)
PL	Photoluminescence
PPV	Poly(Phenylene Vinylene)
p-TSA	*para*-Toluenesulfonic Acid
RBM	Radial Breathing Mode
RDS	Rate-Determining Step
rr-P3DDT	Regioregular Poly(3-Dodecylthiophene)
RT	Room Temperature
sc-SWNT	Semiconducting Single-Walled Carbon Nanotube
SDBS	Sodium Dodecylbenzenesulfonate
SDS	Sodium Dodecyl Sulfate
SEC	Size Exclusion Chromatography
SPAAC	Strain-Promoted Azide-Alkyne Cycloaddition
SPANC	Strain-Promoted Azide-Nitrone Cycloaddition
TCO	*trans*-Cyclooctene
TFA	Trifluoroacetic Acid
TGA	Thermogravimetric Analysis
THF	Tetrahydrofuran
uDEFT	Uniform Driven Equilibrium Fourier Transform
UV/Vis-NIR	Ultraviolet-Visible-Near-Infrared
VE	Vinyl Ether
XPS	X-Ray Photoelectron Spectroscopy

If you don't like how the table is set, turn over the table.

Francis J. Underwood

Chapter 1

Carbon Nanotube Sorting and Functionalization

The carbon nanotube sorting review included in this Introduction has been reprinted with permission from Chemical Science. Fong, D.; Adronov, A. Recent developments in the selective dispersion of single-walled carbon nanotubes using conjugated polymers, **2017**, *8*, 7292-7305. Copyright (2017) Royal Society of Chemistry.

1.1 Introduction

1.1.1 Enrichment of Single-Walled Carbon Nanotubes

Within the realm of nano-scale materials, the recently discovered allotropes of carbon, including fullerenes, carbon nanotubes, and graphene, have attracted significant research attention. In particular, since the first deliberate preparation methods of single-walled carbon nanotubes (SWNTs) were reported,[1,2] a substantial number of studies have focused on exploiting the unique properties of this nanomaterial. The high tensile strength,[3] aspect ratio,[4] thermal and electrical conductivity,[5–8] and extraordinary optical characteristics[9–11] of SWNTs find utility in numerous applications, including high-strength nanocomposites,[12–14] field-effect transistors (FETs),[15] sensors,[16–19] photodetectors,[20] organic photovoltaics (OPVs),[21–23] flexible electronics,[24,25] touch screens,[26] microelectronic interconnects,[27] and other devices.[28] Indeed, semiconducting SWNTs (sc-SWNTs) have demonstrated performance superior to that of traditional silicon-based semiconductors,[15] while metallic SWNTs (m-SWNTs) are superior conductors to traditional metals, such as copper.[29] Though SWNT commercialization has begun,[27] the promise of transformative technologies has not materialized, especially in cases where nanotube purity is critical to the application. Nanotube purity is a challenge because all known commercial synthetic methods, including high-pressure carbon monoxide disproportionation (HiPCO),[30] chemical vapour deposition (CVD),[31] arc-discharge,[32] laser ablation,[33] and plasma torch growth,[34] produce a roughly 2:1 mixture of sc-SWNTs and m-SWNTs. In the pursuit of electronically-pure SWNTs, differences in the exploitable properties used to separate the electronic types are exceedingly small, and thus their separation is extremely difficult.

Several methods for isolating electronically-enriched SWNTs have recently been developed (Figure 1.1). The first, and arguably most transformative, is density gradient ultracentrifugation (DGU), described in the seminal papers by Hersam and co-workers that appeared in 2005[35] and 2006.[36] This technique allowed, for the first time, access to electronically-enriched samples of SWNTs, and enabled follow-up studies that developed a variety of SWNT-based devices.[28] DGU is capable of separating individual SWNT species; also referred to as chiralities (for a thorough discussion on SWNT properties, including chirality, chiral vectors, chiral angles, and electronics, the reader is referred to the excellent review by Charlier[37]). Subsequently, agarose gel filtration,[38] electrophoresis,[39] two-phase extraction,[40,41] and size-exclusion chromatography (SEC)[42,43] were developed as alternative separation methods for m- and sc-SWNTs. As well, single-stranded DNA, in combination with ion exchange chromatography, was found to be capable of separating individual SWNT species.[44–46] However, with all the aforementioned purification methods, the yield of electronically-enriched SWNTs is a major limitation. These methods typically isolate microgram quantities of enriched material after extensive purification procedures, and the difficulty in obtaining large quantities of enriched material is reflected in the exorbitant cost of commercially-available enriched SWNTs. At the time of writing this Thesis, one milligram of $> 99\%$ enriched sc- or m-SWNT samples could be purchased from Raymor Industries Inc. at a cost of $695 and $899 USD, respectively (prices quoted directly from Raymor in March 2019).

An alternative strategy that has the potential to address the scalability challenge involves the selective dispersion of SWNTs using conjugated polymers. Since the initial reports that both aromatic small molecules (i.e., pyrene)[49] and conjugated polymers [i.e., poly(phenylene vinylene) (PPV)][50,51] exhibit interactions with

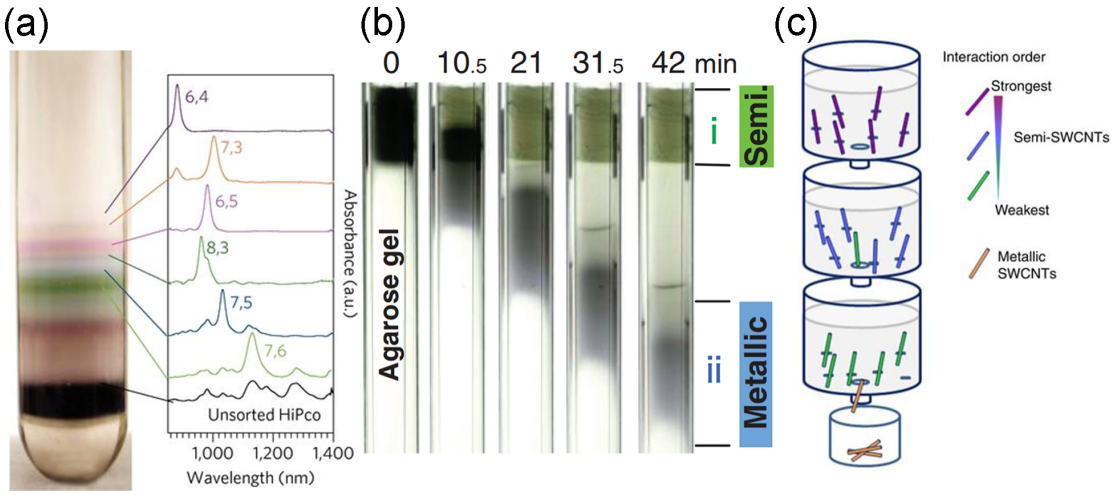


FIGURE 1.1: Methodologies for the selective enrichment of SWNTs, including (a) DGU,[47] (b) agarose gel electrophoresis,[48] and (c) SEC.[38] Reproduced with permission. Copyright Springer Nature Publishing Group (2010), IOP Publishing Ltd. (2008), Springer Nature Publishing Group (2011), respectively.

SWNTs, nanotube dispersions have been prepared using a variety of conjugated polymer structures.[52–54] Amongst the different conjugated polymer structures that have been explored, the vast majority have focused on polymers based on the fluorene monomer unit, followed by thiophene- and carbazole-based polymers (Figure 1.2). Copolymers of these core monomers with other monomer types have also been considered. The potential for selective conjugated polymer-SWNT dispersions went practically unnoticed (except for a brief report in the patent literature)[55] until the ground-breaking work of Nicholas and co-workers in 2007.[56] As shown in Figure 1.3, this group was the first to demonstrate that simple commercially-available conjugated polymers, including poly(9,9-di-*n*-octylfluorene) (PFO), can selectively disperse a small subset of sc-SWNT chiralities. It was found that the PFO-SWNT dispersion in toluene only contained a small subset of the original SWNT population (Figure 1.3a), and had a substantial enrichment of sc-SWNTs

compared to the non-selective SDBS surfactant (Figure 1.3b). Since then, studies of polymer-SWNT interactions have dramatically increased, with numerous reports of highly enriched sc-SWNT dispersions having appeared, some with purities in excess of 99.9%.[57] Recently, polymer structures that utilize backbone conformational changes or depolymerization to desorb from the SWNT surface have been developed to allow for the isolation of pristine SWNTs,[54] with some systems demonstrating both enrichment and release of sc-SWNTs.[58–60] Overall, the selective dispersion of SWNTs using conjugated polymers is arguably the most viable method for time-efficient and scalable SWNT subtype enrichment.

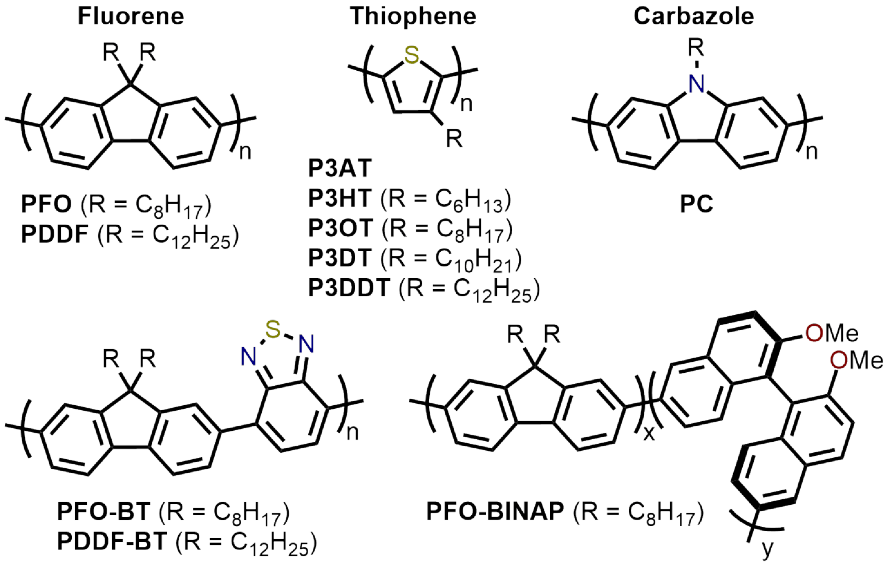


FIGURE 1.2: Chemical structures of homopolymers derived from fluorene, thiophene, and carbazole monomers, as well as copolymers of fluorene with benzothiadiazole (BT) or binaphthol (BINAP) units. Reproduced with permission.[61] Copyright Royal Society of Chemistry, 2017.

Currently, the ability to selectively isolate substantial quantities of a desired SWNT subtype or chirality from its parent mixture using a rationally designed conjugated polymer structure remains elusive. The difficulty in identifying polymer

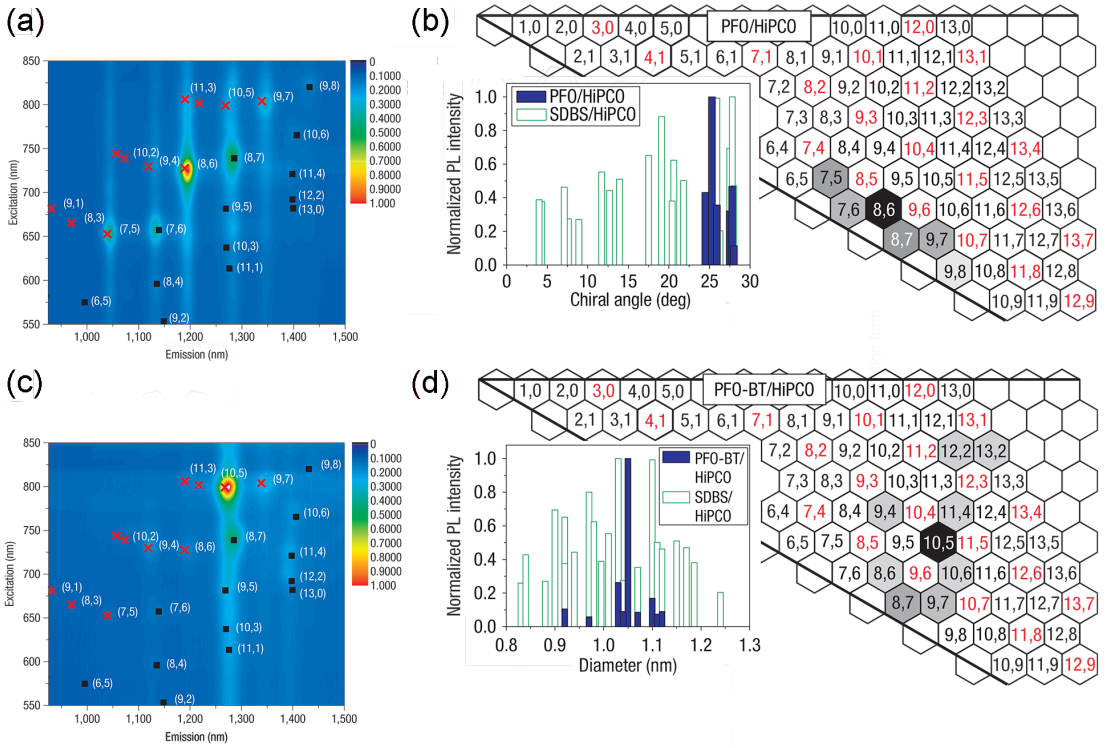


FIGURE 1.3: First example of the selective dispersion of SWNTs using conjugated polymers. (a) PL and (b) graphene sheet maps of PFO-SWNT dispersions in toluene. (c) PL and (d) graphene sheet maps of PFO-BT-SWNT dispersions in toluene. Graphene sheet maps use normalized PL map intensities and compare the relative fluorescence intensities of different SWNT species present in the SWNT dispersion. Reproduced with permission.[56] Copyright 2007, Nature Publishing Group.

characteristics that dictate nanotube selectivity arises from the fact that systematic variation of conjugated polymer structure is non-trivial. Structural changes to monomers result in differences in solubility, stability, and polymerization reactivity, the combination of which makes it difficult to control polymer molecular weight and dispersity (Đ). This is problematic because polymer molecular weight is known to impact dispersion selectivity, and so a rigorous analysis of structure-selectivity relationships necessitates that polymers within a series under investigation have comparable degrees of polymerization (a requirement that is infrequently satisfied).

It is instructive to point out that commercial syntheses of SWNTs lead to samples that differ in their diameter ranges, depending on the synthetic methodology used. In order from smallest to largest average diameters, the different SWNT types include: CoMoCAT (0.7 – 0.9 nm), HiPCO (0.8 – 1.2 nm), plasma torch (1.1 – 1.5 nm), arc-discharge (1.2 – 1.7 nm), and TUBALL (1.5 – 2.0 nm).[54] In addition, batch-to-batch variability within any given SWNT synthesis is significant, and warrants that, if results are to be directly compared, experiments should be performed using SWNTs of the same type and from the same batch. Generally, researchers list the SWNT type used in their experimental work and provide the batch number. Exact reproduction of results necessitates that the same SWNT type and, preferably, batch number be used, which may not always be feasible.

Despite the examples of selective sc-SWNT dispersions using conjugated polymers reported thus far, a fundamental understanding of the underlying principles behind observed selectivity is limited.[61] Insight can be gleaned, however, by considering the SWNT dispersion protocol. As depicted in Figure 1.4, the general process of dispersing SWNTs begins with the sonication of a mixture of SWNT powder and solubilized conjugated polymer. Careful consideration must be made with respect to polymer structure and molecular weight, as well as the SWNT source, sonication temperature, conjugated polymer:SWNT mass ratio, and identity of the solvent. Sonication is followed by mild centrifugation to remove SWNT bundles and isolate polymer-wrapped, individualized SWNTs. Within this protocol, two opportunities arise for control over the outcome of dispersion selectivity: Conjugated polymer structure and dispersion preparation conditions. It has been proposed that the selectivity problem can be considered in terms of the classic chemistry principles of kinetics and thermodynamics.[61] If the system is governed

primarily by kinetics, then selectivity is driven by either the activation energy barrier (E_a) to polymer-SWNT complex formation, or the E_a to aggregation (and flocculation) of specific SWNT species. In this case, if the exfoliation is carried out under conditions favouring kinetic control, the process with the lowest E_a will occur and dictate selectivity. Conversely, if the system is controlled primarily by thermodynamics, where enough energy is available to surmount every E_a and allow microscopic reversibility, then the stability of polymer-SWNT complexes and/or the stability of SWNT bundles become the governing factors. Considering that sonication, a highly energetic process, is nearly always used to disperse SWNTs and promote the formation of polymer-SWNT complexes, it may be argued that thermodynamic control may be the dominant factor that dictates selectivity. By considering the selectivity problem from the vantage point of kinetics versus thermodynamics, the logical consequences of these frameworks can be considered, and this may better enable the rational design of conjugated polymer structures to selectively disperse specific SWNT species. Nevertheless, it is evident that the origin of dispersion selectivity is multifaceted and requires further investigation to identify a clear and predictive mechanism.

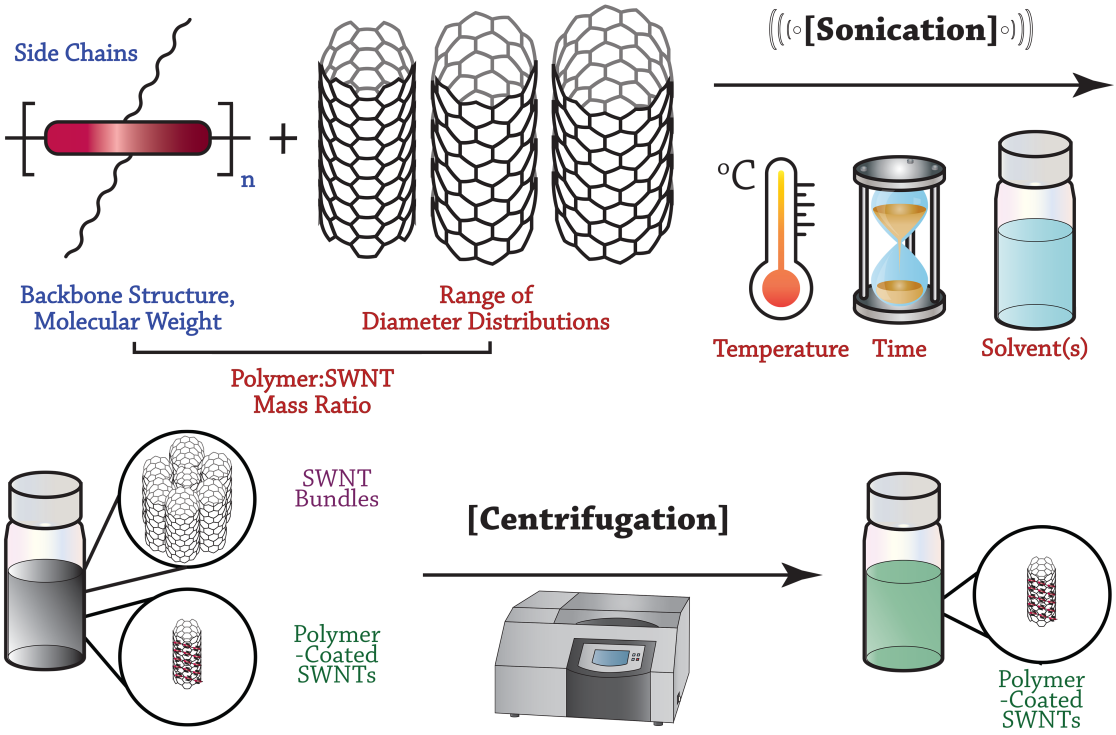


FIGURE 1.4: General overview of the SWNT dispersion protocol. Soluble conjugated polymer is sonicated with insoluble SWNT powder, and then SWNT bundles are removed by mild centrifugation. The variables involved in dispersion selectivity are categorized, where polymer features are labelled in blue and preparation conditions are labelled in red. Reproduced with permission.[61] Copyright Royal Society of Chemistry, 2017.

1.1.2 General Considerations for Dispersion Preparation

As mentioned above, several variables can be considered during the SWNT dispersion process to modulate dispersion selectivity: These include the SWNT type used, sonication temperature, polymer:SWNT mass ratio, and choice of solvent. The author emphasizes that, for the same conjugated polymer sample, different SWNT species may be dispersed depending on the starting SWNT material used, so investigation of different SWNT types is important. In addition, though not necessarily related to dispersion selectivity, there have been conflicting reports on

the effect of sonication time on the length of SWNTs. Below, the author has compiled the reports and establishes that the impact of sonication on SWNT length is dependent on the sonication power used. Additionally, although centrifugation speed is not particularly relevant to dispersion selectivity, it should be noted that an adequate speed must be identified for each individual polymer-SWNT system, such that bundles are efficiently removed. Overall, based on the numerous studies that have been done, the author attempts to highlight the general trends with respect to each variable.

Sonication Time. Sonication is used to temporarily exfoliate SWNT bundles, such that dispersant can access and coat the SWNT surface to prevent re-bundling. Bao and co-workers examined the effect of sonication time on SWNT concentration, length, and bundling, using the solvent *N*-methylpyrrolidine (NMP) as the dispersant.[62] SWNTs in NMP were sonicated at 225 W for up to 480 min, and aliquots were taken at regular intervals for analysis. It was found that increased sonication time decreased bundling, until sufficient diffusion of atmospheric water into NMP resulted in SWNT bundling ($\sim$120 min); a known phenomenon.[63] It was also found that increased sonication time decreased the average SWNT length and length dispersity, and increased the dispersed SWNT concentration.[62] The SWNT dispersions were used to prepare FETs, and it was determined that shorter sonication times ($<$ 30 min) were ideal to minimize sonication-induced SWNT defects. Contrary to these findings, Loi and co-workers found that sonication time up to 2 h had little effect on SWNT length.[64] It is important to note that, in this study, sonication power was 90 W, compared to 225 W used by Bao and co-workers. Thus, we highlight that sonication-induced SWNT damage is dependent on the sonication apparatus used. It is imperative to optimize sonication time such that

SWNTs can be sufficiently de-bundled to allow for polymer wrapping, while being aware that higher sonication power may potentially result in changes to the SWNT material.

Sonication Temperature. Bao and co-workers examined the effect of temperature on the selective dispersion of HiPCO SWNTs using rr-P3DDT.[65] Temperature was varied from –40 to 90 °C, and it was found that the strongest SWNT absorption intensity at 1288 nm was obtained for the dispersion prepared at 50 °C, which coincided with the alkyl side chain melting temperature. The observations were modelled by the authors as follows: (i) At low temperatures, polymer aggregates cannot dissociate, even if the polymer-SWNT complex is more thermodynamically stable; (ii) at high temperatures, entropic penalties may prohibit polymer-SWNT complex formation; and (iii) at an intermediate temperature, enough energy is present to overcome polymer-polymer interactions and allow for equilibration to more stable polymer-SWNT complexes, without excessive entropic penalties. In tandem with this study, Loi and co-workers also investigated rr-P3DDT dispersions with HiPCO SWNTs, varying sonication temperature from 0 – 80 °C.[66] SWNT dispersions prepared with or without polymer aggregation resulted in no difference in the dispersion selectivity. It was found, in contrast to the aforementioned study, that sonication from 10 – 20 °C produced the most concentrated SWNT dispersions. It should be noted that preparation conditions were not identical. For instance, Bao and co-workers used a 2:1 polymer:SWNT mass ratio, while Loi and co-workers used a 3:1 polymer:SWNT mass ratio. The polymer molecular weights and dispersities were also different (M_n = 39.1 kDa and Đ = 1.97, vs M_n = 26.8 kDa and Đ = 1.08), as were the initial SWNT concentrations in toluene (0.20 mg·mL^{-1} vs 0.33 mg·mL^{-1}). These differences in polymer features and dispersion

preparation conditions highlight the difficulty in making generalizable statements about the effect of a single variable, even with extraneous variables held constant within a single study. Though it is clear that sonication temperature influences dispersion selectivity and cannot be ignored, the exact role it plays is unclear and warrants further examination.

Polymer:SWNT Mass Ratio. Several groups have examined the polymer:SWNT mass ratio and its effect on dispersion selectivity. In work by Malenfant and co-workers, it was shown that polymer:SWNT mass ratios of 0.5:1 to 1:1 produced the highest sc-SWNT purity, while larger polymer:SWNT mass ratios resulted in decreased sc-SWNT discrimination.[67] Likewise, Rice et al.[68] and Zaumseil and co-workers[69] found similar results. The appropriate polymer:SWNT mass ratio depends on the polymer system, but in general, there is an ideal mass ratio range where, (i) there is enough polymer to adequately coat SWNT surfaces and produce stable polymer-SWNT dispersions, while (ii) there is not enough polymer present to saturate all SWNT surfaces and indiscriminately disperse all SWNTs. The polymer:SWNT mass ratio should be optimized for each polymer system.[68,70]

Solvent. In general, solvent density must be lower than the buoyant density of SWNT bundles ($\sim$1.3 g·cm^{-3}), otherwise bundles cannot sediment upon centrifugation. This necessarily excludes chlorinated solvents such as CH_2Cl_2 and $CHCl_3$, as these solvents are too dense (densities of $\sim$1.3 and 1.5 g·cm^{-3}, respectively). Beyond this, several groups have examined different solvent properties. Cui and co-workers examined the effect of solvent dielectric constant on dispersion selectivity.[71] Arc discharge SWNTs were dispersed using commercially available poly(9,9-di-*n*-octylfluorene-*co*-bithiophene) (PFO-T2) in various solvents (0 – 1.75

D). It was found that sc-SWNT selectivity only occurred for solvents with a dielectric constant between 0 to 0.5 D (toluene, *m*-xylene, and xylenes). It was argued that selectivity was driven by charge transfer that prevented the formation of the supramolecular polymer-SWNT complexes required to disperse m-SWNTs, and that in solvents with a higher dielectric constant, this charge transfer could be inhibited. Within the solvent series, CH_2Cl_2 and $CHCl_3$ were included as solvents with higher dielectric constants (1.60 and 1.04 D, respectively); yet the absence of selectivity can also be explained by the high densities of these solvents, a possibility that was left unaddressed. Meanwhile, Zaumseil and co-workers examined the relationship between solvent viscosity and dispersion selectivity.[69] It was found that the fluorescence intensity for the (9,4) chirality was correlated with the magnitude of solvent kinematic viscosity for toluene, the individual xylene isomers, and mesitylene, while keeping the conjugated polymer properties (molecular weight, backbone structure) constant. However, for the (10,5) chirality, fluorescence intensity was not linearly correlated with increasing solvent kinematic viscosity. The exact relationship between solvent viscosity and dispersion selectivity is therefore unclear. In work by Bao and co-workers, HiPCO SWNTs were dispersed using rr-P3DDT in THF, decalin, tetralin, *m*-xylene, and *o*-xylene.[72] It was found that decalin and tetralin resulted in higher dispersion selectivity (fewer sc-SWNT chiralities). All the solvents, excluding THF, resulted in enriched sc-SWNT dispersions, which was attributed to solvent polarity differences between THF and the other solvents. Interestingly, the viscosities of the solvents that resulted in enriched sc-SWNT dispersions vary over a wide range (0.59 – 2.09 cP). It is evident from these studies that the effect of solvent on dispersion selectivity involves a complicated

amalgamation of solvent density, polarity, and viscosity, and it is perhaps challenging or impossible to disentangle these individual effects. Overall, non-polar solvents such as toluene are commonly used for the preparation of selective dispersions, and often more polar solvents such as THF result in non-selective dispersions. The author emphasizes, however, that examples of selective sc-SWNT dispersions in THF exist in the literature,[73–75] and that these trends are not absolute.

1.1.3 Functional Polymer-Nanotube Complexes

Beyond the selectivity problem, SWNT conjugates are of substantial interest as drug delivery agents,[76–80] catalysis vectors,[81–83] molecular imaging agents,[84–87] and as components in tissue engineering.[88] As well, the production of SWNT nanohybrids is of significant interest for selective chemiresistive sensors.[89] In each case, SWNTs require functionalization with various molecules, including targeting vectors, catalytically active species, or other molecules to impart functionality to the SWNT complex. Thus, methods must be used to introduce functionality onto the SWNT surface for these applications. To approach this issue, covalent or noncovalent functionalization is used.[90–92] Covalent functionalization directly modifies the SWNT sidewall, destroying the sp^2-hybridized structure and damaging SWNT optoelectronic properties.[92] It is possible, to some extent, to balance the degree of functionalization with the extent of SWNT damage. However, issues with batch-to-batch variability and reaction control are prohibitive in these endeavours. Another route is to use multiwalled carbon nanotubes (MWNTs), wherein covalent functionalization sacrifices the outer carbon nanotube while leaving the inner carbon nanotubes intact and able to transduce an electrical signal.[93] Recently, Reich and co-workers reported a covalent functionalization method that preserved SWNT

optoelectronic properties by utilizing a $[2+1]$ cycloaddition with an electron-poor nitrene.[94] However, the subsequent nucleophilic substitution used to decorate the SWNT surface necessitated raised temperatures (60 – 70 °C) and lengthy reaction times (2 – 4 days). Alternatively, noncovalent functionalization uses sonication in the presence of a dispersant to form dispersant-SWNT supramolecular complexes, which prevents bundle re-aggregation.[95–97] This method is promising for the simple production of nanohybrids that preserve the SWNT optoelectronic properties. Criticism for noncovalent functionalization includes the possibility of dispersant leaching that leads to low long-term complex stability and robustness. Although small molecule dispersants may pose this issue, it is far less likely to be a problem for a conjugated polymer-based dispersant due to kinetic effects that prevent high molecular weight polymer chains from easily desorbing from the SWNT surface. Interestingly, enriched SWNT samples consisting of sc-SWNTs improved chemiresistor response, implying that the ability to simultaneously sort and functionalize SWNT surfaces with various molecular recognition motifs may be of substantial value.[98]

The facile derivatization of carbon nanotube surfaces is evidently a challenging issue. A methodology that establishes a generalizable method to functionalize carbon nanotube surfaces without deleteriously affecting optoelectronic properties would have widespread utility. Furthermore, facile stoichiometric reactions under dilute conditions would avoid waste. The ability to sort carbon nanotube subtypes would also be beneficial. Some efforts have been made in preparing conjugated polymer-SWNT complexes with functional polymer coatings. In work by Nakashima and co-workers, thiol- or porphyrin-containing conjugated polymers were used to produce polymer-SWNT thin films that could be functionalized with

AuNPs using thiol-Au[99] or pyridine-porphyrin[100] coordination bonds. Though this work is intriguing for AuNP-SWNT conjugates, these methods lack solution processability and ease of functionalization with any small molecule or polymer. Meanwhile, Fujigaya and co-workers prepared surfactant-coated SWNTs and then copolymerized polyethylene glycol methacrylate (PEGMA) and furan-protected maleimide-containing acrylates to form a crosslinked polymer shell around the SWNT surface.[101] These polymer-SWNT complexes were then subjected to 80 °C for 90 min to deprotect the maleimide groups, followed by stirring at RT for 24 h in a saturated solution of thiol to functionalize the polymer-SWNT surface. Though interesting, the necessity for saturated thiol solution is suboptimal as the extra reagent is wasted. In work by Arnold, Gopalan, and co-workers, it was shown that the bipyridyl units (BPy) in PFO-BPy could be used to chelate Re metal centres, causing a conformational change in the polymer backbone and resulting in a structure that was no longer capable of dispersing SWNTs (Figure 1.5).[102] The combination of selective sc-SWNT dispersion with PFO-BPy followed by polymer desorption upon metal complexation allowed for the isolation of electronically-enriched samples of pristine sc-SWNTs.

Recently, polymer backbones that are degradable, recyclable, and selectively disperse sc-SWNTs have been prepared, with polymer removal mechanisms including supramolecular metal coordination chemistry,[58] hydrogen bond disruption,[59] and imine hydrolysis[60] (Figure 1.6). In work by Toshimitsu and Nakashima, a fluorene unit appended to two phenanthroline moieties was used to form supramolecular metal-coordination polymers with perchlorate salts of Co(II), Ni(II), Cu(II), and Zn(II) in benzonitrile, which served as a "good" solvent.[58] HiPCO SWNTs

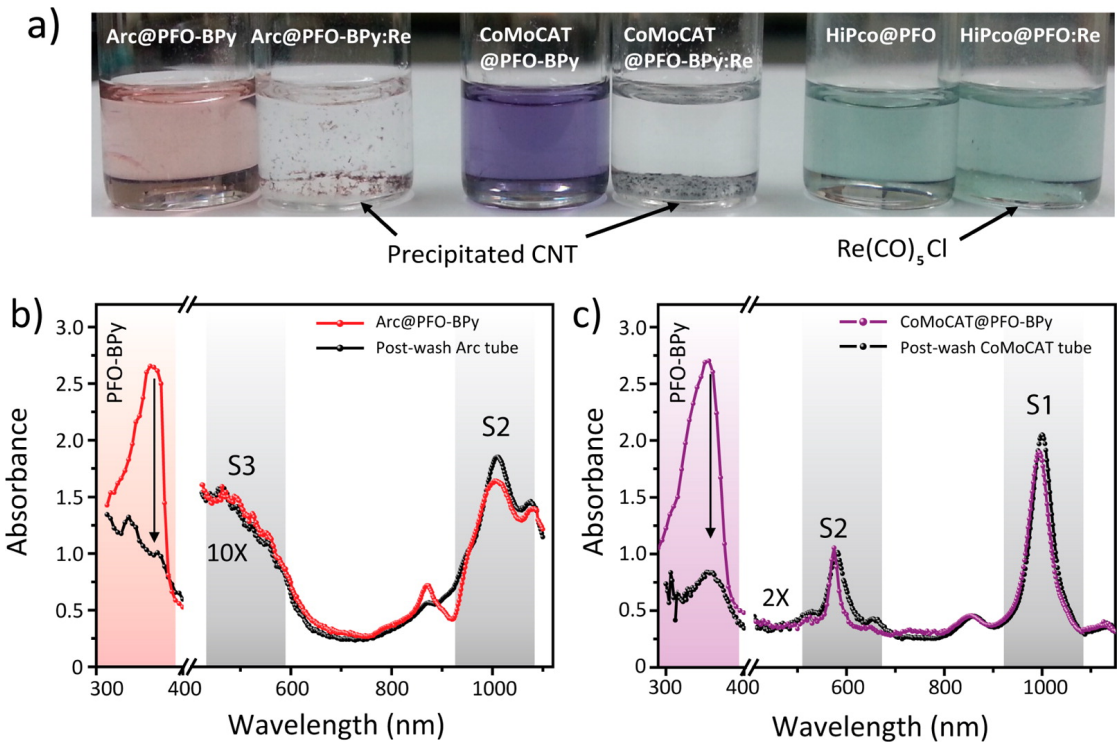


FIGURE 1.5: Selective dispersion and release of sc-SWNTs using PFO-BPy followed by metal complexation with a Re metal centre. Reproduced with permission.[102] Copyright 2015, American Chemical Society.

were then non-selectively dispersed in benzonitrile to prepare homogenous dispersions containing both sc-SWNTs and m-SWNTs. Addition of 50 vol % of toluene, a "poor" polymer solvent, resulted in the preferential flocculation of polymer:m-SWNT complexes, with the Zn(II)-containing polymer affording the best removal of m-SWNTs. Subsequently, removal of the adsorbed polymer from the remaining dispersed sc-SWNT complexes was accomplished *via* depolymerization, which occurred upon addition of trifluoroacetic acid (TFA). To investigate the origin of selectivity, molecular mechanics simulations were performed, and it was found that stabilization energies were higher in toluene for the polymer:sc-SWNT complexes relative to the polymer:m-SWNT complexes. In an alternative approach to

a similar goal, Bao and co-workers prepared a fluorene monomer flanked by self-complementary quadruply hydrogen-bonding 2-ureido-6[1*H*]-pyrimidinone (UPy) groups, which allowed the fluorene units to form a supramolecular polymer.[59] It was shown that this polymer selectively dispersed sc-SWNTs, and could depolymerize on-demand to release the enriched sc-SWNT sample *via* addition of TFA, which acted as a hydrogen-bond disruptor. Subsequently, Bao and co-workers prepared imine-containing polyfluorenes, which were used to selectively disperse large-diameter sc-SWNTs.[60] In this case, depolymerization and SWNT release were initiated *via* imine hydrolysis using catalytic TFA.

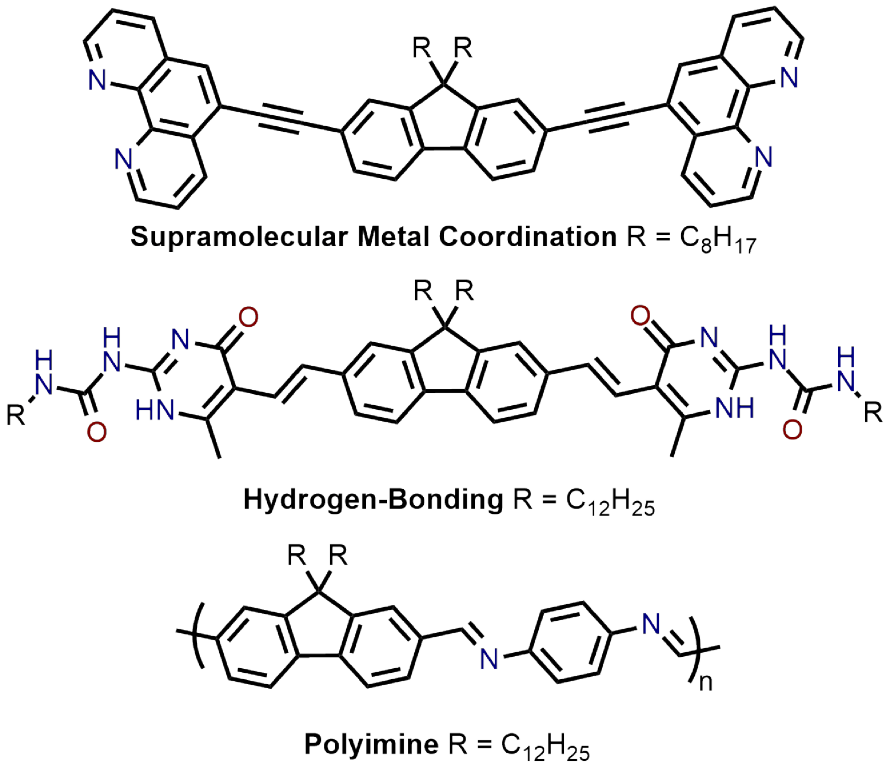


FIGURE 1.6: Chemical structures of monomers used for the enrichment and release of sc-SWNTs, as well as the PDDF-imine derivative. Reproduced with permission.[61] Copyright Royal Society of Chemistry, 2017.

It is apparent that decorating carbon nanotube surfaces without damaging SWNT optoelectronic properties is of substantial interest. Furthermore, the ability to sort specific subsets of SWNTs can be relevant to device performance (e.g., sc-SWNTs for FETs). Thus, the development of a methodology that encompasses the decoration of SWNTs while simultaneously enabling for SWNT subtype sorting/purification and avoiding damage to optoelectronic properties is an unmet and worthy challenge. In this Thesis, I explore the chemistry of polymer-SWNT complexes to decorate the SWNT surface in a facile and reliable manner. Given that conjugated polymer concentrations (and thus the molarity of potential reactive functional groups) are low (10 – 1000 μM) for typical dispersion protocols, the kinetics of coupling chemistry requires examination in order to understand the intricacies of facile decoration of SWNT surfaces.

1.2 Reaction Kinetics

The intention of this section is to give the reader a general sense of what reaction parameters matter for a reaction to go to completion, rather than to provide an in-depth mathematical treatment of reaction kinetics. The author refers the reader to the excellent textbook by Anslyn and Dougherty for detailed information.[103] The study of kinetics examines the timescale for the transformation of reactant into product. The underlying tenet of kinetics is that an energetic barrier must be overcome for a given transformation to occur. During this transformation, the reactant must go through a high energy transition state before proceeding to an intermediate or product. The energy difference between the reactant and transition state is known as the activation energy barrier, or E_a, and dictates the

reaction rate. In a multistep reaction, the step with the highest E_a is referred to as the rate-determining step (RDS). The onset of reactant transformation is due to a molecular collision, wherein the collision provides energy to distort the shape of the reactant into that of the transition state. Within a reaction, any chemical structures that exist for longer than a typical bond vibration (10 to 100 femtoseconds) are called intermediates. To have any influence on the reaction rate, k, the E_a of the RDS must be decreased. The factors influencing reaction rate can be summarized with the Arrhenius rate law:

$$k = Ae^{\frac{-E_a}{RT}} \tag{1.1}$$

Where A and R are constants and T is the temperature in Kelvin. From this equation, it is apparent that the reaction rate scales non-linearly with temperature. Higher kinetic energy of the reactants in solution will increase the overall energy available to overcome the E_a, while also simultaneously increasing the frequency of molecular collisions. The first helpful fact to remember is that the reaction rate roughly doubles for every 10 °C (i.e., going from room temperature to 40 °C would increase the reaction rate by ∼4-fold).

1.2.1 Reaction Order and Half-Lives

The order of a reaction indicates the dependence of reaction rate on the concentration of a given reagent. For the types of reactions typically observed under dilute conditions (as in the case with SWNT functionalization), second-order reactions that are bimolecular (i.e., a first-order dependence on reactants A and B) are the most common and will be the focus here. In general, a second-order reaction rate

can be described using the following equation:

$$rate = k_2[A][B] \tag{1.2}$$

Where k_2 is the second-order rate constant and [A], [B] are the concentrations of reactants A and B, respectively. An important figure to keep in mind is that decreasing the solvent volume two-fold will increase the overall rate 4-fold, as [A] and [B] will both double. In general, the factor by which solvent volume is decreased will increase the reaction rate by the square of that factor (i.e., 10-fold decrease in solvent volume would result in a 100-fold increase in reaction rate). In a case where one reactant is more precious (or difficult to synthesize) than the other, increasing the number of equivalents of the non-precious reactant will increase the reaction rate accordingly (i.e., increasing equivalents from 1 to 10 will increase the reaction rate 10-fold). This is, of course, suboptimal, as the excess equivalents of this reagent will add to reaction waste. To compare reaction rates under various conditions the half-life of a reaction, $t_{1/2}$, can be used. For second-order reactions, $t_{1/2}$ can be calculated as:

$$t_{1/2} = \frac{1}{k_2 \times [A]_0} \tag{1.3}$$

Where $[A]_0$ is the initial concentration of reactant A. It should be noted that this equation only holds true if $[A]_0 = [B]_0$, and that in cases where $[A]_0 \neq [B]_0$, the mathematics become significantly more complicated and will not be discussed here.[103] The number of half-lives required for a specific reaction conversion ($0 \leq \rho \leq 1$) can be described as:

$$\rho = 1 - \frac{1}{2^n} \tag{1.4}$$

Where n is the number of half-lives. This equation can then be rearranged to:

$$n = log_2(\frac{1}{1-\rho}) \tag{1.5}$$

As shown in Figure 1.7, conversion can be plotted against the number of elapsed half-lives, and between 3 and 5 half-lives afford reaction conversions between 88% and 97%, respectively. It should be noted that for second-order reactions, $t_{1/2}$ doubles each half-life. For example, if $t_{1/2}$ was initially 100 s for 50% conversion, it would take 200 s to reach the second half-life for 75% conversion. This can be summarized below:

$$t_{total} = \sum_{i=1}^{n} 2^{n-1} \times t_{1/2} \tag{1.6}$$

Thus, for 97% conversion (5 half-lives), a reaction that has $t_{1/2}$ = 60 s (1 min) would require 31 min overall, while a reaction that has $t_{1/2}$ = 600 s (10 min) would require 5.2 h overall. An interesting cutoff to keep in mind is that at $t_{1/2}$ = 2700 s (45 min), a reaction would require almost a full day (∼23 h) to reach 97% conversion. In other words, if it is desired that a reaction that goes to completion within a single day, $t_{1/2} \leq$ 45 min can be used as a quick heuristic to identify the feasibility of using specific coupling partners that undergo second-order kinetics.

In Figure 1.8, the author has prepared several simulations and plotted the conversion (%) vs time (h) using Python. As shown in Figure 1.8a, if initial substrate concentrations are 100 μM, a k_2 of around 10 $M^{-1} \cdot s^{-1}$ is desirable for full conversion within a day. The $t_{1/2}$, which is indicated by the intersection of the simulated curve with the horizontal black dashed line, is a useful indicator of reaction feasibility (recall that $t_{1/2} \leq$ 45 min is a critical threshold). In Figure 1.8b, simulations are shown where k_2 is held constant at 1 $M^{-1} \cdot s^{-1}$ while [A] and

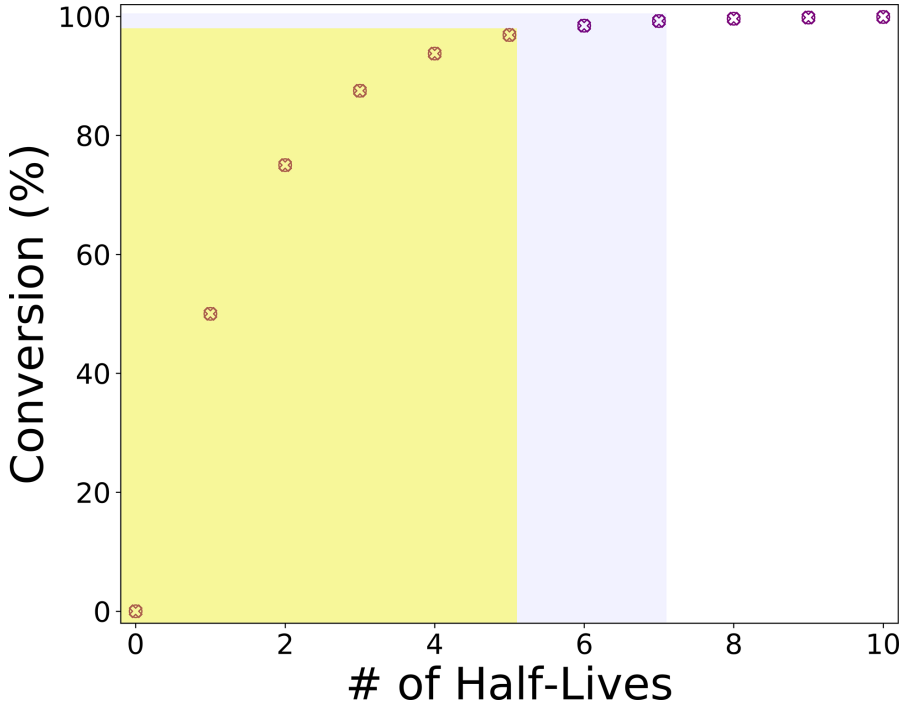


FIGURE 1.7: Plot showing reaction conversion vs number of elapsed half-lives. The shaded yellow region indicates 97% conversion while the shaded blue region indicates 99% conversion.

[B] is varied from 10 μM to 100 mM. At this value of k_2, substrate concentrations of $\geq$ 1 mM will afford full conversion within 24 h. Given these values, the urgency for rapid kinetics under dilute conditions (i.e., "click" chemistry) is apparent.

1.3 Click Chemistry

Synthetic organic chemistry can be broadly divided into several major research areas: (i) the development of novel enantioselective or enantiospecific processes; (ii) the development of novel bond formation processes that enable unrealized bond disconnections; (iii) the improvement upon existing processes with respect to user friendliness, reaction yield and control, byproduct waste, etc.; and (iv) the rapid

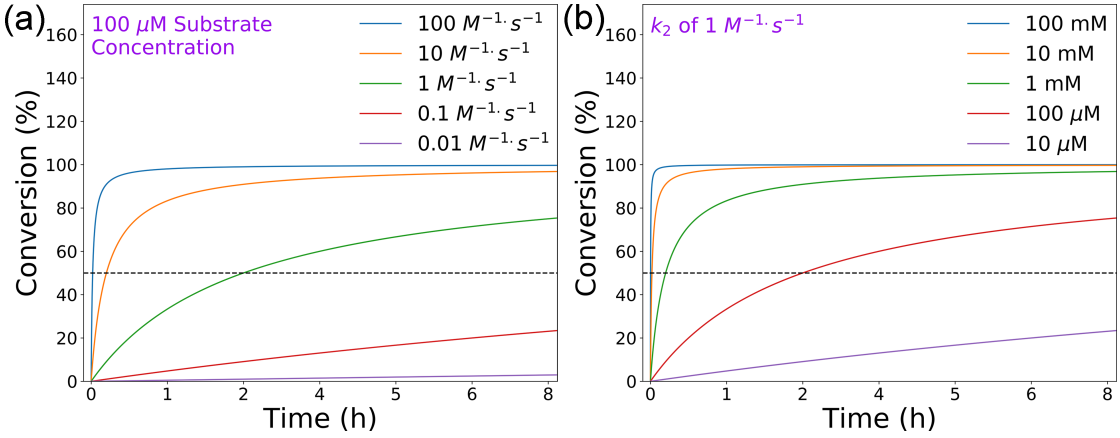


FIGURE 1.8: Second-order reaction simulations plotting reaction conversion (%) vs time (h). (a) Reaction conversion at 100 μM reactant concentrations for both reagents A and B at various k_2 values (0.01 to 100 $M^{-1} \cdot s^{-1}$), and (b) reaction conversion for $k_2 = 1$ $M^{-1} \cdot s^{-1}$ at various concentrations of substrate (10 μM to 100 mM). The horizontal black dashed lines indicate 50% conversion (i.e., the point of intersection with each simulated curve indicates the reaction half-life, $t_{1/2}$).

and efficient linkage of two or more molecular fragments that, together, give rise to a new molecular entity with properties that take advantage of the individual properties of the starting materials. The terminology of "click chemistry", to which the last point refers, was first coined in 2001 by Prof. Barry Sharpless,[104] who is a recipient of the Nobel Prize for his work on asymmetric oxidation reactions. In his seminal paper, Sharpless argues that chemistry should be modular, broad in scope, high yielding, and produce simple byproducts (if any at all) that can be removed non-chromatographically. In his argument for click chemistry, Sharpless envisioned a pharmaceutical application of modular chemistry such that large and diverse molecular libraries could be rapidly stitched together for drug candidate screening. Since then, the interpretation of click chemistry has evolved to encompass both small molecule and polymer functionalization. The spirit of click chemistry encompasses reactions that are fast under dilute conditions (i.e., they occur under ambient conditions with millimolar or sub-millimolar substrate

concentrations on a reasonable timescale). Otherwise, many reactions could be considered fast (and thus "click") if concentrated to the high millimolar or molar concentration regime. If k_2 is not provided (and is not at least $\geq 0.1\ M^{-1} \cdot s^{-1}$), it is difficult to fairly judge whether the reaction is truly fast or not. A brief overview of various click chemistries and their respective rate constants is recorded in Table 1.1 at the end of this Chapter.

1.3.1 Copper-Catalyzed Azide-Alkyne Cycloaddition

In 2002, the groups of Meldal[105] and Sharpless[106] concurrently reported the Copper-Catalyzed Azide-Alkyne Cycloaddition (CuAAC) in organic and aqueous solution, respectively, which is a reaction practically synonymous with the concept of click chemistry. The reaction mechanism occurs *via* a dinuclear Cu(I) complex.[107] As shown in Figure 1.9, the first Cu(I) centre coordinates to the terminal alkyne in a Lewis acidic manner (π-bound), followed by alkyne deprotonation and formation of a copper acetylide with the second Cu(I) centre (σ-bound). The π-bound Cu(I) centre reversibly coordinates with an organic azide, initiating nucleophilic attack of the alkyne to the N-3 of the azide. Lastly, ring annulation generates the triazole ring. The reaction rate is highly dependent on the [Cu(I)] and the identity of the amine ligand. Based on ligand screening studies, it was found that weak donor ligands (e.g., triazole-rich ligands) were ideal under dilute conditions ($< 250\ \mu$M substrate), while strong donor ligands (e.g., pyridine-based or benzimidazole ligands) were ideal under relatively concentrated conditions (> 10 mM substrate).[108]

Since then, click chemistry has been heavily adopted by both the materials science community for the preparation of novel polymeric constructs as well as by

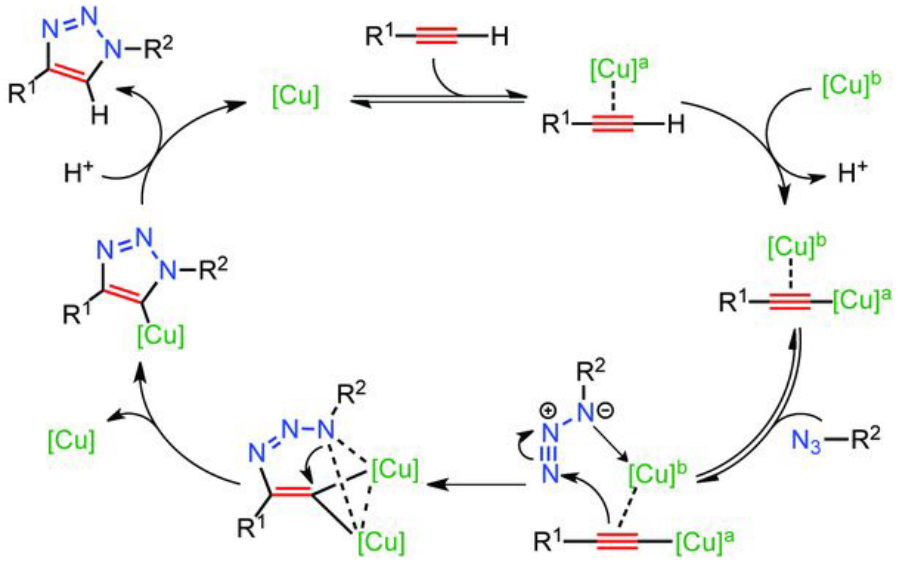


FIGURE 1.9: Proposed mechanism for CuAAC. (a) Reprinted with permission.[107] Copyright American Association for the Advancement of Science, 2013.

the chemical biology community to produce molecular hybrids to study biological systems. With emphasis on the applications in chemical biology, click chemistry's definition has shifted over the past decade to include reactions that encompass the following traits: (i) bio-orthogonality, or the ability for a reaction to occur in the presence of various biologically relevant nucleophiles and electrophiles; (ii) fast reaction rates under very dilute conditions ($<$ 10 mM); (iii) catalyst- and additive-free, perhaps with reaction control using an external stimulus; (iv) reaction compatibility with living organisms (cells, animals, etc.); and (v) ease of purification (or, ideally, no purification or byproduct removal at all). Given these restrictions, and especially given the desire in the materials science community to have the ability to explore biological applications, the field of click chemistry has grown and continued the search for selective and fast reactions having idealized reaction properties and ease of coupling partner synthesis. Given the ease of synthesizing the terminal alkynes and alkyl or aryl azides used in CuAAC, it

would be an ideal bioorthogonal click reaction as it possesses selectivity, fast reactivity, and facile chemical syntheses of the coupling partners. However, Cu is cytotoxic, and [Cu] $\geq$ 1 mM results in substantial cell death.[109] To some extent, low concentrations of Cu ($<$ 500 μM) can allow for some cell survival (for example, mammalian cells can survive for $\sim$1 h when [Cu] $<$ 500 μM), but a tradeoff occurs between cell viability and reaction rate once concentrations of Cu are too low. The toxicity of Cu(I) *in vivo* can be somewhat ameliorated by using tailored water-soluble Cu(I) tris(triazolylmethyl)amine ligands (Figure 1.10).[110] These ligands protect the Cu(I) centres from being released and generating reactive oxygen species, which are thought to bring about the cytotoxicity associated with Cu(I) species.[111] Interestingly, this Cu(I)-ligand system was able to perform CuAAC in developing zebra fish embryos at [Cu] of 25-75 μM, enabling for both a drastic rate enhancement (reaction coupling in $<$ 15 min) as well as the complete development of $>$ 90% of the zebrafish embryos tested.[110] Though impressive, avoidance of Cu in the materials science applications is sometimes desirable, particularly if extensive biological applications are desired downstream.

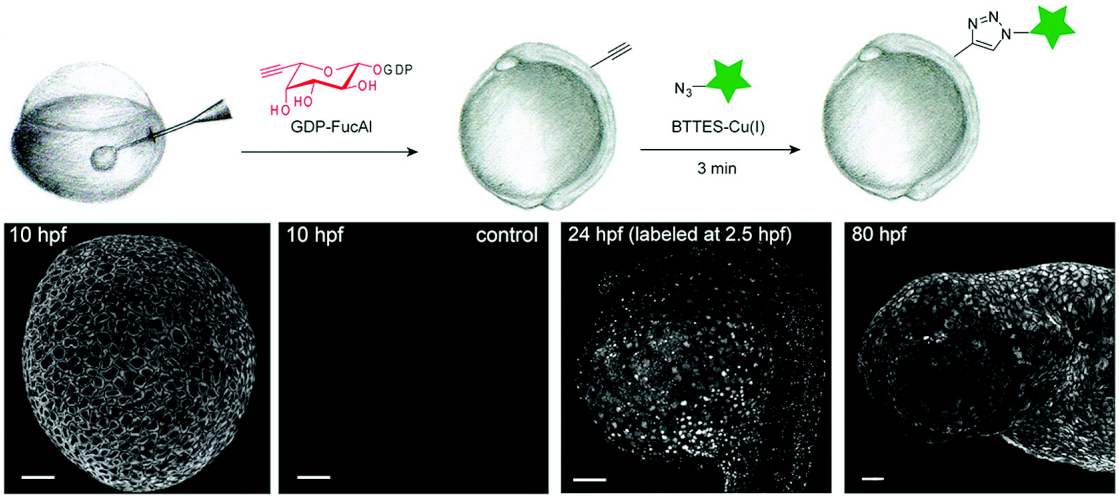


FIGURE 1.10: *In vivo* imaging during early zebrafish embryogenesis with fucosylated glycans containing guanine diphosphate fucose (GDP-fuc) with (GDP-fucAl) or without (control) alkyne functionalization. Embryos were dechorionated and reacted with Alexa Fluor 488-N_3 at 2.5 or 10 h post-fertilization (hpf) using CuAAC. Reproduced with permission.[110] Copyright American Chemical Society, 2010.

1.3.2 Initial Exploration Beyond CuAAC

In an effort to avoid metal contaminants, Bertozzi and co-workers reported the Strain-Promoted [3+2] Azide-Alkyne Cycloaddition (SPAAC) in 2004.[112] This pioneering bioorthogonal reaction utilizes a strained cyclooctyne to increase the alkyne reactivity by inducing extreme bond strain from ideality (R-C≡C-R' bond angle of ∼160°) to enable room temperature coupling to an azide without requiring any metal catalyst or byproduct removal. As shown in Figure 1.11, it is interesting to note that in the initial publication by Bertozzi and co-workers in 2004, the strained cyclooctyne derivative did not have an especially fast rate constant ($\sim 10^{-3}$ $M^{-1} \cdot s^{-1}$). Instead, the concept was compelling enough to warrant further investigation until derivatives with faster rate constants ($\sim 10^{-1}$ $M^{-1} \cdot s^{-1}$) were identified, with the biggest rate increases being due to the incorporation

of additional sp^2-hybridized carbon atoms (i.e., pendant aromatic rings) to further increase the alkyne strain. Other 1,3-dipoles such as nitrones have been employed with strained cyclooctynes (Strain-Promoted Alkyne-Nitrone Cycloaddition, or SPANC) for marginal improvements in reaction rate.[113–116] Although this reaction is ideal in terms of reactivity and ease of purification, synthesis of strained cyclooctyne derivatives is notoriously difficult. To some extent this issue has been addressed by the optimization of the strained cyclooctyne synthetic procedure,[117] but difficulties remain in isolating and purifying the synthetic intermediates. Indeed, the difficulties in synthesis are highlighted by the steep prices from commercial suppliers (e.g., from Sigma-Aldrich simple strained cyclooctyne derivatives are as expensive as $3-5 CAD/mg as of March 2019). Consequently, the search for alternative click chemistry coupling partners has continued.[118] Couplings involving azides and phosphines have been independently reported by the groups of Bertozzi[119] and Raines,[120] utilizing the Staudinger ligation to prepare an amide moiety. A follow-up report by Bertozzi and co-workers utilized a "traceless" Staudinger ligation that avoided the need for distal protecting groups.[121] Although these reactions are sufficiently docile in biological systems, they suffer from both slow reactivity and phosphine oxidation issues.

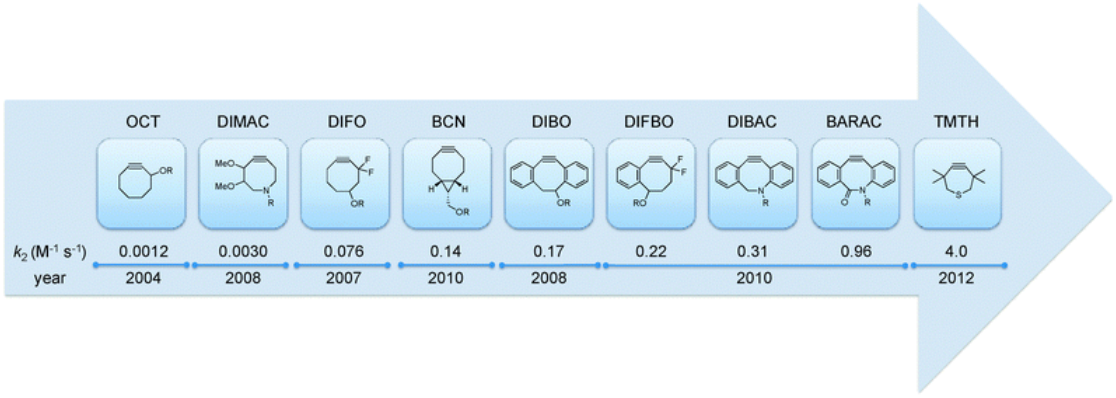


FIGURE 1.11: Second-order rate constants of various strained cyclooctyne derivatives with benzyl azide. Reproduced with permission.[112] Copyright Royal Society of Chemistry, 2013.

1.3.3 Carbonyl Chemistry

Carbonyl condensation chemistries (commonly termed as oxime[122] or hydrazide[123] ligation for the final functional groups produced), are ideal with respect to producing only water as a byproduct. Given the inherent reversibility of this chemistry, hydrolysis rates can vary substantially depending on pH, with oximes being generally more hydrolytically stable than hydrazides.[124] As the first step in the reverse (hydrolytic) reaction is protonation of the imine nitrogen atom, any modifications to the pendant X group that decrease basicity of this nitrogen atom (e.g., a more electronegative pendant atom) will improve bond stability. An ingenious workaround to the lability of carbonyl condensation chemistry was the utilization of Pictet-Spengler ligation by Bertozzi and co-workers,[125] whereby intramolecular attack by a pendant indole post-oxime formation resulted in the formation of a cyclic alkylamine derivative that was more hydrolytically stable (Figure 1.12). Depending on the application, this reversibility can be seen both positively and negatively, as bond lability enables for features like controlled-release of biomolecules

but may be suboptimal in cases where long-term bond stability is desirable. Compared to amines, alkoxyamine and hydrazine moieties are more reactive toward carbonyl electrophiles due to the α-effect,[126,127] which is a phenomenon that originates from the adjacent heteroatom lone pair. The pendant electron density (i) destabilizes the ground state of the nucleophile due to lone pair repulsion; (ii) stabilizes the transition state due to the donation of electron density to the positively charged carbonyl centre; and (iii) impedes the formation of a solvation sphere around the nucleophile that can reduce nucleophilicity. Reactions are often catalyzed with aniline[128,129] or alkyl amine[130] derivatives. Recent advances include the addition of pendant functional groups to accelerate the catalyst-free reaction rate *via* pendant pyridyl or carboxylic acid moieties,[131] as well as boronic acids.[132–134]

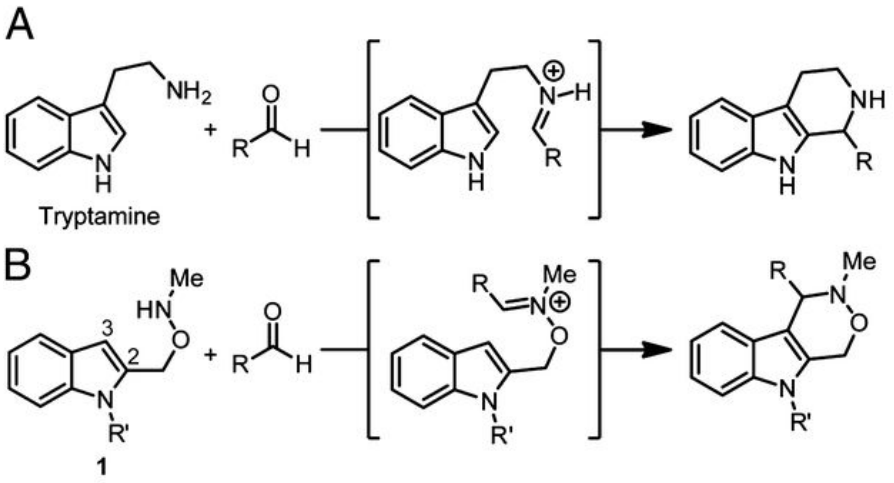


FIGURE 1.12: Pictet-Spengler ligation used by Bertozzi and co-workers. (a) Cannonical Pictet-Spengler reaction between an indole with pendant alkylamine and an aldehyde. (b) Proposed Pictet-Spengler ligation. Reproduced with permission.[125] Copyright Proceedings of the National Academy of Sciences of the United States of America, 2013.

1.3.4 Inverse-Electron Demand Diels-Alder Cycloaddition

Of the available click chemistries, the Inverse-Electron Demand Diels-Alder Cycloaddition (IEDDA) holds the record for fastest reaction kinetics,[118] with a k_2 of up to 10^6 $M^{-1} \cdot s^{-1}$. To put that reaction rate in perspective, the $t_{1/2}$ for substrate concentrations of 10^{-9} M (1 nM) would be ~17 min (97% conversion in ~9 h). The canonical Diels-Alder cycloaddition occurs between an electron-poor dienophile and an electron-rich diene. In IEDDA, the electronic nature of the reactants is reversed, whereby an electron-poor diene (typically a 1,2,4,5-tetrazine) reacts with an electron-rich dienophile (Figure 1.13). The reaction kinetics of IEDDA is governed by the energy gap between the HOMO of the dienophile and the LUMO of the diene, where a smaller energy gap results in a faster cycloaddition. Electron-rich substituents raise both the HOMO and LUMO energy levels, while electron-poor substituents do the opposite. In addition to electronic effects, ring strain of the dienophile can also play a substantial role in rate acceleration by increasing the HOMO energy level. Using this principle, the fastest reaction to date was achieved by imparting extreme ring strain using *trans*-cyclooctenes (TCOs),[135] which are the smallest cyclic *trans*-alkenes that are stable enough to be isolated. Other strained alkenes like norbornene have been employed,[136] although it should be warned that the electronic nature of the tetrazine derivative is extremely important for this coupling to be considered click chemistry (i.e., tetrazines with electron-rich substituents have diminished or no reactivity with norbornene). Interestingly, the stereochemistry of the strained alkene derivative has a substantial impact on reactivity, with *axial*-TCO being ~4x more reactive than *equatorial*-TCO,[137] while *exo*-norbornene reacts ~3x faster than *endo*-norbornene.[138] IEDDA is generally quite sensitive to steric effects, and for dienophiles a sterically bulky electron-rich

substituent can cancel out the rate boosting effect of an increased HOMO energy level.[139] For the tetrazine component, even the substitution of a methyl group in place of a proton at the 6-position can result in a ∼30-fold decrease in reactivity (for both steric and electronic reasons).[140] Lastly, solvent hydrogen bonding with the tetrazine moiety can induce polarity and decrease the diene LUMO energy level, increasing the rate of reaction by as much as 10- to 100-fold.[141] In the case of water, a hydrophobic effect can also further contribute to an increased reaction rate.[142]

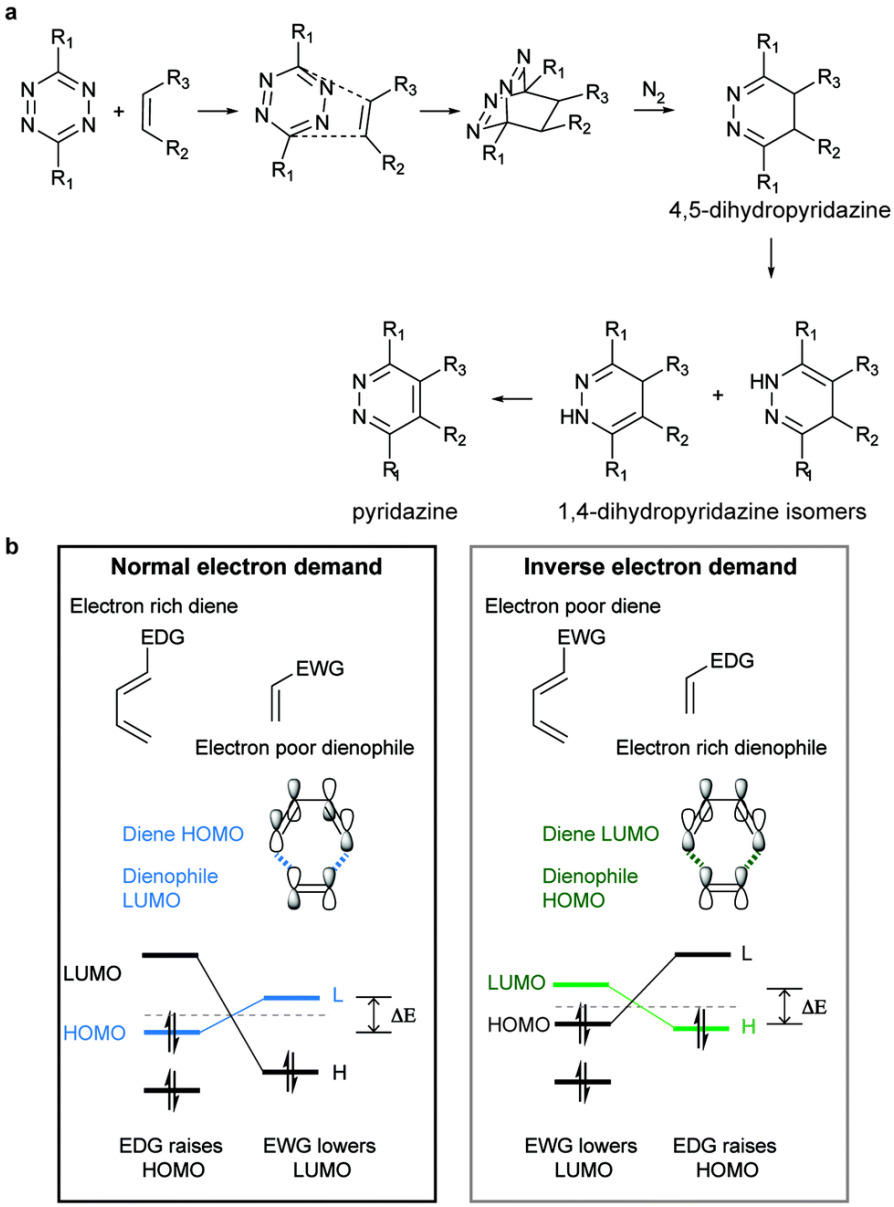


FIGURE 1.13: (a) Mechanism of IEDDA and (b) molecular orbital rationale for reactivity. Reproduced with permission.[118] Copyright Royal Society of Chemistry, 2017.

1.3.5 Light-Controlled Click Chemistry

Beyond fast reactivity, efforts have been made to utilize an external stimulus such as light to trigger click chemistry.[143] Light-triggered reactions offer an interesting

opportunity to couple spatiotemporal control with inherently fast reactions. In several cases, existing click chemistries have been modified to incorporate a photochemical component. For instance, Bowman and co-workers re-tooled CuAAC to be triggered by UV light *via* the formation of radicals followed by the *in situ* reduction of Cu(II).[144] Popik and co-workers have also re-tooled SPAAC to be triggered by UV light (λ_{ex} = 350 nm)[145] or NIR two-photon excitation (λ_{ex} = 800 nm)[146] *via* the use of cyclopropenone, which is a light-sensitive alkyne protecting group. Maynard and co-workers repurposed oxime ligation to unveil an activated aldehyde by photo-deprotection of a tetrahydropyranyl ether using a photoacid generator (λ_{ex} = 365 nm).[147] In terms of distinct photo-click chemistry, Lin and co-workers reported a 1,3-cycloaddition between tetrazole and an electron-deficient alkene, wherein UV light (λ_{ex} = 302 nm) was used to decompose the tetrazole *in situ* to generate a reactive nitrile imine (1,3-dipole) intermediate.[148] Most recently, Zhang and co-workers reported the first example of visible light-mediated photoclick coupling between a 1,10-phenanthrenequinone (PQ) derivative and an electron-rich vinyl ether (Figure 1.14).[149] The reaction proceeds *via* excitation of PQ from the ground state to excited state to generate a biradical, followed by radical addition to the vinyl ether and 1,6-biradical recombination to generate the final product. These additions to the click chemistry repertoire add further synthetic control to the chemist's toolbox, enabling for the spatiotemporally resolved coupling of two molecules, which is an essential feature in complicated systems like biology.

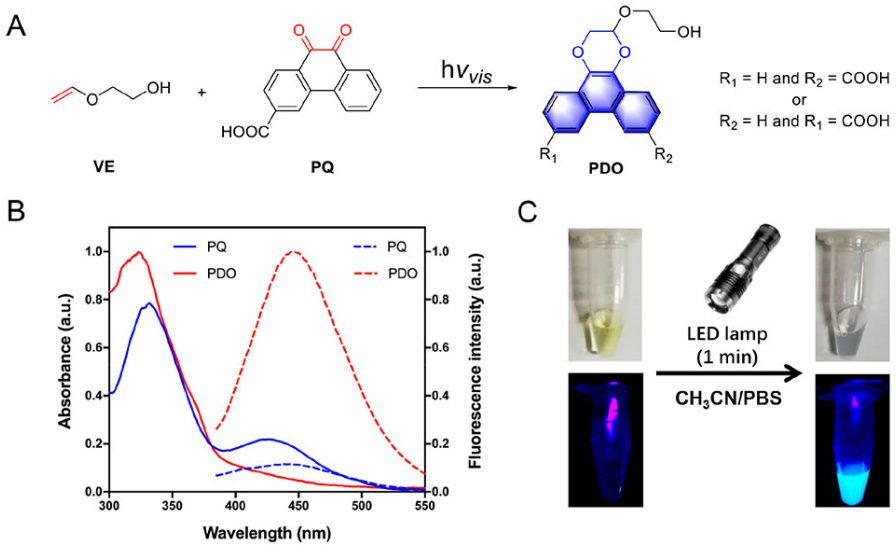


FIGURE 1.14: Visible light-mediated photoclick chemistry. (a) Structures of the vinyl ether (VE) and 9,10-phenanthrenequinone (PQ) coupling partners as well as the product phenanthrodioxine (PDO). (b) Absorption spectra of PQ and PDO. (c) Photographs before and after the click reaction, with the bottom photographs taken while irradiated with a handheld UV lamp at 365 nm. Reproduced with permission.[149] Copyright American Chemical Society, 2018.

Reaction	Catalyst	$k_2(M^{-1} \cdot s^{-1})$
Staudinger Ligation	None	$10^{-4} - 10^{-3}$ (Ref 150)
Carbonyl Condensation	None or Amine	$10^{-4} - 10^{-1}$ (Ref 151)
SPAAC	None	$10^{-3} - 10^{1}$ (Ref 152)
SPANC	Nitrone (*in situ*)	$3 - 60$ (Ref 113)
CuAAC	Cu(I), ± Ligand	$10^{3} - 10^{4}$ (Ref 108)[a]
IEDDA	None	$10^{1} - 10^{6}$ (Ref 137)
Tetrazole-Alkene	$\lambda_{ex} = 290$ nm	11.0 (Ref 148)
PQ-Vinyl Ether	White LEDs	$0.28 - 2.76$ (Ref 149)

TABLE 1.1: Summary of click chemistries and their second-order rate constants (k_2). PBS = phosphate-buffered saline; LED = light-emitting diode. [a]CuAAC rate is highly dependent on [Cu(I)] and ligand identity.

1.4 Summary

SWNTs are nanomaterials that are composed entirely of elemental carbon and possess exceptional physical and optoelectronic properties. The ability to incorporate this nanomaterial in various applications is promising for the production of next-generation devices. In an idealized world, SWNTs would be solution processible, easily purified on an industrial scale, and easily derivatized without perturbation of their properties to tailor SWNT nanocomposite features. In reality, SWNTs are insoluble black powders that are purchased as a complicated mixture of amorphous carbon, metal catalyst particles, and both sc- and m-SWNTs. Furthermore, derivatization of the SWNT sidewall typically results in either detrimental damage to SWNT properties (covalent functionalization) or leaves a limited ability to produce functionalizable SWNT complexes (noncovalent functionalization). These problems, although not insurmountable, have been tackled in a piecemeal fashion thus far. With respect to SWNT purity and dispersibility, efforts have been widespread, but lack scalability outside of conjugated polymer sorting. As for functional SWNT complexes, efforts have been made toward specific conjugates (e.g., AuNP-SWNT conjugates) or have severe limitations (e.g., requiring saturated solutions for functionalization).

In this Thesis, I examine how the structure of a conjugated polymer can be modulated to desired polymer-SWNT complex properties, and demonstrate the versatility of conjugated polymers as SWNT dispersants. In Chapters 2 and 3, I explore the effect of conjugated polymer backbone structure on SWNT sorting. I show that (i) the nature of the conjugated π-system may influence SWNT sorting, and that (ii) complete backbone conjugation is not required to sort sc-SWNTs. In

Chapters 4 to 6, I investigate the incorporation of reactive functional groups in the conjugated polymer side chains to produce latently reactive polymer-SWNT complexes. I develop a system that is capable of simultaneously (i) sorting SWNTs and (ii) decorating the polymer-SWNT surface, while (iii) preserving SWNT optoelectronic properties. Within these Chapters, I show several strategies to functionalize the polymer-SWNT complex in solution phase (both organic and aqueous) and as a polymer-SWNT thin film. Lastly, in Chapter 7 I reveal a conjugated polymer backbone structure that is capable of photoclick coupling chemistry with visible light. This conjugated structure can be rapidly functionalized to alter its photophysical properties, and is the first example of a photopatternable conjugated polymer backbone.

1.5 References

(1) Iijima, S. Mater. *Sci. Eng. B* **1993**, 19, 172–180.

(2) Bethune, D. S.; Kiang, C. H.; de Vries, M. S.; Gorman, G.; Savoy, R.; Vazquez, J.; Beyers, R. *Nature* **1993**, 363, 605–607.

(3) Yu, M.-F.; Files, B. S.; Arepalli, S.; Ruoff, R. S. *Phys. Rev. Lett.* **2000**, 84, 5552–5555.

(4) Terrones, M. *Annu. Rev. Mater. Res.* **2003**, 33, 419–501.

(5) Han, Z.; Fina, A. *Prog. Polym. Sci.* **2011**, 36, 914–944.

(6) Avouris, P.; Chen, Z.; Perebeinos, V. *Nat. Nanotechnol.* **2007**, 2, 605–615.

(7) Avouris, P. *Acc. Chem. Res.* **2002**, 35, 1026–1034.

(8) Collins, P. G.; Avouris, P. *Sci. Am.* **2000**, 283, 62–69.

(9) O'Connell, M. J.; Bachilo, S. M.; Huffman, C. B.; Moore, V. C.; Strano, M. S.;

Haroz, E. H.; Rialon, K. L.; Boul, P. J.; Noon, W. H.; Kittrell, C.; et al. *Science* **2002**, 297, 593–596.

(10) Weisman, R. B.; Bachilo, S. M. *Nano Lett.* **2003**, 3, 1235–1238.

(11) Kataura, H.; Kumazawa, Y.; Maniwa, Y.; Umezu, I.; Suzuki, S.; Ohtsuka, Y.; Achiba, Y. *Synth. Met.* **1999**, 103, 2555–2558.

(12) Zhan, G.-D.; Kuntz, J. D.; Wan, J.; Mukherjee, A. K. *Nat. Mater.* **2003**, 2, 38–42.

(13) Liu, L.; Barber, A. H.; Nuriel, S.; Wagner, H. D. *Adv. Funct. Mater.* **2005**, 15, 975–980.

(14) Coleman, J. N.; Khan, U.; Blau, W. J.; Gun'ko, Y. K. *Carbon* **2006**, 44, 1624–1652.

(15) T. Dürkop; S. A. Getty; Cobas, E.; Fuhrer, M. S. *Nano Lett.* **2003**, 4, 35–39.

(16) Qi, P.; Vermesh, O.; Grecu, M.; Javey, A.; Wang, Q.; Dai, H.; Peng, S.; Cho, K. J. *Nano Lett.* **2003**, 3, 347–351.

(17) Dionisio, M.; Schnorr, J. M.; Michaelis, V. K.; Griffin, R. G.; Swager, T. M.; Dalcanale, E. *J. Am. Chem. Soc.* **2012**, 134, 6540–6543.

(18) Rivas, G. A.; Rubianes, M. D.; Rodríguez, M. C.; Ferreyra, N. F.; Luque, G. L.; Pedano, M. L.; Miscoria, S. A.; Parrado, C. *Talanta* **2007**, 74, 291–307.

(19) Pang, X.; Imin, P.; Zhitomirsky, I.; Adronov, A. *Macromolecules* **2010**, 43, 10376–10381.

(20) Kim, J.-H.; Yee, K.-J.; Lim, Y.-S.; Booshehri, L. G.; Haroz, E. H.; Kono, J. *Adv. Mater.* **2011**, 24, 4977–4994.

(21) Rowell, M. W.; Topinka, M. A.; McGehee, M. D.; Prall, H.-J.; Dennler, G.; Sariciftci, N. S.; Hu, L.; Gruner, G. *Appl. Phys. Lett.* **2006**, 88, 233506.

(22) Bindl, D. J.; Safron, N. S.; Arnold, M. S. *ACS Nano* **2010**, 4, 5657–5664.

(23) Keru, G.; Ndungu, P. G.; Nyamori, V. O. *Int. J. Energy Res.* **2014**, 38, 1635–1653.

(24) Sun, D.-M.; Liu, C.; Ren, W.-C.; Cheng, H.-M. *Small* **2013**, 9, 1188–1205.

(25) Green, A. A.; Hersam, M. C. *Nano Lett.* **2008**, 8, 1417–1422.

(26) Hecht, D. S.; Thomas, D.; Hu, L.; Ladous, C.; Lam, T.; Park, Y.; Irvin, G.; Drzaic, P. *J. Soc. Inf. Disp.* **2009**, 17, 941.

(27) De Volder, M. F. L.; Tawfick, S. H.; Baughman, R. H.; Hart, A. J. *Science* **2013**, 339, 535–539.

(28) Jariwala, D.; Sangwan, V. K.; Lauhon, L. J.; Marks, T. J.; Hersam, M. C. *Chem. Soc. Rev.* **2013**, 42, 2824–2860.

(29) Hong, S.; Myung, S. *Nat. Nanotechnol.* **2007**, 2, 207–208.

(30) Nikolaev, P.; Bronikowski, M. J.; Bradley, R. K.; Rohmund, F.; Colbert, D. T.; Smith, K. .; Smalley, R. E. *Chem. Phys. Lett.* **1999**, 313, 91–97.

(31) Kong, J.; Cassell, A. M.; Dai, H. *Chem. Phys. Lett.* **1998**, 292, 567–574.

(32) Bernier, P.; Journet, C.; Maser, W. K.; Loiseau, A.; de la Chapelle, M. L.; Lefrant, S.; Deniard, P.; Lee, R.; Fischer, J. E. *Nature* **1997**, 388, 756–758.

(33) Guo, T.; Nikolaev, P.; Thess, A.; Colbert, D. T.; Smalley, R. E. *Chem. Phys. Lett.* **1995**, 243, 49–54.

(34) Kim, K. S.; Cota-Sanchez, G.; Kingston, C. T.; Imris, M.; Simard, B.; Soucy, G. *J. Phys. D. Appl. Phys.* **2007**, 40, 2375–2387.

(35) Arnold, M. S.; Stupp, S. I.; Mark C. Hersam. *Nano Lett.* **2005**, 5, 713–718.

(36) Arnold, M. S.; Green, A. A.; Hulvat, J. F.; Stupp, S. I.; Hersam, M. C. *Nat. Nanotechnol.* **2006**, 1, 60–65.

(37) Charlier, J. C. *Acc. Chem. Res.* **2002**, 35, 1063–1069.

(38) Liu, H.; Nishide, D.; Tanaka, T.; Kataura, H.; Mioskowski, C. *Nat. Commun.*

2011, 2, 309.

(39) Tanaka, T.; Jin, H.; Miyata, Y.; Kataura, H. *Appl. Phys. Express* **2008**, 1, 114001.

(40) Khripin, C. Y.; Fagan, J. A.; Zheng, M. *J. Am. Chem. Soc.* **2013**, 135, 6822–6825.

(41) Fagan, J. A.; Khripin, C. Y.; Silvera Batista, C. A.; Simpson, J. R.; Hároz, E. H.; Hight Walker, A. R.; Zheng, M. *Adv. Mater.* **2014**, 26, 2800–2804.

(42) Flavel, B. S.; Kappes, M. M.; Krupke, R.; Hennrich, F. *ACS Nano* **2013**, 7, 3557–3564.

(43) Flavel, B. S.; Moore, K. E.; Pfohl, M.; Kappes, M. M.; Hennrich, F. *ACS Nano* **2014**, 8, 1817–1826.

(44) Zheng, M.; Jagota, A.; Semke, E. D.; Diner, B. A.; McLean, R. S.; Lustig, S. R.; Richardson, R. E.; Tassi, N. G. *Nat. Mater.* **2003**, 2, 338–342.

(45) Tu, X.; Manohar, S.; Jagota, A.; Zheng, M. *Nature* **2009**, 460, 250–253.

(46) Zheng, M.; Semke, E. D. *J. Am. Chem. Soc.* **2007**, 129, 6084–6085.

(47) Ghosh, S.; Bachilo, S. M.; Weisman, R. B. *Nat. Nanotechnol.* **2010**, 5, 443–450.

(48) Tanaka, T.; Jin, H.; Miyata, Y.; Kataura, H. *Appl. Phys. Express* **2008**, 1, 1140011–1140013.

(49) Chen, R. J.; Zhang, Y.; Wang, D.; Dai, H. *J. Am. Chem. Soc.* **2001**, 123, 3838–3839.

(50) Star, A.; Stoddart, J. F.; Steuerman, D.; Diehl, M.; Boukai, A.; Wong, E. W.; Yang, X.; Chung, S.-W.; Choi, H.; Heath, J. R. *Angew. Chemie - Int. Ed.* **2001**, 40, 1721–1725.

(51) David W. Steuerman; Alexander Star; Narizzano, R.; Hyeon Choi; Ryan S.

Ries; Nicolini, C.; Stoddart, J. F.; Heath, J. R. *J. Phys. Chem. B* **2002**, 106, 3124–3130.

(52) Wang, H.; Bao, Z. *Nano Today* **2015**, 10, 737–758.

(53) Samanta, S. K.; Fritsch, M.; Scherf, U.; Gomulya, W.; Bisri, S. Z.; Loi, M. A. *Acc. Chem. Res.* **2014**, 47, 2446–2456.

(54) Lei, T.; Pochorovski, I.; Bao, Z. *Acc. Chem. Res.* **2017**, 50, 1096–1104.

(55) Malenfant, P. R. L.; Cicha, W. V.; Bui, P.-A.; Simone, D. L. US20060045838A1, 2006.

(56) Nish, A.; Hwang, J.-Y.; Doig, J.; Nicholas, R. J. *Nat. Nanotechnol.* **2007**, 2, 640–646.

(57) Brady, G. J.; Joo, Y.; Wu, M.-Y.; Shea, M. J.; Gopalan, P.; Arnold, M. S. *ACS Nano* **2014**, 8, 11614–11621.

(58) Toshimitsu, F.; Nakashima, N. *Nat. Commun.* **2014**, 5, 5041.

(59) Pochorovski, I.; Wang, H.; Feldblyum, J. I.; Zhang, X.; Antaris, A. L.; Bao, Z. *J. Am. Chem. Soc.* **2015**, 137, 4328–4331.

(60) Lei, T.; Chen, X.; Pitner, G.; Wong, H.-S. P.; Bao, Z. *J. Am. Chem. Soc.* **2016**, 138, 802–805.

(61) Fong, D.; Adronov, A. *Chem. Sci.* **2017**, 8, 7292–7305.

(62) Barman, S. N.; LeMieux, M. C.; Baek, J.; Rivera, R.; Bao, Z. *ACS Appl. Mater. Interfaces* **2010**, 2, 2672–2678.

(63) Sun, Z.; O'Connor, I.; Bergin, S. D.; Coleman, J. N. *J. Phys. Chem. C* **2009**, 113, 1260–1266.

(64) Gomulya, W.; Costanzo, G. D.; De Carvalho, E. J. F.; Bisri, S. Z.; Derenskyi, V.; Fritsch, M.; Fröhlich, N.; Allard, S.; Gordiichuk, P.; Herrmann, A.; et al. *Adv. Mater.* **2013**, 25, 2948–2956.

(65) Lee, H. W.; Yoon, Y.; Park, S.; Oh, J. H.; Hong, S.; Liyanage, L. S.; Wang, H.; Morishita, S.; Patil, N.; Park, Y. J.; et al. *Nat. Commun.* **2011**, 2, 541.

(66) Gomulya, W.; Rios, J. M. S.; Derenskyi, V.; Bisri, S. Z.; Jung, S.; Fritsch, M.; Allard, S.; Scherf, U.; Dos Santos, M. C.; Loi, M. A. *Carbon* **2015**, 84, 66–73.

(67) Ding, J.; Li, Z.; Lefebvre, J.; Cheng, F.; Dubey, G.; Zou, S.; Finnie, P.; Hrdina, A.; Scoles, L.; Lopinski, G. P.; et al. *Nanoscale* **2014**, 6, 2328–2339.

(68) Rice, N. A.; Subrahmanyam, A. V.; Laengert, S. E.; Adronov, A. *J. Polym. Sci. Part A Polym. Chem.* **2015**, 53, 2510–2516.

(69) Jakubka, F.; Schießl, S. P.; Martin, S.; Englert, J. M.; Hauke, F.; Hirsch, A.; Zaumseil, J. *ACS Macro Lett.* **2012**, 1, 815–819.

(70) Lei, T.; Lai, Y. C.; Hong, G.; Wang, H.; Hayoz, P.; Weitz, R. T.; Chen, C.; Dai, H.; Bao, Z. *Small* **2015**, 11, 2946–2954.

(71) Qian, L.; Xu, W.; Fan, X.; Wang, C.; Zhang, J.; Zhao, J.; Cui, Z. *J. Phys. Chem. C* **2013**, 117, 18243–18250.

(72) Wang, H.; Hsieh, B.; Jiménez-Osés, G.; Liu, P.; Tassone, C. J.; Diao, Y.; Lei, T.; Houk, K. N.; Bao, Z. *Small* **2014**, 1–8.

(73) Rice, N. A.; Adronov, A. *Macromolecules* **2013**, 46, 3850–3860.

(74) Rice, N. A.; Adronov, A. *J. Polym. Sci. Part A Polym. Chem.* **2014**, 52, 2738–2747.

(75) Fong, D.; Bodnaryk, W. J.; Rice, N. A.; Saem, S.; Moran-Mirabal, J. M.; Adronov, A. *Chem. - A Eur. J.* **2016**, 22, 14560–14566.

(76) Prato, M.; Kostarelos, K.; Bianco, A. *Acc. Chem. Res.* **2008**, 41, 60–68.

(77) Liu, Z.; Chen, K.; Davis, C.; Sherlock, S.; Cao, Q.; Chen, X.; Dai, H. *Cancer Res.* **2008**, 68, 6652–6660.

(78) Bianco, A.; Kostarelos, K.; Prato, M. *Curr. Opin. Chem. Biol.* **2005**, 9,

674–679.

(79) Kam, N. W. S.; Jessop, T. C.; Wender, P. A.; Dai, H. *J. Am. Chem. Soc.* **2004**, 126, 6850–6851.

(80) Liu, Z.; Winters, M.; Holodniy, M.; Dai, H. *Angew. Chemie - Int. Ed.* **2007**, 46, 2023–2027.

(81) Asuri, P.; Karajanagi, S. S.; Sellitto, E.; Kim, D. Y.; Kane, R. S.; Dordick, J. S. *Biotechnol. Bioeng.* **2006**, 95, 804–811.

(82) Ramasamy, R. P.; Luckarift, H. R.; Ivnitski, D. M.; Atanassov, P. B.; Johnson, G. R. *Chem. Commun.* **2010**, 46, 6045–6047.

(83) Yim, T. J.; Liu, J.; Lu, Y.; Kane, R. S.; Dordick, J. S. *J. Am. Chem. Soc.* **2005**, 127, 12200–12201.

(84) Liu, Z.; Tabakman, S.; Welsher, K.; Dai, H. *Nano Res.* **2009**, 2, 85–120.

(85) Kostarelos, K.; Bianco, A.; Prato, M. *Nat. Nanotechnol.* **2009**, 4, 627–633.

(86) De La Zerda, A.; Zavaleta, C.; Keren, S.; Vaithilingam, S.; Bodapati, S.; Liu, Z.; Levi, J.; Smith, B. R.; Ma, T. J.; Oralkan, O.; et al. *Nat. Nanotechnol.* **2008**, 3, 557–562.

(87) Lacerda, L.; Soundararajan, A.; Singh, R.; Pastorin, G.; Al-Jamal, K. T.; Turton, J.; Frederik, P.; Herrero, M. A.; Li, S.; Bao, A.; et al. *Adv. Mater.* **2008**, 20, 225–230.

(88) Harrison, B. S.; Atala, A. *Biomaterials* **2007**, 28, 344–353.

(89) Lin, S.; Schroeder, V.; Swager, T. M.; Savagatrup, S.; He, M. *Chem. Rev.* **2018**, 119, 599–663.

(90) Hirsch, A. *Angew. Chemie - Int. Ed.* **2002**, 41, 1853–1859.

(91) Britz, D. A.; Khlobystov, A. N. *Chem. Soc. Rev.* **2006**, 35, 637–659.

(92) Campidelli, S.; Klumpp, C.; Bianco, A.; Guldi, D. M.; Prato, M. *J. Phys.*

Org. Chem. **2006**, 19, 531–539.

(93) Wang, F.; Swager, T. M. *J. Am. Chem. Soc.* **2011**, 133, 11181–11193.

(94) Setaro, A.; Adeli, M.; Glaeske, M.; Przyrembel, D.; Bisswanger, T.; Gordeev, G.; Maschietto, F.; Faghani, A.; Paulus, B.; Weinelt, M.; et al. *Nat. Commun.* **2017**, 8, 14281.

(95) Zhao, Y. L.; Stoddart, J. F. *Acc. Chem. Res.* **2009**, 42, 1161–1171.

(96) Bilalis, P.; Katsigiannopoulos, D.; Avgeropoulos, A.; Sakellariou, G. *RSC Adv.* **2014**, 4, 2911–2934.

(97) Gavrel, G.; Jousselme, B.; Filoramo, A.; Campidelli, S. *Top. Curr. Chem.* **2014**, 348, 95–126.

(98) Ishihara, S.; O'Kelly, C. J.; Tanaka, T.; Kataura, H.; Labuta, J.; Shingaya, Y.; Nakayama, T.; Ohsawa, T.; Nakanishi, T.; Swager, T. M. *ACS Appl. Mater. Interfaces* **2017**, 9, 38062–38067.

(99) Ozawa, H.; Ide, N.; Fujigaya, T.; Niidome, Y.; Nakashima, N. *Chem. - A Eur. J.* **2011**, 17, 13438–13444.

(100) Ozawa, H.; Yi, X.; Fujigaya, T.; Niidome, Y.; Asano, T.; Nakashima, N. *J. Am. Chem. Soc.* **2011**, 133, 14771–14777.

(101) Nagai, Y.; Tsutsumi, Y.; Nakashima, N.; Fujigaya, T. *J. Am. Chem. Soc.* **2018**, 140, 8544–8550.

(102) Joo, Y.; Brady, G. J.; Shea, M. J.; Oviedo, M. B.; Kanimozhi, C.; Schmitt, S. K.; Wong, B. M.; Arnold, M. S.; Gopalan, P. *ACS Nano* **2015**, 9, 10203–10213.

(103) Anslyn, E. V.; Dougherty, D. A. *Modern Physical Organic Chemistry.* In *Modern Physical Organic Chemistry*; **2006**.

(104) Kolb, H. C.; Finn, M. G.; Sharpless, K. B. *Angew. Chemie - Int. Ed.* **2001**, 40, 2004–2021.

(105) Tornøe, C. W.; Christensen, C.; Meldal, M. *J. Org. Chem.* **2002**, 67, 3057–3064.

(106) Rostovtsev, V. V.; Green, L. G.; Fokin, V. V.; Sharpless, K. B. *Angew. Chemie - Int. Ed.* **2002**, 41, 2596–2599.

(107) Worrell, B. T.; Malik, J. A.; Fokin, V. V. *Science* **2013**, 340, 457–460.

(108) Presolski, S. I.; Hong, V.; Cho, S. H.; Finn, M. G. *J. Am. Chem. Soc.* **2010**, 132, 14570–14576.

(109) Sletten, E. M.; Bertozzi, C. R. *Angew. Chemie - Int. Ed.* **2009**, 48, 6974–6998.

(110) Soriano Del Amo, D.; Wang, W.; Jiang, H.; Besanceney, C.; Yan, A. C.; Levy, M.; Liu, Y.; Marlow, F. L.; Wu, P. *J. Am. Chem. Soc.* **2010**, 132, 16893–16899.

(111) Gaetke, L. M.; Chow, C. K. *Toxicology* **2003**, 189, 147–163.

(112) Ramil, C. P.; Lin, Q. *Chem. Commun.* **2013**, 49, 11007–11022.

(113) McKay, C. S.; Chigrinova, M.; Blake, J. A.; Pezacki, J. P. *Org. Biomol. Chem.* **2012**, 10, 3066–3070.

(114) Ning, X.; Temming, R. P.; Dommerholt, J.; Guo, J.; Ania, D. B.; Debets, M. F.; Wolfert, M. A.; Boons, G.-J.; van Delft, F. L. *Angew. Chemie - Int. Ed.* **2010**, 49, 3065–3068.

(115) McKay, C. S.; Blake, J. A.; Cheng, J.; Danielson, D. C.; Pezacki, J. P. *Chem. Commun.* **2011**, 47, 10040–10042.

(116) Sanders, B. C.; Friscourt, F.; Ledin, P. A.; Mbua, N. E.; Arumugam, S.; Guo, J.; Boltje, T. J.; Popik, V. V.; Boons, G. J. *J. Am. Chem. Soc.* **2011**, 133, 949–957.

(117) Chadwick, R. C.; Van Gyzen, S.; Liogier, S.; Adronov, A. *Synth.* **2014**, 46, 669–677.

(118) Oliveira, B. L.; Guo, Z.; Bernardes, G. J. L. *Chem. Soc. Rev.* **2017**, 46, 4895–4950.

(119) Saxon, E.; Bertozzi, C. R. *Science* **2000**, 287, 2007–2010.

(120) Nilsson, B. L.; Kiessling, L. L.; Raines, R. T. *Org. Lett.* **2000**, 2, 1939–1941.

(121) Saxon, E.; Armstrong, J. I.; Bertozzi, C. R. *Org. Lett.* **2000**, 2, 2141–2143.

(122) Axup, J. Y.; Bajjuri, K. M.; Ritland, M.; Hutchins, B. M.; Kim, C. H.; Kazane, S. A.; Halder, R.; Forsyth, J. S.; Santidrian, A. F.; Stafin, K.; et al. *Proc. Natl. Acad. Sci.* **2012**, 109, 16101–16106.

(123) Kölmel, D. K.; Kool, E. T. *Chem. Rev.* **2017**, 117, 10358–10376.

(124) Kalia, J.; Raines, R. T. *Angew. Chemie - Int. Ed.* **2008**, 47, 7523–7526.

(125) Agarwal, P.; van der Weijden, J.; Sletten, E. M.; Rabuka, D.; Bertozzi, C. R. *Proc. Natl. Acad. Sci.* **2013**, 110, 46–51.

(126) Fina, N. J.; Edwards, J. O. *Int. J. Chem. Kinet.* **1973**, 5, 1–26.

(127) Ren, Y.; Yamataka, H. *Org. Lett.* **2006**, 8, 119–121.

(128) Crisalli, P.; Kool, E. T. *Org. Lett.* **2013**, 15, 1646–1649.

(129) Crisalli, P.; Kool, E. T. *J. Org. Chem.* **2013**, 78, 1184–1189.

(130) Larsen, D.; Pittelkow, M.; Karmakar, S.; Kool, E. T. *Org. Lett.* **2015**, 17, 274–277.

(131) Kool, E. T.; Park, D. H.; Crisalli, P. *J. Am. Chem. Soc.* **2013**, 135, 17663–17666.

(132) Stress, C. J.; Schmidt, P. J.; Gillingham, D. G. *Org. Biomol. Chem.* **2016**, 14, 5529–5533.

(133) Cal, P. M. S. D.; Vicente, J. B.; Pires, E.; Coelho, A. V.; Veiros, L. F.; Cordeiro, C.; Gois, P. M. P. *J. Am. Chem. Soc.* **2012**, 134, 10299–10305.

(134) Schmidt, P.; Stress, C.; Gillingham, D. *Chem. Sci.* **2015**, 6, 3329–3333.

(135) Devaraj, N. K.; Upadhyay, R.; Haun, J. B.; Hilderbrand, S. A.; Weissleder, R. *Angew. Chemie - Int. Ed.* **2009**, 48, 7013–7016.

(136) Han, H. S.; Devaraj, N. K.; Lee, J.; Hilderbrand, S. A.; Weissleder, R.; Bawendi, M. G. *J. Am. Chem. Soc.* **2010**, 132, 7838–7839.

(137) Darko, A.; Wallace, S.; Dmitrenko, O.; Machovina, M. M.; Mehl, R. A.; Chin, J. W.; Fox, J. M. *Chem. Sci.* **2014**, 5, 3770–3776.

(138) Vrabel, M.; Kölle, P.; Brunner, K. M.; Gattner, M. J.; Lõpez-Carrillo, V.; De Vivie-Riedle, R.; Carell, T. *Chem. - A Eur. J.* **2013**, 19, 13309–13312.

(139) Sauer, J.; Heldmann, D. K.; Hetzenegger, J.; Krauthan, J.; Sichert, H.; Schuster, J. *Eur. J. Org. Chem.* **1998**, No. 12, 2885–2896.

(140) Karver, M. R.; Weissleder, R.; Hilderbrand, S. A. *Bioconjug. Chem.* **2011**, 22, 2263–2270.

(141) Wijnen, J. W.; Zavarise, S.; Charton, M.; Engbert, J. B. F. N. *J. Org. Chem.* **1996**, 61, 2001–2005.

(142) Meijer, A.; Otto, S.; Engberts, J. B. F. N. J. Org. Chem. **1998**, 63, 8989–8994.

(143) Tasdelen, M. A.; Yagci, Y. *Angew. Chemie - Int. Ed.* **2013**, 52, 5930–5938.

(144) Adzima, B. J.; Tao, Y.; Kloxin, C. J.; DeForest, C. A.; Anseth, K. S.; Bowman, C. N. *Nat. Chem.* **2011**, 3, 256–259.

(145) Poloukhtine, A. A.; Mbua, N. E.; Wolfert, M. A.; Boons, G. J.; Popik, V. V. *J. Am. Chem. Soc.* **2009**, 131, 15769–15776.

(146) McNitt, C. D.; Cheng, H.; Ullrich, S.; Popik, V. V.; Bjerknes, M. *J. Am. Chem. Soc.* **2017**, 139, 14029–14032.

(147) Christman, K. L.; Broyer, R. M.; Tolstyka, Z. P.; Maynard, H. D. *J. Mater. Chem.* **2007**, 17, 2021–2027.

(148) Song, W.; Wang, Y.; Qu, J.; Madden, M. M.; Lin, Q. *Angew. Chemie - Int. Ed.* **2008**, 47, 2832–2835.

(149) Li, J.; Kong, H.; Huang, L.; Cheng, B.; Qin, K.; Zheng, M.; Yan, Z.; Zhang, Y. *J. Am. Chem. Soc.* **2018**, 140, 14542–14546.

(150) Van Berkel, S. S.; Van Eldijk, M. B.; Van Hest, J. C. M. *Angew. Chemie - Int. Ed.* **2011**, 50, 8806–8827.

(151) Lang, K.; Chin, J. W. *Chem. Rev.* **2014**, 114, 4764–4806.

(152) Spicer, C. D.; Davis, B. G. *Nat. Commun.* **2014**, 5:4740.

Chapter 2

Influence of Polymer Electronics on Selective Dispersion of Single-Walled Carbon Nanotubes

This chapter has been reprinted with permission from Chemistry – A European Journal. Fong, D.; Bodnaryk, W. J.; Rice, N. A.; Saem, S.; Moran-Mirabal, J. M.; Adronov, A. **2016**, *22*, 14560-14566. Copyright (2016) John Wiley & Sons.

D. Fong planned the study and synthesized the polymers with assistance from W. J. Bodnaryk for **P1**. D. Fong performed the UV/Vis-NIR, Raman, and electrical conductivity experiments. Computational work was performed by W. J. Bodnaryk. N. A. Rice performed the AFM and PL mapping experiments, and S. Saem performed thin film thickness measurements.

Abstract

The separation and isolation of semiconducting and metallic single-walled carbon nanotubes (SWNTs) on a large scale remains a barrier to many commercial applications. Selective extraction of semiconducting SWNTs by wrapping and dispersion with conjugated polymers has been demonstrated to be effective, but the structural parameters of conjugated polymers that dictate selectivity are poorly understood. Here, we report nanotube dispersions with a poly(fluorene-*co*-pyridine) copolymer and its cationic methylated derivative, and show that electron-deficient conjugated π-systems bias the dispersion selectivity toward metallic SWNTs. Differentiation of semiconducting and metallic SWNT populations was carried out by a combination of UV/Vis-NIR absorption spectroscopy, Raman spectroscopy, fluorescence spectroscopy, and electrical conductivity measurements. These results provide new insight into the rational design of conjugated polymers for the selective dispersion of metallic SWNTs.

2.1 Introduction

Single-walled carbon nanotubes (SWNTs) have attracted tremendous attention from the scientific community since their discovery.[1–3] Their unique properties, which include high tensile strength,[5] a high aspect ratio,[5] thermal and electrical conductivity,[6–8] and extraordinary optical characteristics,[9–11] make nanotubes potentially valuable as advanced materials in a variety of applications. Indeed, SWNTs have been incorporated into field-effect transistors,[12] photovoltaics,[13] flexible electronics,[14] sensors,[15] touch screens,[16] high-strength fibers,[17–19] biotechnological constructs,[20] and various other devices.[21] Despite recent progress toward commercialization, applications involving the electrical and optical properties of nanotubes have not kept pace with expectations. This is in part due to the nontrivial isolation of electronically pure nanotubes on an industrial scale.[22] All known SWNT synthesis methods, including high-pressure carbon monoxide disproportionation (HiPCO),[23] carbon vapor deposition (CVD),[24] arc discharge,[25] laser ablation,[26] and plasma torch growth,[27] produce mixtures of metallic SWNTs (m-SWNTs) and semiconducting SWNTs (sc-SWNTS). Since components of electronic devices require either pure m-SWNTs (electrodes, interconnects, etc.) or pure sc-SWNTs (transistors, sensors, etc.), purification of as-produced SWNTs is imperative. Several methods for separating and purifying SWNTs have recently been reported, including density-gradient ultracentrifugation (DGU),[28] agarose gel filtration,[29] electrophoresis,[30] and selective dispersion using conjugated polymers.[31] Of these, the latter is promising as it is a low-cost and scalable process. Indeed, it has been demonstrated that sc-SWNTs can be selectively dispersed using a variety of conjugated polymers.[31–35] However, despite this progress, the selective

dispersion of m-SWNTs remains elusive.

Dispersion selectivity is influenced by a combination of polymer attributes, including the backbone structure and conformation, the degree of polymerization, and the nature of the side chains.[36–38] It has been suggested that selectivity arises from a difference in polarity between sc- and m-SWNTs, with both p-type and n-type conjugated polymers appearing to be selective for sc-SWNTs.[39] This was based on calculations of polarizability, which show that m-SWNTs are more than three orders of magnitude more polarizable than sc-SWNTs.[40] This polarizability difference between m- and sc-SWNTs has been further supported by a recent study that found m-SWNTs to be more readily oxidized than sc-SWNTs,[41] indicating that the metallic tubes can donate electrons more easily, and are more "electron rich", than their semiconducting counterparts. In light of these results, we set out to show that the electronic nature of the conjugated polymer backbone actually does have a significant effect on dispersion selectivity through inductive effects.[38] We expect that relatively electron-poor conjugated polymers should disperse m-SWNTs to a greater extent when compared to structurally similar electron-rich conjugated polymers. Here, we demonstrate this concept through the comparison of a poly(fluorene-*co*-pyridine) conjugated polymer before and after post-polymerization functionalization. By partially methylating the pyridine units, cationic charges are introduced onto the conjugated backbone, which convert the polymer from being electron-rich to electron-poor. This enables the comparison of two polymers that are identical in length and polydispersity, and differ primarily in their electronic characteristics. We show that the electron-poor conjugated polymer results in dispersions that are enriched in m-SWNTs, while the electron-rich counterpart solely selects for sc-SWNTs, thus providing evidence that

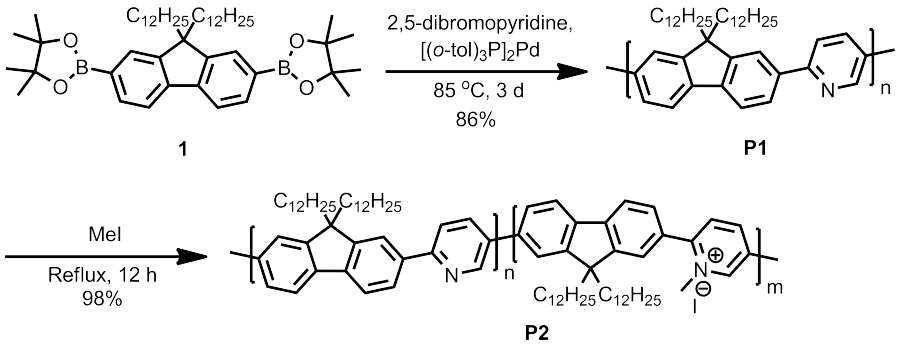
the electronic structure of a conjugated polymer plays an important role in determining its selectivity for different SWNT types.

2.2 Results and Discussion

Considering that the degree of polymerization (DP) of a conjugated polymer can significantly influence its SWNT dispersion selectivity,[42] it is imperative to minimize length variability when comparing different polymers. For this reason, post-polymerization functionalization is an ideal strategy for the comparison of polymers with different structural and electronic properties. We, therefore, chose to prepare a poly(9,9′-didodecylfluorene-*co*-pyridine) (**P1**) copolymer, as the pyridine units within this structure can undergo post-polymerization chemistry. Pyridine-containing polymers have been previously used to disperse SWNTs,[43,44] with some efficiency demonstrated for dispersing sc-SWNTs, but to the best of our knowledge, the effect of post-polymerization chemistry on SWNT selectivity has not been investigated. Methylation of the pyridine units within this polymer using methyl iodide is a facile process that introduces multiple cationic charges without significantly perturbing the steric bulk of repeat units or the DP. Thus, a drastic effect on polymer electronics can be achieved, and the interaction selectivity of the polymer before and after methylation can be directly compared.

Polymer **P1** was synthesized by the Suzuki polycondensation of 2,2′-(9,9-didodecylfluorene-2,7-diyl)bis(4,4,5,5-tetramethyl-1,3,2-dioxaborolane) (**1**), prepared according to literature procedures (see the Supporting Information),[45] with commercially available 2,5-dibromopyridine (Scheme 2.1). GPC analysis showed that **P1** had a number-average molecular weight (M_n) of 13.5 kDa, corresponding to a

DP of ∼23 and a polydispersity index (PDI) of 1.84. To prepare the methylated polymer **P2**, **P1** was dissolved in $CHCl_3$ and heated to reflux with an excess of methyl iodide (Scheme 2.1). The methylation was monitored by ^{1}H NMR, which indicated the appearance of new sets of peaks centered at 4.72 and 4.84 ppm, corresponding to the pyridine-CH_3 (Py-CH_3) group (Supporting Information, Figure 2.5). The appearance of two new sets of peaks suggests incomplete methylation, as the electronic environment of these protons will differ depending on whether or not adjacent repeat units are methylated, and also the relative orientation of the methyl groups. Broadening of the peaks in the aromatic region was also observed, corroborating the incomplete methylation of **P1**. We determined the degree of methylation by comparing the relative integration of the Py-CH_3 group to the aromatic region in the ^{1}H NMR spectrum, and observed a maximum methylation of ∼50% of the pyridine units after 12 h (Supporting Information, Figure 2.6). Heating at reflux for a total of 36 h did not result in any further methylation (Supporting Information, Figure 2.6). We hypothesize that pyridine methylation is limited by the decreased nucleophilicity of the nitrogen atom after adjacent pyridines are methylated, resulting in the observed maximum. Despite the non-quantitative methylation, it was still possible to carry out SWNT dispersion studies using the nonmethylated **P1** and its partially methylated analogue, **P2**.



SCHEME 2.1: Synthesis of fluorene–pyridine copolymers **P1** and **P2**.

Prior to nanotube complexation, we investigated the influence of methylation on the electronic properties of **P2** *via* density functional theory (DFT) calculations using the 6-31G(d) basis set.[46] Calculations were performed on trimers with methyl groups substituted for the dodecyl chains in order to decrease the calculation complexity and time. Electron density maps, color-coded to illustrate electron-rich and electron-poor segments (red and blue, respectively), are shown in Figure 2.1. Our calculations suggest that methylation drastically alters the electronic landscape of the polymer backbone. Figure 2.1A shows that the conjugated system for the trimer of **P1** is relatively electron-rich, while Figure 2.1B shows that the conjugated system for the trimer of **P2** is electron-poor. Additionally, we performed DFT calculations on the trimers of **P2** with varying degrees and positions of methylation to more accurately model incomplete functionalization (Figure S2.7, Supporting Information). These calculations show that wherever methylation occurs, the adjacent conjugated backbone units become electron-poor. Thus, **P1** and **P2** should be significantly different in terms of their electronics, despite being extremely similar in structure.

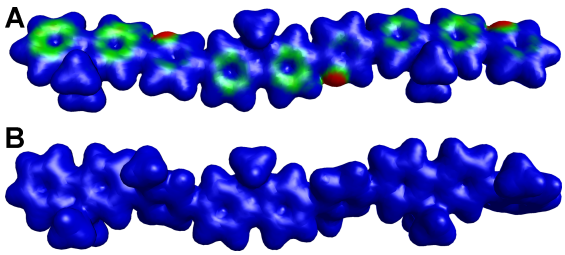


FIGURE 2.1: Electron density maps of trimers for (A) **P1** and (B) fully methylated **P2**. Red denotes electron-rich regions, green denotes less electron-rich regions, and blue denotes electron-poor regions.

Supramolecular polymer-SWNT complexes of **P1** and **P2** were prepared with raw HiPCO SWNTs following previously reported procedures.[47] A few different polymer:SWNT weight ratios were investigated and it was found that a ratio of 1.5:1 polymer:SWNT produced the best dispersions for both **P1** and **P2** (see Supporting Information, Figure S2.8). Additionally, THF, toluene, and a 1:1 mixture of these solvents were chosen for dispersion selectivity studies. The optimized dispersion protocol involved dissolving 15 mg of polymer in 20 mL of solvent before adding 10 mg of SWNTs. The mixture was sonicated for 2 h in a bath sonicator chilled with ice before being centrifuged at 8,346 *g* for 30 minutes. The supernatant was carefully removed, filtered through a Teflon filtration membrane with 0.2 μm diameter pores, and the resulting polymer-SWNT residue ("bucky paper") was washed with $CHCl_3$ until the filtrate did not exhibit any observable fluorescence when excited at 365 nm with a hand-held UV lamp. The bucky paper was re-dispersed in 5 mL of solvent, sonicated for 1 h in a bath sonicator chilled with ice, and centrifuged again. The resulting polymer-SWNT dispersions were stable on the bench top for at least several months, with no observable flocculation.

To investigate the polymer-SWNT dispersions, we initially performed UV/Vis-NIR absorption spectroscopy shown in Figure 2.2. Nanotube absorption features

depend on their respective diameters and chiralities, and arise from the interband transitions of the van Hove singularities, resulting in specific nanotube chiralities having specific transition energies. The absorbance features in the observed range can be grouped into three categories: two semi-conducting regions, S_{11} (830 – 1600 nm) and S_{22} (600 – 800 nm), and a metallic region, M_{11} (440 – 645 nm).[48] The absorption spectrum for **P1**-SWNT in THF shows sharp peaks in the S_{11} and S_{22} regions, suggesting that the electron-rich **P1** efficiently exfoliates sc-SWNTs in THF. This is corroborated by the intense green color of the **P1**-SWNT solution in THF (Supporting Information, Figure S2.9). The absence of a broad, featureless absorption background in the spectrum indicates effective nanotube exfoliation and the removal of m-SWNTs, consistent with previous reports.[43] The absorption spectrum for **P2**-SWNT in THF also shows sharp peaks in the S_{11} and S_{22} regions, which suggests that the electron-poor **P2** likewise exfoliates sc-SWNTs in THF. However, the presence of a broad, featureless, and relatively intense absorption background in this spectrum indicates the presence of m-SWNTs, which is confirmed by the presence of peaks in the M_{11} region (and is consistent with the dark brown-black color of the **P2**-SWNT solution in THF, Figure S2.8). The overlap of polymer absorption with the M_{11} region precludes a detailed analysis of the specific m-SWNT chiralities present in the sample. In toluene and the 1:1 THF:toluene co-solvent mixture, the **P2**-SWNT dispersions have no discernible absorbance features outside of the polymer absorbance, which suggests that **P2** does not form a stable colloidal dispersion with SWNTs in either of these solvents. As a consequence, these solvent options were not pursued in subsequent studies. A control sodium dodecylbenzenesulfonate (SDBS) dispersion was prepared in D_2O and showed no SWNT selectivity (see Supporting Information, Figure S2.13).

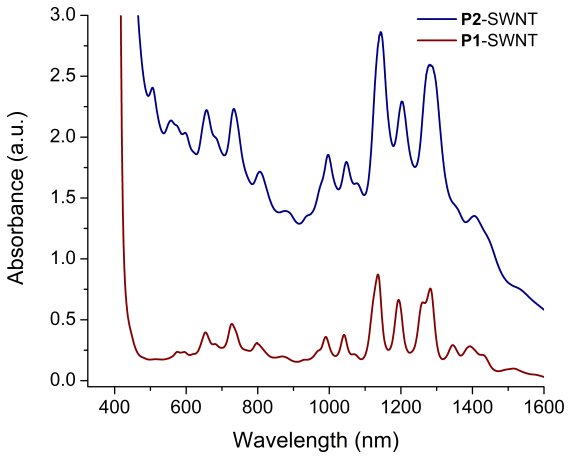


FIGURE 2.2: UV/Vis-NIR absorption spectra for **P1**-SWNT (red) and **P2**-SWNT (blue) in THF.

To further investigate the differences in nanotube populations dispersed by **P1** and **P2**, resonance Raman spectroscopy was performed. This technique allows for the examination of both m- and sc-SWNT species within a given sample,[49] and utilizes laser excitation wavelengths that overlap with the van Hove singularities present in the 1D density of states for a particular SWNT.[50] As the electronic transitions depend on nanotube chirality and diameter, only a subset of the total nanotube population will be observed for each individual excitation wavelength.[51]

Thin film samples were prepared from the polymer-SWNT complexes by drop-casting the dispersions onto silicon wafers. A reference SWNT sample was also prepared by sonicating a small amount of the SWNT starting material in $CHCl_3$ and making a solid film with the same drop-casting method. Raman spectra were collected using three excitation wavelengths: 514, 633, and 785 nm. These excitation wavelengths have previously been shown to be adequate for characterizing the electronic character of HiPCO SWNT samples, as both m- and sc-SWNTs can be separately probed.[52] Figure 2.3 shows the radial breathing mode (RBM) regions from the three samples at each excitation wavelength (full Raman spectra

are provided in the Supporting Information, Figure S2.10). All Raman spectra were normalized to the G-band at ~1590 cm^{-1} and offset for clarity. Upon excitation at 514 nm, two dominant RBM features are observed in the Raman spectrum: a broad feature arising from sc-SWNTs centered at 180 cm^{-1}, and several sharp peaks from 225 to 290 cm^{-1} arising from m-SWNTs.[53] The **P1**-SWNT sample shows a single peak in the sc-SWNT region, confirming that m-SWNTs are not present in the dispersions prepared using this polymer. Meanwhile, the **P2**-SWNT sample exhibits peaks corresponding to both sc- and m-SWNTs. This observation is corroborated by analysis of the G-band region at this excitation wavelength, which is shown in the inset of Figure 2.3A. The G-band consists of two peaks: a lower frequency G^- and a higher frequency G^+. For sc-SWNTs, both the G^- and G^+ have Lorentzian line shapes, but for m-SWNTs the G^- exhibits a broader Breit–Wigner–Fano (BWF) line shape.[54] A broad G^- is observed for both the raw SWNT and **P2**-SWNT samples, confirming that m-SWNTs are present. The **P1**-SWNT sample, however, lacks a BWF line shape in the G-band, which is consistent with the absence of m-SWNTs. Both m- and sc-SWNTs are in resonance when the 633 nm excitation wavelength is used. For HiPCO SWNTs at this wavelength, m-SWNT features are found at ~175 – 230 cm^{-1}, while sc-SWNTs give rise to peaks at ~230 – 300 cm^{-1}.[48,52] Both m- and sc-SWNT features are observed in the SWNT and **P2**-SWNT samples, while only sc-SWNT features are observed for the **P1**-SWNT sample.

While mainly sc-SWNTs are in resonance with the 785 nm excitation wavelength for HiPCO SWNTs, a few larger diameter metallic species, most notably the (16,7) and (12,9) chiralities, have been observed in the low-frequency region.[53,55] In our case, neither polymer-SWNT sample exhibits any signals below 200 cm^{-1},

which indicates the absence of large diameter m-SWNTs in both samples. The most intense peak in the raw SWNT spectrum occurs at 265 cm^{-1} and corresponds to (10,2) SWNTs, which are in resonance with this excitation wavelength when bundled.[56] This peak is often referred to as the "bundling peak" and can be used to identify bundling in a nanotube sample, but only if (10,2) SWNTs are present. Figure 2.3C shows that a significant decrease in the bundling peak occurs when SWNTs are dispersed with either **P1** or **P2**, giving further evidence that SWNTs are efficiently exfoliated using both of these polymers. This removes the possibility that the increased suspension of m-SWNTs using **P2** is due to bundles in the dispersion, as opposed to a genuine effect originating from the differences in electronic properties between these conjugated polymers.

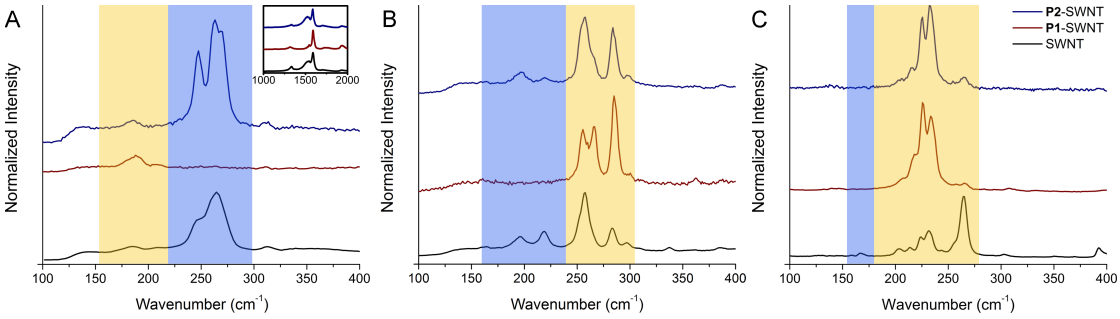


FIGURE 2.3: RBM regions of the Raman spectra using (A) 514 nm, (B) 633 nm, and (C) 785 nm excitation wavelengths. The yellow boxes denote the locations of signals arising from sc-SWNTs, while the blue boxes represent the locations of signals arising from m-SWNTs. The inset in (A) shows the G-band region, located at ~1590 cm^{-1}, upon excitation at 514 nm.

To confirm the absence of nanotube bundles, we investigated these samples using atomic force microscopy (AFM). Polymer-SWNT samples were prepared by spin-coating dilute dispersions onto freshly cleaved mica. These samples were analyzed using tapping-mode AFM, and representative images are shown in Figure S2.11. Long, filamentous structures were observed in both samples, with heights

ranging from 1 – 5 nm. The smallest diameter features correspond to individual polymer-coated nanotubes, while the larger features could originate from small bundles formed upon spin-coating the polymer-SWNT complexes. The height profiles observed suggest that significant SWNT exfoliation occurs for both polymer samples upon sonication, and that there is no palpable difference in the degree of nanotube exfoliation between **P1** and **P2**. On the basis of these results, it is clear that **P1** disperses only sc-SWNTs while **P2** disperses a higher proportion of m-SWNTs, alongside some sc-SWNTs.

Photoluminescence (PL) maps were recorded for the polymer-SWNT samples (Figure 2.4). The locations of various SWNT fluorescence maxima were assigned according to previously published data.[10] A SDBS-SWNT dispersion was prepared as a control experiment and a multitude of high intensity PL signals were observed, with the most intense peak corresponding to the (8,6) chirality (see Supporting Information, Figure S2.14). High intensity PL signals were also observed for the **P1**-SWNT dispersion, with the most intense peak corresponding to the (7,6) chirality (Figure 2.4A). The **P2**-SWNT sample similarly contains the (7,6) chirality as the most intense peak, but the relative fluorescence is dramatically lower (Figure 2.4B). Despite matching the sample concentrations by obtaining comparable absorption intensities for the (7,6) chirality at 1120 nm (see Figure S2.12), the fluorescence intensity for the **P2**-SWNT sample is an order of magnitude lower than the **P1**-SWNT sample. The observed fluorescence quenching can be attributed to two possibilities: the presence of nanotube bundles or the presence of m-SWNTs. We have already dispelled the possibility of bundles in our polymer-SWNT dispersions (*vide supra*), so we attribute the observed fluorescence quenching to the

increased amount of m-SWNTs dispersed by **P2**, in contrast to the enriched sc-SWNT dispersion with **P1**.

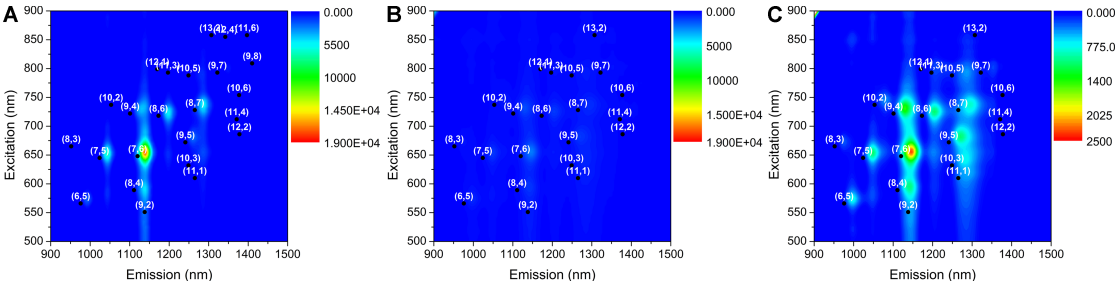


FIGURE 2.4: PL maps (A) and (B) correspond to **P1**-SWNT and **P2**-SWNT at a similar concentration and plotted on the same scale. (C) is the same **P2**-SWNT dispersion as (B) with an adjusted intensity scale.

To confirm the difference in m-SWNT quantities between our dispersions, we performed electrical conductivity measurements using the Van der Pauw method.[57] We first prepared square-shaped thin films with dimensions of 0.5 × 0.5 cm for our polymer-SWNT samples by filtering 100 μL of polymer-SWNT dispersion through a Teflon filtration membrane with 0.2 μm pore diameters clamped between two solvent-resistant aluminum masks under vacuum. The thin films were dried under vacuum for 15 min and then resistivity was measured by direct contact with four platinum probes placed in the corners of the square-shaped thin film. Voltages from 0 to 250 mV were applied to one pair of contiguous electrodes and the current was measured on the opposite pair of electrodes (e.g. if the thin film corners were labelled from 1 – 4 clockwise, the first measurement would apply V_{12} and measure I_{43}). The thin film resistance (R) was calculated from the slope of the resulting I–V curve. The measurements were repeated for all four electrode combinations (i.e. V_{12}, V_{23}, V_{34}, and V_{41}) and the total resistance for the thin film (R_T) was calculated as $R_T = \frac{1}{4}(\frac{V_{12}}{I_{43}} + \frac{V_{23}}{I_{14}} + \frac{V_{34}}{I_{21}} + \frac{V_{41}}{I_{32}})$ (measured in triplicate). The sheet resistance (R_s) was then calculated as $R_s = \frac{\pi R_T}{ln2}$. Thin film thickness ($t$) was measured

using white light interference microscopy, and bulk conductivity (σ) was calculated as $\sigma = {R_S}^{-1}t^{-1}$. The thickness measurements obtained for **P1**-SWNT and **P2**-SWNT (2.5 and 3.0 μm, respectively, with relative standard errors of 4 – 14%) allowed us to calculate conductivities of 3.1 ± 0.8 x 10^{-4} S/m and 1.4 ± 0.6 S/m, respectively, which gives a difference of four orders of magnitude. This stark contrast suggests that there are more m-SWNTs in the nanotube population dispersed by **P2**, which corroborates our previous spectroscopic analyses. However, it should be noted that the presence of charges and/or salts within the **P2**-SWNT sample can impact its conductivity. We performed conductivity measurements involving just the polymers **P1** and **P2** in thin films with mass loadings equivalent to those expected for the polymer-SWNT samples, and observed non-linear *I-V* curves, indicating that the polymers are non-conductive and are unlikely to contribute appreciably to the observed conductivity of the polymer-SWNT films. An uncentrifuged SDBS suspension of the raw SWNTs was also cast as a reference thin film using the same protocol described above. Its conductivity was measured to be 785 ± 114 S/m (full details of these control experiments are provided in the Supporting Information). Although the bulk conductivity of this SDBS-SWNT sample is higher than the **P2**-SWNT sample, the two materials cannot be directly compared as the SDBS suspension contains a mixture of amorphous carbon, metal catalyst particles, and the raw nanotube mixture that is significantly bundled. Thus, it is not surprising that this sample exhibits higher conductivity, as nanotubes are able to come into closer contact within the SDBS-SWNT sample. Considering the extent of insulating material around the nanotubes in the **P2**-SWNT sample, the finding that its conductivity is only 2 orders of magnitude lower than the raw nanotube sample is again indicative of the selectivity for metallic SWNTs by the

electron-poor cationic copolymer.

2.3 Conclusions

In the pursuit of next-generation polymers for the selective dispersion and purification of SWNTs, understanding the key parameters dictating polymer selectivity is imperative. We have demonstrated that the simple modification of a poly(fluorene-*co*-pyridine) backbone, such that it is transformed from being electron-rich to being electron-poor, has a significant impact on the electronic nature of SWNTs dispersed. The unmodified copolymer bearing an electron-rich fluorene co-monomer preferentially forms stable colloids with sc-SWNTs, while the methylated copolymer bearing electron-withdrawing cationic charges produces dispersions that are more enriched with m-SWNTs. Although the exact mechanism that directs specificity in conjugated polymer interactions with SWNTs is still under investigation, this work provides a clear indication that polymer electronics plays an important role. Further investigation of rationally-designed, electron-deficient conjugated polymers for selective dispersion of m-SWNTs is warranted.

2.4 Supporting Information

2.4.1 General

Raw HiPCO SWNTs were purchased from NanoIntegris (batch #R10-02, 10 wt % solid) and used without further purification. All other reagents were purchased from commercial suppliers and used as received. NMR was performed on a Bruker Avance 600 MHz or 700 MHz instrument and shift-referenced to the residual $CHCl_3$

resonance. Polymer molecular weights and polydispersity indices were analyzed (relative to polystyrene standards) *via* GPC using a Waters 2695 Separations Module equipped with a Waters 2414 refractive index detector and a Jordi Fluorinated DVB mixed bed column. THF was used as the eluent at a flow rate of 3.0 mL/min. Sonication was performed in a Branson Ultrasonic B2800 bath sonicator. Centrifugation of the polymer samples was performed using a Beckman Coulter Allegra X-22 centrifuge. Filtration was done through a Teflon filtration membrane with a pore diameter of 0.2 μm (Sartorius). UV/Vis-NIR spectra were recorded on a Cary 5000 spectrometer in dual beam mode, using matching 10 mm quartz cuvettes. Fluorescence spectra were measured on a Jobin-Yvon SPEX Fluorolog 3.22 equipped with a 450 W Xe arc lamp, digital photon counting photomultiplier, and an InGaAs detector, also using a 10 mm quartz cuvette. Slit widths for both excitation and emission were set to 10 nm band-pass, and correction factor files were applied to account to instrument variations. Photoluminescence maps were obtained at 25 °C, with 5 nm intervals for both the excitation and emission. Raman spectra were collected with a Renishaw InVia Laser Raman spectrometer, using three different lasers: a 25 mW argon ion laser (514 nm, 1800L/mm grating); a 500 mW HeNe Renishaw laser (633 nm, 1800 L/mm grating); and a 300 mW Renishaw laser (785 nm, 1200 L/mm grating). Laser intensity for both 514 and 633 nm excitations was set to 1% for the SWNT sample dispersed in $CHCl_3$ and polymer-SWNT samples. For spectra obtained at 785 nm, laser intensity was set to 10% for the SWNT sample and 0.1% for the polymer-SWNT samples. Tapping mode atomic force microscopy (AFM) was performed using a Digital Instruments NanoScope IIIa Multimode AFM using standard tips, with a scan rate of 0.85 Hz. AFM samples were prepared by spin coating (3500 rpm for 45 sec) a few drops of

dilute polymer-SWNT dispersions on freshly cleaved mica. Conductivity measurements were recorded using the Model 2450 Interactive Source Meter Instrument (Keithley) with Pt-wire probes. Thin film thickness was measured by white light interference microscopy using a Zygo NewView 5000 optical profilometer (Zygo Corporation, Middlefield, Connecticut, USA). Microscopy samples were prepared by drop-casting 100 μL of SWNT suspension onto a silicon wafer with a square-shaped Teflon mask (0.5 $\times$ 0.5 cm inner dimensions). Thin films for microscopy were prepared identically to the thin films used for electrical conductivity measurements, but the silicon wafer substrate was used because it has ideal reflectivity for interferometry. Half of the square-shaped thin films were removed and then ten images at different locations along each long edge of the resulting rectangle-shaped thin film were taken (20 images per replicate) using a charge-coupled device (CCD) camera. A 50$\times$ objective with a 2$\times$ optical zoom was used to obtain a field of view of 50 $\times$ 70 μm, with a camera resolution of 112 nm. Topographical maps were obtained for each surveyed area and a fast Fourier transform (FFT) band pass filter was applied to remove noise (cut-off frequencies of 183.35 mm^{-1} and 558.79 mm^{-1}). MetroPro software was used for data analysis. Thickness measurements were performed in duplicate per SWNT suspension sample.

2.4.2 Synthetic Procedures

2,7-dibromofluorene (adapted from reference 58)

A round bottom flask equipped with a stir bar was charged with fluorene (16.6 g, 100 mmol), NBS (34.8 g, 200 mmol) and acetic acid (200 mL). While the mixture was stirring, conc. HBr (5 mL) was slowly added and then the reaction mixture was stirred at RT for 3 h. Water (100 mL) was added and the resulting suspension

was filtered to obtain an off-colour orange-white solid. The solid was recrystallized from a 2.5:1 mixture of EtOH:acetone (∼850 mL total volume), and the mother liquor was recrystallized again from the same solvent mixture (∼650 mL total volume). The crops were combined to afford **1** (15.3 g, 47%) as a white solid. ^{1}H NMR (600 MHz; $CDCl_3$): δ 7.67 (d, J = 0.9 Hz, 2H), 7.61 (d, J = 8.1 Hz, 2H), 7.52-7.50 (m, 2H), 3.88 (s, 2H).

2,7-dibromo-9,9-didodecylfluorene (2) (adapted from reference 59)

A round bottom flask equipped with a stir bar was charged with 2,7-dibromofluorene (5 g, 15.4 mmol), 1-bromododecane (9.6 g, 38.6 mmol), toluene (30 mL), and sat. KOH (60 mL) and sparged with nitrogen for 1 h. $^{n}Bu_4NBr$ (993 mg, 3 mmol) was then added and the reaction mixture was heated to 60 °C and stirred vigorously for 12 h under a nitrogen atmosphere. The biphasic mixture was allowed to separate and the organic layer was isolated and concentrated *in vacuo* to obtain a viscous green oil. The crude product was purified by silica column chromatography (100% hexanes) twice then recrystallized from hexanes to afford **2** as a white solid (7.52 g, 74%). ^{1}H NMR (600 MHz; $CDCl_3$): δ 7.51 (s, 2H), 7.46-7.44 (m, 4H), 1.92-1.89 (m, 4H), 1.28-1.04 (m, 36H), 0.87 (t, J = 7.1 Hz, 6H), 0.57 (s, 4H).

2,2′-(9,9-didodecylfluorene-2,7-diyl)bis(4,4,5,5-tetramethyl-1,3,2-dioxaborolane) (3) (adapted from reference 59)

A round bottom flask equipped with a stir bar was charged with 2,7-dibromo-9,9-didodecylfluorene (7 g, 10.6 mmol), B_2Pin_2 (5.92 g, 23.3 mmol), KOAc (3.12 g, 31.8 mmol), DMSO (25 mL) and dioxane (75 mL) and sparged with nitrogen for 1 h. $Pd(dppf)_2Cl_2$ (260 mg, 318 μmol) was added and then the reaction mixture was stirred at 80 °C for 12 h. The reaction mixture was partitioned with water

and extracted thrice with CH_2Cl_2. The organic extracts were combined and concentrated *in vacuo*, then the extract was passed through a celite/silica plug. The plug was washed thoroughly with CH_2Cl_2 and the resulting organic extract was concentrated *in vacuo*. The crude product was purified by silica column chromatography (100% CH_2Cl_2) to obtain a yellow solid. The solid was recrystallized from a 1.25:1 mixture of MeOH:acetone (∼450 mL total volume) to afford **3** as a white solid (4.88 g, 63%). ^{1}H NMR (700 MHz; $CDCl_3$): δ 7.80 (dd, J = 7.5, 0.8 Hz, 2H), 7.74 (s, 2H), 7.72 (d, J = 7.6 Hz, 2H), 1.99 (dt, J = 7.9, 4.1 Hz, 4H), 1.39 (s, 24H), 1.26-1.00 (m, 36H), 0.86 (t, J = 7.2 Hz, 6H), 0.55 (s, 4H).

Poly(9,9′-didodecylfluorene-*co*-pyridine) (P1)

A Schlenk tube equipped with a stir bar was charged with **3** (700 mg, 0.93 mmol), 2,5-dibromopyridine (219.7 mg, 0.93 mmol), toluene (6.75 mL), and 3M $K_3PO_{4(aq)}$ (7.4 mL) then the mixture was degassed by three freeze-pump-thaw cycles. The biphasic mixture was frozen under liquid nitrogen and $[(o\text{-tol})_3P]_2Pd$ (33.2 mg, 46 μmol) was added under a positive pressure of nitrogen. The Schlenk tube was evacuated and backfilled with nitrogen four times and then the reaction mixture was vigorously stirred at 85 °C for 3 days. The phases were allowed to separate and the organic layer was isolated then filtered through a celite and neutral alumina plug. The plug was thoroughly washed with THF and the flow-through was concentrated *in vacuo*. The crude polymer was precipitated into MeOH (200 mL) and then filtered to afford **P1** as a yellow solid (460 mg, 86%). ^{1}H NMR (700 MHz; $CDCl_3$): δ 9.07 (m), 8.60-8.59 (m), 8.14-7.66 (m), 2.15 (m), 1.27-0.82 (m).

Methylated Poly(9,9′-didodecylfluorene-*co*-pyridine) (P2)

A Schlenk tube equipped with a stir bar was charged with **P1** (50 mg, 87 μmol), MeI (123 mg, 870 μmol, 540 μL), and $CHCl_3$ (5 mL) and the reaction mixture

was heated to reflux. The RM was transferred to a pre-weighed glass vial and the solution was removed by a stream of nitrogen gas followed by drying the sample under high vacuum overnight to afford **P2** as a red solid (62 mg, 98%). ^{1}H NMR (600 MHz; $CDCl_3$): δ 9.06-7.43 (m), 4.84 (m), 4.72 (m), 2.27-2.09 (m), 1.25-0.85 (m).

Sodium dodecylbenzenesulfonate (SDBS) Dispersion Preparation

A SDBS-SWNT control was prepared following a previously reported procedure,[60] with a few minor modifications. 350 mg of SDBS was dissolved in 35 mL of D_2O before 5 mg of HiPCO SWNTs were added. The mixture was sonicated for 4 h in a bath sonicator chilled with ice followed by centrifugation at 40,000 *g* for 4 hours at 15 °C. The supernatant was carefully recovered and analysed by UV/Vis-NIR absorption spectroscopy and PL mapping.

Control Electrical Conductivity Experiments

Polymer only. The resistance for thin films of **P1** or **P2** at mass loadings equivalent to the amount expected in the polymer-SWNT thin films (100 μL of a 0.75 mg/mL THF solution, or 75 μg of polymer) were measured under identical experimental conditions. The inability to obtain a linear *I–V* curve demonstrates that the polymers have a resistance higher than measurable with our current apparatus, and suggests that the polymers are not contributing to the conductive pathways in the polymer-SWNT thin films.

SWNT only. An uncentrifuged SDBS suspension of SWNTs (for the preparation protocol, *vide supra*) was used to obtain resistance measurements. Thin films were prepared by vacuum filtration of 100 μL of the uncentrifuged suspension, and resistance was measured in an identical fashion to the polymer-SWNT thin films.

Film thickness was measured and the bulk conductivity was calculated as 785 ± 114 S/m. Although the bulk conductivity of the SDBS-SWNT sample is higher than the **P2**-SWNT sample, the SDBS suspension contains a complicated mixture of amorphous carbon, leftover metal catalyst nanoparticles, and a 2:1 ratio of semiconducting:metallic SWNTs that are significantly bundled. It is non-trivial to ascertain the effects of these contaminants and their contributions to the conductivity observed in the sample, so any decisive statement about these differences is untenable. Although removal of these contaminants is possible through centrifugation, the resulting dispersions are too dilute to obtain reasonable conductivity measurements. The leftover metal catalysts could help decrease junction resistance in the SWNT only thin film, or that the conjugated polymers **P1** and **P2** are insulating in nature and decrease the bulk conductivity of the samples relative to the SWNT only sample. It may also be a combination of these factors. The most important finding, in our view, is that the conductivity between the polymer-SWNT samples prepared using **P1** and **P2** are significantly different and corroborate spectroscopic analyses.

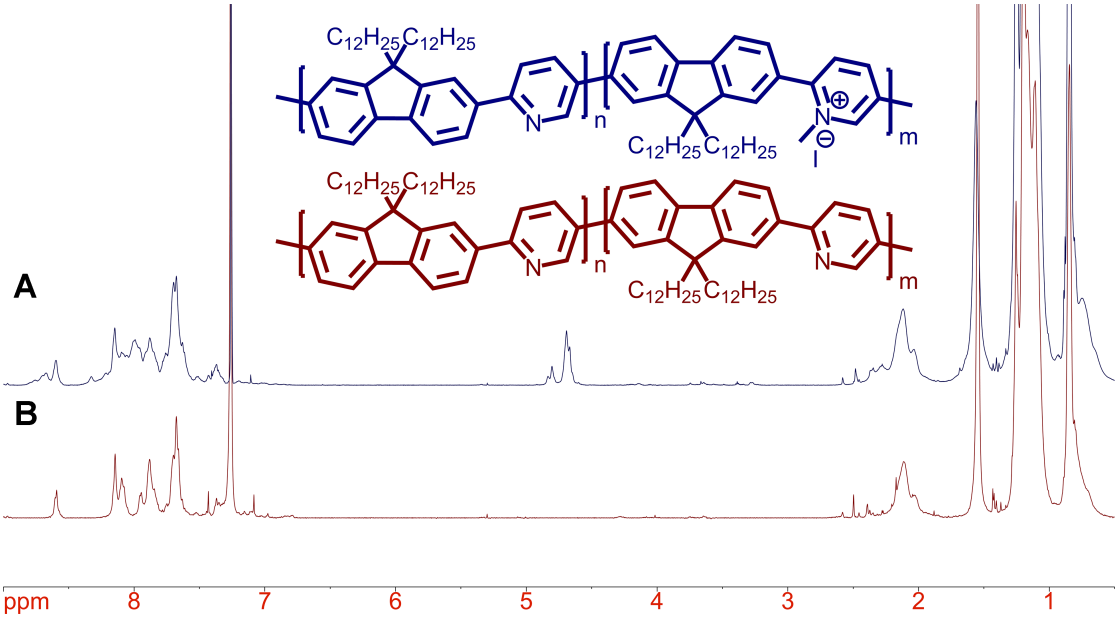


FIGURE 2.5: ^{1}H NMR overlay for (A) **P2** and (B) **P1**.

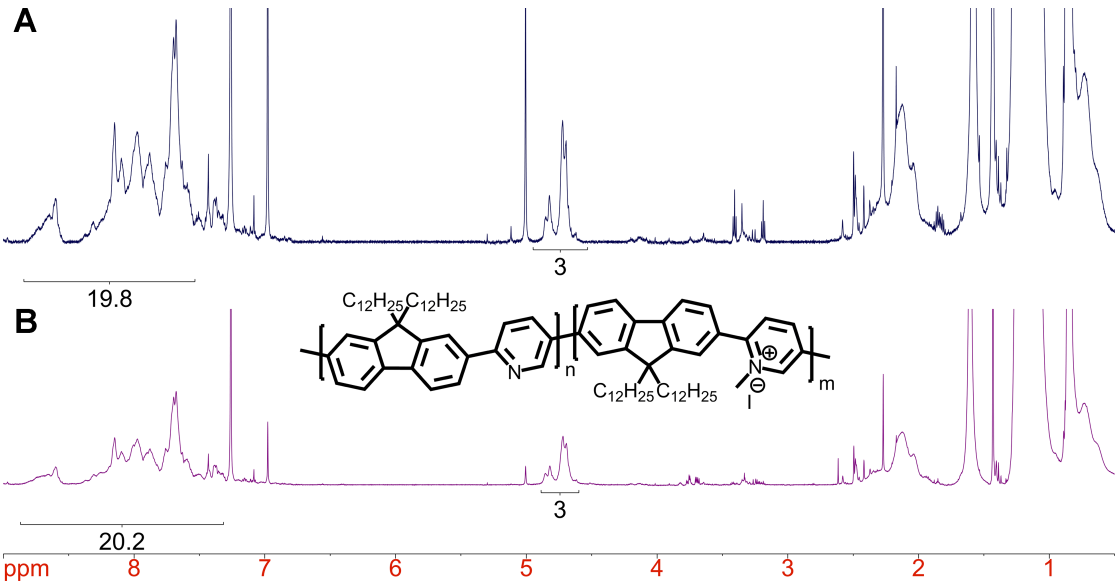


FIGURE 2.6: Crude ^{1}H NMR spectra for **P2** after a reaction time of (A) 12 h (blue) and (B) 36 h (purple). If fully methylated, an integration of 9:3 aromatic:Py-CH_3 protons is expected; however, the aromatic region integrates to about twice this, which indicates that **P2** is ∼50% methylated.

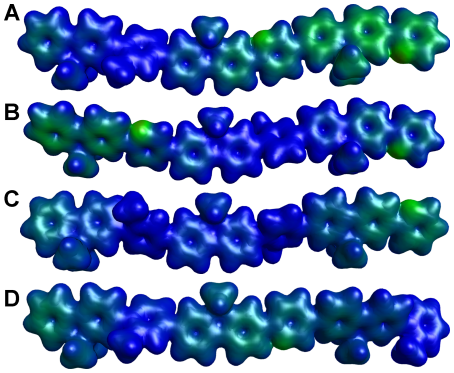


FIGURE 2.7: Electron density maps of trimers for partially methylated **P2**: (A) mono-methylation in the 1 position, (B) mono-methylation in the 2 position, (C) di-methylation in the 1 and 2 positions, and (D) di-methylation in the 1 and 3 positions. Red denotes electron-rich regions, green denotes less electron-rich regions, and blue denotes electron-poor regions.

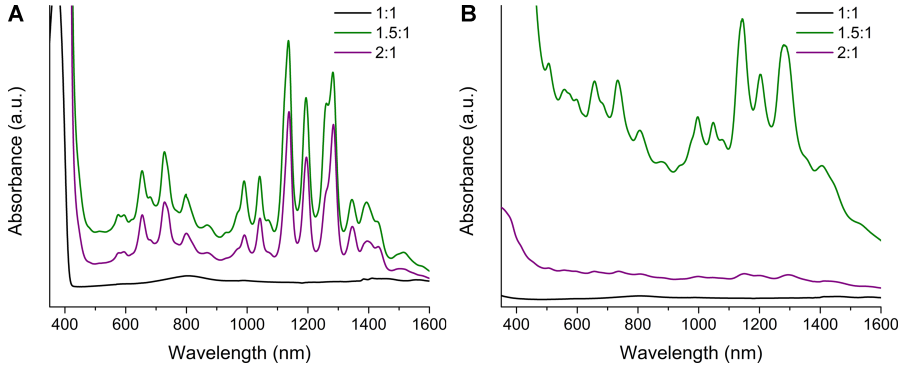


FIGURE 2.8: UV/Vis-NIR absorption spectra (no normalization) for (A) **P1**-SWNT and (B) **P2**-SWNT in THF at varying polymer:SWNT ratios.



FIGURE 2.9: Photograph of **P1**, **P1**-SWNT, **P2**, and **P2**-SWNT (left to right) in THF solution.

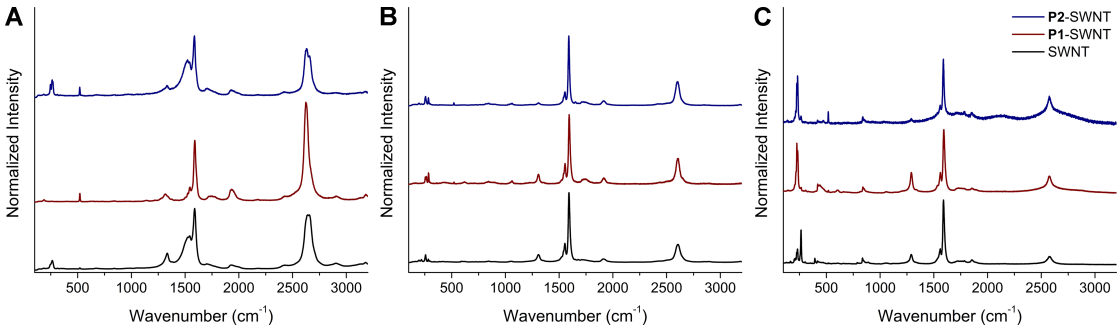


FIGURE 2.10: Full Raman spectra of **P1**-SWNT (red), **P2**-SWNT (blue), and SWNT material (black) obtained at (A) 514 nm, (B) 633 nm, and (C) 785 nm excitation wavelengths.

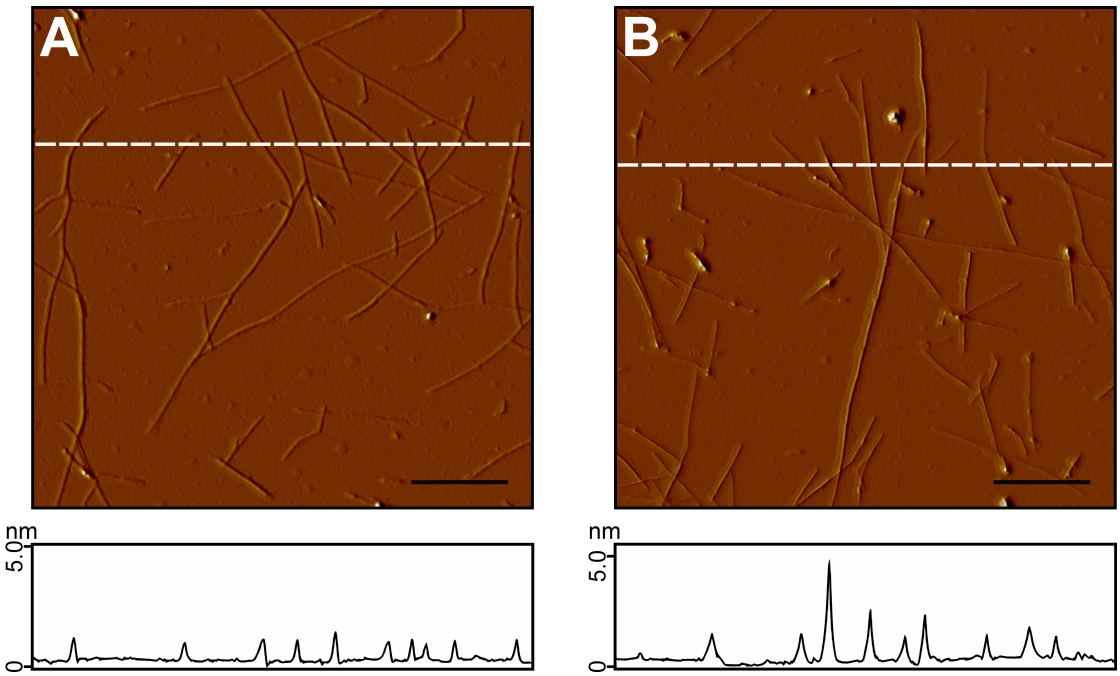


FIGURE 2.11: Representative AFM images and corresponding height profiles of (A) **P1** and (B) **P2** with HiPCO SWNTs. The dashed white line is the location height trace, and the black scale bar represents 500 nm.

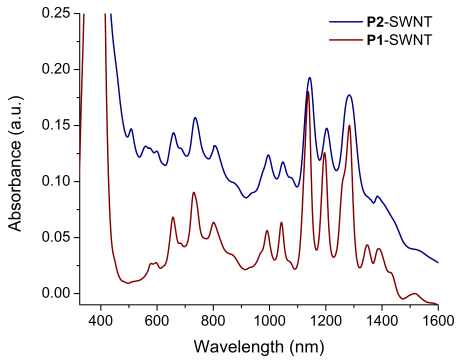


FIGURE 2.12: UV/Vis-NIR absorption spectra for **P1**-SWNT (red) and **P2**-SWNT (blue) in THF used for PL mapping.

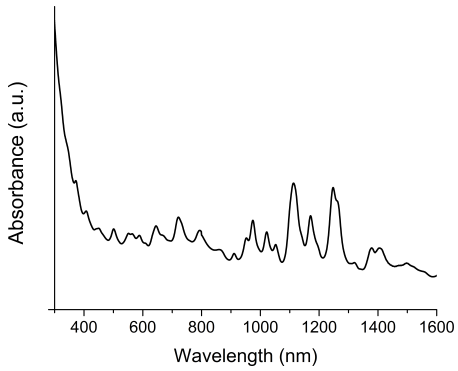


FIGURE 2.13: UV/Vis-NIR absorption spectra for SDBS-SWNT in D_2O.

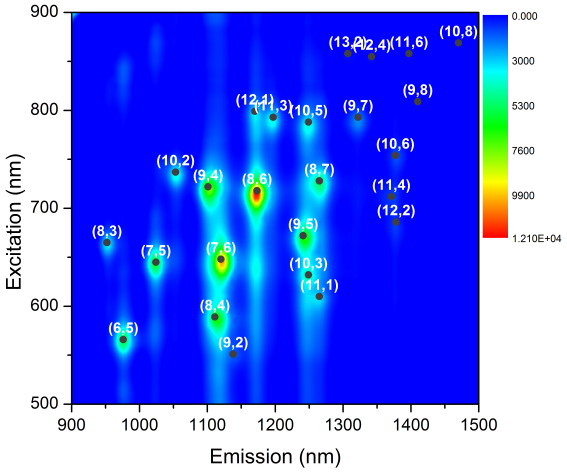


FIGURE 2.14: PL map of SDBS-SWNT dispersion in D_2O.

Computational Methods

All calculations were performed using GAMESS[46] (64-bit Linux), run in Mac OSX 10.9 on a desktop computer equipped with an Intel i5-3570k processor. Trimers were used to calculate the respective polymer backbone conformations and electron density maps, and the initial coordinates for each trimer were optimized by using the molecular mechanics geometry optimization in Avogadro.[61] The M06 functional and 6-31G(d) basis set were used for all geometry and frequency calculations on the trimers.[62] In all cases alkyl chains were replaced by methyl groups to minimize computational load.

Coordinates of M06/6-31G(d) stationary point:

Unmethylated Trimer

E = -2477.1486424795

ATOM	CHARGE	X	Y	Z
C	6	-5.458114468	-6.035973777	2.402824388
C	6	-3.935429959	-7.599570854	0.876265941
C	6	-1.546230495	-6.767316632	0.076496108
C	6	-0.734876642	-4.374394408	0.8296464
C	6	-2.214324221	-2.83218903	2.324041712
C	6	-4.598043479	-3.633224979	3.136208147
C	6	1.592339809	-3.079195113	0.285783261
C	6	1.540240064	-0.749824375	1.443127045
C	6	-0.913058906	-0.334538192	2.881095138
C	6	3.654673369	-3.868231302	-1.136859154
C	6	5.724490243	-2.232068748	-1.385811656

C	6	5.726134304	0.186667133	-0.212235126
C	6	3.578574103	0.916158056	1.224655824
C	6	7.981219915	1.874948331	-0.530049242
C	6	8.136404213	4.287637088	0.563554084
C	6	10.28781946	5.765969728	0.194906338
C	6	12.33594228	4.877061521	-1.272711556
C	6	12.08434416	2.435441059	-2.331884074
N	7	9.964676311	1.042883081	-1.936043172
C	6	-2.41011873	1.903993419	1.800360846
C	6	-0.43323858	-0.000812582	5.723356407
H	1	-5.762568222	-2.428222305	4.308140615
H	1	-7.297781614	-6.688477264	3.01294132
H	1	-4.60975978	-9.447949637	0.318456624
H	1	-0.369044588	-7.95939358	-1.095606436
H	1	3.670452581	-5.704459147	-2.036501005
H	1	7.325314922	-2.855262584	-2.495534345
H	1	3.454305722	2.717822813	2.161959914
H	1	6.634053155	5.062802688	1.697465266
H	1	10.29539726	7.596830752	1.073723409
H	1	13.54103943	1.596062569	-3.46783616
H	1	-4.269457924	2.074578984	2.760152675
H	1	-1.352930424	3.69645521	2.077243498
H	1	-2.745658477	1.641604966	-0.256681481
H	1	0.651067295	-1.631324856	6.483990015
H	1	0.66503237	1.752078347	6.081724044

H	1	-2.252005357	0.130674552	6.763669461
C	6	14.69401795	6.468135214	-1.692873232
C	6	14.9743966	8.893825286	-0.534168845
C	6	17.14788384	10.35998809	-0.922866583
C	6	19.04720963	9.418904549	-2.464826298
C	6	18.84633176	7.099133618	-3.609452226
C	6	16.70551788	5.5944393	-3.258133267
C	6	21.42837776	10.53240669	-3.159546262
C	6	22.68667071	8.889913553	-4.73334786
C	6	21.16493106	6.498937747	-5.197294487
C	6	22.46039492	12.84786905	-2.470457681
C	6	24.84708105	13.50483229	-3.416851353
C	6	26.19377537	11.84567177	-5.048119517
C	6	25.06755538	9.497951787	-5.70264501
C	6	28.74091814	12.62669552	-6.016868648
C	6	30.19411742	11.10274489	-7.631582812
C	6	32.54998212	11.94000689	-8.467522
C	6	33.51408252	14.3157893	-7.71635592
C	6	31.97622351	15.77686874	-6.08967979
N	7	29.69139362	14.90653654	-5.30803243
C	6	22.55161199	4.150972105	-4.204262378
C	6	20.48219196	6.205463301	-8.00263051
H	1	16.65971092	3.801297208	-4.209383535
H	1	13.55079042	9.688719625	0.676011678
H	1	17.33313368	12.19158611	-0.032163136

H	1	21.45003402	14.12231915	-1.2310242
H	1	25.64208877	15.3095773	-2.87521809
H	1	25.98065208	8.154035356	-6.927452012
H	1	29.55416172	9.277817607	-8.26704097
H	1	33.57196483	10.69573571	-9.705387009
H	1	32.55111595	17.6005677	-5.410587859
H	1	21.34500305	2.445040867	-4.406463058
H	1	24.32784104	3.838203556	-5.278666088
H	1	23.03589207	4.385335922	-2.173657317
H	1	19.48025924	7.915155094	-8.699674838
H	1	22.21558092	5.935345869	-9.155703513
H	1	19.23244058	4.542409946	-8.284407552
C	6	36.07893202	15.25515319	-8.613673408
C	6	37.68104171	13.70943292	-10.1461278
C	6	40.04514561	14.576477	-10.97318528
C	6	40.82136946	16.98230605	-10.2799015
C	6	39.33561019	18.52103433	-8.811206466
C	6	36.97243226	17.71062534	-7.957220395
C	6	43.12485095	18.29953955	-10.87268965
C	6	43.0472966	20.64998073	-9.764724405
C	6	40.60064946	21.05313487	-8.315833695
C	6	45.18680657	17.51216632	-12.29742966
C	6	47.22897675	19.17418032	-12.59918111
C	6	47.20297412	21.61653778	-11.47624923
C	6	45.05707688	22.34272168	-10.0357867

C	6	49.42774852	23.33274913	-11.84833628
C	6	49.54865319	25.78440403	-10.79774312
C	6	51.67977278	27.28199298	-11.22087166
C	6	53.67127941	26.35736895	-12.67155761
C	6	53.50732678	23.93421111	-13.68694518
N	7	51.42105039	22.49743355	-13.25941357
C	6	39.05876534	23.24502805	-9.429505912
C	6	41.09929146	21.4536434	-5.485118652
H	1	35.89676243	19.0046908	-6.820852569
H	1	37.15318455	11.83389877	-10.71826124
H	1	41.23739263	13.38413549	-12.13047237
H	1	45.22327828	15.65802387	-13.15882346
H	1	48.82959356	18.55251717	-13.70999984
H	1	44.91321204	24.16156405	-9.135181089
H	1	48.04581081	26.56212076	-9.666761009
H	1	51.78489823	29.16206247	-10.42166875
H	1	55.03989456	23.19134093	-14.81756824
H	1	37.20513312	23.40750669	-8.457563144
H	1	40.08964866	25.05925948	-9.199148314
H	1	38.7100731	22.93441379	-11.47760983
H	1	42.21608172	19.85669266	-4.700693395
H	1	42.17233457	23.23081731	-5.172935919
H	1	39.28825366	21.57842201	-4.430783832
H	1	55.32821005	27.5087601	-13.00647375

Mono-methylation in the 1 position

E = -2516.8145503584

ATOM	CHARGE	X	Y	Z
C	6	-33.82235352	-2.253290371	0.213331167
C	6	-32.75276861	-4.399357689	-0.94612911
C	6	-30.13090609	-4.544299672	-1.327570301
C	6	-28.63475333	-2.523445598	-0.534490098
C	6	-29.66720512	-0.416155457	0.602709207
C	6	-32.27449786	-0.242924276	0.996622589
C	6	-25.94174262	-2.189719988	-0.692244424
C	6	-25.32554077	0.116558299	0.336749171
C	6	-27.65132103	1.508190311	1.291476535
C	6	-24.10814149	-3.80073029	-1.656911746
C	6	-21.57456696	-3.029060683	-1.577184207
C	6	-20.87663447	-0.636969939	-0.554426708
C	6	-22.81464295	0.929707391	0.431934669
C	6	-28.04345807	4.008883608	-0.12731084
C	6	-27.53141792	1.936780165	4.158927851
H	1	-35.84445482	-2.153286071	0.502213579
C	6	-18.11591487	0.098700388	-0.506522154
C	6	-16.35385877	-1.820939962	-0.002078699
C	6	-13.78390702	-1.31798939	0.031993061
C	6	-12.87098039	1.123083052	-0.464929285
C	6	-14.68275518	3.010371293	-1.002083897
N	7	-17.2322979	2.513959173	-1.014877342

H	1	-33.95607053	-5.941015047	-1.54426518
H	1	-33.08966896	1.406995484	1.888157515
H	1	-29.29901091	-6.187151856	-2.216195049
H	1	-24.61574079	-5.613922375	-2.454508394
H	1	-20.1605228	-4.286295383	-2.351234868
H	1	-22.42681449	2.700834176	1.325472705
H	1	-16.96756618	-3.728448271	0.408161916
H	1	-14.07080522	4.896053267	-1.445016771
H	1	-12.55059625	-2.872780344	0.469823675
C	6	-18.92050351	4.612669958	-1.727908751
H	1	-29.83777179	4.918937849	0.472318113
H	1	-28.12743749	3.675082409	-2.199603255
H	1	-26.46219205	5.3323721	0.267774173
H	1	-25.94230954	3.219790727	4.644303971
H	1	-29.31656647	2.80184003	4.846164501
H	1	-27.24542678	0.114876443	5.164734508
H	1	-20.16823288	4.038514511	-3.315184095
H	1	-19.99628672	5.318407025	-0.092502087
H	1	-17.85358311	6.300044087	-2.380865772
C	6	-10.05396586	1.697276293	-0.443518689
C	6	-9.134330712	4.2351405	-0.581638762
C	6	-6.535787404	4.757441866	-0.56096516
C	6	-4.846674727	2.758621997	-0.405213944
C	6	-5.658897854	0.297839713	-0.269040289
C	6	-8.234178635	-0.282457343	-0.282684111

C	6	-2.128209407	2.784643524	-0.355211794
C	6	-1.277228001	0.334878342	-0.190427688
C	6	-3.453020708	-1.537216502	-0.11710632
C	6	-0.468198511	4.81948157	-0.448639847
C	6	2.139585558	4.341834429	-0.371992561
C	6	3.072845634	1.820902167	-0.201728249
C	6	1.307520308	-0.193337866	-0.111021402
C	6	-3.483785447	-3.028833916	2.372002957
C	6	-3.395006121	-3.319095828	-2.406925093
C	6	5.844015412	1.228851015	-0.116955141
C	6	7.719190509	3.104215086	-0.198780277
C	6	10.26550179	2.426408168	-0.114574087
C	6	11.0054618	-0.135814607	0.053441451
C	6	9.043264817	-1.949592507	0.130806833
N	7	6.581651054	-1.227433721	0.04489989
H	1	-10.38005698	5.836664378	-0.684043013
H	1	-8.752870624	-2.244692117	-0.189785181
H	1	-5.86775037	6.687721373	-0.661800938
H	1	-1.165960934	6.737288886	-0.578577406
H	1	3.387598395	5.947194451	-0.447317039
H	1	1.924345768	-2.138716284	0.018254753
H	1	7.267357026	5.084761304	-0.326658034
H	1	9.41627783	-3.939776328	0.256020077
H	1	11.61351893	3.943914828	-0.182698709
H	1	-1.77192047	-4.234214534	2.526450262

H	1	-3.525227138	-1.720066389	4.014666169
H	1	-5.177263391	-4.265943034	2.465922339
H	1	-5.086178599	-4.562800089	-2.412915525
H	1	-3.373047505	-2.218765077	-4.196231042
H	1	-1.681081341	-4.530145624	-2.351045896
C	6	13.7757812	-0.902627618	0.145508901
C	6	14.50835237	-3.497051324	0.341813637
C	6	17.06190131	-4.202051398	0.425622984
C	6	18.89334814	-2.330296705	0.314299226
C	6	18.26389932	0.179750736	0.125572292
C	6	15.73748685	0.941404795	0.038323643
C	6	21.60296955	-2.549826173	0.364358068
C	6	22.63211432	-0.169017092	0.20579116
C	6	20.59931718	1.851666906	0.034638677
C	6	23.10887329	-4.696252538	0.537740427
C	6	25.74513553	-4.406198497	0.54972129
C	6	26.86151005	-1.960628507	0.387507211
C	6	25.24938481	0.173004414	0.213841393
C	6	20.76343988	3.309911759	-2.469002592
C	6	20.70315762	3.653898581	2.306788513
C	6	29.66898147	-1.570192221	0.394083458
C	6	31.40611208	-3.590876219	0.560719495
C	6	33.99675633	-3.088605949	0.55641092
C	6	34.85616592	-0.606923296	0.388527663
C	6	33.10624186	1.35281704	0.226124612

N	7	30.58990163	0.835750215	0.232398502
H	1	13.15067874	-5.003899929	0.434070059
H	1	15.3688391	2.932287815	-0.111323758
H	1	17.58656483	-6.173111192	0.574514495
H	1	22.27166798	-6.557840506	0.661252918
H	1	26.87214921	-6.094914331	0.685309129
H	1	26.00812869	2.067662587	0.086795115
H	1	30.81186885	-5.53285313	0.693019212
H	1	33.74642433	3.28976728	0.094694169
H	1	35.33817833	-4.627731074	0.683532787
H	1	36.86165652	-0.20524314	0.384237985
H	1	20.6867548	1.986631136	-4.098683387
H	1	22.56149526	4.388491764	-2.573504439
H	1	19.16730172	4.663144539	-2.636848054
H	1	19.10571555	5.014255628	2.238890659
H	1	20.58321671	2.577642939	4.106828106
H	1	22.49996578	4.739602853	2.300760287

Mono-methylation in the 2 position E = -2516.8154961762

ATOM	CHARGE	X	Y	Z
C	6	-33.87622961	-1.261222022	-1.485778161
C	6	-32.83659686	-3.594769055	-2.239098528
C	6	-30.20698645	-3.949357239	-2.234223035
C	6	-28.67277462	-1.945813055	-1.470301305
C	6	-29.67589786	0.344648226	-0.730076738

C	6	-32.29057943	0.727903553	-0.724313074
C	6	-25.96413587	-1.803705661	-1.290210418
C	6	-25.30821198	0.566728824	-0.442347059
C	6	-27.62250271	2.208995193	0.011262767
C	6	-24.15228549	-3.627366828	-1.829746085
C	6	-21.59607205	-3.01411295	-1.493752804
C	6	-20.85951355	-0.58061831	-0.620245864
C	6	-22.77427841	1.225940837	-0.092161936
C	6	-27.62834196	4.536060466	-1.722145087
C	6	-27.84702105	2.978264848	2.800195969
H	1	-35.90452921	-0.999986301	-1.493658318
C	6	-18.10306474	-0.008352589	-0.286501357
C	6	-17.21568721	2.344016115	0.562609221
C	6	-14.6261012	2.755107107	0.83620375
C	6	-12.85892394	0.832518784	0.272536282
C	6	-13.8502553	-1.500442434	-0.575591639
N	7	-16.38245033	-1.839818324	-0.824298476
H	1	-34.06901946	-5.118662988	-2.823250626
H	1	-33.08286595	2.521782639	-0.144790805
H	1	-29.39816483	-5.736641181	-2.810494975
H	1	-24.69450457	-5.483436796	-2.494854044
H	1	-20.19289381	-4.440780482	-1.91591759
H	1	-22.35048846	3.101002551	0.574552289
H	1	-18.47458487	3.875790206	1.023588979
H	1	-12.65591068	-3.067781169	-1.060665402

H	1	-14.05973142	4.588594849	1.502029804
H	1	-27.46499405	3.95617915	-3.734570983
H	1	-29.40965437	5.621745841	-1.486231695
H	1	-26.01532855	5.798435221	-1.261902323
H	1	-29.63283101	4.031957162	3.128894907
H	1	-27.84067157	1.279476775	4.035906689
H	1	-26.23856188	4.208287494	3.354377012
C	6	-10.0302498	1.251168679	0.5661997
C	6	-9.034836639	3.666200697	1.259351193
C	6	-6.426750214	4.050514271	1.533361461
C	6	-4.803022057	2.034384512	1.121457887
C	6	-5.688283093	-0.311521329	0.452362607
C	6	-8.275147895	-0.752451094	0.162459743
C	6	-2.090868422	1.931470035	1.280478329
C	6	-1.317309089	-0.485149353	0.713938478
C	6	-3.543746453	-2.193726207	0.110908018
C	6	-0.370386294	3.830058837	1.867880755
C	6	2.21356833	3.237478562	1.89012283
C	6	3.06218758	0.743569382	1.354990225
C	6	1.244479049	-1.12102325	0.72641067
C	6	-3.738558305	-4.381688751	2.007418122
C	6	-3.418684387	-3.177498659	-2.616306733
C	6	5.845924035	0.161911723	1.34316054
C	6	7.472543473	1.994832547	0.329776082
C	6	10.04893919	1.549594207	0.146378175

C	6	11.09291832	-0.748085827	0.972623069
C	6	9.410835419	-2.539489371	2.019191115
N	7	6.866772911	-2.084443354	2.22005009
H	1	-10.22791514	5.276417314	1.588012337
H	1	-8.850342691	-2.630252911	-0.354002369
H	1	-5.701284408	5.889463322	2.057287991
H	1	-1.002972068	5.726361072	2.297812315
H	1	3.548395179	4.714186038	2.357811115
H	1	1.801135633	-3.019366389	0.214653975
H	1	6.742239968	3.766507352	-0.386052122
H	1	10.11850001	-4.302735999	2.747264744
H	1	11.17850401	3.019158519	-0.68786026
H	1	-3.827432118	-3.646906595	3.973394554
H	1	-5.466259187	-5.517395172	1.644042712
H	1	-2.068153916	-5.643326512	1.845789859
H	1	-1.743952525	-4.416988832	-2.873574029
H	1	-5.14120742	-4.285615081	-3.076776264
H	1	-3.275858897	-1.577940097	-3.970465478
C	6	13.91187926	-1.266758919	0.772708956
C	6	14.92526372	-3.724517641	1.257253597
C	6	17.52650934	-4.198082974	1.072249423
C	6	19.12465061	-2.228856214	0.407783971
C	6	18.22013326	0.155732319	-0.072319814
C	6	15.63895653	0.68510126	0.093125697
C	6	21.82573045	-2.216913145	0.096999635

C	6	22.57425091	0.180015298	-0.571963365
C	6	20.33879955	1.972930623	-0.754813251
C	6	23.55496201	-4.175330673	0.378398732
C	6	26.12640664	-3.674477697	-0.034865445
C	6	26.95386096	-1.207459317	-0.729604307
C	6	25.12111021	0.729679896	-0.994373815
C	6	20.55005202	4.129674893	1.175333975
C	6	20.02502945	3.003870636	-3.449260154
C	6	29.68326779	-0.594677871	-1.186899098
C	6	31.62685097	-2.411536025	-0.962909877
C	6	34.12956628	-1.708104423	-1.416122861
C	6	34.69916748	0.772595573	-2.084840196
C	6	32.74982064	2.529190365	-2.293522637
N	7	30.32218415	1.817614044	-1.846734722
H	1	13.747492	-5.30306245	1.756916045
H	1	15.0453936	2.591173377	-0.286161206
H	1	18.26616699	-6.068968393	1.43978223
H	1	22.93762632	-6.052055346	0.906142508
H	1	27.42986404	-5.22002789	0.194471701
H	1	25.65733886	2.632161534	-1.518413728
H	1	31.25846779	-4.346180799	-0.44979258
H	1	33.16419976	4.462852482	-2.811402044
H	1	35.6279867	-3.090438983	-1.247861659
H	1	36.63513507	1.329630102	-2.438521312
H	1	22.20923144	5.341178224	0.74330482

H	1	20.77630891	3.360934361	3.117159709
H	1	18.82563926	5.32609821	1.131643511
H	1	18.28922164	4.176237741	-3.58942113
H	1	21.67313507	4.192489385	-3.976739369
H	1	19.87468285	1.426667532	-4.828627844
C	6	5.38906388	-4.0496261	3.530159323
H	1	3.441625661	-3.496427714	4.011037895
H	1	6.26519754	-4.441101736	5.398984941
H	1	5.389101675	-5.823492987	2.407416422

Di-methylation in the 1 and 2 positions

E = -2556.4300943479

ATOM	CHARGE	X	Y	Z
C	6	-5.938048177	-5.437044023	2.289554212
C	6	-4.132963016	-7.354189935	2.690024944
C	6	-1.544737611	-6.824991069	2.44143149
C	6	-0.822692209	-4.373392853	1.793746805
C	6	-2.578209857	-2.485840051	1.398831868
C	6	-5.16258022	-2.982214376	1.638921555
C	6	1.662032904	-3.335914389	1.420828278
C	6	1.431089491	-0.822163086	0.804947682
C	6	-1.319614555	0.003231431	0.719229711
C	6	4.009545012	-4.49507231	1.618607
C	6	6.186887295	-3.0530791	1.155964284
C	6	6.010500271	-0.454441306	0.487794969

C	6	3.569408932	0.653486144	0.344326972
C	6	-2.080267059	0.885317728	-1.938405329
C	6	-1.87502392	2.047782669	2.70191132
H	1	-7.930046135	-5.857149007	2.484007016
C	6	8.300394634	1.180077188	-0.008711637
C	6	8.222953663	3.681885423	0.873525838
C	6	10.2219625	5.321789635	0.456727874
C	6	12.36986286	4.531978658	-0.886300386
C	6	12.3819571	2.015468355	-1.782918675
N	7	10.40723124	0.3848238	-1.3496423
H	1	-4.743609072	-9.240665594	3.190670049
H	1	-6.543648664	-1.506017126	1.330480479
H	1	-0.150422189	-8.28911297	2.746130908
H	1	4.164408056	-6.467133659	2.137261195
H	1	7.970902011	-3.972166232	1.404028614
H	1	3.32659804	2.620860972	-0.155089812
H	1	6.613474039	4.372807038	1.930298405
H	1	13.9626751	1.339003143	-2.864030913
H	1	10.04241964	7.196378917	1.219364591
C	6	10.59078033	-2.148864112	-2.493436749
H	1	-4.1330764	1.319614555	-2.007399225
H	1	-1.016899349	2.615645329	-2.469871866
H	1	-1.669043787	-0.608926405	-3.356531299
H	1	-1.316723274	1.388438375	4.616713972
H	1	-0.806856305	3.801845228	2.266253891

H	1	-3.92348689	2.506494756	2.728348587
H	1	12.25833123	-2.327972342	-3.758060277
H	1	10.90823539	-3.616935541	-1.053673416
H	1	8.897718121	-2.541586967	-3.670339197
C	6	14.57209283	6.317524052	-1.370977307
C	6	14.39872937	8.946850997	-0.769458628
C	6	16.42292826	10.59686524	-1.220781885
C	6	18.62532831	9.636563188	-2.26846487
C	6	18.86413298	7.123208727	-2.86839618
C	6	16.88105453	5.433037804	-2.442622017
C	6	20.93878755	10.91150462	-2.911538624
C	6	22.59583158	9.173259068	-3.9075565
C	6	21.44706715	6.543346308	-3.986849403
C	6	21.57861098	13.4495767	-2.671278862
C	6	23.98649983	14.23139413	-3.457801715
C	6	25.75031338	12.46824199	-4.460358043
C	6	25.00217086	9.90717195	-4.707704278
C	6	22.93314767	4.686898395	-2.323758253
C	6	21.22729202	5.566679226	-6.710813825
C	6	28.31389675	13.29068854	-5.377593243
C	6	29.20960798	12.20779996	-7.6268396
C	6	31.49727246	12.95958965	-8.661143325
C	6	32.97450906	14.82353977	-7.480669295
C	6	32.04128678	15.84703426	-5.196689775
N	7	29.78901686	15.08258341	-4.165749762

H	1	12.71944327	9.767105459	0.026928595
H	1	17.19197115	3.48790505	-2.937276692
H	1	16.26078977	12.58315623	-0.761672957
H	1	20.24599511	14.80239374	-1.913007412
H	1	24.44940711	16.21764732	-3.328355485
H	1	26.2728982	8.503672458	-5.479562858
H	1	28.10362694	10.81229401	-8.634025757
H	1	33.13092168	17.22963338	-4.175708618
H	1	32.04640794	12.08389062	-10.41114297
H	1	21.97577469	2.81935779	-2.271261665
H	1	24.87344272	4.417064421	-3.078609298
H	1	23.07994158	5.41381929	-0.358367636
H	1	20.14939232	6.9254678	-7.896031067
H	1	23.13245707	5.314551984	-7.555937081
H	1	20.23388197	3.717714627	-6.750252406
C	6	35.47550471	15.68232575	-8.60352558
C	6	36.60002396	14.36915516	-10.67978642
C	6	38.90518731	15.16189521	-11.7199294
C	6	40.09401393	17.26434765	-10.70008208
C	6	39.07042495	18.57415453	-8.707233742
C	6	36.77894321	17.82843086	-7.628483662
C	6	42.43398603	18.45011291	-11.41454968
C	6	42.84133536	20.49139493	-9.857094211
C	6	40.72215884	20.79773841	-7.94304745
C	6	44.12854111	17.80356206	-13.3150471

C	6	46.30248189	19.2853529	-13.63405175
C	6	46.7748	21.40760967	-12.0530314
C	6	44.99248604	21.99930178	-10.13454378
C	6	39.33309686	23.32135408	-8.295330168
C	6	41.69839129	20.50851584	-5.225508096
C	6	49.12333256	22.94064988	-12.46238384
C	6	49.72938659	25.07420721	-10.97594428
C	6	51.94900204	26.41587487	-11.46241644
C	6	53.55171644	25.64923193	-13.40384533
C	6	52.91276229	23.53959853	-14.84285277
N	7	50.74577571	22.25165579	-14.34787684
H	1	35.74403478	12.72303375	-11.50897929
H	1	36.06268037	18.94200859	-6.087242043
H	1	39.7362888	14.14624308	-13.28840197
H	1	43.78468657	16.19311868	-14.52724963
H	1	47.6155391	18.77459776	-15.11639061
H	1	45.23217889	23.57767651	-8.873057197
H	1	48.53604352	25.72234543	-9.459892706
H	1	54.13974248	22.92239513	-16.35695792
H	1	52.42489173	28.05232088	-10.33103749
H	1	55.27480639	26.68113571	-13.79046437
H	1	37.68922422	23.44284456	-6.995368764
H	1	40.61937665	24.9301912	-7.889965047
H	1	38.63550451	23.50913615	-10.26788285
H	1	42.69987047	18.67655878	-4.99361982

H	1	43.03342601	22.0591683	-4.756081263
H	1	40.10351925	20.57055555	-3.861806234

Di-methylation in the 1 and 3 positions

E = -2556.4455386916

ATOM	CHARGE	X	Y	Z
C	6	-34.33979829	-1.201695653	0.417761724
C	6	-33.54841884	-3.052304313	-1.326663232
C	6	-30.98294574	-3.274517192	-1.966618938
C	6	-29.26166993	-1.627243048	-0.83758325
C	6	-30.02122639	0.189369441	0.872807742
C	6	-32.56893607	0.43461808	1.530148927
C	6	-26.56744979	-1.448928504	-1.150691948
C	6	-25.67963763	0.474982627	0.359199116
C	6	-27.79989129	1.735354272	1.831220071
C	6	-24.954323	-2.885743864	-2.647884054
C	6	-22.36171343	-2.333282472	-2.611147781
C	6	-21.39886024	-0.328150918	-1.101634662
C	6	-23.10683238	1.061213423	0.424337971
C	6	-28.06626706	4.534151843	1.113086401
C	6	-27.44207167	1.416217347	4.692964415
H	1	-36.31987208	-1.040388643	0.903194536
C	6	-18.60431455	0.197003934	-1.051141183
C	6	-16.96888899	-1.890387392	-1.077672936
C	6	-14.37342594	-1.564730912	-0.914362816

C	6	-13.3185431	0.864417359	-0.719588759
C	6	-15.01268245	2.929226459	-0.737749026
N	7	-17.57756973	2.602549528	-0.923490193
H	1	-34.92255199	-4.306553245	-2.175754913
H	1	-33.17036026	1.856863653	2.870720543
H	1	-30.36426835	-4.691736093	-3.304337068
H	1	-25.67531015	-4.401096236	-3.816226043
H	1	-21.11099828	-3.447257044	-3.784138496
H	1	-22.45493361	2.540642104	1.674032664
H	1	-17.70225385	-3.79817916	-1.162030304
H	1	-14.30259901	4.834693864	-0.66537252
H	1	-13.23480934	-3.24845787	-0.901890625
C	6	-19.08143257	4.93989491	-1.115335175
H	1	-28.32378002	4.741341401	-0.961454788
H	1	-29.72642914	5.383980517	2.076865552
H	1	-26.34979115	5.602999759	1.67826565
H	1	-25.71480543	2.422817689	5.333713806
H	1	-29.09066862	2.199962303	5.729875962
H	1	-27.2494897	-0.615880597	5.189282049
H	1	-18.94709195	6.035010017	0.670701548
H	1	-18.32688388	6.119537461	-2.681369999
H	1	-21.07424311	4.649935354	-1.639412883
C	6	-10.47796368	1.248844316	-0.524928085
C	6	-9.425065056	3.669243156	0.053668218
C	6	-6.803901727	4.018785772	0.233362262

C	6	-5.225375815	1.963557582	-0.164349469
C	6	-6.167876651	-0.388811122	-0.723198136
C	6	-8.76938683	-0.796991935	-0.911566022
C	6	-2.51108679	1.822451743	-0.094013868
C	6	-1.791649209	-0.621020651	-0.613877487
C	6	-4.064649422	-2.314385212	-1.076728073
C	6	-0.747046478	3.707245546	0.392609471
C	6	1.826892599	3.077928997	0.346594643
C	6	2.628684438	0.567730379	-0.185892345
C	6	0.760860374	-1.298770877	-0.671778691
C	6	-4.225861946	-4.434884537	0.897941098
C	6	-4.053197682	-3.389998347	-3.772082044
C	6	5.401876222	-0.019501972	-0.21737518
C	6	6.352465086	-2.443453497	-0.730001149
C	6	8.954825641	-2.865089159	-0.732760149
C	6	10.67211413	-0.883012262	-0.223195536
C	6	9.617760415	1.520549119	0.282967569
N	7	7.074793947	1.869600406	0.268870214
H	1	-10.5854324	5.302079793	0.394650375
H	1	-9.394186933	-2.675096108	-1.371733197
H	1	-6.033857284	5.860512719	0.677769123
H	1	-1.338908657	5.621915916	0.798673792
H	1	3.192692056	4.552028651	0.726165005
H	1	1.234482399	-3.233453446	-1.08744282
H	1	5.13347844	-4.024228183	-1.128676641

H	1	10.77070114	3.142878879	0.679035239
H	1	9.570668443	-4.759501667	-1.129734887
H	1	-2.583765651	-5.730612955	0.719569862
H	1	-4.232419295	-3.634075355	2.839974701
H	1	-5.983836237	-5.551655904	0.634381014
H	1	-5.807184652	-4.485472502	-4.133265372
H	1	-2.407284141	-4.663768149	-4.047207251
H	1	-3.936129157	-1.838778975	-5.183726254
C	6	13.51431871	-1.313378459	-0.220436537
C	6	14.57077002	-3.706754217	-0.898300146
C	6	17.1916121	-4.102065996	-0.896996235
C	6	18.76751129	-2.119346593	-0.221211324
C	6	17.82300735	0.204241585	0.442554929
C	6	15.2219885	0.656641986	0.458447525
C	6	21.48066648	-2.034894738	-0.067217553
C	6	22.19734506	0.345271835	0.685573691
C	6	19.92387242	2.048481868	1.106755819
C	6	23.24578394	-3.919953103	-0.534508996
C	6	25.8163404	-3.352222724	-0.232568577
C	6	26.62448172	-0.893141194	0.515384969
C	6	24.74726572	0.95950837	0.994260431
C	6	19.95529856	4.317891601	-0.701844232
C	6	19.74209967	2.912842535	3.871198172
C	6	29.42138957	-0.38440806	0.820235565
C	6	30.92793582	-2.36571017	1.790326401

C	6	33.51663365	-2.057212402	2.078887559
C	6	34.63914979	0.198818071	1.383808546
C	6	33.15958882	2.135428161	0.398694389
N	7	30.59233938	1.867653988	0.124476251
H	1	13.41601516	-5.286413964	-1.441766442
H	1	14.60007967	2.511351351	1.003312219
H	1	17.96354627	-5.923176033	-1.416765368
H	1	22.65828702	-5.789005488	-1.119983901
H	1	27.1770565	-4.82658694	-0.622740302
H	1	25.19647248	2.812516982	1.660861273
H	1	30.09868626	-4.146077714	2.357886704
H	1	34.09405833	3.871746193	-0.155921291
H	1	34.65426759	-3.577818213	2.839294399
H	1	36.65868105	0.449433532	1.591565021
C	6	29.22774935	3.993161087	-1.044262581
H	1	20.08705026	3.669337642	-2.695542943
H	1	18.20233204	5.452766543	-0.487057976
H	1	21.60177902	5.55609676	-0.296857055
H	1	17.9833128	4.01617795	4.181453385
H	1	19.72286226	1.255156001	5.161333001
H	1	21.38166374	4.124667119	4.371446436
H	1	28.06131598	5.008983292	0.348748931
H	1	28.11135592	3.327164958	-2.692198128
H	1	30.5411278	5.469377235	-1.758201059

Full Methylation of the Trimer

E = -2596.00763434149

ATOM	CHARGE	X	Y	Z
C	6	-5.686884696	-5.834321117	2.3586048
C	6	-3.874391809	-7.75477405	2.706276587
C	6	-1.290796233	-7.220246157	2.423460196
C	6	-0.580712796	-4.760049688	1.795390866
C	6	-2.343524786	-2.869208762	1.452141038
C	6	-4.923435397	-3.370798731	1.72681271
C	6	1.897095919	-3.71576821	1.396564197
C	6	1.654851945	-1.194684769	0.816172654
C	6	-1.09743947	-0.370669753	0.784274079
C	6	4.248160712	-4.875190692	1.543055755
C	6	6.417018126	-3.425525195	1.065068464
C	6	6.228688034	-0.818742681	0.432633868
C	6	3.784724311	0.288598953	0.340925465
C	6	-1.900591912	0.544392263	-1.849588208
C	6	-1.622783295	1.648105623	2.801310907
C	6	8.509908554	0.82420399	-0.077346485
C	6	8.442615412	3.315580937	0.835447859
C	6	10.43457558	4.96209919	0.410864224
C	6	12.56441015	4.189598104	-0.969826274
C	6	12.56639436	1.684463951	-1.896869152
N	7	10.59884946	0.047016383	-1.45667638
C	6	10.76894369	-2.472366304	-2.633597726

H	1	12.4185422	-2.63384339	-3.92390263
H	1	11.10911327	-3.957331883	-1.216511105
H	1	9.059837714	-2.853032707	-3.791130482
H	1	-3.954516191	0.977763123	-1.880579714
H	1	-0.846899599	2.282222075	-2.375763512
H	1	-1.510873722	-0.931408145	-3.292847534
H	1	-1.033831293	0.965007473	4.69852021
H	1	-0.562798194	3.408479867	2.371171478
H	1	-3.670887217	2.104682319	2.86597733
H	1	-6.310191916	-1.892031453	1.458944052
H	1	-7.67525438	-6.258545704	2.579287001
H	1	-4.475797105	-9.647958236	3.192710954
H	1	0.109150573	-8.686881393	2.687624992
H	1	4.412434592	-6.853507034	2.034384512
H	1	8.205001266	-4.346275286	1.274204439
H	1	3.532559275	2.261888624	-0.129597408
C	6	14.75928909	5.981190621	-1.460342449
C	6	14.584017	8.607305032	-0.846710626
C	6	16.60315143	10.26276169	-1.301076343
C	6	18.80226335	9.310434277	-2.36329132
C	6	19.04210737	6.799971097	-2.975468054
C	6	17.06365875	5.104905783	-2.547747474
C	6	21.1115652	10.59130945	-3.009709889
C	6	22.76705965	8.859564554	-4.019636149
C	6	21.6212054	6.228650239	-4.106922592

C	6	21.74968787	13.1288524	-2.759377887
C	6	24.15459096	13.91669806	-3.549188864
C	6	25.9170439	12.1599332	-4.565256733
C	6	25.17022419	9.59965684	-4.82362007
C	6	23.11609204	4.366514251	-2.458079976
C	6	21.39209502	5.26417189	-6.834401905
C	6	28.47877535	12.98787884	-5.482586419
C	6	29.37087719	11.91778371	-7.739278296
C	6	31.65810704	12.6737119	-8.77173009
C	6	33.13878294	14.52898818	-7.581637355
C	6	32.20843304	15.54010497	-5.290892615
N	7	29.95652217	14.77170459	-4.262144685
C	6	29.33393305	15.85500891	-1.772657463
H	1	30.9418442	15.53511609	-0.458957751
H	1	29.01196153	17.92246362	-1.943696562
H	1	27.7273825	14.94824279	-0.810125531
H	1	22.16130799	2.497518557	-2.410421086
H	1	25.05376038	4.102576222	-3.221642658
H	1	23.26957559	5.084629023	-0.489949257
H	1	20.30788364	6.62698558	-8.009187859
H	1	23.29427431	5.01837523	-7.688047825
H	1	20.40082036	3.414167942	-6.878394725
H	1	17.37465096	3.161568269	-3.050452381
H	1	12.90635606	9.420265152	-0.038852766
H	1	16.44010587	12.24672831	-0.832310914

H	1	20.41841371	14.47662387	-1.989862568
H	1	24.61672345	15.90253552	-3.410634154
H	1	26.44017675	8.201013944	-5.605550889
C	6	35.6411014	15.39034418	-8.700600804
C	6	36.75851528	14.09280163	-10.79069444
C	6	39.06562504	14.88661882	-11.82586744
C	6	40.26363573	16.97442589	-10.78716065
C	6	39.2472844	18.26902047	-8.780838569
C	6	36.95398853	17.52229525	-7.706888393
C	6	42.60750067	18.15828253	-11.49199065
C	6	43.02620725	20.17694452	-9.914182833
C	6	40.91028107	20.47697632	-7.996375517
C	6	44.30504152	17.51961184	-13.39005033
C	6	46.48693804	18.99524217	-13.69954965
C	6	46.96367812	21.11415413	-12.11331366
C	6	45.18616406	21.66945011	-10.17844212
C	6	39.53478731	23.01125004	-8.323430394
C	6	41.88759065	20.15653548	-5.282747896
C	6	49.2955244	22.74937182	-12.35952606
C	6	50.39457013	23.66146696	-10.10188932
C	6	52.50907903	25.21160919	-10.17693033
C	6	53.53425538	25.89563331	-12.48226376
C	6	52.43080658	25.02422396	-14.70342879
N	7	50.35263711	23.46962198	-14.65926589
C	6	49.26802888	22.7549843	-17.12040722

H	1	50.18632233	23.77940476	-18.70828728
H	1	49.62401547	20.75170468	-17.5585213
H	1	47.22674687	23.23899982	-17.18664212
H	1	37.89255874	23.12909336	-7.021087935
H	1	40.83030786	24.60895668	-7.903741149
H	1	38.83687371	23.22163324	-10.29358312
H	1	42.87939444	18.3170762	-5.069265551
H	1	43.23177165	21.69535825	-4.800414235
H	1	40.29449496	20.21437999	-3.916816158
H	1	36.24484996	18.62370314	-6.153798193
H	1	35.89566639	12.45805637	-11.63489173
H	1	39.89118964	13.88290976	-13.40490357
H	1	43.96702623	15.90525672	-14.59902143
H	1	47.79774648	18.40821769	-15.12071808
H	1	45.44947848	23.25763252	-8.919279895
H	1	6.847705575	3.992537478	1.92281509
H	1	14.13314728	1.023475595	-3.008065827
H	1	10.26591753	6.827409918	1.198993345
H	1	28.26272298	10.52866503	-8.752946214
H	1	33.29991988	16.91567431	-4.262692705
H	1	32.2045591	11.80704577	-10.52694538
H	1	53.25678691	25.61391296	-16.4826625
H	1	55.17570916	27.11403414	-12.55679455
H	1	53.34962915	25.88792322	-8.438930446
H	1	49.63705457	23.14868982	-8.273352655

GAMESS File Headers:

Unmethylated Trimer

$BASIS GBASIS=N31 NGAUSS=6 NDFUNC=1 $END

$CONTRL SCFTYP=RHF RUNTYP=OPTIMIZE DFTTYP=m06 $END

$STATPT OPTTOL=0.0005 NSTEP=25 $END

$contrl nzvar=1 $end

$zmat dlc=.t. auto=.t. $end

$SYSTEM mwords=100 $END

$scf dirscf =.t. $end

Mono-methylation in the 1 position

$BASIS GBASIS=N31 NGAUSS=6 NDFUNC=1 $END

$CONTRL SCFTYP=RHF RUNTYP=OPTIMIZE DFTTYP=m06 ICHARG=1

$END

$STATPT OPTTOL=0.0005 NSTEP=25 $END

$contrl nzvar=1 $end

$zmat dlc=.t. auto=.t. $end

$SYSTEM mwords=100 $END

$scf dirscf =.t. $end

Mono-methylation in the 2 position

$BASIS GBASIS=N31 NGAUSS=6 NDFUNC=1 $END

$CONTRL SCFTYP=RHF RUNTYP=OPTIMIZE DFTTYP=m06 ICHARG=1

$END

$STATPT OPTTOL=0.0005 NSTEP=25 $END

$contrl nzvar=1 $end

$zmat dlc=.t. auto=.t. $end

$SYSTEM mwords=100 $END

$scf dirscf =.t. $end

Di-methylation in the 1 and 2 positions

$BASIS GBASIS=N31 NGAUSS=6 NDFUNC=1 $END

$CONTRL SCFTYP=RHF RUNTYP=OPTIMIZE DFTTYP=m06 ICHARG=2 $END

$STATPT OPTTOL=0.0005 NSTEP=25 $END

$contrl nzvar=1 $end

$zmat dlc=.t. auto=.t. $end

$SYSTEM mwords=100 $END

$scf dirscf =.t. $end

Di-methylation in the 1 and 3 positions

$BASIS GBASIS=N31 NGAUSS=6 NDFUNC=1 $END

$CONTRL SCFTYP=RHF RUNTYP=OPTIMIZE DFTTYP=m06 ICHARG=2 $END

$STATPT OPTTOL=0.0005 NSTEP=25 $END

$contrl nzvar=1 $end

$zmat dlc=.t. auto=.t. $end

$SYSTEM mwords=100 $END

$scf dirscf =.t. $end

Full Methylation of the Trimer

$BASIS GBASIS=N31 NGAUSS=6 NDFUNC=1 $END

$CONTRL SCFTYP=RHF RUNTYP=OPTIMIZE DFTTYP=m06 ICHARG=3 $END

$STATPT OPTTOL=0.0005 NSTEP=25 $END

$contrl nzvar=1 $end

$zmat dlc=.t. auto=.t. $end

$SYSTEM mwords=100 $END

$scf dirscf =.t. $end

2.5 References

(1) Iijima, S.; Ichihashi, T. *Nature* **1993**, 363, 603–605.

(2) Saito, R.; Dresselhaus, G.; Dresselhaus, M. S. *Physical Properties of Carbon Nanotubes*, **1998**.

(3) Ajayan, P. M. *Chem. Rev.* **1999**, 99, 1787–1800.

(4) Yu, M.; Files, B.; Arepalli, S.; Ruoff, R. *Phys. Rev. Lett.* **2000**, 84, 5552–5555.

(5) Terrones, M. *Annu. Rev. Mater. Res.* **2003**, 33, 419–501.

(6) Avouris, P.; Chen, Z.; Perebeinos, V. *Nat. Nanotechnol.* **2007**, 2, 605–615.

(7) Avouris, P. *Acc. Chem. Res.* **2002**, 35, 1026–1034.

(8) Han, Z.; Fina, A. *Prog. Polym. Sci.* **2011**, 36, 914–944.

(9) O'Connell, M. J.; Bachilo, S. M.; Huffman, C. B.; Moore, V. C.; Strano, M. S.; Haroz, E. H.; Rialon, K. L.; Boul, P. J.; Noon, W. H.; Kittrell, C.; et al. *Science* **2002**, 297, 593–596.

(10) Weisman, R. B.; Bachilo, S. M. *Nano Lett.* **2003**, 3, 1235–1238.

(11) Kataura, H.; Kumazawa, Y.; Maniwa, Y.; Umezu, I.; Suzuki, S.; Ohtsuka, Y.; Achiba, Y. *Synth. Met.* **1999**, 103, 2555–2558.

(12) Dürkop, T.; Getty, S. A.; Cobas, E.; Fuhrer, M. S. *Nano Lett.* **2004**, 4, 35–39.

(13) Rowell, M. W.; Topinka, M. A.; McGehee, M. D.; Prall, H. J.; Dennler, G.; Sariciftci, N. S.; Hu, L.; Gruner, G. *Appl. Phys. Lett.* **2006**, 88, 86–89.

(14) Wang, H.; Wei, P.; Li, Y.; Han, J.; Lee, H. R.; Naab, B. D.; Liu, N.; Wang, C.; Adijanto, E.; Tee, B. C.-K.; et al. *Proc. Natl. Acad. Sci. U. S. A.* **2014**, 111, 4776–4781.

(15) Tee, B. C.-K.; Chortos, A.; Berndt, A.; Nguyen, A. K.; Tom, A.; McGuire, A.; Lin, Z. C.; Tien, K.; Bae, W.-G.; Wang, H.; et al. *Science* **2015**, 350, 313–316.

(16) Hecht, D. S.; Thomas, D.; Hu, L.; Ladous, C.; Lam, T.; Park, Y.; Irvin, G.; Drzaic, P. *J. SID* **2009**, 17, 941–946.

(17) Jiang, C.; Saha, A.; Xiang, C.; Young, C. C.; Tour, J. M.; Pasquali, M.; Martí, A. A. *ACS Nano* **2013**, 7, 4503–4510.

(18) Jiang, C.; Saha, A.; Young, C. C.; Hashim, D. P.; Ramirez, C. E.; Ajayan, P. M.; Pasquali, M.; Martí, A. A. *ACS Nano* **2014**, 8, 9107–9112.

(19) Behabtu, N.; Young, C. C.; Tsentalovich, D. E.; Kleinerman, O.; Wang, X.; Ma, A. W. K.; Bengio, E. A.; ter Waarbeek, R. F.; de Jong, J. J.; Hoogerwerf, R. E.; et al. *Science* **2013**, 339, 182–186.

(20) Serpell, C. J.; Kostarelos, K.; Davis, B. G. *ACS Cent. Sci.* **2016**, 2, 190–200.

(21) Jariwala, D.; Sangwan, V. K.; Lauhon, L. J.; Marks, T. J.; Hersam, M. C. *Chem. Soc. Rev.* **2013**, 42, 2824–2860.

(22) De Volder, M. F. L.; Tawfick, S. H.; Baughman, R. H.; Hart, A. J. *Science* **2013**, 339, 535–539.

(23) Bladh, K.; Falk, L. K. L.; Rohmund, F. *Appl. Phys. A Mater. Sci. Process.*

2000, 70, 317–322.

(24) Kong, J. *Chem. Phys. Lett.* **1998**, 292, 567–574.

(25) Journet, C.; Maser, W. K.; Bernier, P.; Loiseau, A.; Lamy De La Chapelle, M.; Lefrant, S.; Deniard, P.; Lee, R.; Fischer, J. E. *Nature* **1997**, 388, 20–22.

(26) Guo, T.; Nikolaev, P.; Thess, A.; Colbert, D. T.; Smalley, R. E. *Chem. Phys. Lett.* **1995**, 243, 49–54.

(27) Kim, K. S.; Cota-Sanchez, G.; Kingston, C. T.; Imris, M.; Simard, B.; Soucy, G. *J. Phys. D. Appl. Phys.* **2007**, 40, 2375–2387.

(28) Arnold, M. S.; Green, A. A.; Hulvat, J. F.; Stupp, S. I.; Hersam, M. C. *Nat. Nanotechnol.* **2006**, 1, 60–65.

(29) Liu, H.; Feng, Y.; Tanaka, T.; Urabe, Y.; Kataura, H. *J. Phys. Chem. C* **2010**, 114, 9270–9276.

(30) Tanaka, T.; Jin, H.; Miyata, Y.; Kataura, H. *Appl. Phys. Express* **2008**, 1, 1140011–1140013.

(31) Nish, A.; Hwang, J.-Y.; Doig, J.; Nicholas, R. J. *Nat. Nanotechnol.* **2007**, 2, 640–646.

(32) Ding, J.; Li, Z.; Lefebvre, J.; Cheng, F.; Dubey, G.; Zou, S.; Finnie, P.; Hrdina, A.; Scoles, L.; Lopinski, G. P.; et al. *Nanoscale* **2014**, 6, 2328–2339.

(33) Hwang, J.-Y.; Nish, A.; Doig, J.; Douven, S.; Chen, C.-W.; Chen, L.-C.; Nicholas, R. J. *J. Am. Chem. Soc.* **2008**, 130, 3543–3553.

(34) Jakubka, F.; Schießl, S. P.; Martin, S.; Englert, J. M.; Hauke, F.; Hirsch, A.; Zaumseil, J. *ACS Macro Lett.* **2012**, 1, 815–819.

(35) Berton, N.; Lemasson, F.; Hennrich, F.; Kappes, M. M.; Mayor, M. *Chem. Commun.* **2012**, 48, 2516–2518.

(36) Ozawa, H.; Fujigaya, T.; Niidome, Y.; Hotta, N.; Fujiki, M.; Nakashima, N.

J. Am. Chem. Soc. **2011**, 133, 2651–2657.

(37) Gao, J.; Kwak, M.; Wildeman, J.; Herrmann, A.; Loi, M. A. *Carbon* **2011**, 49, 333–338.

(38) Rice, N. A.; Subrahmanyam, A. V.; Coleman, B. R.; Adronov, A. *Macromolecules* **2015**, 48, 5155–5161.

(39) Wang, H.; Bao, Z. *Nano Today* **2015**, 10, 737–758.

(40) Wang, H.; Hsieh, B.; Jiménez-Osés, G.; Liu, P.; Tassone, C. J.; Diao, Y.; Lei, T.; Houk, K. N.; Bao, Z. *Small* **2015**, 11, 126–133.

(41) Wang, J.; Nguyen, T. D.; Cao, Q.; Wang, Y.; Tan, M. Y. C.; Chan-Park, M. B. *ACS Nano* **2016**, 10, 3222–3232.

(42) Rice, N. A.; Subrahmanyam, A. V.; Laengert, S. E.; Adronov, A. *J. Polym. Sci. Part A Polym. Chem.* **2015**, 53, 2510–2516.

(43) Tange, M.; Okazaki, T.; Iijima, S. *ACS Appl. Mater. Interfaces* **2012**, 4, 6458–6462.

(44) Berton, N.; Lemasson, F.; Poschlad, A.; Meded, V.; Tristram, F.; Wenzel, W.; Hennrich, F.; Kappes, M. M.; Mayor, M. *Small* **2014**, 10, 360–367.

(45) Jo, J.; Chi, C.; Höger, S.; Wegner, G.; Yoon, D. Y. *Chem. Eur. J.* **2004**, 10, 2681–2688.

(46) Schmidt, M. W.; Baldridge, K. K.; Boatz, J. A.; Elbert, S. T.; Gordon, M. S.; Jensen, J. H.; Koseki, S.; Matsunaga, N.; Nguyen, K. A.; Su, S.; Windus, T. L.; Dupuis, M.; Montgomery, J. A. *J. Comput. Chem.* **1993**, 14, 1347–1363.

(47) Imin, P.; Imit,; Adronov, A. *Macromolecules* **2012**, 45, 5045–5050.

(48) Strano, M. S.; Dyke, C. A.; Usrey, M. L.; Barone, P. W.; Allen, M. J.; Shan, H.; Kittrell, C.; Hauge, R. H.; Tour, J. M.; Smalley, R. E. *Science* **2003**, 301, 1519–1522.

(49) Dresselhaus, M. S.; Jorio, A.; Hofmann, M.; Dresselhaus, G.; Saito, R. *Nano Lett.* **2010**, 10, 751–758.

(50) Dresselhaus, M. S.; Dresselhaus, G.; Saito, R.; Jorio, A. *Phys. Rep.* **2005**, 409, 47–99.

(51) Doorn, S. K. *J. Nanosci. Nanotechnol.* **2005**, 5, 1023–1034.

(52) Strano, M. S.; Zheng, M.; Jagota, A.; Onoa, G. B.; Heller, D. A.; Barone, P. W.; Usrey, M. L. *Nano Lett.* **2004**, 4, 543–550.

(53) Strano, M. S.; Doorn, S. K.; Haroz, E. H.; Kittrell, C.; Hauge, R. H.; Smalley, R. E. *Nano Lett.* **2003**, 3, 1091–1096.

(54) Brown, S.; Jorio, A.; Corio, P.; Dresselhaus, M.; Dresselhaus, G.; Saito, R.; Kneipp, K. *Phys. Rev. B* **2001**, 63, 1–8.

(55) Doorn, S. K.; Heller, D. A.; Barone, P. W.; Usrey, M. L.; Strano, M. S. *Appl. Phys. A* **2004**, 78, 1147–1155.

(56) Heller, D. A.; Barone, P. W.; Swanson, J. P.; Mayrhofer, R. M.; Strano, M. S. *J. Phys. Chem. B* **2004**, 108, 6905–6909.

(57) van der Pauw, L. J. *Philips Tech. Rev.* **1958**, 20, 220–224.

(58) Xia, C.; Advincula, R. C. *Macromolecules* **2001**, 34, 5854–5859.

(59) Jo, J.; Chi, C.; Höger, S.; Wegner, G.; Yoon, D. Y. *Chem. - A Eur. J.* **2004**, 10, 2681–2688.

(60) Rice, N. A.; Adronov, A. *J. Polym. Sci. Part A Polym. Chem.* **2014**, 52, 2738–2747.

(61) Hanwell, M. D.; Curtis, D. E.; Lonie, D. C.; Vandermeerschd, T.; Zurek, E.; Hutchison, G. R. J. *Cheminform.* **2012**, 4.

(62) Zhao, Y.; Truhlar, D. G. *Theor. Chem. Acc.* **2007**, 120, 215–241.

Chapter 3

Investigation of Hybrid Conjugated/Nonconjugated Polymers for Sorting of Single-Walled Carbon Nanotubes

This chapter has been reprinted with permission from Macromolecules. Fong, D.; Adronov, A. **2017**, *50*, 8002-8009. Copyright (2017) American Chemical Society.

Abstract

Structure–selectivity relationships between conjugated polymer backbone structure and enriched semiconducting carbon nanotube dispersions remain unclear. A significant focus has been on the structure of the aromatic monomer incorporated into the conjugated polymer backbone, particularly with respect to derivatives of fluorene, thiophene, and carbazole. Less attention has been given to challenging the necessity of complete backbone conjugation in preparing samples of enriched semiconducting carbon nanotubes. Here, we synthesize and study a series of polymer backbone structures containing nonconjugated flexible linkers with lengths of 3–12 carbon atoms and incorporation percentages of 5–50%. We prepare nanotube dispersions with HiPCO starting material and characterize the dispersions using UV/vis–NIR, Raman, and fluorescence spectroscopy. We find that at an optimized alkyl spacer length (six carbon atoms) and incorporation percentage (25%) an enriched sample of semiconducting carbon nanotubes can be prepared in THF, showing that complete polymer conjugation is not necessary for nanotube sorting. Furthermore, we demonstrate that these polymers are efficient at dispersing higher average diameter plasma torch carbon nanotubes in both THF and toluene and that enriched, concentrated dispersions of semiconducting tubes can be achieved in toluene.

3.1 Introduction

Single-walled carbon nanotubes (SWNTs) have attracted significant attention since their discovery in the early 1990s.[1] Their structural,[2–4] mechanical,[5–7] and opto-electronic properties[8–10] make SWNTs potentially valuable in a multitude of applications, including flexible electronics,[11] sensors,[12] and high-strength fibers,[13–15] among others.[16–19] Although SWNTs possess many interesting attributes, all commercial synthetic methods produce an impure mixture of leftover metal catalyst particles, amorphous carbon, and both semiconducting and metallic SWNTs.[20–24] Furthermore, intertube π–π interactions result in the formation of SWNT bundles that are insoluble in typical aqueous and organic solvents.[25] In order to render SWNTs processable, nanotube exfoliation and solubilization are necessary, using either covalent or noncovalent functionalization.[26–28] Covalent functionalization typically destroys many of the interesting SWNT properties, as this method breaks the extended π-system of the SWNT sidewall.[28] A notable exception was reported recently, where SWNTs could be functionalized via a [2 + 1] cycloaddition with an electron-poor nitrene, generated *in situ* from azidodichlorotriazine.[29] Noncovalent functionalization, in contrast, maintains the integrity of the SWNT sidewall and thus preserves desirable SWNT properties. To noncovalently functionalize SWNTs, bundles are temporarily perturbed using sonication, and then a dispersant is used to coat the SWNT sidewall, preventing reaggregation. Several dispersant categories have been identified, including surfactants,[30–32] small molecule aromatic compounds,[33–35] biomacromolecules,[36–38] and conjugated polymers.[39–41]

Of the aforementioned dispersants, numerous researchers have focused on conjugated polymers, as these macromolecules offer a synthetic diversity that enables

the fine-tuning of polymer structure for various purposes, including the isolation of specific subtypes of SWNTs.[42–44] Though many conjugated polymers are capable of exfoliating SWNTs effectively, polymer structure–selectivity relationships are poorly understood. To date, the primary focus of investigations on polymer backbone structure has been on variation of the aromatic monomer. A significant bulk of this work has involved modification of three core aromatic units: fluorene,[45–47] thiophene,[48–50] and carbazole.[51–53] Though these studies provide substantial insight into the nature of the aromatic backbone and the consequent SWNT selectivity, it is unclear whether a fully conjugated polymer backbone is necessary for efficient polymer wrapping and dispersion of SWNTs. Recently, nonconjugated flexible linkers (NCLs) have been incorporated into conjugated polymer backbones to modify the solid-phase morphology of organic semiconductors.[54–57] In these exploratory studies, the general theme was that the incorporation of NCLs into conjugated polymer backbones could enhance charge mobility through improved thin film morphology. To the best of our knowledge, NCLs within conjugated polymers have not been examined for any purpose outside of semiconductor applications. We thus wish to expand the scope of NCLs by investigating their impact on conjugated polymers as a SWNT dispersant. In this work, we examine the consequences of introducing a NCL into the conjugated polymer backbone to produce a hybrid conjugated/nonconjugated structure. We examine the effect of the NCL length and percent incorporation on SWNT dispersion quality, concentration, and subtypes dispersed and find that both the NCL length and percent incorporation are important factors in obtaining high quality SWNT dispersions. At a medium length of six carbon atoms, it is possible to prepare an enriched dispersion of sc-SWNTs using NCL-containing polymers, which demonstrates that

a fully conjugated polymer is not necessarily required to sort SWNTs.

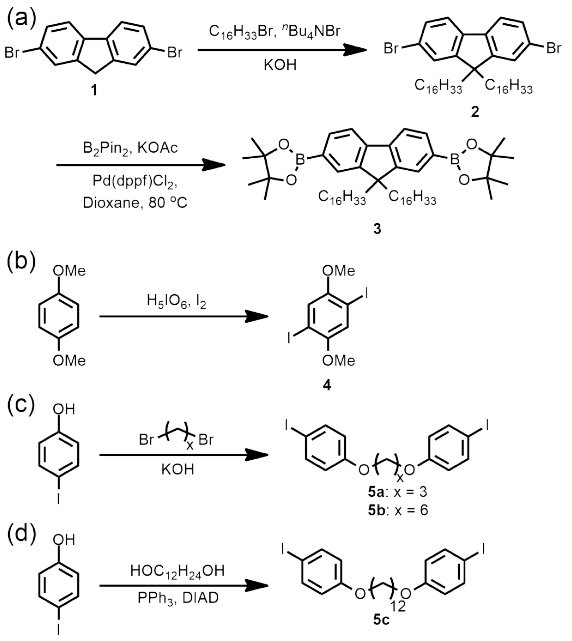
3.2 Results and Discussion

For this work we decided to use poly(fluorene-*co*-dimethoxybenzene) (PFdOMB) as the backbone scaffold, as we have previously used this polymer structure to prepare high quality SWNT dispersions.[58] If NCLs deleteriously affect SWNT dispersion quality, a direct comparison with this polymer should be instructive. PFdOMB can be prepared by Suzuki polycondensation between a boronic ester-containing fluorene monomer and an aryl halide-containing benzene monomer, and thus the monomers 2,2′-(9,9-dihexadecylfluorene-2,7-diyl)bis(4,4,5,5-tetramethyl-1,3,2-dioxaborolane) (**3**) and 1,4-diiodo-2,5-dimethoxybenzene (dOMB) (**4**) were prepared following modified literature procedures (Scheme 3.1a,b).[58] To prepare the NCL monomer, 4-iodophenol was alkylated with a terminally functionalized dibromoalkane (n = 3 or 6) using KOH in DMSO (Scheme 3.1c). The reaction mixture was then poured into water, and the slurry was filtered. The crude material was purified by flash chromatography to afford the NCL monomers **5a** (n = 3) and **5b** (n = 6). To prepare the 12-carbon NCL (**5c**), 1,12-dodecanol was coupled to 4-iodophenol using the Mitsunobu reaction (Scheme 3.1d).[59] With monomers **5a**–**c** in hand, we prepared a series of NCL-containing PFdOMB polymers with varying lengths of NCL. To prepare PFdOMB with NCLs, the ratio between the aryl iodide monomers **4** and **5** was varied, while maintaining an overall 1:1 stoichiometry of boronic ester:aryl iodide. The amount of NCL was varied from 10% to 50%, and the length of alkyl spacer was varied from 3 to 12 carbon atoms, resulting in a total of nine polymers (Table 3.1). The polymer naming convention

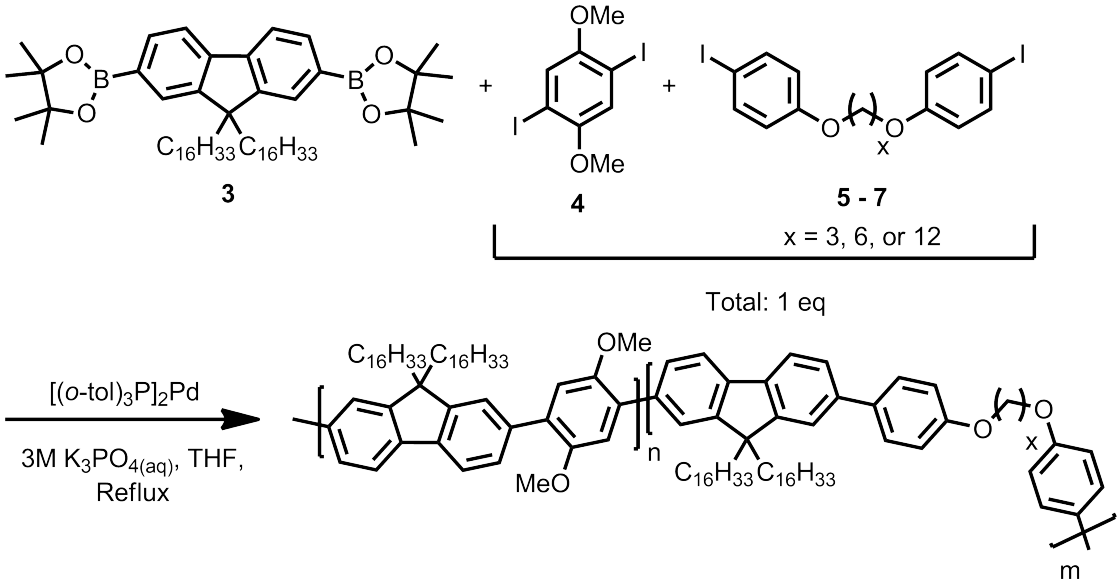
used hereafter is PFdOMB-Cα-β, where α refers to the NCL alkyl spacer length (3, 6, or 12) and β refers to the NCL feed percentage (10–50%). The percentage of NCL incorporation was controlled by the stoichiometry of monomers **4** and **5** used in the polymerization reaction, and the ratios were verified using ^{1}H NMR. The integration of the methoxy group resonance at ~3.84 ppm from monomer **4** was compared to the integration of the resonance for the methylene group adjacent to the oxygen atom from monomer **5**, which appears slightly above 4 ppm. A reference polymer, PFdOMB-C6-100, was prepared to unequivocally confirm the location of these resonances (NMR spectra can be found in the Supporting Information, Figure S3.5). If monomers **4** and **5** were incorporated in a 1:1 ratio, their expected ^{1}H integration ratio would be 6:4. To calculate the percent incorporation of the NCL, the incorporation (I) of the two monomers based on ^{1}H NMR integration (i) can be defined, where $I_{NCL} = \frac{i_{NCL}}{4}$ and $I_{DMB} = \frac{i_{NCL}}{6}$. The percentage of NCL can then be calculated as

$$\%NCL = \frac{I_{NCL}}{I_{NCL} + I_{DMB}} \times 100\% \tag{3.1}$$

Calculations based on ^{1}H NMR data indicated that the feed stoichiometry roughly matched the incorporated stoichiometry in most cases, as shown in Table 3.1. Unexpectedly, the NCL incorporation in the PFdOMB-C3 series, as determined by ^{1}H NMR, was consistently half of what was expected. The reason for this discrepancy is unclear, as the polymerization conditions were kept constant between all polymer series.



SCHEME 3.1: Synthesis of Monomers **3** (a), **4** (b), **5a,b** (c), and **5c** (d)



SCHEME 3.2: Synthesis of PFdOMB-Cα-β Copolymers

Polymer	Feed Ratio	Integration	% NCL	M_n (kDa)	Đ
PFdOMB-C3-10	0.1:0.9	0.2:6	5	21.6	4.56
PFdOMB-C3-25	0.25:0.75	0.5:6	11	16.5	2.47
PFdOMB-C3-50	0.5:0.5	1.5:6	27	6.8	1.72
PFdOMB-C6-10	0.1:0.9	0.4:6	9	54.4	2.65
PFdOMB-C6-25	0.25:0.75	1:6	20	24.7	3.61
PFdOMB-C6-50	0.5:0.5	4:6	50	35.9	2.87
PFdOMB-C12-10	0.1:0.9	0.4:6	9	17.1	2.38
PFdOMB-C12-25	0.25:0.75	1:6	20	10.0	2.73
PFdOMB-C12-50	0.5:0.5	4:6	50	16.5	2.12

TABLE 3.1: Summary of PFdOMB-Cα-β Attributes, Including % NCL (by ^{1}H NMR Integration), M_n, and Dispersity

Gel permeation chromatography (GPC) analysis of our polymer series was also performed, and molecular weight values are recorded in Table 3.1. Previously, we have demonstrated that molecular weight is an important factor in the preparation of polymer–SWNT dispersions.[60] In this study, we maintained identical polymerization conditions in an attempt to achieve constant molecular weights. However, as seen from the data in Table 3.1, the different NCL monomers seem to exhibit different reactivity in the polymerizations, leading to significant molecular weight differences and the possibility for formation of tapered or gradient copolymers. Nevertheless, NMR analysis showed that the NCL monomers were incorporated within all the prepared polymers. Although molecular weight could not be kept identical between the polymers, the primary question we sought to address was whether complete backbone conjugation was necessary to disperse and sort SWNTs, which we could still probe by varying the length of the NCL and degree of NCL incorporation.

We first set out to identify the key polymer parameters involved in obtaining stable polymer–SWNT dispersions. Supramolecular polymer–SWNT complexes

were prepared with raw HiPCO SWNTs following previously reported literature procedures.[58] Polymer:SWNT mass ratios were previously optimized for PFdOMB, and thus to compare the NCL-containing polymers to the fully conjugated polymer, a mass ratio of 1.5:1 polymer:SWNT, which is consistent with previous studies, was used.[58] Additionally, THF and toluene were examined as solvents for dispersion optimization studies. To prepare polymer–SWNT dispersions, 6 mg of polymer and 4 mg of HiPCO SWNTs were added to 8 mL of solvent. The mixture was sonicated for 2 h in a bath sonicator that was chilled with ice, and then the black suspension was centrifuged at 8346 *g* for 30 min. The supernatant was carefully removed, and the resulting polymer–SWNT dispersions were analyzed as isolated. Any stable dispersions produced had no observable flocculation for at least several months.

To investigate the polymer–SWNT dispersions, we initially performed UV/vis–NIR absorption spectroscopy (Figure 3.1). Nanotube absorption features depend on their respective diameters and chiralities and arise from the interband transitions of the van Hove singularities, resulting in specific nanotube chiralities having specific transition energies. The absorption features in the observed range can be grouped into three categories: two semiconducting regions, S_{11} (830–1600 nm) and S_{22} (600–800 nm), and a metallic region, M_{11} (440–645 nm).[61] For the PFdOMB-C3 series in THF, only PFdOMB-C3-10–SWNT produced a stable dispersion (Figure 3.1a). To maintain the same absorption intensity scale between each polymer series, the spectrum for the as-produced PFdOMB-C3-10–SWNT dispersion was divided by a factor of 4. The absorption spectrum for PFdOMB-C3-10–SWNT in THF indicated the presence of sharp peaks in the S_{11} and S_{22} regions corresponding to semiconducting SWNTs (sc-SWNTs) as well as signals in the M_{11} region

and a broad, featureless absorption background, both of which can be attributed to the presence of metallic SWNTs (m-SWNTs). Conversely, with the longer NCL of the PFdOMB-C6 series in THF, all polymers produced stable SWNT dispersions (Figure 3.1b). The absorption spectrum for PFdOMB-C6-10–SWNT did not possess sharp peaks, which indicated that bundles were dispersed. However, the absorption spectra for SWNT dispersions prepared using PFdOMB-C6-25 and PFdOMB-C6-50 had relatively sharp peaks, although some peak broadness suggested mild bundling of SWNTs. The absence of a broad, featureless absorption background in these spectra suggested that a significant proportion of m-SWNTs was removed from the dispersions in THF. Interestingly, the most intense absorption from both of these polymer–SWNT dispersions occurs slightly above 1400 nm, which is consistent with predominantly the presence of the (9,8) species (Figure 3.1b). Precise assignment of a SWNT species based on absorption spectra alone is difficult, and this peak may contain other SWNT species as well. Nonetheless, the (9,8) structure has a diameter of 1.170 nm, which seems to indicate that these two polymers may be selective for SWNTs in the upper diameter range of the HiPCO starting material (which contains species with diameters ranging from 0.8 to 1.2 nm).[62] Finally, for the PFdOMB-C12 series in THF, stable SWNT dispersions could only be produced using PFdOMB-C12-10 and PFdOMB-C12-25 (Figure 3.1c). However, the peaks for both samples were ill-defined, suggesting that SWNT bundles were dispersed. In terms of solvent, switching from THF to toluene resulted in no stable polymer–SWNT dispersions with any of the samples (see Figure S3.6).

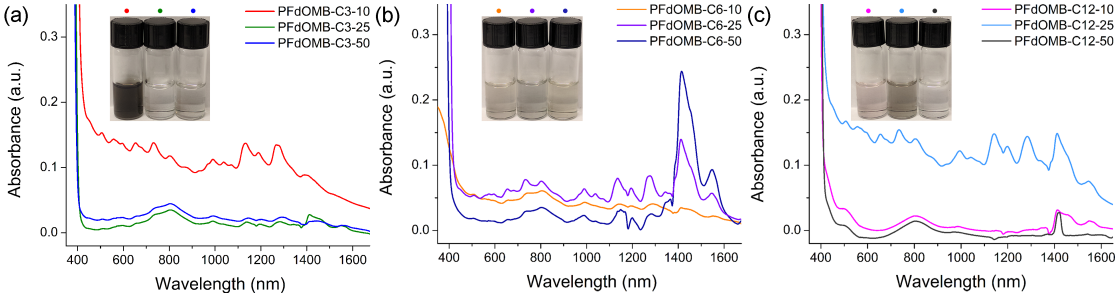


FIGURE 3.1: UV/vis–NIR spectra for polymer–SWNT dispersions produced in THF for the (a) PFdOMB-C3 series, (b) PFdOMB-C6 series, and (c) PFdOMB-C12 series. Photographs of the polymer–SWNT dispersions are color-coded with the appropriately colored dot above each dispersion. Note that the spectrum for the PFdOMB-C3-10–SWNT dispersion (red trace) was divided by a factor of 4.

Within the series of NCL-containing polymers, the results in aggregate suggest that alkyl spacer length and percent incorporation can influence both the SWNT subtypes dispersed and the SWNT exfoliation efficiency. It should be noted that we assume statistical incorporation of monomers in the copolymer, but deviation from such a statistical incorporation could also have an influence on the nanotube dispersions. Interestingly, the removal of a significant proportion of m-SWNTs was accomplished for some polymers in the C6-NCL series, despite the lack of full conjugation along the polymer length. We hypothesize that alkyl spacer length influences the ability for the conjugated fragments to organize on the nanotube surface. A previous study on alkyl chain folding demonstrated that the average length of a folded alkane chain segment was between six and ten carbons at 293 K.[63] This suggests that a length of six to ten carbons provides enough flexibility to allow for chain folding and reorganization, which may allow for conjugated fragments in the NCL-containing polymers to adopt a thermodynamically ideal arrangement on the nanotube surface. Too short of an alkyl spacer may prohibit reorganization, while too long of an alkyl spacer may result in an entropic penalty

that disallows optimal conjugated fragment arrangement. Although we could not maintain consistent molecular weights within the polymer series, which precluded absolute comparison, the results nonetheless demonstrate that complete backbone conjugation is not necessary to produce stable SWNT dispersions.

To further investigate the nanotube populations dispersed by the PFdOMB-Cα-β polymers, resonance Raman spectroscopy was performed. This technique allows for the examination of both m- and sc-SWNT species within a given sample[64] and utilizes laser excitation wavelengths that overlap with the van Hove singularities present in the 1D density of states for a particular SWNT.[65] As the electronic transitions depend on nanotube chirality and diameter, only a subset of the total nanotube population will be observed for each individual excitation wavelength.[66] Thin film samples were prepared from the polymer–SWNT complexes by drop-casting the dispersions onto silicon wafers. A reference SWNT sample was also prepared by sonicating a small amount of the SWNT starting material in $CHCl_3$ and making a solid film with the same drop-casting method. Raman spectra were collected using three excitation wavelengths: 514, 633, and 785 nm. These excitation wavelengths have previously been shown to adequately allow characterization of HiPCO SWNT electronic character, as both m- and sc-SWNTs can be separately probed.[67] Figure 3.2 shows the radial breathing mode (RBM) regions for SWNT complexes at each excitation wavelength, prepared using only the polymers that produced stable and concentrated dispersions, including PFdOMB-C3-10, PFdOMB-C6-10, PFdOMB-C6-25, and PFdOMB-C6-50 (full Raman spectra are provided in Figure S3.7). All Raman spectra were normalized to the G-band at ~1590 cm^{-1} and offset for clarity. Upon excitation at 514 nm, two dominant RBM features are

expected in the Raman spectrum: a broad peak arising from sc-SWNTs centered at 180 cm^{-1} and several sharp peaks from 225 to 290 cm^{-1} arising from m-SWNTs.[68] The SWNT dispersions prepared using PFdOMB-C3-10, PFdOMB-C6-10, and PFdOMB-C6-50 all exhibit peaks in both of these regions (Figure 3.2a). However, the PFdOMB-C6-25–SWNT sample exhibits no RBM signals with this excitation wavelength, indicating the absence of both small diameter m- and sc-SWNTs. This observation is corroborated by analysis of the G-band region at this excitation wavelength, which is shown in the inset of Figure 3.2a. The G-band consists of two peaks: a lower frequency G^- and a higher frequency G^+. For sc-SWNTs, both the G^- and G^+ have Lorentzian line shapes, but for m-SWNTs the G– exhibits a broader Breit–Wigner–Fano (BWF) line shape.[69] A broad G^- is observed for the SWNT dispersions prepared using PFdOMB-C3-10, PFdOMB-C6-10, and PFdOMB-C6-50, confirming that m-SWNTs are present. The PFdOMB-C6-25–SWNT sample, however, lacks a BWF line shape in the G-band, which is consistent with the absence of m-SWNTs. At the 633 nm excitation wavelength, both m- and sc-SWNTs are in resonance. For HiPCO SWNTs at this wavelength, m-SWNT features are found at ∼175–230 cm^{-1}, while sc-SWNTs give rise to peaks at ∼230–300 cm^{-1}.[61,67] Both m- and sc-SWNT features are observed in the SWNT dispersions prepared using PFdOMB-C3-10, PFdOMB-C6-10, and PFdOMB-C6-50. However, in the PFdOMB-C6-25–SWNT sample, only sc-SWNT features are observed, again indicating the enrichment of sc-SWNTs. Finally, for the 785 nm excitation, it is mainly semiconducting HiPCO SWNTs that are in resonance, with only a few large diameter metallic species exhibiting absorptions in the low-frequency region.[68,70] At this excitation wavelength, none of the polymer–SWNT samples prepared exhibit any signals below 200 cm^{-1}, which indicates the

absence of large diameter m-SWNTs in all samples, but all four samples exhibited signals corresponding to sc-SWNTs (Figure 3.3c).

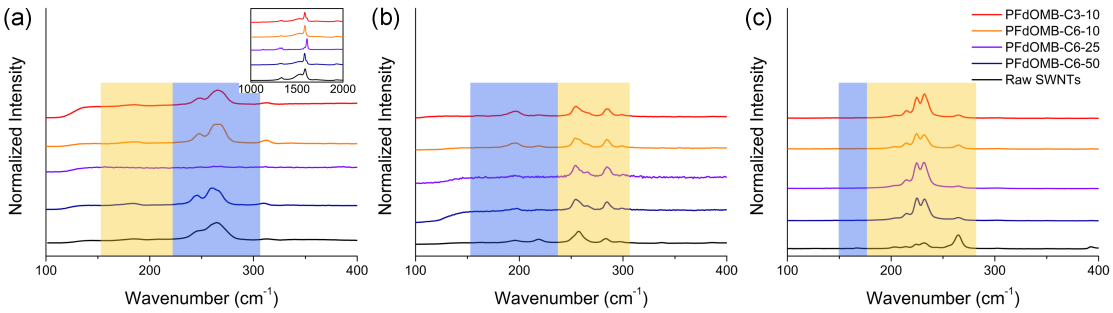


FIGURE 3.2: RBM regions of the Raman spectra using (a) 514, (b) 633, and (c) 785 nm excitation wavelengths. The yellow boxes denote the locations of signals arising from sc-SWNTs, while the blue boxes represent the locations of signals arising from m-SWNTs. The inset in (a) shows the G-band region, located at ~1590 cm^{-1}, upon excitation at 514 nm.

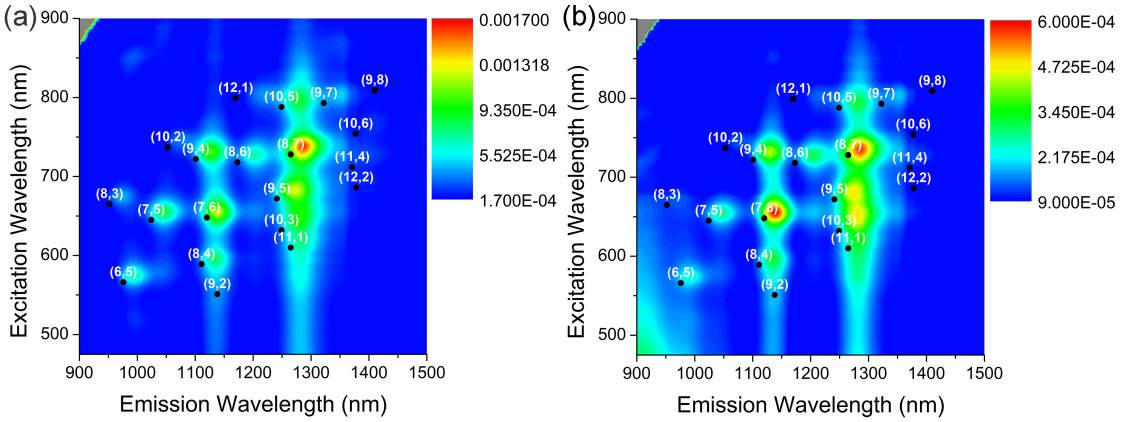


FIGURE 3.3: PL maps in THF corresponding to (a) PFdOMB-C6-25–SWNT and (b) PFdOMB-C6-50–SWNT.

Altogether, UV/vis–NIR and Raman spectroscopy demonstrated that PFdOMB-C6-25 dispersed an enriched sample of sc-SWNTs in THF, in comparison to the raw SWNT starting material. It is instructive to compare the performance of the NCL polymers to the fully conjugated analogue, PFdOMB, which has been shown

to disperse high concentrations of HiPCO SWNTs in both THF and toluene.[58] Enriched dispersions of sc-SWNTs could be prepared using PFdOMB in both solvents, although a molecular weight dependence was found, where higher molecular weight polymer (M_n ~60 kDa) was more discriminative for sc-SWNTs than lower molecular weight polymer (M_n ~21 kDa).[58] Interestingly, the incorporation of the C6 NCL allowed for PFdOMB-C6-25, which has a M_n of 24.7 kDa, to produce an enriched sc-SWNT dispersion, even though the comparable conjugated polymer dispersed a mixture of both m- and sc-SWNTs. Thus, these results demonstrate that if optimized, a NCL can be incorporated into the conjugated polymer scaffold to significantly influence the outcome of SWNT selectivity.

To identify the nanotube species present in the C6 series, photoluminescence (PL) maps were recorded for the PFdOMB-C6-25–SWNT and PFdOMB-C6-50–SWNT samples, as shown in Figure 3.3. The locations of various SWNT fluorescence maxima were assigned according to previously published data.[71] The sample concentrations were adjusted such that absorption spectra were in a similar intensity range (Figure S3.8). For the PFdOMB-C6-25–SWNT dispersion, the most intense spot corresponded to the (8,7) structure (Figure 3.3a). Relatively intense spots were also found for the (6,5), (7,5), (7,6), (8,3), (8,4), (8,6), (9,4), (9,5), (9,7), and (10,5) species, indicating that PFdOMB-C6-25 did not discriminate among individual sc-SWNT types. For the PFdOMB-C6-50–SWNT dispersion, the most intense spots corresponded to the (7,6) and (8,7) species (Figure 3.3b). Relatively intense spots were found for the same sc-SWNT species as dispersed by PFdOMB-C6-25, which indicated that PFdOMB-C6-50 was also nonselective for specific sc-SWNTs. Surprisingly, no emission from the (9,8) species is observed in either of these PL maps, despite the significant absorption from this structure in

the UV–vis–NIR absorption spectra (Figure 3.1b). The lack of observed emission from this species may be the result of its low quantum yield of fluorescence, which has previously been reported.[41,72]

Considering that the incorporation of C6 NCLs within some of the polymers resulted in the dispersion of a significant proportion of SWNT species in the upper diameter range of HiPCO nanotubes, we hypothesized that the wrapping efficiency of NCL-containing polymers and their dispersion concentration may improve by using a SWNT starting material with a higher average diameter. Large diameter sc-SWNTs (>1.3 nm) are of significant interest for organic electronic device applications, as they possess higher charge carrier mobility and a smaller Schottky barrier.[73] Thus, we investigated dispersions of PFdOMB-C6-50 with plasma torch-grown SWNTs (Raymor Industries, Inc.). In comparison to HiPCO SWNTs, which have average diameters of 0.8–1.2 nm, plasma torch SWNTs have average diameters of 0.9–1.5 nm.[62] The PFdOMB-C6-50 polymer was chosen for these studies because it showed the greatest proclivity for dispersing large diameter HiPCO SWNTs (Figure 3.1b). Supramolecular polymer–SWNT complexes with plasma torch SWNTs were prepared with slight modifications to the HiPCO SWNT procedure. A modified dispersion protocol was as follows: PFdOMB-C6-50 was dissolved in 8 mL of solvent (THF or toluene) before adding 4 mg of plasma torch SWNTs. The mixture was sonicated for 1.5 h in a bath sonicator chilled with ice and then centrifuged at 15000 g for 20 min at 10 °C. The supernatant was carefully removed, and the resulting polymer–SWNT dispersions were analyzed as isolated. The dispersions prepared were stable on the benchtop for at least several months. As shown in Figure 3.4, polymer:SWNT mass ratio optimization studies were performed in THF and toluene, and the dispersions were then analyzed using UV/vis–NIR

spectroscopy. The absorption features in the observed range can be grouped into four categories: three semiconducting regions—S_{11} (1400–1900 nm), S_{22} (750–1150 nm), and S_{33} (420–580 nm)—and a metallic region, M_{11} (600–750 nm).[42] Absorption spectra were normalized to the most intense peak in the S_{22} region to compare the relative areas of the S_{22}/M_{11} regions, which provide quantitative information on the degree of sc-SWNT enrichment. In contrast to the prior results with the lower average diameter HiPCO SWNTs, stable polymer–SWNT dispersions were obtained not only in both THF and toluene but also at polymer:SWNT mass ratios as low as 0.25:1 (though, in toluene, the 0.25:1 polymer:SWNT mass ratio was insufficient to stabilize polymer–SWNT dispersions after centrifugation). Although dispersions in THF were generally more concentrated, the dispersions prepared in toluene had significantly depressed M_{11} peaks, and as the polymer:SWNT mass ratio was decreased, discrimination for sc-SWNTs improved. These results suggest that conjugated scaffolds containing NCLs can effectively disperse SWNTs with a higher average diameter and can exhibit selectivity for sc-SWNTs, in spite of the absence of complete polymer backbone conjugation.

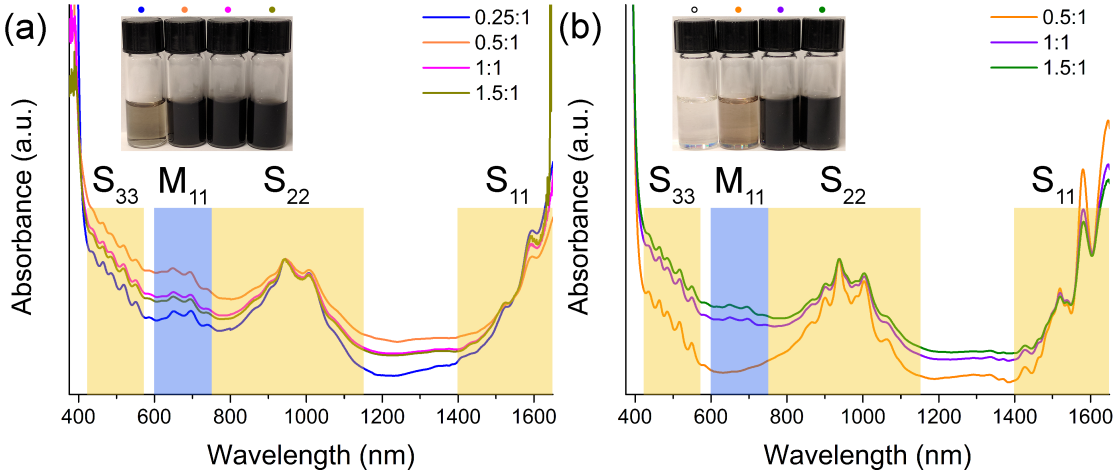


FIGURE 3.4: UV/vis–NIR absorption spectra for PFdOMB-C6-50–SWNT dispersions prepared using plasma torch SWNTs in (a) THF and (b) toluene. Photographs of the polymer–SWNT dispersions are color-coded with the appropriately colored dot above each dispersion. The sample prepared in toluene with a polymer:SWNT mass ratio of 0.25:1 did not produce a stable SWNT dispersion, and the photograph is labeled with a black circle. The yellow boxes highlight the absorption regions corresponding to sc-SWNT chiralities, while the blue boxes highlight the regions corresponding to m-SWNT chiralities.

3.3 Conclusions

SWNT dispersions prepared using a series of nine NCL-containing polymers with various lengths of NCL (3–12 carbon atoms) and incorporation percentages (10–50%) were investigated. We verified the incorporation percentage by ^{1}H NMR spectroscopy and found that the feed stoichiometry roughly matched the observed NCL incorporation by ^{1}H NMR. We demonstrate that PFdOMB-C6-25 can disperse an enriched sample of HiPCO sc-SWNTs in THF, showing that complete conjugation of the polymer backbone is not necessary for adequate nanotube sorting. Although stable SWNT dispersions with PFdOMB-C6-50 cannot be produced in toluene with HiPCO SWNTs, using higher average diameter plasma torch SWNTs allowed for

the preparation of stable dispersions. Using PFdOMB-C6-50, only substoichiometric amounts of polymer were required to prepare enriched sc-SWNT dispersions in toluene. Altogether, this study demonstrates that (i) conjugation is advantageous, but unnecessary for nanotube sorting; (ii) polymer backbone scaffolds containing an optimal alkyl spacer length of six carbon atoms can produce enriched HiPCO sc-SWNT dispersions in THF and enriched, concentrated plasma torch sc-SWNT dispersions in toluene; and (iii) the choice of SWNT starting material can significantly influence the dispersion outcome and warrants consideration for polymer structures that may not initially appear to produce stable SWNT dispersions under the given conditions.

3.4 Supporting Information

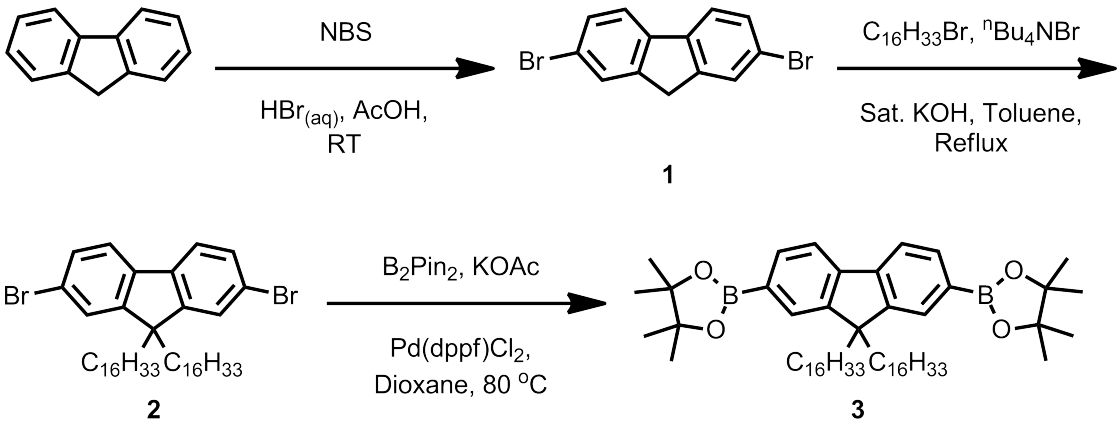
3.4.1 General

Raw HiPCO SWNTs were purchased from NanoIntegris (batch #R10-02, 10 wt % solid in anhydrous EtOH) and used without further purification. Semi-purified plasma torch SWNTs (RN120, batch #RNB735-120-X464) were purchased from Raymor Industries Inc. and also used without further purification. All other reagents were purchased from commercial suppliers and used as received. Flash chromatography was performed using an IntelliFlash 280 system from Analogix. Unless otherwise noted, compounds were monitored using a variable wavelength detector at 254 nm. Solvent amounts used for gradient or isocratic elution were reported in column volumes (CV). Columns were prepared in Biotage® SNAP KP-Sil cartridges using 40 – 63 μm silica or 25 – 40 μm silica purchased from

Silicycle. NMR was performed on a Bruker Avance 600 MHz or 700 MHz instrument and shift-referenced to the residual solvent resonance. Monomer purities were analyzed via HPLC using a Waters 2695 Separations Module equipped with a Waters 2996 photodiode array. High-resolution (HR) electron ionization (EI) MS measurements were carried out on the Micromass GCT instrument (GC-EI/CI time-of-flight). A Phenomenex Luna 3 μ (50 x 4.6 mm) phenyl-hexyl column was used for monomers **5a**, **5b**, and **5c**. Polymer molecular weights and dispersities were analyzed (relative to polystyrene standards) via GPC using a Waters 2695 Separations Module equipped with a Waters 2414 refractive index detector and a Jordi Fluorinated DVB mixed bed column. THF with 1% acetonitrile was used as the eluent at a flow rate of 3.0 mL/min. Sonication was performed in a Branson Ultrasonic B2800 bath sonicator. Centrifugation of the polymer-SWNT samples was performed using a Beckman Coulter Allegra X-22 centrifuge (raw HiPCO SWNT dispersions) or a Sorvall Legend X1R centrifuge (semi-purified plasma torch SWNT dispersions). UV/Vis-NIR spectra were recorded on a Cary 5000 spectrometer in dual beam mode, using matching 10 mm quartz cuvettes. Fluorescence spectra were measured on a Jobin-Yvon SPEX Fluorolog 3.22 equipped with a 450 W Xe arc lamp, digital photon counting photomultiplier, and an InGaAs detector, also using a 10 mm quartz cuvette. Slit widths for both excitation and emission were set to 10 nm band-pass, and correction factor files were applied to account for instrument variations. Photoluminescence maps were obtained at 25 °C, with 5 nm intervals for both the excitation and emission. Raman spectra were collected with a Renishaw InVia Laser Raman spectrometer, using three different lasers: a 25 mW argon ion laser (514 nm, 1800L/mm grating); a 500 mW HeNe Renishaw laser (633 nm, 1800 L/mm grating); and a 300 mW Renishaw laser (785 nm, 1200

L/mm grating). For spectra obtained at 514 nm, excitations were set to 5% for polymer-SWNT samples and 1% for the SWNT sample dispersed in $CHCl_3$. For the polymer-SWNT samples, laser intensity for both 633 and 785 nm excitations was set to 1%. For the SWNT sample dispersed in $CHCl_3$, laser intensity was set to 1% for 633 nm and 10% for 785 nm.

3.4.2 Synthetic Procedures



2,7-dibromofluorene (1) (Adapted from Ref. 74)

A round bottom flask equipped with a stir bar was charged with fluorene (33.2 g, 200 mmol), NBS (89.0 g, 500 mmol) and acetic acid (400 mL). While the mixture was stirring, conc. HBr (10 mL) was slowly added and then the reaction mixture was stirred at RT for 1.5 h. Water (200 mL) was added and the resulting suspension was filtered and washed with water to obtain an off-colour orange-white solid. The solid was recrystallized from a 1.5:1 v/v mixture of EtOH:acetone (∼1.8 L total volume), and the mother liquor was recrystallized again from the same solvent mixture (∼1.5 L total volume). The crops were combined to afford **1** (41.2 g, 64%) as a white solid. ^{1}H-NMR (600 MHz; $CDCl_3$): δ 7.67 (d, J = 1.1 Hz, 2H),

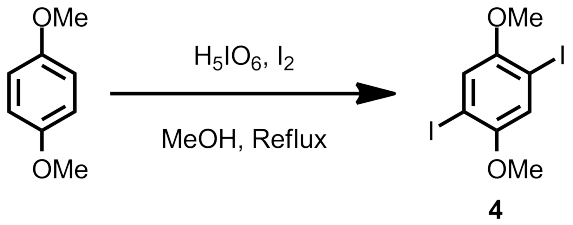
7.61 (d, J = 8.1 Hz, 2H), 7.51 (dd, J = 8.1, 1.8 Hz, 2H), 3.88 (s, 2H).

2,7-dibromo-9,9-dihexadecylfluorene (2) (Adapted from Ref. 74)

A round bottom flask equipped with a stir bar was charged with **1** (2.7 g, 8.3 mmol), 1-bromohexadecane (6.36 g, 20.8 mmol), $^{n}Bu_4NBr$ (537 mg, 1.7 mmol), toluene (16.6 mL), and sat. $KOH_{(aq)}$ (16.6 mL). The reaction mixture was heated to 60 °C and stirred vigorously for 1 h under a nitrogen atmosphere. The biphasic mixture was allowed to separate and the organic layer was isolated. The aqueous phase was extracted twice with diethyl ether (2 x 20 mL) and the organic extracts were combined and concentrated *in vacuo* to obtain a viscous green oil. The crude product was purified by flash chromatography (100 g column, 100% hexanes over 10 CV) to afford **2** as a white solid (5.19 g, 81%). ^{1}H-NMR (600 MHz; $CDCl_3$): δ 7.51 (d, J = 8.0 Hz, 1H), 7.46-7.43 (m, 2H), 1.92-1.88 (m, 2H), 1.24-1.03 (m, 26H), 0.88 (t, J = 7.0 Hz, 3H), 0.59-0.57 (m, 2H).

2,2'-(9,9-dihexadecylfluorene-2,7-diyl)bis(4,4,5,5-tetramethyl-1,3,2-dioxaborolane) (3) (Adapted from Ref. 74)

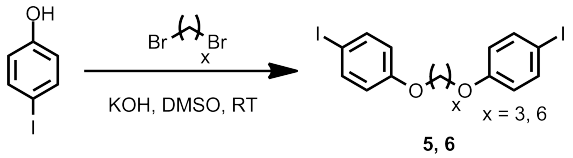
A round bottom flask equipped with a stir bar was charged with **2** (5.2 g, 6.7 mmol), B_2Pin_2 (3.76 g, 14.8 mmol), KOAc (1.98 g, 20.2 mmol), and dioxane (28 mL). $Pd(dppf)_2Cl_2$ (165 mg, 202 μmol) was added and then the reaction mixture was stirred at 80 °C for 12 h. The reaction mixture was partitioned with water and extracted thrice with Et_2O. The organic extracts were combined and dry loaded onto silica (9.9 g). The crude product was purified by flash chromatography (100 g column, 0 to 70% CH_2Cl_2 in hexanes over 10 CV) to afford **3** as a white solid (4.88 g, 63%). ^{1}H-NMR (600 MHz; $CDCl_3$): δ 7.80 (d, J = 7.5 Hz, 1H), 7.74-7.71 (m, 2H), 2.00-1.97 (m, 2H), 1.39 (s, 12H), 1.24-0.99 (m, 26H), 0.87 (t, J = 7.0 Hz, 3H), 0.55-0.53 (m, 2H).



4

2,5-dimethoxy-1,4-diiodobenzene (4) (Adapted from Ref. 75)

A round bottom flask equipped with a stir bar was charged with 1,4-dimethoxy benzene (10 g, 72.4 mmol), periodic acid (10.6 g, 228.0 mmol), iodine (23 g, 90.4 mmol) and MeOH (86 mL). The reaction mixture was stirred at reflux for 3 h and then poured into 0.5 M Na_2SO_3 (500 mL) chilled in an ice bath. The suspension was filtered and the precipitate was washed with dH_2O and MeOH to afford **4** as a white solid (12.4 g, 88%). ^{1}H NMR (600 MHz; $CDCl_3$): δ 7.19 (s, 1H), 3.83 (s, 3H).



5, 6

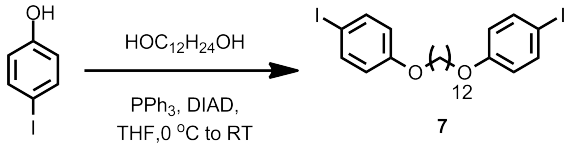
Bis(4-iodophenoxy)propane (5a)

A round bottom flask equipped with a stir bar was charged with 1,3-dibromopropane (1 g, 5.0 mmol), 4-iodophenol (2.72 g, 12.4 mmol), KOH (1.67 g, 29.7 mmol) and DMSO (3 mL). The reaction mixture was stirred at RT for 12 h and dH_2O (20 mL) was poured into the RM. The suspension was filtered and the precipitate was washed with dH_2O. The crude material was purified by flash chromatography (50 g column, 5 CV of hexanes followed by a gradient of 0 to 75% CH_2Cl_2 in hexanes over 10 CV) to afford **5a** as a white solid (1.33 g, 56%). Purity: >99% by HPLC; M.W.: 480.08 g/mol; ^{1}H-NMR (700 MHz; $CDCl_3$): δ 7.54 (d, J = 9.0 Hz, 2H), 6.68 (d, J = 9.0 Hz, 2H), 4.10 (t, J = 6.1 Hz, 2H), 2.26-2.21 (m, 1H); ^{13}C-NMR

(176 MHz; $CDCl_3$): δ 158.8, 138.4, 117.1, 83.0, 64.6, 29.2; HRMS (EI^+) (m/z) for $C_{15}H_{14}I_2O_2$ $[M]^+$ calculated: 479.9083, found: 479.9101.

Bis(4-iodophenoxy)hexane (5b)

A round bottom flask equipped with a stir bar was charged with 1,6-dibromohexane (1 g, 4.1 mmol), 4-iodophenol (2.24 g, 10.2 mmol), KOH (1.38 g, 24.6 mmol) and DMSO (3 mL). The reaction mixture was stirred at RT for 12 h and dH_2O (20 mL) was poured into the RM. The suspension was filtered and the precipitate was washed with dH_2O. The crude material was purified by flash chromatography (50 g column, 5 CV of hexanes followed by a gradient of 0 to 75% CH_2Cl_2 in hexanes over 10 CV) to afford **5b** as a white solid (1.76 g, 82%). Purity: >99% by HPLC; M.W.: 522.16 g/mol; ^{1}H-NMR (700 MHz; $CDCl_3$): δ 7.54 (d, J = 9.0 Hz, 1H), 6.66 (d, J = 9.0 Hz, 1H), 3.92 (t, J = 6.4 Hz, 1H), 1.82-1.77 (m, 1H), 1.53-1.50 (m, 1H); ^{13}C-NMR (176 MHz; $CDCl_3$): δ 159.1, 138.3, 117.1, 82.6, 68.0, 29.2, 25.9; HRMS (EI^+) (m/z) for $C_{18}H_{20}I_2O_2$ $[M]^+$ calculated: 521.9553, found: 521.9547.

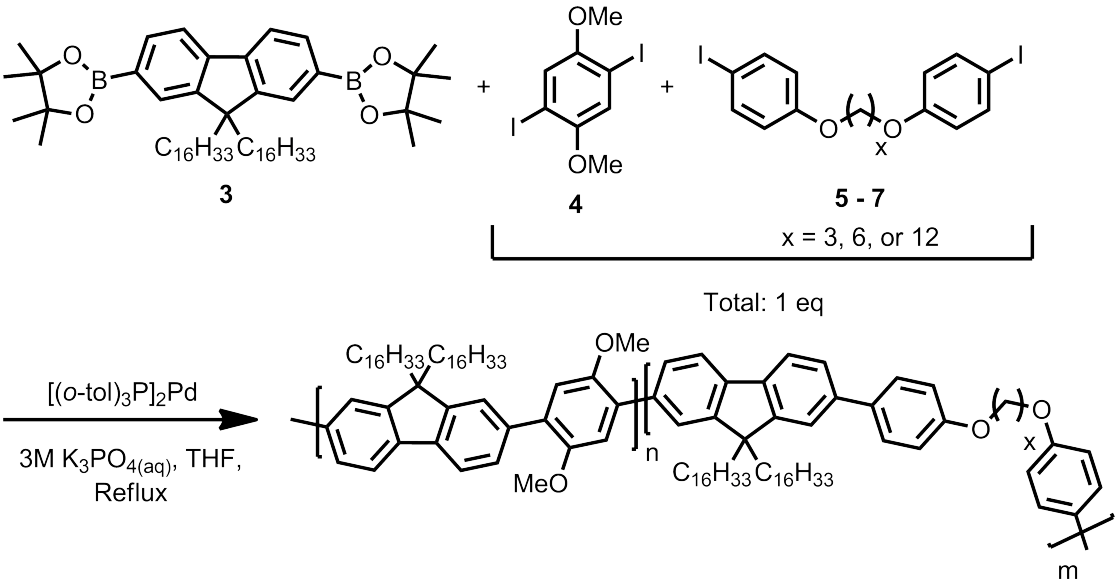


7

Bis(4-iodophenoxy)dodecane (5c)

A round bottom flask equipped with a stir bar was charged with 1,12-dodecanol (1 g, 4.94 mmol), 4-iodophenol (2.72 g, 12.4 mmol), PPh_3 (3.24 g, 12.4 mmol), and THF (5 mL) then cooled to 0 °C under a nitrogen atmosphere. Diisopropylazodicarboxylate (2.5 g, 12.4 mmol) was added dropwise at 0 °C. The reaction mixture was stirred at RT for 2 h and the resulting yellow precipitate was sonicated in Et_2O and filtered through a silica plug. The suspension was filtered and the precipitate was washed with dH_2O. The crude material was purified by flash

silica chromatography (50 g column, 5 CV of hexanes followed by a gradient of 0 to 75% CH_2Cl_2 in hexanes over 10 CV) to afford **5c** as a white solid (1.76 g, 82%). Purity: >99% by HPLC; M.W.: 606.32 g/mol; ^{1}H-NMR (700 MHz; $CDCl_3$): δ 7.53 (d, J = 9.0 Hz, 1H), 6.67 (d, J = 9.0 Hz, 1H), 3.90 (t, J = 6.6 Hz, 1H), 1.76 (dd, J = 8.2, 7.0 Hz, 1H), 1.44-1.41 (m, 1H), 1.34-1.28 (m, 3H); ^{13}C-NMR (176 MHz; $CDCl_3$): δ 159.1, 138.3, 117.1, 82.5, 68.3, 29.67, 29.49, 29.28, 29.27, 26.1; HRMS (EI$^+$) (m/z) for $C_{24}H_{32}I_2O_2$ $[M]^+$ calculated: 606.0492, found: 606.0479.



PFdOMB-C3-10. A Schlenk tube equipped with a stir bar was charged with monomer **3** (200 mg, 0.23 mmol), monomer **4** (81.0 mg, 0.21 mmol), monomer **5a** (4.3 mg, 23 μmol), THF (0.9 mL), and 3M $K_3PO_{4(aq)}$ (0.9 mL) then the mixture was degassed by three freeze-pump-thaw cycles. The biphasic mixture was frozen under liquid nitrogen and $[(o\text{-tol})_3P]_2Pd$ (8 mg, 12 μmol) was added under a positive pressure of nitrogen. The Schlenk tube was evacuated and backfilled with nitrogen four times and then the reaction mixture was vigorously stirred at reflux for 12 h. The phases were allowed to separate and the organic layer was

isolated, then filtered through a celite and neutral alumina plug. The plug was thoroughly washed with THF and the flow-through was concentrated *in vacuo*. The crude polymer was precipitated into MeOH (200 mL) and then filtered to afford **PFdOMB-C3-10** as a white solid (154 mg). M_n: 21.6 kDa (GPC), M_w: 98.5 kDa (GPC). ^{1}H-NMR (700 MHz; $CDCl_3$): δ 7.83-7.78 (m, 2H), 7.67-7.58 (m, 4H), 7.14 (s, 2H), 4.29-4.26 (m, 0.165H), 3.87-3.82 (m, 6H), 2.06-2.01 (m, 3H), 1.29-1.12 (m, 63H), 0.87 (t, J = 7.1 Hz, 16H).

PFdOMB-C3-25. A Schlenk tube equipped with a stir bar was charged with monomer **3** (200 mg, 0.23 mmol), monomer **4** (67.5 mg, 0.17 mmol), monomer **5a** (10.8 mg, 58 μmol), THF (0.9 mL), and 3M $K_3PO_{4(aq)}$ (0.9 mL) then the mixture was degassed by three freeze-pump-thaw cycles. The biphasic mixture was frozen under liquid nitrogen and $[(o\text{-tol})_3P]_2Pd$ (8 mg, 12 μmol) was added under a positive pressure of nitrogen. The Schlenk tube was evacuated and backfilled with nitrogen four times and then the reaction mixture was vigorously stirred at reflux for 12 h. The phases were allowed to separate and the organic layer was isolated then filtered through a celite and neutral alumina plug. The plug was thoroughly washed with THF and the flow-through was concentrated *in vacuo*. The crude polymer was precipitated into MeOH (200 mL) and then filtered to afford **PFdOMB-C3-25** as a white solid (75 mg). M_n: 16.5 kDa (GPC), M_w: 40.8 kDa (GPC). ^{1}H-NMR (700 MHz; $CDCl_3$): δ 7.82-7.77 (m, 3H), 7.68-7.54 (m, 6H), 7.14-7.05 (m, 3H), 4.29-4.26 (m, 0.503H), 3.85-3.83 (m, 6H), 2.10-2.00 (m, 5H), 1.28-1.09 (m, 74H), 0.87 (t, J = 6.9 Hz, 16H).

PFdOMB-C3-50. A Schlenk tube equipped with a stir bar was charged with monomer **3** (200 mg, 0.23 mmol), monomer **4** (45.0 mg, 0.12 mmol), monomer **5a**

(21.6 mg, 116 μmol), THF (0.9 mL), and 3M $K_3PO_{4(aq)}$ (0.9 mL) then the mixture was degassed by three freeze-pump-thaw cycles. The biphasic mixture was frozen under liquid nitrogen and $[(o\text{-tol})_3P]_2Pd$ (8 mg, 12 μmol) was added under a positive pressure of nitrogen. The Schlenk tube was evacuated and backfilled with nitrogen four times and then the reaction mixture was vigorously stirred at reflux for 12 h. The phases were allowed to separate and the organic layer was isolated then filtered through a celite and neutral alumina plug. The plug was thoroughly washed with THF and the flow-through was concentrated *in vacuo*. The crude polymer was precipitated into MeOH (200 mL) and then filtered to afford **PFdOMB-C3-50** as a yellow solid (22 mg). M_n: 6.8 kDa (GPC), M_w: 11.7 kDa (GPC). ^{1}H-NMR (700 MHz; $CDCl_3$): δ 7.83-7.50 (m, 12H), 7.13-7.04 (m, 4H), 4.27 (m, 1.49H), 3.83 (m, 6H), 2.02-2.01 (m, 7H), 1.28-1.02 (m, 98H), 0.88-0.86 (m, 20H).

PFdOMB-C6-10. A Schlenk tube equipped with a stir bar was charged with monomer **3** (200 mg, 0.23 mmol), monomer **4** (81.0 mg, 0.21 mmol), monomer **5b** (12.0 mg, 23 μmol), THF (0.9 mL), and 3M $K_3PO_{4(aq)}$ (0.9 mL) then the mixture was degassed by three freeze-pump-thaw cycles. The biphasic mixture was frozen under liquid nitrogen and $[(o\text{-tol})_3P]_2Pd$ (8 mg, 12 μmol) was added under a positive pressure of nitrogen. The Schlenk tube was evacuated and backfilled with nitrogen four times and then the reaction mixture was vigorously stirred at reflux for 12 h. The phases were allowed to separate and the organic layer was isolated, then filtered through a celite and neutral alumina plug. The plug was thoroughly washed with THF and the flow-through was concentrated *in vacuo*. The crude polymer was precipitated into MeOH (200 mL) and then filtered to afford **PFdOMB-C6-10** as a white solid (170 mg). M_n: 54.4 kDa (GPC), M_w:

144.2 kDa (GPC). ^{1}H-NMR (600 MHz; $CDCl_3$): δ 7.82-7.79 (m, 2H), 7.68-7.54 (m, 5H), 7.14-7.12 (m, 2H), 4.08-4.05 (m, 0.405H), 3.86-3.83 (m, 6H), 2.07-1.99 (m, 2H), 1.25-1.12 (m, 75H), 0.88-0.86 (m, 19H).

PFdOMB-C6-25. A Schlenk tube equipped with a stir bar was charged with monomer **3** (200 mg, 0.23 mmol), monomer **4** (67.5 mg, 0.17 mmol), monomer **6** (30.1 mg, 58 μmol), THF (0.9 mL), and 3M $K_3PO_{4(aq)}$ (0.9 mL) then the mixture was degassed by three freeze-pump-thaw cycles. The biphasic mixture was frozen under liquid nitrogen and $[(o\text{-tol})_3P]_2Pd$ (8 mg, 12 μmol) was added under a positive pressure of nitrogen. The Schlenk tube was evacuated and backfilled with nitrogen four times and then the reaction mixture was vigorously stirred at reflux for 12 h. The phases were allowed to separate and the organic layer was isolated, then filtered through a celite and neutral alumina plug. The plug was thoroughly washed with THF and the flow-through was concentrated *in vacuo*. The crude polymer was precipitated into MeOH (200 mL) and then filtered to afford **PFdOMB-C6-25** as a white solid (29 mg). M_n: 24.7 kDa (GPC), M_w: 89.2 kDa (GPC). ^{1}H-NMR (600 MHz; $CDCl_3$): δ 7.82-7.75 (m, 3H), 7.67-7.53 (m, 6H), 7.14-7.11 (m, 2H), 7.03-7.01 (m, 1H), 4.08-4.04 (m, 1.04H), 3.85-3.82 (m, 6H), 2.10-1.88 (m, 5H), 1.28-1.08 (m, 72H), 0.88-0.86 (m, 14H).

PFdOMB-C6-50. A Schlenk tube equipped with a stir bar was charged with monomer **3** (200 mg, 0.23 mmol), monomer **4** (45.0 mg, 0.12 mmol), monomer **5b** (60.2 mg, 116 μmol), THF (0.9 mL), and 3M $K_3PO_{4(aq)}$ (0.9 mL) then the mixture was degassed by three freeze-pump-thaw cycles. The biphasic mixture was frozen under liquid nitrogen and $[(o\text{-tol})_3P]_2Pd$ (8 mg, 12 μmol) was added under a positive pressure of nitrogen. The Schlenk tube was evacuated and backfilled with nitrogen four times and then the reaction mixture was vigorously stirred at

reflux for 12 h. The phases were allowed to separate and the organic layer was isolated, then filtered through a celite and neutral alumina plug. The plug was thoroughly washed with THF and the flow-through was concentrated *in vacuo*. The crude polymer was precipitated into MeOH (200 mL) and then filtered to afford **PFdOMB-C6-50** as a white solid (163 mg). M_n: 35.9 kDa (GPC), M_w: 103.0 kDa (GPC). ^{1}H-NMR (600 MHz; $CDCl_3$): δ 7.81-7.72 (m, 4H), 7.67-7.51 (m, 12H), 7.13-7.11 (m, 2H), 7.03-7.00 (m, 4H), 4.07-4.04 (m, 3.99H), 3.84 (t, J = 5.0 Hz, 6H), 2.05-1.87 (m, 11H), 1.28-1.05 (m, 115H), 0.88-0.86 (m, 22H).

PFdOMB-C6-100. A Schlenk tube equipped with a stir bar was charged with monomer **3** (200 mg, 0.23 mmol) monomer **5b** (120.5 mg, 0.23 mmol), THF (0.9 mL), and 3M $K_3PO_{4(aq)}$ (0.9 mL) then the mixture was degassed by three freeze-pump-thaw cycles. The biphasic mixture was frozen under liquid nitrogen and $[(o\text{-tol})_3P]_2Pd$ (8 mg, 12 μmol) was added under a positive pressure of nitrogen. The Schlenk tube was evacuated and backfilled with nitrogen four times and then the reaction mixture was vigorously stirred at reflux for 12 h. The phases were allowed to separate and the organic layer was isolated, then filtered through a celite and neutral alumina plug. The plug was thoroughly washed with THF and the flow-through was concentrated *in vacuo*. The crude polymer was precipitated into MeOH (200 mL) and then filtered to afford **PFdOMB-C6-100** as a white solid (108 mg, 56%). M_n: 79.4 kDa (GPC), M_w: 141.3 kDa (GPC). ^{1}H-NMR (600 MHz; $CDCl_3$): δ 7.72 (d, J = 7.9 Hz, 1H), 7.60 (d, J = 8.6 Hz, 2H), 7.54-7.51 (m, 2H), 7.01 (d, J = 8.7 Hz, 2H), 4.05 (t, J = 6.4 Hz, 2H), 2.02-1.88 (m, 4H), 1.61 (m, 2H), 1.28-1.05 (m, 26H), 0.87 (t, J = 7.1 Hz, 3H), 0.73-0.71 (m, 2H).

PFdOMB-C12-10. A Schlenk tube equipped with a stir bar was charged with monomer **3** (200 mg, 0.23 mmol), monomer **4** (81.0 mg, 0.21 mmol), monomer **5c**

(14.0 mg, 23 μmol), THF (0.9 mL), and 3M $K_3PO_{4(aq)}$ (0.9 mL) then the mixture was degassed by three freeze-pump-thaw cycles. The biphasic mixture was frozen under liquid nitrogen and $[(o\text{-tol})_3P]_2Pd$ (8 mg, 12 μmol) was added under a positive pressure of nitrogen. The Schlenk tube was evacuated and backfilled with nitrogen four times and then the reaction mixture was vigorously stirred at reflux for 12 h. The phases were allowed to separate and the organic layer was isolated, then filtered through a celite and neutral alumina plug. The plug was thoroughly washed with THF and the flow-through was concentrated *in vacuo*. The crude polymer was precipitated into MeOH (200 mL) and then filtered to afford **PFdOMB-C12-10** as a white solid (155 mg). M_n: 17.1 kDa (GPC), M_w: 40.7 kDa (GPC). ^{1}H-NMR (600 MHz; $CDCl_3$): δ 7.83-7.77 (m, 2H), 7.69-7.53 (m, 5H), 7.14-7.12 (m, 2H), 7.02-7.00 (m,), 4.04-4.01 (m, 0.415), 3.85-3.83 (m, 6H), 2.07-2.00 (m, 4H), 1.29-1.09 (m, 68H), 0.87 (t, J = 7.0 Hz, 14H).

PFdOMB-C12-25. A Schlenk tube equipped with a stir bar was charged with monomer **3** (200 mg, 0.23 mmol), monomer **4** (67.5 mg, 0.17 mmol), monomer **5c** (35.0 mg, 58 μmol), THF (0.9 mL), and 3M $K_3PO_{4(aq)}$ (0.9 mL) then the mixture was degassed by three freeze-pump-thaw cycles. The biphasic mixture was frozen under liquid nitrogen and $[(o\text{-tol})_3P]_2Pd$ (8 mg, 12 μmol) was added under a positive pressure of nitrogen. The Schlenk tube was evacuated and backfilled with nitrogen four times and then the reaction mixture was vigorously stirred at reflux for 12 h. The phases were allowed to separate and the organic layer was isolated, then filtered through a celite and neutral alumina plug. The plug was thoroughly washed with THF and the flow-through was concentrated *in vacuo*. The crude polymer was precipitated into MeOH (200 mL) and then filtered to afford **PFdOMB-C12-25** as a white solid (126 mg). M_n: 10.0 kDa (GPC), M_w:

27.3 kDa (GPC). ^{1}H-NMR (600 MHz; $CDCl_3$): δ 7.82-7.76 (m, 3H), 7.68-7.54 (m, 7H), 7.14-7.12 (m, 2H), 7.02-7.01 (m, 1H), 4.03 (m, 1.15H), 3.86-3.84 (m, 6H), 2.05-2.02 (m, 6H), 1.29-1.10 (m, 80H), 0.89-0.86 (m, 15H).

PFdOMB-C12-50. A Schlenk tube equipped with a stir bar was charged with monomer **3** (200 mg, 0.23 mmol), monomer **4** (45.0 mg, 0.12 mmol), monomer **5c** (69.5 mg, 116 μmol), THF (0.9 mL), and 3M $K_3PO_{4(aq)}$ (0.9 mL) then the mixture was degassed by three freeze-pump-thaw cycles. The biphasic mixture was frozen under liquid nitrogen and $[(o\text{-tol})_3P]_2Pd$ (8 mg, 12 μmol) was added under a positive pressure of nitrogen. The Schlenk tube was evacuated and backfilled with nitrogen four times and then the reaction mixture was vigorously stirred at reflux for 12 h. The phases were allowed to separate and the organic layer was isolated, then filtered through a celite and neutral alumina plug. The plug was thoroughly washed with THF and the flow-through was concentrated *in vacuo*. The crude polymer was precipitated into MeOH (200 mL) and then filtered to afford **PFdOMB-C12-50** as a white solid (136 mg). M_n: 16.5 kDa (GPC), M_w: 35.0 kDa (GPC). ^{1}H-NMR (600 MHz; $CDCl_3$): δ 7.82-7.50 (m, 17H), 7.13-7.11 (m, 2H), 7.02-6.99 (m, 4H), 4.03-4.01 (m, 4.18H), 3.85-3.82 (m, 6H), 2.06-1.99 (m, 8H), 1.84-1.81 (m, 5H), 1.34-1.05 (m, 134H), 0.87 (m, J = 8.1, 5.9, 2.0 Hz, 25H).

Sample Calculation for NCL Incorporation Determination by ^{1}H NMR (PFdOMB-C6-25)

^{1}H NMR integration ratio (NCL:dOMB) of 1:6.

Thus: $I_{NCL} = \frac{1}{4} = 0.25$ and $I_{DMB} = \frac{6}{6} = 1$.

Therefore:

$$\%NCL = \frac{I_{NCL}}{I_{NCL} + I_{DMB}} \times 100 = \frac{0.25}{0.25 + 1} \times 100 = 20\% \tag{3.2}$$

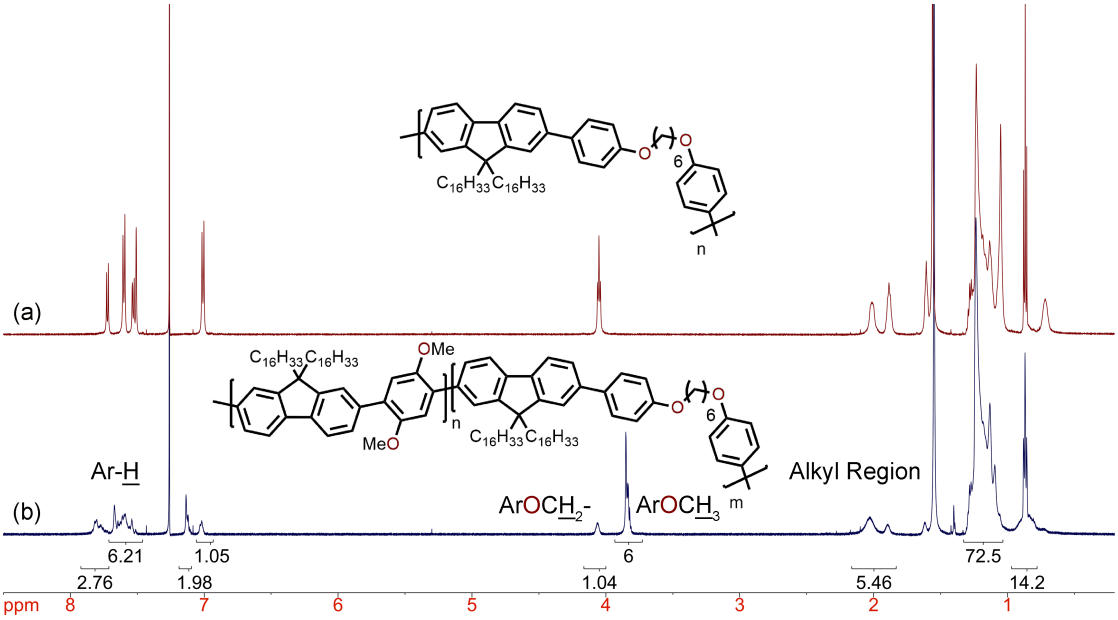


FIGURE 3.5: ^{1}H NMR data for (a) PFdOMB-C6-100 and (b) PFdOMB-C6-50 in $CDCl_3$.

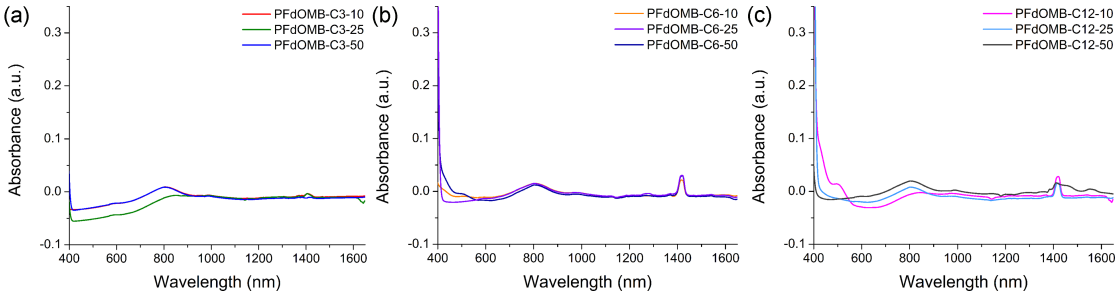


FIGURE 3.6: UV/Vis-NIR spectra for polymer-SWNT dispersions produced in toluene. (a) PFdOMB-C3 series, (b), PFdOMB-C6 series, and (c) PFdOMB-C12 series.

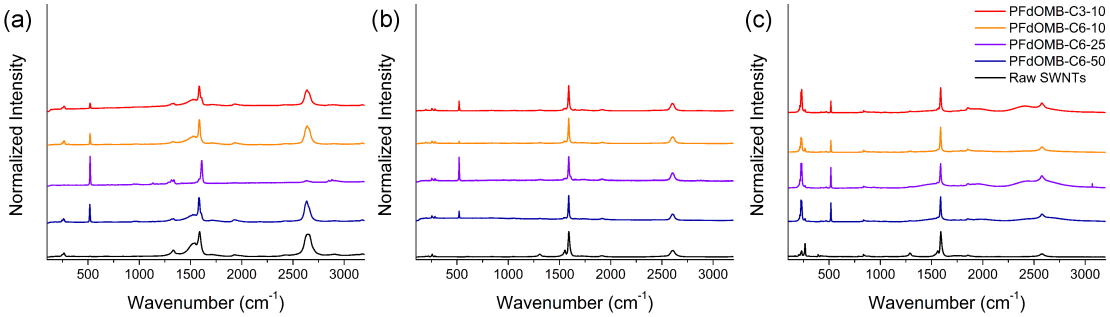


FIGURE 3.7: Full Raman spectra using (a) 514 nm, (b) 633 nm, and (c) 785 nm excitation wavelengths.

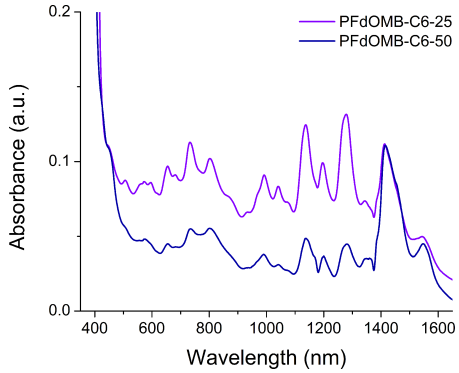


FIGURE 3.8: UV/Vis-NIR spectra of polymer-HiPCO dispersions in THF used for PL mapping.

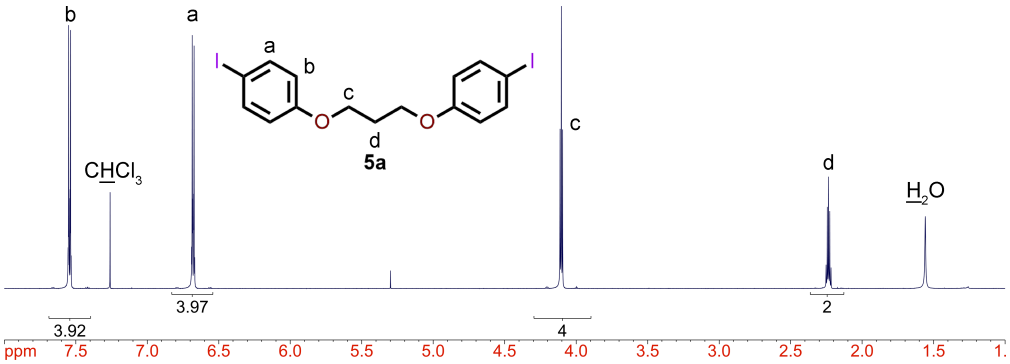


FIGURE 3.9: ^{1}H NMR spectrum of **5a** in $CDCl_3$.

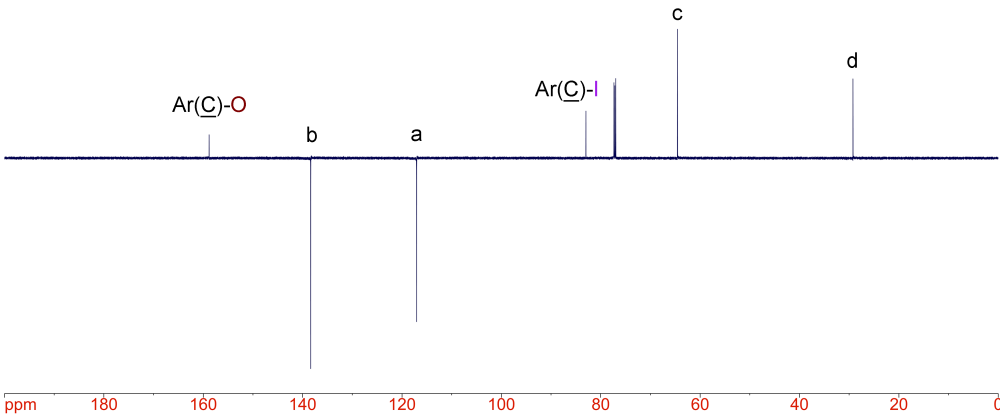
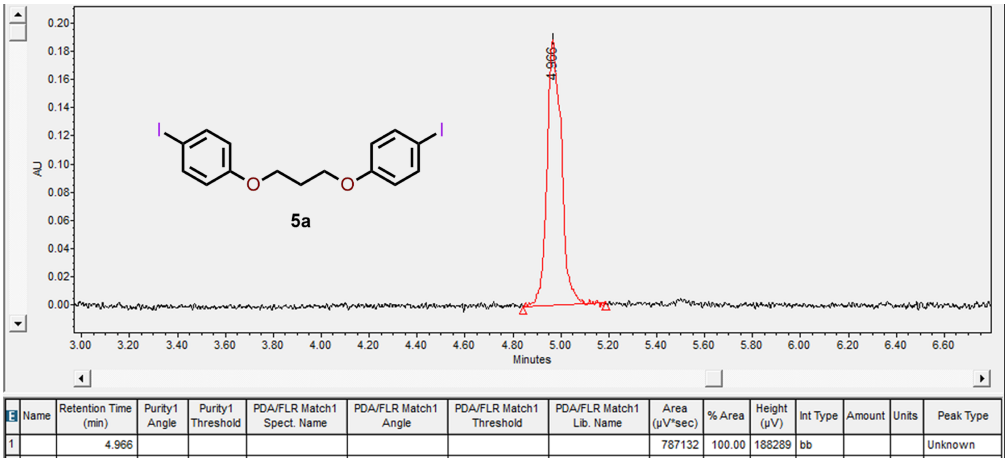


FIGURE 3.10: DEPTq spectrum of **5a** in $CDCl_3$.



	Name	Retention Time (min)	Purity1 Angle	Purity1 Threshold	PDA/FLR Match1 Spect. Name	PDA/FLR Match1 Angle	PDA/FLR Match1 Threshold	PDA/FLR Match1 Lib. Name	Area (µV*sec)	% Area	Height (µV)	Int Type	Amount	Units	Peak Type
1		4.966							787132	100.00	188289	bb			Unknown

FIGURE 3.11: HPLC trace of **5a** at 254 nm.

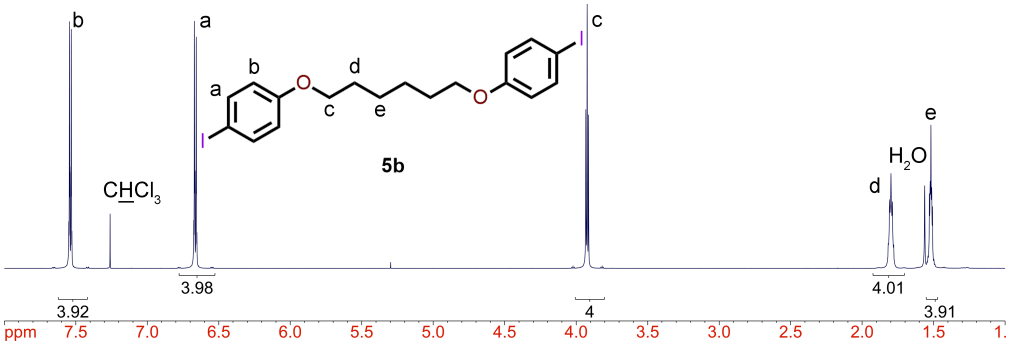


FIGURE 3.12: ^{1}H NMR spectrum of **5b** in $CDCl_3$.

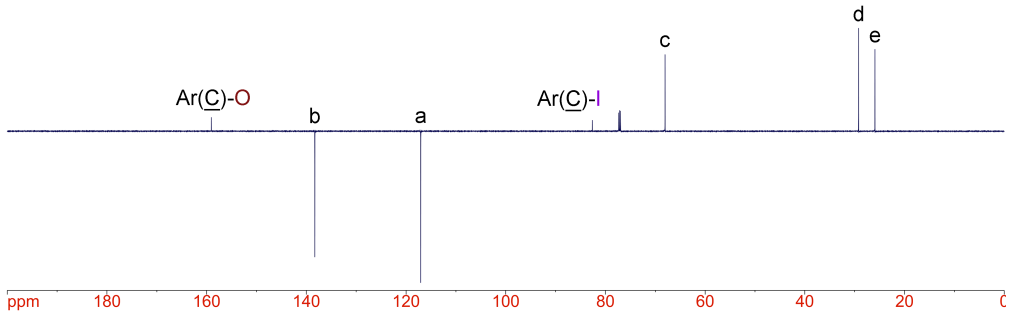
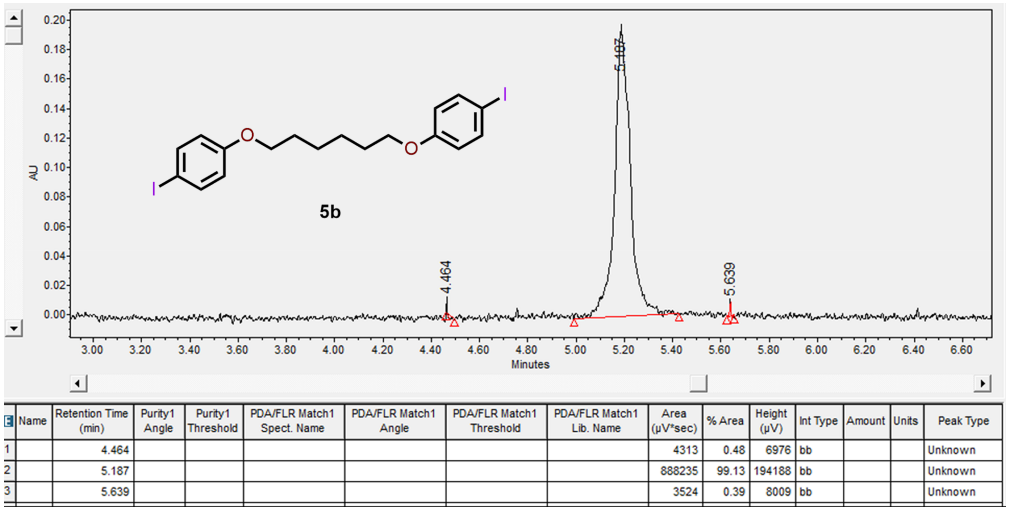


FIGURE 3.13: DEPTq spectrum of **5b** in $CDCl_3$.



	Name	Retention Time (min)	Purity1 Angle	Purity1 Threshold	PDA/FLR Match1 Spect. Name	PDA/FLR Match1 Angle	PDA/FLR Match1 Threshold	PDA/FLR Match1 Lib. Name	Area (µV*sec)	% Area	Height (µV)	Int Type	Amount	Units	Peak Type
1		4.464							4313	0.48	6976	bb			Unknown
2		5.187							888235	99.13	194188	bb			Unknown
3		5.639							3524	0.39	8009	bb			Unknown

FIGURE 3.14: HPLC trace of **5b** at 254 nm.

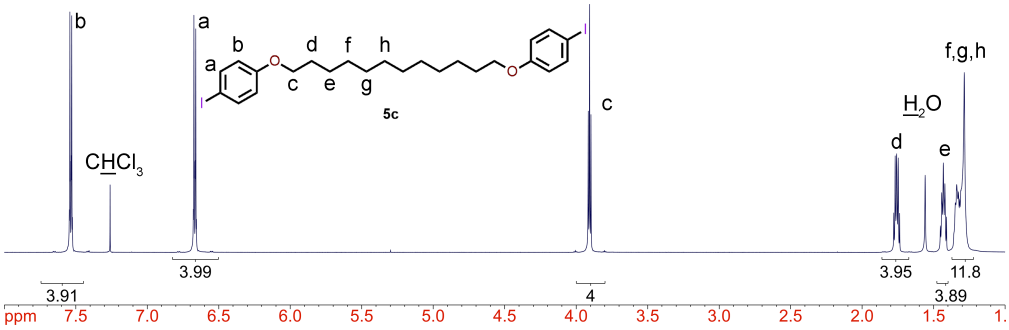


FIGURE 3.15: ^{1}H NMR spectrum of **5c** in $CDCl_3$.

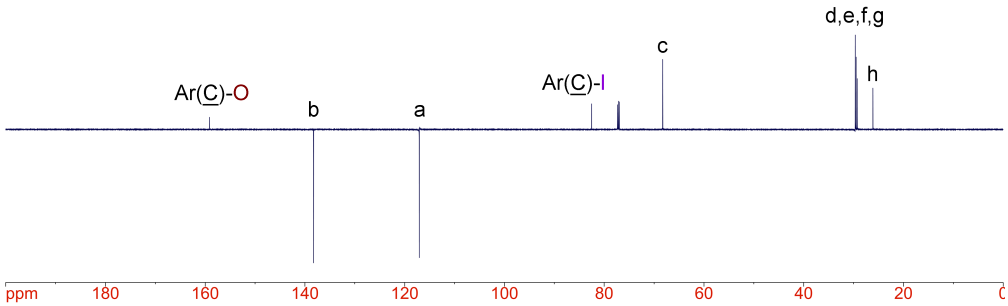
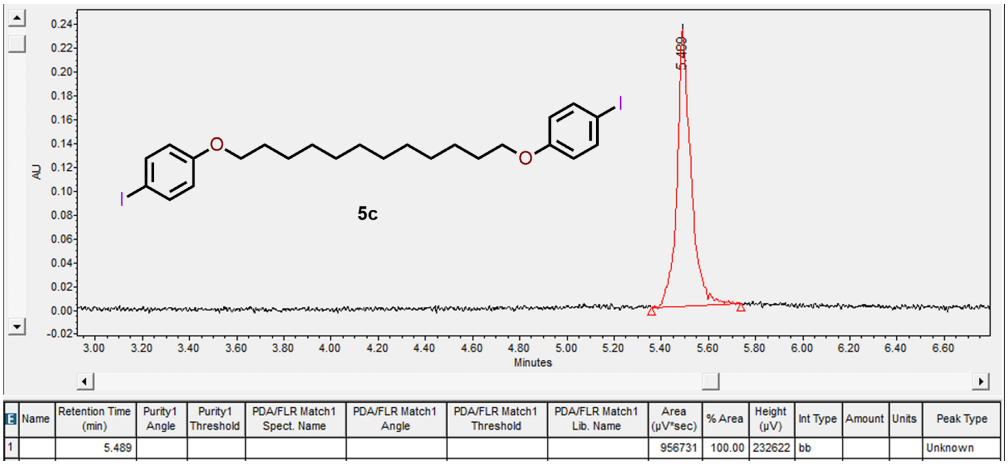


FIGURE 3.16: DEPTq spectrum of **5c** in $CDCl_3$.



	Name	Retention Time (min)	Purity1 Angle	Purity1 Threshold	PDA/FLR Match1 Spect. Name	PDA/FLR Match1 Angle	PDA/FLR Match1 Threshold	PDA/FLR Match1 Lib. Name	Area (µV*sec)	% Area	Height (µV)	Int Type	Amount	Units	Peak Type
1		5.489							956731	100.00	232622	bb			Unknown

FIGURE 3.17: HPLC trace of **5c** at 254 nm.

3.5 References

(1) Iijima, S.; Ichihashi, T. *Nature* **1993**, 363, 603–605.

(2) Park, S.; Vosguerichian, M.; Bao, Z. *Nanoscale* **2013**, 5, 1727–1752.

(3) Terrones, M. *Annu. Rev. Mater. Res.* **2003**, 33, 419–501.

(4) Ajayan, P. M. *Chem. Rev.* **1999**, 99, 1787–1800.

(5) Saito, R.; Dresselhaus, G.; Dresselhaus, M. S. *Physical Properties of Carbon Nanotubes*, vol. 3.; Imperial College Press: London, **2005**.

(6) Coleman, J. N.; Khan, U.; Blau, W. J.; Gun'ko, Y. K. *Carbon* **2006**, 44, 1624–1652.

(7) Zhang, Q.; Huang, J.-Q.; Qian, W.-Z.; Zhang, Y.-Y.; Wei, F. *Small* **2013**, 9, 1237–1265.

(8) O'Connell, M. J.; Bachilo, S. M.; Huffman, C. B.; Moore, V. C.; Strano, M. S.; Haroz, E. H.; Rialon, K. L.; Boul, P. J.; Noon, W. H.; Kittrell, C.; et al. *Science* **2002**, 297, 593–596.

(9) Bachilo, S. M.; Strano, M. S.; Kittrell, C.; Hauge, R. H.; Smalley, R. E.; Weisman, R. B. *Science* **2002**, 298, 2361–2366.

(10) Kataura, H.; Kumazawa, Y.; Maniwa, Y.; Umezu, I.; Suzuki, S.; Ohtsuka, Y.; Achiba, Y. *Synth. Met.* **1999**, 103, 2555–2558.

(11) Wang, H.; Wei, P.; Li, Y.; Han, J.; Lee, H. R.; Naab, B. D.; Liu, N.; Wang, C.; Adijanto, E.; Tee, B. C.-K.; et al. *Proc. Natl. Acad. Sci. U. S. A.* **2014**, 111, 4776–4781.

(12) Tee, B. C.-K.; Chortos, A.; Berndt, A.; Nguyen, A. K.; Tom, A.; McGuire, A.; Lin, Z. C.; Tien, K.; Bae, W.-G.; Wang, H.; et al. *Science* **2015**, 350, 313–316.

(13) Jiang, C.; Saha, A.; Xiang, C.; Young, C. C.; Tour, J. M.; Pasquali, M.;

Martí, A. A. *ACS Nano* **2013**, 7, 4503–4510.

(14) Jiang, C.; Saha, A.; Young, C. C.; Hashim, D. P.; Ramirez, C. E.; Ajayan, P. M.; Pasquali, M.; Martí, A. A. *ACS Nano* **2014**, 8, 9107–9112.

(15) Behabtu, N.; Young, C. C.; Tsentalovich, D. E.; Kleinerman, O.; Wang, X.; Ma, A. W. K.; Bengio, E. A.; ter Waarbeek, R. F.; de Jong, J. J.; Hoogerwerf, R. E.; et al. *Science* **2013**, 339, 182–186.

(16) Dürkop, T.; Getty, S. A.; Cobas, E.; Fuhrer, M. S. *Nano Lett.* **2004**, 4, 35–39.

(17) Rowell, M. W.; Topinka, M. A.; McGehee, M. D.; Prall, H. J.; Dennler, G.; Sariciftci, N. S.; Hu, L.; Gruner, G. *Appl. Phys. Lett.* **2006**, 88, 86–89.

(18) Hecht, D. S.; Thomas, D.; Hu, L.; Ladous, C.; Lam, T.; Park, Y.; Irvin, G.; Drzaic, P. *J. SID* **2009**, 17, 941–946.

(19) Jariwala, D.; Sangwan, V. K.; Lauhon, L. J.; Marks, T. J.; Hersam, M. C. *Chem. Soc. Rev.* **2013**, 42, 2824–2860.

(20) Nikolaev, P.; Bronikowski, M. J.; Bradley, R. K.; Rohmund, F.; Colbert, D. T.; Smith, K. .; Smalley, R. E. *Chem. Phys. Lett.* **1999**, 313, 91–97.

(21) Kong, J.; Cassell, A. M.; Dai, H. *Chem. Phys. Lett.* **1998**, 292, 567–574.

(22) Bernier, P.; Journet, C.; Maser, W. K.; Loiseau, A.; de la Chapelle, M. L.; Lefrant, S.; Deniard, P.; Lee, R.; Fischer, J. E. *Nature* **1997**, 388, 756–758.

(23) Guo, T.; Nikolaev, P.; Thess, A.; Colbert, D. T.; Smalley, R. E. *Chem. Phys. Lett.* **1995**, 243, 49–54.

(24) Kim, K. S.; Cota-Sanchez, G.; Kingston, C. T.; Imris, M.; Simard, B.; Soucy, G. *J. Phys. D. Appl. Phys.* **2007**, 40, 2375–2387.

(25) Tasis, D.; Tagmatarchis, N.; Bianco, A.; Prato, M. *Chem. Rev.* **2006**, 106, 1105–1136.

(26) Hirsch, A. *Angew. Chemie - Int. Ed.* **2002**, 41, 1853.

(27) Britz, D. A.; Khlobystov, A. N. *Chem. Soc. Rev.* **2006**, 35, 637–659.

(28) Campidelli, S.; Klumpp, C.; Bianco, A.; Guldi, D. M.; Prato, M. *J. Phys. Org. Chem.* **2006**, 19, 531–539.

(29) Setaro, A.; Adeli, M.; Glaeske, M.; Przyrembel, D.; Bisswanger, T.; Gordeev, G.; Maschietto, F.; Faghani, A.; Paulus, B.; Weinelt, M.; et al. *Nat. Commun.* **2017**, 8, 14281.

(30) Islam, M. F.; Rojas, E.; Bergey, D. M.; Johnson, A. T.; Yodh, A. G. *Nano Lett.* **2003**, 3, 269–273.

(31) Moore, V. C.; Strano, M. S.; Haroz, E. H.; Hauge, R. H.; Smalley, R. E.; Schmidt, J.; Talmon, Y. *Nano Lett.* **2003**, 3, 1379–1382.

(32) Gong, X.; Liu, J.; Baskaran, S.; Voise, R. D.; Young, J. S. *Chem. Mater.* **2000**, 12, 1049–1052.

(33) Yang, K.; Zhu, L.; Xing, B. *Environ. Sci. Technol.* **2006**, 40, 1855–1861.

(34) Tomonari, Y.; Murakami, H.; Nakashima, N. *Chem. - A Eur. J.* **2006**, 12, 4027–4034.

(35) Chen, R. J.; Zhang, Y.; Wang, D.; Dai, H. *J. Am. Chem. Soc.* **2001**, 123, 3838–3839.

(36) Guo, Z.; Sadler, P. J.; Tsang, S. C. *Adv. Mater.* **1998**, 10, 701–703.

(37) Zheng, M.; Jagota, A.; Strano, M. S.; Santos, A. P.; Barone, P.; Chou, S. G.; Diner, B. A.; Dresselhaus, M. S.; McLean, R. S.; Onoa, G. B.; et al. *Science* **2003**, 302, 1545–1548.

(38) Zheng, M.; Jagota, A.; Semke, E. D.; Diner, B. A.; McLean, R. S.; Lustig, S. R.; Richardson, R. E.; Tassi, N. G. *Nat. Mater.* **2003**, 2, 338–342.

(39) Chen, J.; Liu, H.; Weimer, W. A.; Halls, M. D.; Waldeck, D. H.; Walker, G. C. *J. Am. Chem. Soc.* **2002**, 124, 9034–9035.

(40) Star, A.; Stoddart, J. F.; Steuerman, D.; Diehl, M.; Boukai, A.; Wong, E. W.; Yang, X.; Chung, S. W.; Choi, H.; Heath, J. R. *Angew. Chemie - Int. Ed.* **2001**, 40, 1721–1725.

(41) Nish, A.; Hwang, J.-Y.; Doig, J.; Nicholas, R. J. *Nat. Nanotechnol.* **2007**, 2, 640–646.

(42) Ding, J.; Li, Z.; Lefebvre, J.; Cheng, F.; Dubey, G.; Zou, S.; Finnie, P.; Hrdina, A.; Scoles, L.; Lopinski, G. P.; et al. *Nanoscale* **2014**, 6, 2328–2339.

(43) Jakubka, F.; Schießl, S. P.; Martin, S.; Englert, J. M.; Hauke, F.; Hirsch, A.; Zaumseil, J. *ACS Macro Lett.* **2012**, 1, 815–819.

(44) Hwang, J.-Y.; Nish, A.; Doig, J.; Douven, S.; Chen, C.-W.; Chen, L.-C.; Nicholas, R. J. *J. Am. Chem. Soc.* **2008**, 130, 3543–3553.

(45) Nish, A.; Hwang, J.-Y.; Doig, J.; Nicholas, R. J. *Nat. Nanotechnol.* **2007**, 2, 640–646.

(46) Hwang, J.-Y.; Nish, A.; Doig, J.; Douven, S.; Chen, C.-W.; Chen, L.-C.; Nicholas, R. J. *J. Am. Chem. Soc.* **2008**, 130, 3543–3553.

(47) Stürzl, N.; Hennrich, F.; Lebedkin, S.; Kappes, M. M. *J. Phys. Chem. C* **2009**, 113, 14628–14632.

(48) Lee, H. W.; Yoon, Y.; Park, S.; Oh, J. H.; Hong, S.; Liyanage, L. S.; Wang, H.; Morishita, S.; Patil, N.; Park, Y. J.; et al. *Nat. Commun.* **2011**, 2, 541.

(49) Park, S.; Lee, H. W.; Wang, H.; Selvarasah, S.; Dokmeci, M. R.; Park, Y. J.; Cha, S. N.; Kim, J. M.; Bao, Z. *ACS Nano* **2012**, 6, 2487–2496.

(50) Bucella, S. G.; Salazar-Rios, J. M.; Derenskyi, V.; Fritsch, M.; Scherf, U.; Loi, M. A.; Caironi, M. *Adv. Electron. Mater.* **2016**, 2, 1600094.

(51) Lemasson, F. A.; Strunk, T.; Gerstel, P.; Hennrich, F.; Lebedkin, S.; Barner-Kowollik, C.; Wenzel, W.; Kappes, M. M.; Mayor, M. *J. Am. Chem. Soc.* **2011**,

133, 652–655.

(52) Rice, N. A.; Adronov, A. *Macromolecules* **2013**, 46, 3850–3860.

(53) Rice, N. A.; Adronov, A. *J. Polym. Sci. Part A Polym. Chem.* **2014**, 52, 2738–2747.

(54) Zhao, M.; Hashimoto, K.; Tajima, K. *Jpn. J. Appl. Phys.* **2013**, 52.

(55) Gasperini, A.; Jeanbourquin, X. A.; Rahmanudin, A.; Yu, X.; Sivula, K. *Adv. Mater.* **2015**, 27, 5541–5546.

(56) Schroeder, B. C.; Chiu, Y.-C.; Gu, X.; Zhou, Y.; Xu, J.; Lopez, J.; Lu, C.; Toney, M. F.; Bao, Z. *Adv. Electron. Mater.* **2016**, 2, 1600104.

(57) Gasperini, A.; Bivaud, S.; Sivula, K. *Chem. Sci.* **2014**, 5, 4922–4927.

(58) Rice, N. A.; Subrahmanyam, A. V.; Coleman, B. R.; Adronov, A. *Macromolecules* **2015**, 48, 5155–5161.

(59) Manhas, M. S.; Hoffman, W. H.; Lal, B.; Bose, A. K. *J. Chem. Soc. Perkin Trans. 1* **1975**, No. 5, 461.

(60) Rice, N. A.; Subrahmanyam, A. V.; Laengert, S. E.; Adronov, A. *J. Polym. Sci. Part A Polym. Chem.* **2015**, 53, 2510–2516.

(61) Strano, M. S.; Dyke, C. A.; Usrey, M. L.; Barone, P. W.; Allen, M. J.; Shan, H.; Kittrell, C.; Hauge, R. H.; Tour, J. M.; Smalley, R. E. *Science* **2003**, 301, 1519–1522.

(62) Lei, T.; Pochorovski, I.; Bao, Z. *Acc. Chem. Res.* **2017**, 50, 1096–1104.

(63) Grasso, G.; Titman, J. J. *Macromolecules* **2009**, 42, 4175–4180.

(64) Dresselhaus, M. S.; Jorio, A.; Hofmann, M.; Dresselhaus, G.; Saito, R. *Nano Lett.* **2010**, 10, 751–758.

(65) Dresselhaus, M. S.; Dresselhaus, G.; Saito, R.; Jorio, A. *Phys. Rep.* **2005**, 409, 47–99.

(66) Doorn, S. K. *J. Nanosci. Nanotechnol.* **2005**, 5, 1023–1034.

(67) Strano, M. S.; Zheng, M.; Jagota, A.; Onoa, G. B.; Heller, D. A.; Barone, P. W.; Usrey, M. L. *Nano Lett.* **2004**, 4, 543–550.

(68) Strano, M. S.; Doorn, S. K.; Haroz, E. H.; Kittrell, C.; Hauge, R. H.; Smalley, R. E. *Nano Lett.* **2003**, 3, 1091–1096.

(69) Brown, S.; Jorio, A.; Corio, P.; Dresselhaus, M.; Dresselhaus, G.; Saito, R.; Kneipp, K. *Phys. Rev. B* **2001**, 63, 1–8.

(70) Heller, D. A.; Barone, P. W.; Usrey, M. L.; Strano, M. S.; Doorn, S. K. *Appl. Phys. A Mater. Sci. Process.* **2004**, 78, 1147–1155.

(71) Weisman, R. B.; Bachilo, S. M. *Nano Lett.* **2003**, 3, 1235–1238.

(72) Oyama, Y.; Saito, R.; Sato, K.; Jiang, J.; Samsonidze, G. G.; Grüneis, A.; Miyauchi, Y.; Maruyama, S.; Jorio, A.; Dresselhaus, G.; et al. *Carbon* **2006**, 44, 873–879.

(73) Lei, T.; Lai, Y. C.; Hong, G.; Wang, H.; Hayoz, P.; Weitz, R. T.; Chen, C.; Dai, H.; Bao, Z. *Small* **2015**, 11, 2946–2954.

(74) Xia, C.; Advincula, R. C. *Macromolecules* **2001**, 34, 5854–5859.

(75) Rice, N. A.; Subrahmanyam, A. V.; Coleman, B. R.; Adronov, A. *Macromolecules* **2015**, 48, 5155–5161.

Chapter 4

Decoration of Polyfluorene-Wrapped Carbon Nanotubes via Strain-Promoted Azide–Alkyne Cycloaddition

This chapter has been reprinted with permission from Macromolecules. Fong, D.; Yeung, J.; McNelles, S. A.; Adronov, A. **2018**, *51*, 755-762. Copyright (2018) American Chemical Society.

D. Fong planned the study and performed the Raman and fluorescence mapping experiments. D. Fong and J. Yeung performed the remaining experiments. S. A. McNelles synthesized the strained cyclooctyne derivatives.

Abstract

Developing methodologies that can efficiently decorate carbon nanotube surfaces with various molecular structures while avoiding damage to nanotube optoelectronic properties is an ongoing challenge. Here, we outline a methodology to perform chemistry on the nanotube surface without perturbing optoelectronic properties. Reactive, noncovalently functionalized polymer–nanotube complexes were prepared using polyfluorene with azide groups in its side chains. The azides enable strain-promoted azide–alkyne cycloaddition to occur between polymer–nanotube complexes and small molecules or polymers derivatized with a strained cyclooctyne. This reaction was found to occur efficiently at room temperature, without any catalyst or byproduct removal required. The reaction was monitored by infrared spectroscopy via the disappearance of the polymer azide stretch at ∼2090 cm^{-1}, and this chemistry resulted in no damage to the nanotube sidewall, as evidenced by Raman spectroscopy. The azide-containing polyfluorene was used to prepare an enriched dispersion of semiconducting carbon nanotubes in organic media, which could then be redispersed in aqueous solution post-click with strained cyclooctyne-functionalized poly(ethylene glycol). Taking advantage of the ability to preserve optoelectronic properties, solvatochromism of an identical subset of semiconducting carbon nanotubes was investigated using absorption, fluorescence, and Raman spectroscopy. It was found that, in aqueous media, fluorescence was nonuniformly quenched among the different semiconducting species and that there was a significant red-shift in the emission of all nanotubes in D_2O relative to nonpolar toluene.

4.1 Introduction

Since the discovery of single-walled carbon nanotubes (SWNTs) in 1991,[1] significant efforts have been made to exploit their extraordinary structural,[2–4] mechanical,[5–7] and optoelectronic properties.[8–10] This task, however, is nontrivial as all known commercial SWNT synthetic methods result in a complex mixture of amorphous carbon, leftover metal catalyst particles, and both semiconducting and metallic SWNTs.[11–15] Furthermore, due to intertube π–π interactions, SWNTs form bundles that are insoluble in typical aqueous and organic solvents.[16] In order to take advantage of the exceptional properties possessed by SWNTs, nanotube exfoliation and dispersion are imperative, typically relying on either covalent or noncovalent functionalization methods.[17–19] Covalent functionalization involves directly performing chemistry on the SWNT sidewall, which typically disrupts the extended π-system and destroys the advantageous SWNT properties.[19] Recently, Reich and co-workers reported a covalent functionalization method that preserved SWNT optoelectronic properties by utilizing a [2 + 1] cycloaddition with an electron-poor nitrene.[20] However, subsequent SWNT decoration via nucleophilic substitution required elevated temperatures ($60 - 70\,^{\circ}\mathrm{C}$) and long reaction times (2–4 days). Alternatively, noncovalent functionalization involves the formation of supramolecular complexes that do not disrupt the SWNT π-system, which has led to significant interest in this area of research.[21–28] For noncovalent functionalization, a dispersant is required to prevent SWNT bundle reaggregation and render SWNTs processable. Numerous dispersants have been identified, including surfactants,[29–31] aromatic compounds,[32–34] conjugated polymers,[35–39] proteins,[40–42] polysaccharide–iodine complexes,[43] and DNA.[44–46]

Conjugated polymers are of particular interest, as synthetic control allows for a large variety of structures to be produced and for polymer structure to be tailored to a desired application. To date, conjugated polymers have been primarily viewed as a vehicle for dispersing SWNTs rather than as a functional coating that can impart reactivity to the polymer–SWNT supramolecular complex. In particular, the use of conjugated polymers in the context of nanotube science has been focused on the selective dispersion of semiconducting SWNTs (sc-SWNTs), with recent endeavors toward developing polymer backbone structures capable of conformational changes or depolymerization in response to a stimulus.[47–51] Little attention has been given to the use of conjugated polymers that not only form polymer–SWNT complexes but can also be derivatized after supramolecular functionalization of the SWNTs.

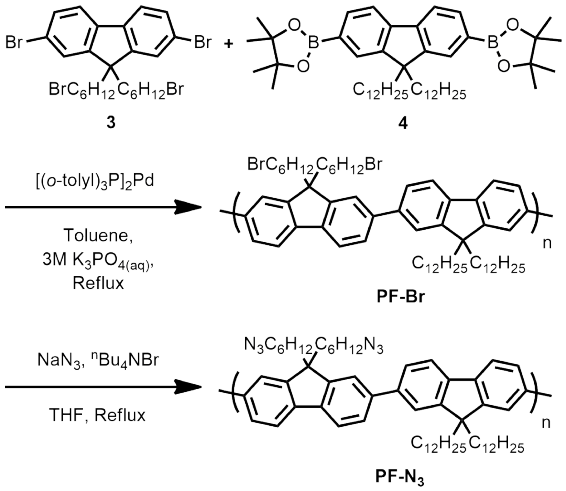
In the seminal work by Bertozzi and co-workers in 2004,[52] the strain-promoted azide–alkyne cycloaddition (SPAAC) was reported as a rapid and efficient "click" reaction. SPAAC involves the catalyst-free [3 + 2] cycloaddition between a strained cyclooctyne and azide to form a triazole ring. The reaction occurs rapidly at room temperature and is free of byproducts. As a result of these qualities, SPAAC has been extensively used in chemical biology,[53–57] as it is bioorthogonal and facile under biological conditions. SPAAC has found less use in materials science to date,[58–62] and with respect to SWNT work, only a single report has been published on the use of SPAAC to produce nanohybrids of covalently functionalized SWNTs and gold nanoparticles (AuNPs).[63] Here, we sought to combine the efficacy of noncovalent functionalization in preserving SWNT optoelectronic properties with the rapid and efficient chemistry of SPAAC. We prepared a polyfluorene with side chains that are decorated with azide groups and used this conjugated polymer

to produce reactive polymer–SWNT complexes that can undergo SPAAC with small molecules or polymers derivatized with dibenzoazacyclooctyne (DIBAC). The reactive polymer–SWNT complexes can be rapidly and efficiently modified under ambient conditions without the addition of catalyst. We show that SPAAC can be used to dramatically alter the dispersion properties of the polymer–SWNT complex and that, unlike with covalent functionalization methods, the SWNT optoelectronic properties are completely preserved after chemical derivatization. This property enables the study of solvatochromism for the same subset of enriched sc-SWNTs in solvents with very different dielectric constants by sorting sc-SWNTs in an organic solvent followed by modification of the dispersion properties using SPAAC.

4.2 Results and Discussion

To prepare reactive polymer–SWNT complexes, we first synthesized an azide-containing polyfluorene (**PF-N$_3$**) from commercially available fluorene (synthetic details provided in the Supporting Information). Bromination of fluorene with *N*-bromosuccinimide (NBS) produced monomer precursor **1**, which was then alkylated under phase-transfer conditions with either 1-bromododecane or 1,6-dibromo hexane to afford compounds **2** and **3**, respectively (Supporting Information, Scheme S4.6). Compound **2** was borylated using the Miyaura reaction to afford compound **4**. Compounds **3** and **4** were copolymerized using Suzuki polycondensation to afford **PF-Br**, as depicted in Scheme 4.1. GPC analysis showed that **PF-Br** had an M_n of 61.0 kDa, corresponding to a degree of polymerization of ∼62, and a dispersity (Đ) of 2.31. The alkyl bromides in **PF-Br** were then cleanly converted to

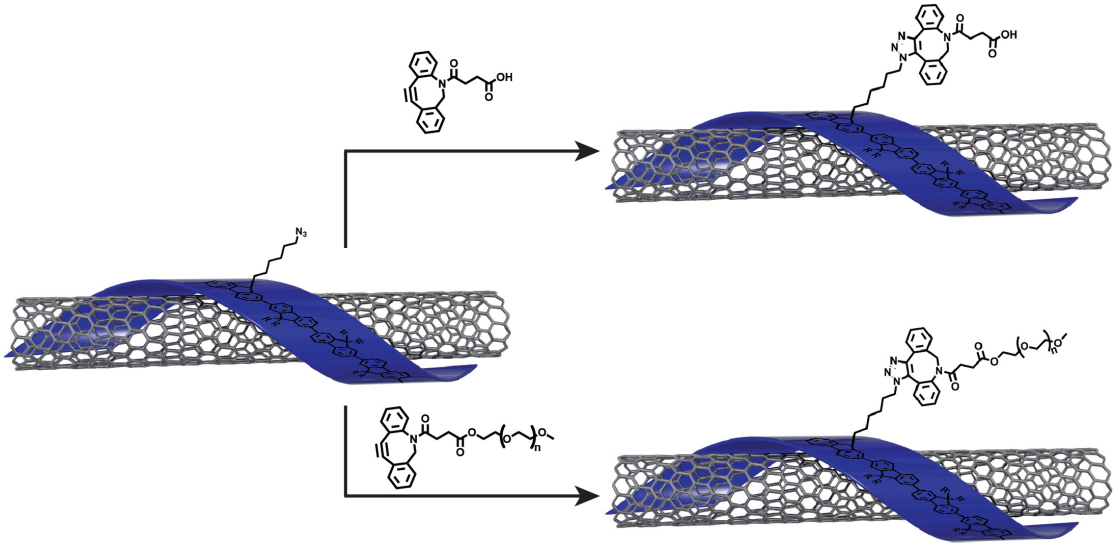
azides using tetrabutylammonium azide generated *in situ* in THF to obtain **PF-N$_3$**. It was necessary to prepare **PF-N$_3$** postpolymerization from the alkyl halide precursor **PF-Br**, as azide moieties can be reduced by the phosphine ligands used in Pd cross-coupling reactions, also known as the Staudinger reaction.[64] The polymer samples were characterized by ^{1}H NMR and FT-IR spectroscopy to confirm the presence of azide moieties in **PF-N$_3$** (Supporting Information, Figures S1 and S2). The ^{1}H NMR spectra clearly show that the signal corresponding to the methylene groups adjacent to the alkyl bromide in **PF-Br** shifts from 3.30 to 3.15 ppm upon azidification (Figure S4.7). The FT-IR spectra also show the appearance of a peak centered at ∼2090 cm^{-1} upon azidification, which is consistent with the presence of alkyl azide in **PF-N$_3$** (Figure S4.8).



SCHEME 4.1: Synthesis of Fluorene–Azide Copolymer **PF-N$_3$**

With **PF-N$_3$** in hand, we prepared reactive polymer–SWNT complexes with semipurified plasma torch SWNTs (Raymor Industries, Inc.) following modified literature procedures.[65] Briefly, a mixture of 10 mg of **PF-N$_3$** and 5 mg of SWNTs in 20 mL of THF was sonicated in a bath sonicator chilled with ice for 1.5 h. The resulting black suspension was centrifuged at 15000 *g* for 20 min at 10 °C, and

the supernatant was carefully removed to isolate the **PF-N_3**–SWNT dispersion. The **PF-N_3**–SWNT dispersion was stable on the benchtop for at least several months, with no observable flocculation. To explore the reactivity of this **PF-N_3**–SWNT dispersion, it was initially treated with DIBAC-COOH (Scheme 4.2), which was prepared according to literature procedures.[66] In a glass vial, a 4 mL aliquot of **PF-N_3**–SWNT dispersion was introduced, then 2 equiv of DIBAC-COOH was added, and the dispersion was agitated until DIBAC-COOH was dissolved (see Supporting Information for experimental details). As shown in Figure 4.1, the SPAAC reaction could be monitored by the disappearance of the IR peak centered at ∼2090 cm^{-1}, indicating the consumption of the azide moiety in the polymer side chains of the **PF-N_3**–SWNT complex. Complete consumption of the azide moiety was found to occur within 30 min, without any stirring of the SWNT dispersion required. Raman spectroscopy confirmed that SPAAC with the side chains of the adsorbed polymer did not damage the SWNT surface, as indicated by the absence of change in the disorder (D) band centered at ∼1290 cm^{-1} (Figure S4.10). An increase in the D band would be indicative of an increase in the amount of sp^3-hybridized carbon atoms in the SWNT sidewall, but this is not observed post-SPAAC in our SWNT sample.[67,68] This demonstrates that, unlike covalent functionalization, nondisruptive chemistry is possible on the SWNT surface if it is performed on the adsorbed conjugated polymer, rather than directly with the SWNT sidewall. This avoids the introduction of defects in the SWNT structure, which is a significant drawback of the covalent functionalization method. Furthermore, SPAAC functionalization using reactive polymer–SWNT complexes can be accomplished rapidly under mild conditions and requires no removal of catalysts or byproducts.



SCHEME 4.2: SPAAC Functionalization of Azide-Bearing Polymer–SWNT Complexes Using DIBAC-COOH and $mPEG_{5000}$–DIBAC

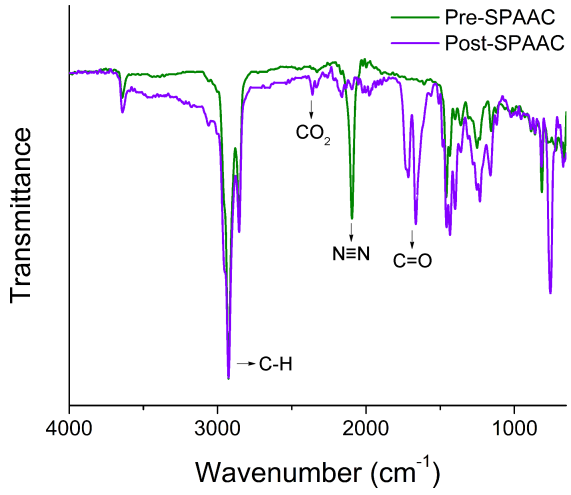


FIGURE 4.1: FT-IR overlay of the **PF-N_3**–SWNT dispersion before (green) and 30 min after the addition of DIBAC-COOH (purple).

To further investigate the reactivity of the **PF-N_3**–SWNT complex, we prepared DIBAC-functionalized poly(ethylene glycol) (PEG) (M_n of 5 kDa) via the Steglich esterification of monomethyl ether PEG_{5000} ($mPEG_{5000}$-OH) with DIBAC-COOH (see Supporting Information for details). We treated 4 mL of **PF-N_3**–SWNT

dispersion with 2 equiv of $mPEG_{5000}$–DIBAC (Scheme 4.2) and found that the reaction was complete within 30 min, as determined by FT-IR spectroscopy (Figure S4.11). To demonstrate the dramatic change in **PF-N_3**–SWNT dispersion properties post-SPAAC, we partitioned the **PF-N_3**–SWNT dispersion pre- and post-SPAAC with a D_2O brine solution. Strikingly, the solubility of the **PF-N_3**–SWNT complex was drastically altered upon SPAAC with $mPEG_{5000}$–DIBAC. As shown in Figure 4.2, UV/Vis–NIR absorption spectroscopy of the organic (Figure 4.2a) and aqueous (Figure 4.2b) phases confirms the presence of SWNTs in the organic phase prior to SPAAC and in the aqueous phase post-SPAAC. A photograph of the biphasic mixture pre- and post-SPAAC with $mPEG_{5000}$–DIBAC is shown in Figure 4.2c. The denser aqueous phase is evidently colorless prior to SPAAC with $mPEG_{5000}$–DIBAC, but post-SPAAC and after extraction of the organic phase (carried out by simply shaking the biphasic mixture and allowing it to separate on standing), it acquires the dark color associated with dispersed SWNTs. To confirm that the covalent introduction of $mPEG_{5000}$–DIBAC upon SPAAC was responsible for the observed change, we performed a control experiment in which 500 μL of **PF-N_3**–SWNT dispersion in THF was mixed with 2 equiv of $mPEG_{5000}$-OH (containing no DIBAC) and allowed to stand for 30 min. Subsequent addition of 500 μL of D_2O to this dispersion resulted in rapid precipitation of nanotubes. Similar addition of D_2O to the as-produced **PF-N_3**–SWNT dispersion also resulted in SWNT precipitation. However, D_2O addition to the post-SPAAC **PF-N_3**–$mPEG_{5000}$–SWNT dispersion resulted in no observable precipitation (Figure S4.12). These experiments demonstrate that SPAAC results in a covalent linkage to $mPEG_{5000}$, which alters the dispersion properties of the polymer–SWNT complex, and that simple addition of $mPEG_{5000}$ alone is insufficient for dispersion of

the polymer–SWNT complex in a 1:1 mixture of D_2O:THF.

To demonstrate that SPAAC chemistry with the reactive polymer–SWNT complex can be performed irrespective of SWNT diameter, we performed the phase extraction study on HiPCO SWNTs. Compared to plasma torch SWNTs, which have a diameter range of 1.1–1.5 nm, HiPCO SWNTs have a lower average diameter of 0.8–1.2 nm.[69] To prepare the HiPCO dispersion with **PF-N$_3$**, 15 mg of **PF-N$_3$** and 15 mg of raw HiPCO SWNTs were sonicated in 20 mL of THF for 2 h in a bath sonicator chilled with ice. The black suspension was then centrifuged at 8346 *g* for 30 min followed by careful removal of the supernatant to isolate the **PF-N$_3$**–SWNT HiPCO dispersion, which was stable on the benchtop for at least several months. UV/Vis–NIR absorption spectroscopy of the organic (Figure 4.2d) and aqueous (Figure 4.2e) phases confirmed the same dispersibility change upon SPAAC with mPEG$_{5000}$–DIBAC. A photograph of the biphasic mixture pre- and post-SPAAC with HiPCO SWNTs is shown in Figure 4.2f, again illustrating that the polymer–SWNT dispersion properties post-SPAAC are drastically different. Thus, irrespective of SWNT diameter, SPAAC with the side chains in the adsorbed polymer of the polymer–SWNT complex can be performed in a facile manner.

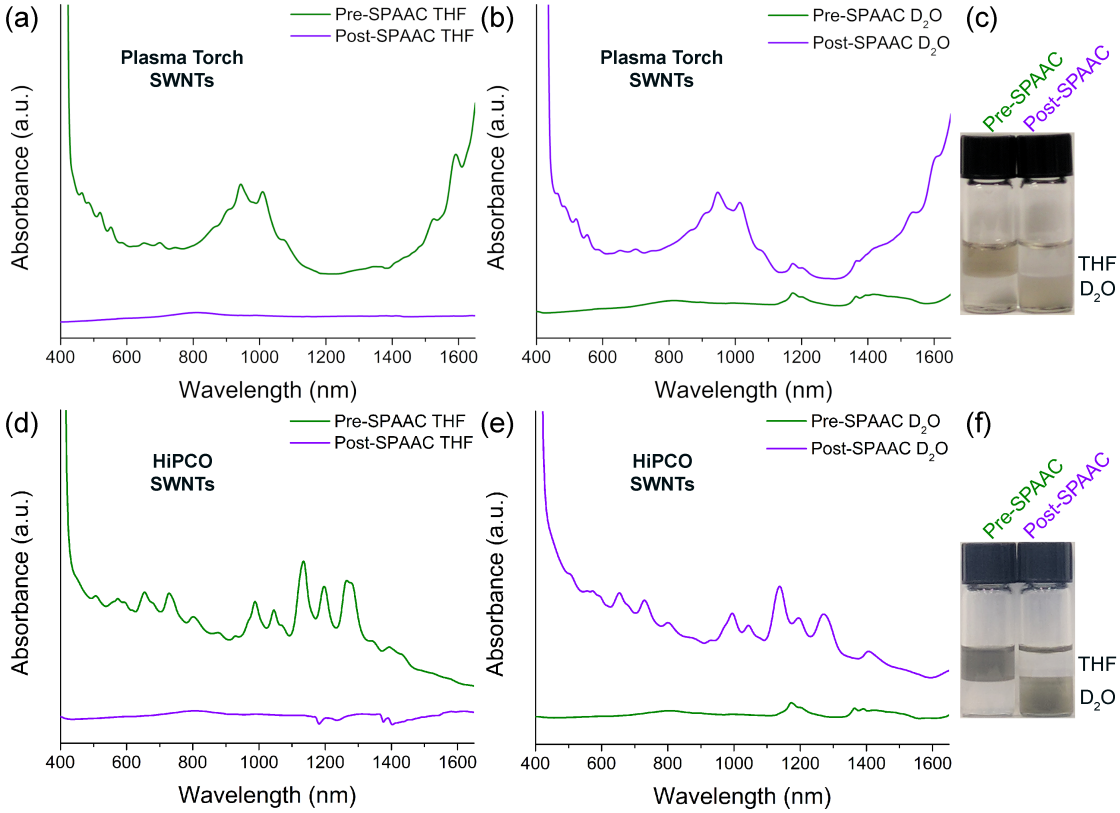


FIGURE 4.2: SPAAC of **PF-N$_3$**–SWNT complex with mPEG$_{5000}$–DIBAC. UV/Vis–NIR spectra of **PF-N$_3$**-coated plasma torch SWNTs pre-SPAAC (green) and post-SPAAC (purple) in (a) THF and (b) D_2O brine. (c) Photograph of organic/aqueous partitions pre- and post-SPAAC for **PF-N$_3$**-coated plasma torch SWNTs. UV/Vis–NIR spectra of **PF-N$_3$**-coated HiPCO SWNTs pre-SPAAC (green) and post-SPAAC (purple) in (d) THF and (e) D_2O brine. (f) Photograph of organic/aqueous partitions pre- and post-SPAAC for **PF-N$_3$**-coated HiPCO SWNTs. The photographs show the biphasic mixtures pre- and post-SPAAC under ambient conditions.

With these results in hand, we were interested in demonstrating the utility of reactive polymer–SWNT complexes by preparing aqueous SWNT dispersions enriched in sc-SWNTs. It is well-known that polyfluorenes can selectively disperse sc-SWNTs in toluene. However, to the best of our knowledge, the selective dispersion of sc-SWNTs in aqueous media using conjugated polymers has not been reported. Here, we show that aqueous dispersions of sc-SWNTs can be achieved if they are first prepared in toluene and then subsequently transferred to water via

SPAAC modification of the surface-bound polymer. Using a protocol adapted from the literature,[65] an enriched dispersion of sc-SWNTs from raw HiPCO SWNTs was prepared. HiPCO SWNTs were used in this study, as methods to extensively characterize the SWNT populations are well-established. Briefly, 15 mg of **PF-N$_3$** and 15 mg of raw HiPCO SWNTs were sonicated in 20 mL of toluene for 2 h in a bath sonicator chilled with ice. The black suspension was then centrifuged at 8346 *g* for 30 min followed by careful removal of the supernatant to isolate the SWNT dispersion. To 4 mL of this dispersion, 2 equiv of mPEG$_{5000}$–DIBAC was added, and the mixture was allowed to stand for 30 min. The solvent was removed *in vacuo*, and the dispersion was easily reconstituted in the same volume of D_2O with gentle shaking. To investigate the polymer–SWNT dispersions, we initially performed UV/Vis–NIR spectroscopy, as shown in Figure S4.13. The absorption features in these spectra can be grouped into three categories: two semiconducting regions, S_{11} (830–1600 nm) and S_{22} (600–800 nm), and a metallic region, M_{11} (440–645 nm).[70] The absorption spectrum for **PF-N$_3$**–SWNT in toluene shows sharp peaks in the S_{11} and S_{22} regions, suggesting that sc-SWNTs are efficiently exfoliated in toluene. In addition, there is an absence of both M_{11} signals and a broad, featureless absorption background, which in tandem indicates the removal of metallic SWNTs (m-SWNTs), consistent with previous reports.[71] This analysis is corroborated by the intense bluish-green color of the **PF-N$_3$**–SWNT dispersion in toluene (Figure S4.13). The UV/Vis–NIR spectrum of the reconstituted post-SPAAC dispersion in D_2O exhibited identical spectral features to the pre-SPAAC sample, indicating that all the same SWNT species were redispersed in D_2O (Figure S4.13).

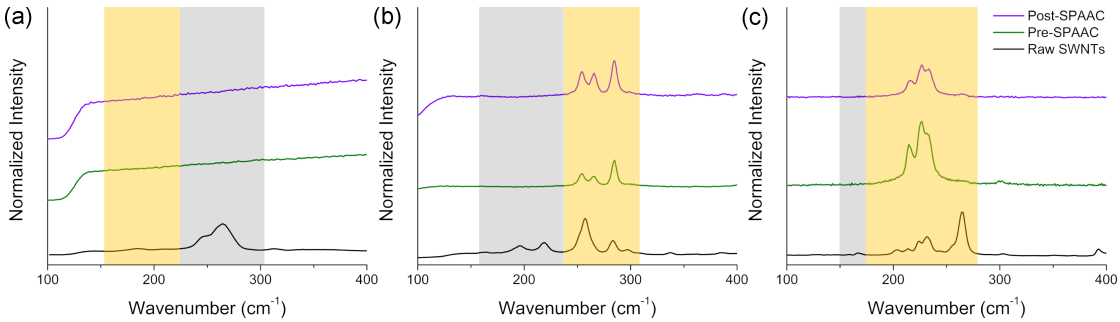


FIGURE 4.3: Raman spectra of **PF-N$_3$**–HiPCO dispersions pre- and post-SPAAC with mPEG$_{5000}$–DIBAC in toluene or D_2O at (a) 514, (b) 633, and (c) 785 nm. The yellow boxes denote the locations of signals arising from sc-SWNTs, while the gray boxes represent the locations of signals arising from m-SWNTs.

To further investigate the nanotube populations dispersed by **PF-N$_3$** in toluene and D_2O, resonance Raman spectroscopy was performed. This technique allows for the identification of both m- and sc-SWNT species within a given sample[72] and utilizes laser excitation wavelengths that overlap with the van Hove singularities present in the 1D density of states for a particular SWNT.[73] As the electronic transitions depend on nanotube chirality and diameter, only a subset of the total nanotube population is observable at each individual excitation energy, necessitating the use of multiple excitation wavelengths, which include 514, 633, and 785 nm for HiPCO SWNTs.[74] These excitation wavelengths have previously been shown to be adequate for characterizing the electronic character of HiPCO SWNT samples, as both m- and sc-SWNTs can be separately probed.[75] Thin film samples were prepared from the polymer–SWNT complexes by drop-casting the dispersions onto silicon wafers. A reference SWNT sample was also prepared by sonicating a small amount of the SWNT starting material in $CHCl_3$ and making a solid film with the same drop-casting method. Figure 4.3 shows the radial breathing mode (RBM) regions, from 100 to 400 cm^{-1}, for the three samples at each excitation wavelength. All Raman spectra were normalized to the G-band at ~1590

cm^{-1} and offset for clarity. Upon excitation at 514 nm, mainly m-SWNTs are generally observed in the 225–290 cm^{-1} region.[76] The polymer–SWNT samples pre- and post-SPAAC exhibit no peaks in this RBM region, indicating the absence of m-SWNTs. With 633 nm excitation, both m- and sc-SWNTs are typically in resonance, with m-SWNT features found at ~175–230 cm^{-1} and sc-SWNT features at ~230–300 cm^{-1}.[70,75] In our experiments, only sc-SWNT features were detected for the polymer–SWNT samples, again indicating selective dispersion of sc-SWNTs. Excitation at 785 nm, where mainly sc-SWNTs are in resonance, again confirmed that only sc-SWNTs were present in the polymer–SWNT dispersions, both pre- and post-SPAAC.

To further characterize the polymer–SWNT dispersions, photoluminescence (PL) maps were recorded in toluene (pre-SPAAC) and D_2O (post-SPAAC), depicted in Figure 4.4. The locations of various SWNT fluorescence maxima were assigned according to previously published data.[77] In toluene, high intensity PL signals were observed for the **PF-N_3**–SWNT dispersion, with the most intense peaks corresponding to the (7,6) and (8,6) chiralities (Figure 4.4a). In D_2O, the highest intensity PL signal corresponds to the (7,6) chirality (Figure 4.4b). The ability to transfer an identical population of sc-SWNTs from toluene to D_2O allows direct comparison of their photophysical properties in the two different environments. As seen in Figure S4.14, the absorption spectra of the HiPCO SWNTs are practically identical in toluene and D_2O prior to recording the respective PL maps. However, the intensity of SWNT emission is significantly affected upon going from toluene to D_2O. Furthermore, the magnitude of quenching is not identical for all polymer-wrapped sc-SWNT species. Figure 4.5 shows the fluorescence intensity

(I_{PL}) of the major sc-SWNT species present in both toluene and D_2O, normalized to the intensity of the (7,6) signal in each PL map. Based on this data, the polymer-wrapped (8,7) and (9,5) species exhibited substantial quenching (~40% the I_{PL} in D_2O), while the (8,4) species exhibited a slight increase in I_{PL} (~104% the I_{PL} in D_2O). It is striking that among the different PF-sc-SWNT complexes, solvent effects on fluorescence emission intensity substantially differ.

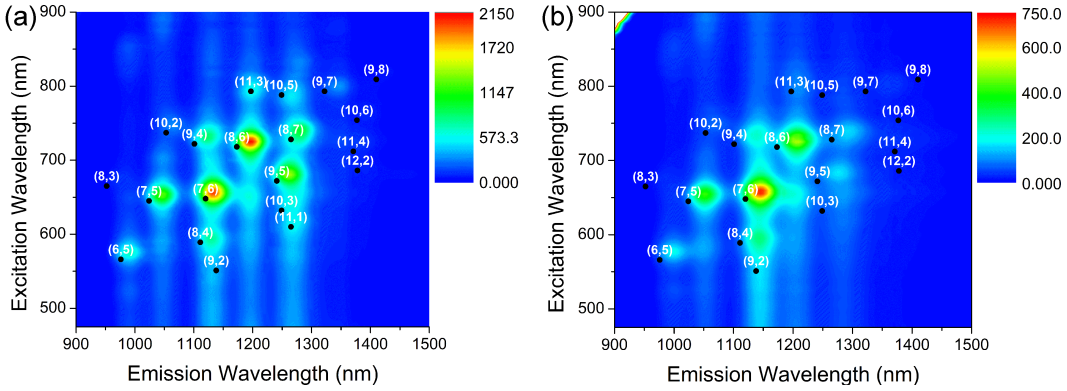


FIGURE 4.4: Photoluminescence maps of **PF-N_3**–HiPCO dispersions in (a) toluene (pre-SPAAC) and (b) D_2O (post-SPAAC with $mPEG_{5000}$–DIBAC).

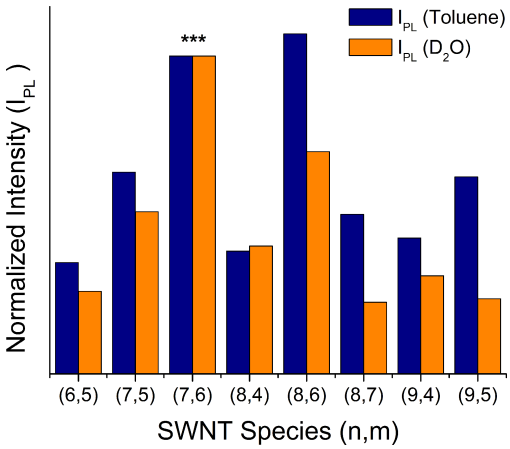


FIGURE 4.5: Relative I_{PL} values for **PF-N_3**–$mPEG_{5000}$-coated sc-SWNTs dispersed in toluene (blue) or D_2O (orange). ***I_{PL} values in a given solvent are normalized to the IPL of the (7,6) species for that solvent.

In addition to substantial variation in fluorescence emission intensity, significant bathochromic shifts in the λ_{em}, ranging from 5 to 16 nm, were found for each of the PF–sc-SWNT species upon transitioning from toluene to D_2O (Table 4.1). To test whether these red-shifts could have simply been caused by the presence of $mPEG_{5000}$, a control sample was prepared where 2 equiv of $mPEG_{5000}$-OH was added to the toluene dispersion. The PL map from this sample did not exhibit λ_{em} shifts beyond ± 1 nm (Figure S4.15 and Table S4.2). Thus, the presence of $mPEG_{5000}$-OH cannot account for the magnitude of the observed shifts in λ_{em} seen when transferring the polymer-wrapped sc-SWNT population from toluene to D_2O. Several studies have attempted to probe solvatochromism in SWNT emission,[78–80] but the majority of these studies could only compare polar organic and aqueous solvents.[78,80] To the best of our knowledge, this study is the first example of direct measurement of solvatochromic effects on SWNTs in an identical sc-SWNT population, where the SWNTs are completely immersed in either nonpolar toluene or polar D_2O.

Chirality	λ_{em} (nm) (toluene)	λ_{em} (nm) (+D_2O)	$\Delta[\lambda_{em}]^a$ (nm)
(6,5)	990	997	+7
(7,5)	1047	1052	+5
(7,6)	1134	1145	+11
(8,4)	1131	1143	+12
(8,6)	1196	1207	+11
(8,7)	1280	1293	+13
(9,4)	1125	1141	+16
(9,5)	1265	1278	+13

TABLE 4.1: $^a\Delta[\lambda_{em}]$ was calculated as $\lambda_{em}[D_2O] - \lambda_{em}$[toluene].

The ability to quantitatively compare the emission properties of sc-SWNTs in

dramatically different environments relies on the ability to decorate SWNT surfaces in a reliable manner without affecting the SWNT side-wall structure – a capability made possible by the SPAAC reaction with the side chains of a conjugated polymer. It is conceivable that the order of operations could be reversed, whereby **PF-N$_3$** is reacted with mPEG$_{5000}$–DIBAC and then used to disperse HiPCO SWNTs. This would then, in principle, allow for any PEG-functionalized conjugated polymer to be used to study solvatochromic effects on the same subset of sc-SWNTs. To determine whether or not the order of operations matters, we prepared the graft copolymer **PF-N$_3$**–mPEG$_{5000}$ by click coupling **PF-N$_3$** with mPEG$_{5000}$–DIBAC and then used this graft copolymer to disperse HiPCO SWNTs in toluene using the procedure outlined above (see Supporting Information for details). A UV/Vis–NIR spectrum of the as-produced **PF-N$_3$**–mPEG$_{5000}$–SWNT dispersion in toluene (diluted 16-fold) is shown in Figure S4.16. The spectrum exhibits sharp peaks, indicative of good SWNT exfoliation by **PF-N$_3$**–mPEG$_{5000}$; however, it is evident that M_{11} signals and an exponentially increasing background at low wavelengths are present, indicative of the presence of m-SWNTs. Thus, although **PF-N$_3$**–mPEG$_{5000}$ is excellent for the production of concentrated SWNT dispersions, it cannot selectively disperse sc-SWNTs.

4.3 Conclusions

Here, we demonstrate that SPAAC can be used to derivatize polymer–SWNT complexes containing azide moieties in the polymer side chains. SPAAC was monitored using IR spectroscopy for the disappearance of the azide stretch at ~2090 cm^{-1}, and the reaction was found to occur at room temperature within half an

hour, without the addition of any catalysts. Reactive polymer–SWNT complexes could be modified with $mPEG_{5000}$ to alter the dispersion properties, as shown using UV/Vis–NIR spectroscopy and solvent partitioning between THF and D_2O (brine) pre- and post-click. This SPAAC modification could be performed with both HiPCO and plasma torch SWNTs, indicating that polymer–SWNT functionalization can be performed irrespective of SWNT diameter. An enriched dispersion of sc-SWNTs was prepared with the latently reactive polyfluorene, and then derivatized via SPAAC with $mPEG_{5000}$ to, for the first time, enable the study of solvatochromic effects on SWNT emission in solvents with drastically different dielectric constants. We characterized these dispersions using absorption, Raman, and fluorescence spectroscopy, and nonuniform fluorescence quenching was observed among the different sc-SWNT species. In addition, significant red-shifts were found in the emission wavelength when comparing SWNTs dispersed in nonpolar toluene versus aqueous media. Overall, we demonstrate that the functionalization of polymer–SWNT complexes using latently reactive side chains of the adsorbed polymer is a facile decoration method that avoids perturbing SWNT optoelectronic properties.

4.4 Supporting Information

4.4.1 General

Semi-purified plasma torch SWNTs (RN120, batch #RNB735-120-X464) were purchased from Raymor Industries Inc. and used without further purification. Raw HiPCO SWNTs were purchased from NanoIntegris (batch #HR27-104, 10 wt % in anhydrous EtOH) and also used without further purification. Reagents were purchased from commercial suppliers and used as received. Monomethyl ether

$mPEG_{5000}$ was purchased from Fluka. Flash chromatography was performed using an IntelliFlash 280 system from Analogix. Unless otherwise noted, compounds were monitored using a variable wavelength detector at 254 nm. Solvent amounts used for gradient or isocratic elution were reported in column volumes (CV). Columns were prepared in Biotage® SNAP KP-Sil cartridges using 40 – 63 μm silica or 25 – 40 μm silica purchased from Silicycle. NMR was performed on a Bruker Avance 600 MHz or 700 MHz instrument and shift-referenced to the residual solvent resonance. Polymer molecular weights and dispersities were analyzed (relative to polystyrene standards) via GPC using a Waters 2695 Separations Module equipped with a Waters 2414 refractive index detector and a Jordi Fluorinated DVB mixed bed column in series with a Jordi Fluorinated DVB 10^5 Å pore size column. THF with 2% acetonitrile was used as the eluent at a flow rate of 2.0 mL/min. Sonication was performed in a Branson Ultrasonic B2800 bath sonicator. Centrifugation of the polymer-SWNT samples was performed using a Sorvall Legend X1R centrifuge (semi-purified plasma torch SWNT dispersions) or a Beckman Coulter Allegra X-22 centrifuge (raw HiPCO SWNT dispersions). Infrared spectra were recorded using a Thermo Scientific Nicolet 6700 FT-IR spectrometer equipped with a Smart iTX attenuated total reflectance (ATR) sample analyzer. UV/Vis-NIR spectra were recorded on a Cary 5000 spectrometer in dual beam mode, using matching 10 mm quartz cuvettes. Fluorescence spectra were measured on a Jobin-Yvon SPEX Fluorolog 3.22 equipped with a 450 W Xe arc lamp, digital photon counting photomultiplier, and an InGaAs detector, also using a 10 mm quartz cuvette. Slit widths for both excitation and emission were set to 10 nm band-pass, and correction factor files were applied to account for instrument variations. Photoluminescence maps were obtained at 25 °C, with 5 nm intervals for

both the excitation and emission. Raman spectra were collected using a Renishaw InVia Laser Raman spectrometer, with three different lasers: a 25 mW argon ion laser (514 nm, 1800 L/mm grating); a 500 mW HeNe Renishaw laser (633 nm, 1800 L/mm grating); and a 300 mW Renishaw laser (785 nm, 1200 L/mm grating). Laser intensity was set to 0.5% for the 785 nm excitation wavelength and 5% for the 514 nm and 633 nm excitations for the polymer-SWNT samples. For the SWNT sample dispersed in $CHCl_3$, laser intensity was set to 1% for 514 nm and 633 nm, and 10% for 785 nm.

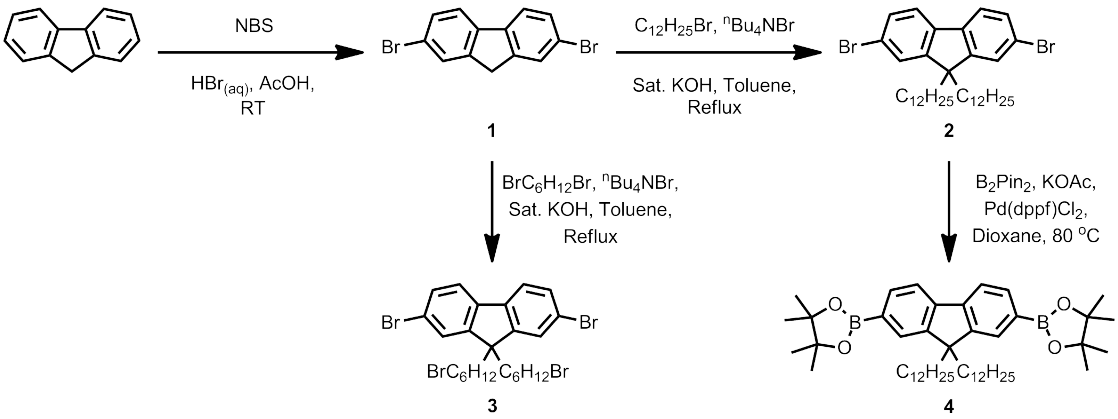


FIGURE 4.6: Synthesis of monomers **3** and **4**.

4.4.2 Synthetic Procedures

2,7-dibromofluorene (1) (adapted from reference 76)

A round bottom flask equipped with a stir bar was charged with fluorene (33.2 g, 200 mmol), NBS (89.0 g, 500 mmol) and acetic acid (400 mL). While the mixture was stirring, conc. HBr (10 mL) was slowly added and then the reaction mixture was stirred at RT for 1.5 h. Water (200 mL) was added and the resulting suspension was filtered and washed with water to obtain an orange-white solid. The solid was recrystallized from a 1.5:1 v/v mixture of EtOH:acetone (∼1.8 L total volume),

and the mother liquor was recrystallized again from the same solvent mixture (∼1.5 L total volume). The crops were combined to afford **1** (41.2 g, 64%) as a white solid. ^{1}H-NMR (600 MHz; $CDCl_3$): δ 7.67 (d, J = 1.1 Hz, 2H), 7.61 (d, J = 8.1 Hz, 2H), 7.51 (dd, J = 8.1, 1.8 Hz, 2H), 3.88 (s, 2H).

2,7-dibromo-9,9-didodecylfluorene (2) (adapted from reference 76)

A round bottom flask equipped with a stir bar was charged with **1** (5 g, 15.4 mmol), 1-bromododecane (7.88 g, 31.6 mmol), toluene (31 mL), and sat. KOH (31 mL). ^{n}Bu_4NBr (1.0 g, 3.1 mmol) was then added and the reaction mixture was heated to 60 °C and stirred vigorously for 1 h under a nitrogen atmosphere. The biphasic mixture was allowed to separate, and the organic layer was isolated. The aqueous phase was extracted twice with diethyl ether (2 x 120 mL) and the organic extracts were combined and concentrated *in vacuo* to obtain a viscous green oil. The crude mixture was purified by flash chromatography (100 g column, 100% hexanes) to afford **2** as a white solid (9.34 g, 92%). ^{1}H-NMR (600 MHz; $CDCl_3$): δ 7.51 (d, J = 8.0 Hz, ^{1}H), 7.45-7.43 (m, 2H), 1.92-1.89 (m, 2H), 1.29-1.04 (m, 18H), 0.87 (t, 3H), 0.59-0.56 (m, 2H).

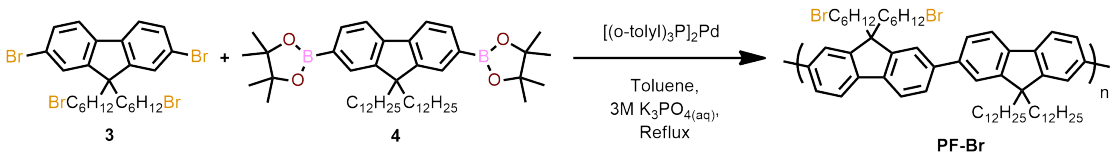
2,7-dibromo-9,9-bis(6-bromohexyl)fluorene (3) (adapted from reference 76)

A round bottom flask equipped with a stir bar was charged with **1** (5 g, 15.4 mmol), 1,6-dibromohexane (37.7 g, 154 mmol), toluene (31 mL), and sat. KOH (31 mL). ^{n}Bu_4NBr (1.0 g, 3.1 mmol) was then added and the reaction mixture was heated to 60 °C and stirred vigorously for 1 h under a nitrogen atmosphere. The biphasic mixture was allowed to separate, and the organic layer was isolated. The aqueous phase was extracted twice with diethyl ether (2 x 120 mL) and the organic extracts were combined and concentrated *in vacuo* to obtain a viscous green oil. Excess 1,6-dibromohexane was removed using vacuum distillation (1

mbar, 115 °C) to obtain a viscous yellow oil. The crude mixture was purified by flash chromatography (100 g column, 0 to 20% CH_2Cl_2 in hexanes over 10 CV) to obtain a white solid containing two spots by TLC. The crude product was recrystallized from MeOH (∼250 mL) to afford **3** as a white solid (4.4 g, 44%). ^{1}H-NMR (600 MHz; $CDCl_3$): δ 7.53-7.52 (m, ^{1}H), 7.47-7.43 (m, 2H), 3.31-3.28 (t, 2H), 1.94-1.91 (m, 2H), 1.68-1.66 (m, 2H), 1.22-1.19 (m, 2H), 1.10-1.07 (m, 2H), 0.60-0.57 (m, 2H).

2,2'-(9,9-didodecylfluorene-2,7-diyl)bis(4,4,5,5-tetramethyl-1,3,2-dioxaborolane) (4) (adapted from reference 76)

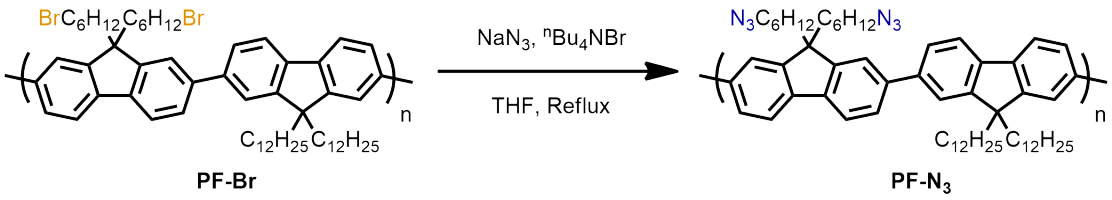
A round bottom flask equipped with a stir bar was charged with **2** (7.0 g, 10.6 mmol), B_2Pin_2 (5.92 g, 23.3 mmol), KOAc (3.12 g, 31.8 mmol), and dioxane (100 mL). $Pd(dppf)_2Cl_2$ (260 mg, 318 μmol) was added and the reaction mixture was stirred at 80 °C for 12 h. The reaction mixture was partitioned with water and extracted thrice with Et_2O. The organic extracts were combined and dry loaded onto silica (10 g). The crude mixture was purified by flash chromatography (100 g column, 0 to 80% CH_2Cl_2 in hexanes over 10 CV) to obtain a yellow solid. The solid was recrystallized from a 1.25:1 v/v mixture of MeOH:acetone (∼450 mL total volume) to afford **4** as a white solid (4.88 g, 63%). ^{1}H-NMR (600 MHz; $CDCl_3$): δ 7.80 (d, J = 7.6 Hz, ^{1}H), 7.74-7.71 (m, 2H), 2.00-1.97 (m, 2H), 1.39 (s, 12H), 1.26-0.99 (m, 18H), 0.86 (t, J = 7.1 Hz, 3H), 0.54 (m, 2H).



Poly(didodecylfluorene-alt-bis(bromohexyl)fluorene) (PF-Br)

A Schlenk tube equipped with a stir bar was charged with **3** (646 mg, 0.99 mmol),

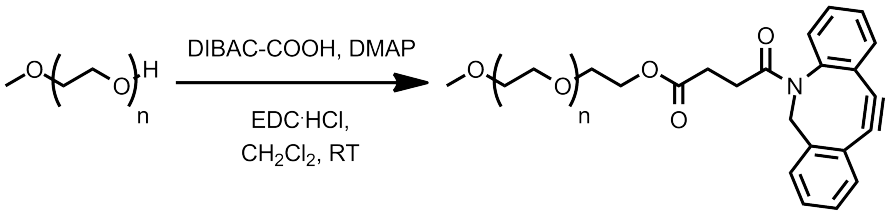
4 (750 mg, 0.99 mmol), toluene (7.1 mL), and 3M $K_3PO_{4(aq)}$ (7.1 mL). The biphasic mixture was degassed by three freeze-pump-thaw cycles, then, while frozen under liquid nitrogen, $[(o\text{-tol})_3P]_2Pd$ (36 mg, 50 μmol) was added under a positive pressure of nitrogen. The Schlenk tube was evacuated and backfilled with nitrogen four times, and the reaction mixture was vigorously stirred at 80 °C for 12 h. The phases were allowed to separate, and the organic layer was isolated and filtered through a single plug of celite and neutral alumina. The plug was thoroughly washed with THF and the flow-through was concentrated *in vacuo*. The crude polymer was precipitated into MeOH (∼400 mL) and then filtered to afford **PF-Br** as a yellow solid (760 mg, 77%). ^{1}H-NMR (600 MHz; $CDCl_3$): δ 7.86-7.83 (m, 4H), 7.73-7.66 (m, 8H), 3.31-3.28 (m, 4H), 2.20-2.10 (m, 4H), 1.72-1.69 (m, 4H), 1.29-1.11 (m, 50H), 0.86 (t, J = 7.1 Hz, 12H).



Poly(didodecylfluorene-alt-bis(azidohexyl)fluorene) (PF-N_3)

A round bottom flask equipped with a stir bar and reflux condenser was charged with **PF-Br** (600 mg, 0.61 mmol), NaN_3 (394 mg, 6.1 mmol), ^{n}Bu$_4$NBr (390 mg, 1.2 mmol), and THF (90 mL) and the reaction mixture was heated to reflux for 12 h. The reaction mixture was filtered through an alumina plug and washed thoroughly with THF, then the solution was concentrated *in vacuo* and precipitated into MeOH (∼400 mL) to afford **PF-N_3** as a yellow solid (407 mg, 73%). ^{1}H-NMR (600 MHz; $CDCl_3$): δ 7.86-7.83 (m, 4H), 7.73-7.64 (m, 8H), 3.15-3.12

(m, 4H), 2.16-2.11 (m, 4H), 1.45-1.42 (m, 4H), 1.27-1.10 (m, 50H), 0.86 (t, J = 7.0 Hz, 12H).



mPEG$_{5000}$-DIBAC. A round bottom flask equipped with a stir bar was charged with mPEG$_{5000}$-OH (250 mg, 50 μmol), DIBAC-COOH (46 mg, 150 μmol) and 4-dimethylaminopyridine (3 mg, 25 μmol) and CH_2Cl_2 (1 mL). To the solution, *N*-(3-dimethylaminopropyl)-*N'*-ethylcarbodiimide hydrochloride (EDC·HCl) (33 mg, 175 μmol) was added, and the reaction mixture was stirred overnight at RT. The reaction mixture diluted with 5 mL of CH_2Cl_2 and then precipitated into 1:1 Et_2O:hexanes (∼100 mL). The precipitate was collected on a Hirsch funnel, then washed with ice cold ethanol (3 x 20 mL), Et_2O (3 x 20 mL), and dried *in vacuo* to afford **mPEG$_{5000}$-DIBAC** as a fine white powder (246 mg, 93%). ^{1}H NMR (600 MHz; DMSO-d6): δ 7.66 (dd, J = 7.6, 1.2, ^{1}H), 7.62 (d, J = 7.3, ^{1}H), 7.52-7.45 (m, 3H), 7.38 (td, J = 7.4, 1.5, ^{1}H), 7.34 (td, J = 7.4, 1.3, ^{1}H), 7.30 (dd, J = 7.5, 1.2, ^{1}H), 5.03 (d, J = 14.2, ^{1}H), 4.03-3.99 (m, ^{1}H), 3.95-3.91 (m, ^{1}H), 3.51 (s, ^{1}H), 3.24 (s, 3H), 2.67-2.62 (m, 2H), 2.37-2.35 (m, ^{1}H), 2.29 (dt, J = 17.1, 6.4, ^{1}H), 1.81 (dt, J = 16.7, 6.3, ^{1}H).

General SPAAC procedure. A glass vial was charged with 4 mL of polymer-SWNT dispersion and 2.05 equivalents of DIBAC derivative was added directly. Equivalents were calculated by determining the polymer concentration in solution (based on the SWNT dispersion protocol), calculating the mass of polymer present,

and then using the molecular weight of the repeat unit to determine the number of moles of azide moiety (two per repeat unit). The glass vial was agitated until the DIBAC derivative was dissolved, and then the reaction progress was monitored by IR spectroscopy.

SPAAC with DIBAC-COOH. 4 mL of **PF-N_3**-SWNT dispersion, 1.4 mg of DIBAC-COOH.

SPAAC with $mPEG_{5000}$-DIBAC (plasma torch SWNTs). 4 mL of **PF-N_3**-SWNT plasma torch dispersion, 23.7 mg of **$mPEG_{5000}$-DIBAC**.

SPAAC with $mPEG_{5000}$-DIBAC (HiPCO SWNTs). 4 mL of **PF-N_3**-SWNT HiPCO dispersion, 35.5 mg of **$mPEG_{5000}$-DIBAC**.

HiPCO Dispersion with PF-N_3-$mPEG_{5000}$

PF-N_3 (3 mg) and **$mPEG_{5000}$-DIBAC** (35.5 mg) were dissolved in toluene (4 mL) and allowed to stand at RT overnight. HiPCO SWNTs (3 mg dry weight) were then added and the mixture was sonicated for 2 h in a bath sonicator chilled with ice. The suspension was centrifuged at 8,346 *g* for 30 min, and the supernatant was carefully removed and filtered through a cotton plug. The as-produced sample was analyzed using UV/Vis-NIR spectroscopy, and was diluted 16-fold (200 μL of the as-produced dispersion was added to 3.0 mL of toluene) to obtain the spectrum shown in Figure S4.16.

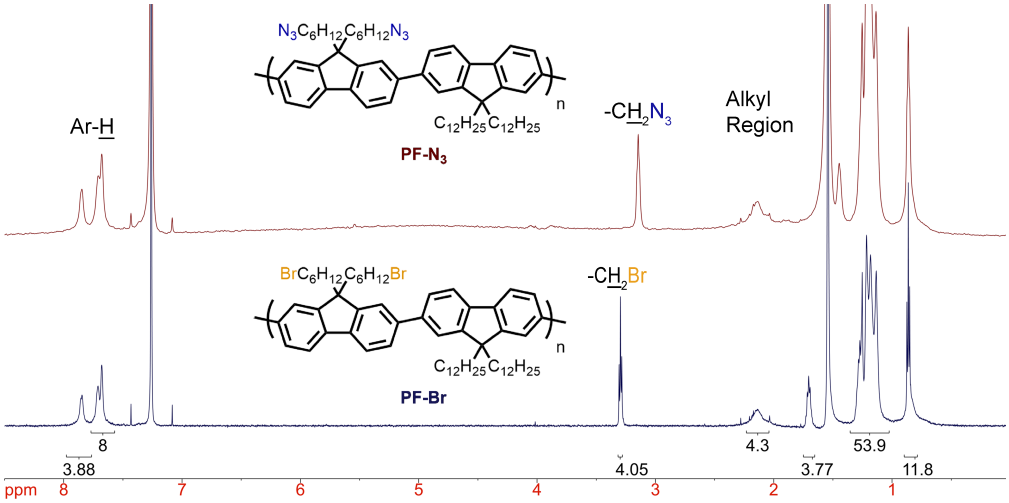


FIGURE 4.7: ^{1}H NMR overlay of (a) **PF-Br** (blue) and (b) **PF-N_3** (red).

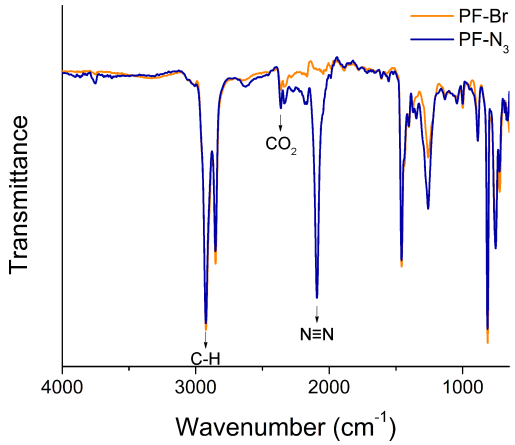


FIGURE 4.8: FT-IR overlay of (a) **PF-Br** (orange) and (b) **PF-N_3** (blue).

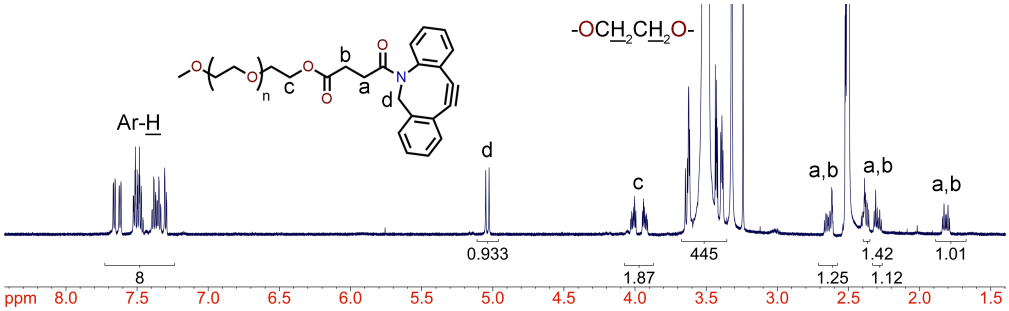


FIGURE 4.9: ^{1}H NMR spectrum of **mPEG$_{5000}$-DIBAC**.

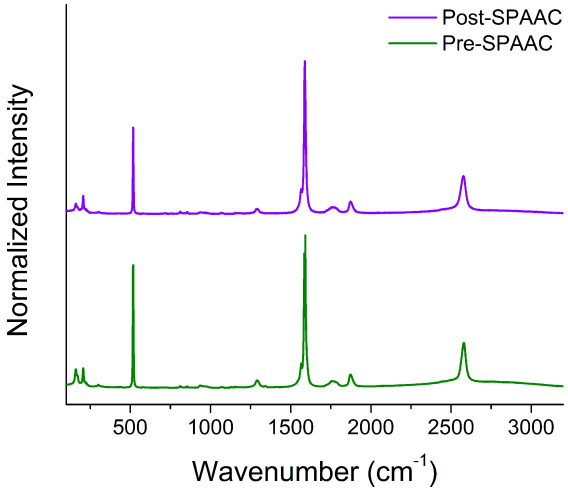


FIGURE 4.10: Raman spectra collected at 785 nm of **PF-N$_3$**-SWNT dispersions (a) pre- (green) and (b) post-SPAAC (purple) with DIBAC-COOH. Spectra were normalized to the G-band at ~1590 cm^{-1} and offset for clarity.

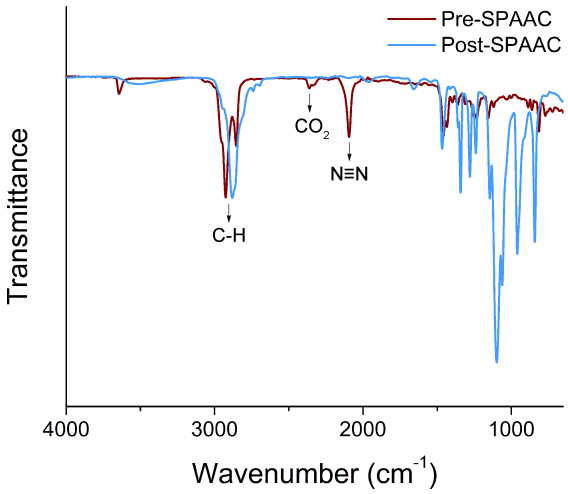


FIGURE 4.11: FT-IR overlay of the SPAAC reaction between **PF-N$_3$**-SWNT and **mPEG$_{5000}$-DIBAC** (a) pre- (dark red) and (b) post-SPAAC (light blue). The post-SPAAC spectrum was obtained after 30 min.

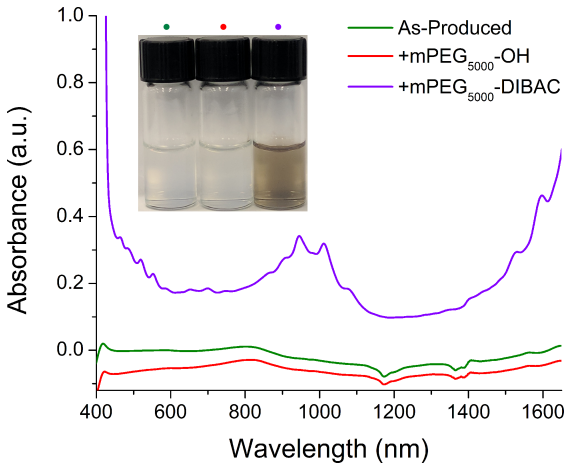


FIGURE 4.12: UV/Vis-NIR spectra of **PF-N$_3$**-SWNT dispersions in 50/50 THF:D_2O with (i) nothing, (ii) two equivalents of mPEG$_{5000}$-OH (containing no DIBAC), or (iii) two equivalents of **mPEG$_{5000}$-DIBAC**. Photographs of the filtered dispersions are colour-coded accordingly with coloured dots above.

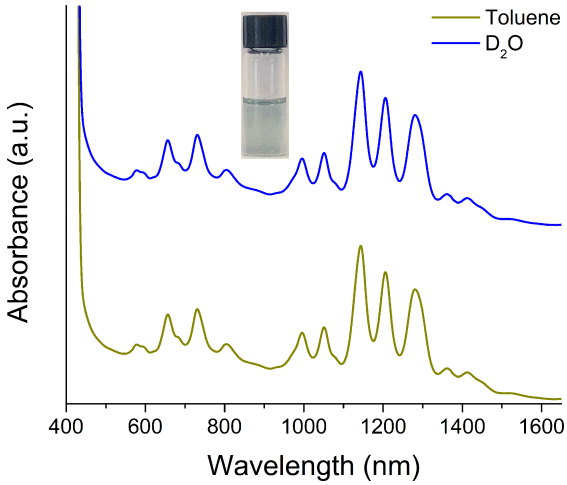


FIGURE 4.13: UV/Vis-NIR spectra of **PF-N$_3$**-HiPCO dispersions pre-SPAAC (toluene, dark yellow trace) and post-SPAAC with **mPEG$_{5000}$-DIBAC** (D_2O, blue trace). Spectra are offset for clarity. The photograph shows the pre-SPAAC polymer-SWNT dispersion in toluene.

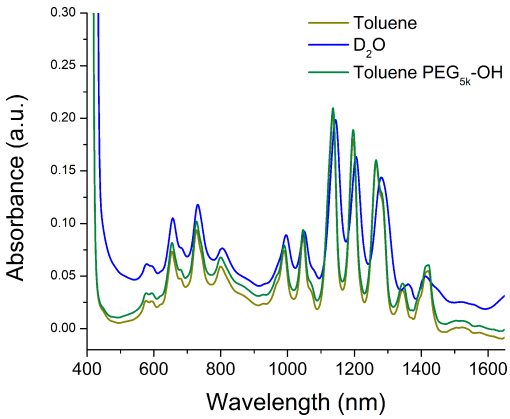


FIGURE 4.14: UV/Vis-NIR spectra of **PF-N$_3$**-HiPCO dispersions diluted for PL mapping.

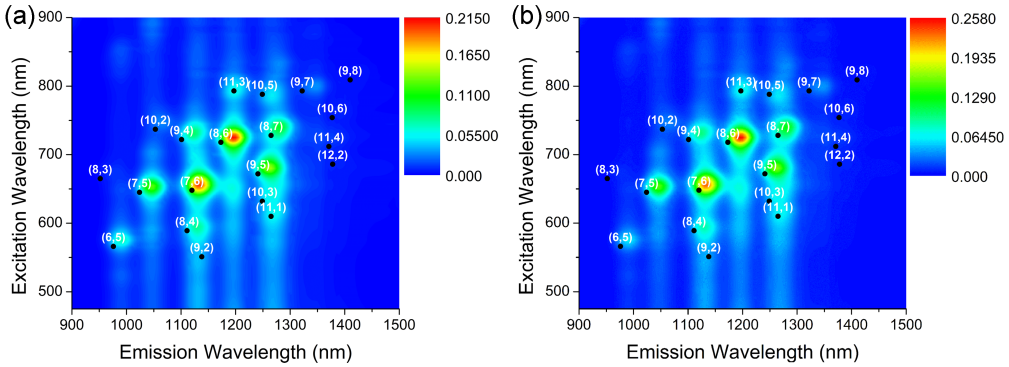


FIGURE 4.15: PL maps of **PF-N$_3$**-HiPCO in (a) toluene and (b) toluene mixed with 2.05 eq of mPEG$_{5000}$-OH.

Chirality	λ_{em} (nm) (-PEG$_{5k}$)	λ_{em} (nm) (+PEG$_{5k}$)	$\Delta[\lambda_{em}]$ (nm)
(6,5)	990	990	0
(7,5)	1047	1046	-1
(7,6)	1133	1133	0
(8,4)	1131	1130	-1
(8,6)	1196	1196	0
(8,7)	1280	1279	-1
(9,4)	1125	1126	1
(9,5)	1265	1264	-1

TABLE 4.2: Emission Wavelengths of sc-SWNT Chiralities Dispersed by **PF-N$_3$** in Toluene and Toluene with mPEG$_{5000}$-OH

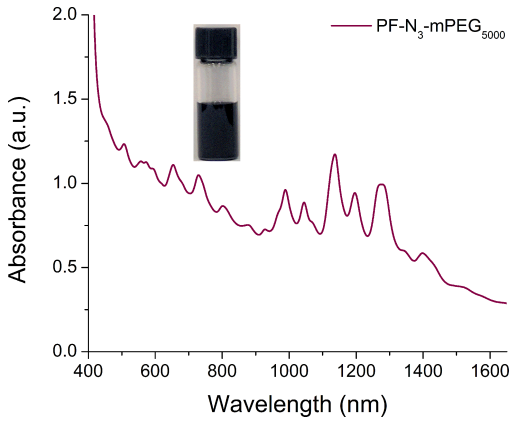


FIGURE 4.16: UV/Vis-NIR spectrum of **PF-N$_3$**-mPEG$_{5000}$ used to disperse HiPCO SWNTs in toluene. Note that the spectrum was obtained by diluting the as-produced dispersion by a factor of 16 in toluene. The photograph shows the as-produced polymer-SWNT dispersion (undiluted).

4.5 References

(1) Iijima, S. *Nature* **1991**, 354, 56–58.

(2) Park, S.; Vosguerichian, M.; Bao, Z. *Nanoscale* **2013**, 5, 1727–1752.

(3) Terrones, M. *Annu. Rev. Mater. Res.* **2003**, 33, 419–501.

(4) Ajayan, P. M. *Chem. Rev.* **1999**, 99, 1787–1800.

(5) Saito, R.; Dresselhaus, G.; Dresselhaus, M. S. *Physical Properties of Carbon Nanotubes*, vol. 3.; Imperial College Press: London, **2005**.

(6) Coleman, J. N.; Khan, U.; Blau, W. J.; Gun'ko, Y. K. *Carbon* **2006**, 44, 1624–1652.

(7) Zhang, Q.; Huang, J.-Q.; Qian, W.-Z.; Zhang, Y.-Y.; Wei, F. *Small* **2013**, 9, 1237–1265.

(8) O'Connell, M. J.; Bachilo, S. M.; Huffman, C. B.; Moore, V. C.; Strano, M. S.; Haroz, E. H.; Rialon, K. L.; Boul, P. J.; Noon, W. H.; Kittrell, C.; et al. *Science* **2002**, 297, 593–596.

(9) Bachilo, S. M.; Strano, M. S.; Kittrell, C.; Hauge, R. H.; Smalley, R. E.; Weisman, R. B. *Science* **2002**, 298, 2361–2366.

(10) Kataura, H.; Kumazawa, Y.; Maniwa, Y.; Umezu, I.; Suzuki, S.; Ohtsuka, Y.; Achiba, Y. *Synth. Met.* **1999**, 103, 2555–2558.

(11) Nikolaev, P.; Bronikowski, M. J.; Bradley, R. K.; Rohmund, F.; Colbert, D. T.; Smith, K. .; Smalley, R. E. *Chem. Phys. Lett.* **1999**, 313, 91–97.

(12) Kong, J.; Cassell, A. M.; Dai, H. *Chem. Phys. Lett.* **1998**, 292, 567–574.

(13) Bernier, P.; Journet, C.; Maser, W. K.; Loiseau, A.; de la Chapelle, M. L.; Lefrant, S.; Deniard, P.; Lee, R.; Fischer, J. E. *Nature* **1997**, 388, 756–758.

(14) Guo, T.; Nikolaev, P.; Thess, A.; Colbert, D. T.; Smalley, R. E. *Chem. Phys. Lett.* **1995**, 243, 49–54.

(15) Kim, K. S.; Cota-Sanchez, G.; Kingston, C. T.; Imris, M.; Simard, B.; Soucy, G. J. *Phys. D. Appl. Phys.* **2007**, 40, 2375–2387.

(16) Tasis, D.; Tagmatarchis, N.; Bianco, A.; Prato, M. *Chem. Rev.* **2006**, 106, 1105–1136.

(17) Hirsch, A. *Angew. Chemie - Int. Ed.* **2002**, 41, 1853–1859.

(18) Britz, D. A.; Khlobystov, A. N. *Chem. Soc. Rev.* **2006**, 35, 637–659.

(19) Campidelli, S.; Klumpp, C.; Bianco, A.; Guldi, D. M.; Prato, M. *J. Phys. Org. Chem.* **2006**, 19, 531–539.

(20) Setaro, A.; Adeli, M.; Glaeske, M.; Przyrembel, D.; Bisswanger, T.; Gordeev, G.; Maschietto, F.; Faghani, A.; Paulus, B.; Weinelt, M.; et al. *Nat. Commun.* **2017**, 8, 14281.

(21) Zhao, Y. L.; Stoddart, J. F. *Acc. Chem. Res.* **2009**, 42, 1161–1171.

(22) Bilalis, P.; Katsigiannopoulos, D.; Avgeropoulos, A.; Sakellariou, G. *RSC Adv.* **2014**, 4, 2911–2934.

(23) Gavrel, G.; Jousselme, B.; Filoramo, A.; Campidelli, S. *Top. Curr. Chem.* **2014**, 348, 95–126.

(24) Islam, M. F.; Rojas, E.; Bergey, D. M.; Johnson, A. T.; Yodh, A. G. *Nano Lett.* **2003**, 3, 269–273.

(25) Moore, V. C.; Strano, M. S.; Haroz, E. H.; Hauge, R. H.; Smalley, R. E.; Schmidt, J.; Talmon, Y. *Nano Lett.* **2003**, 3, 1379–1382.

(26) Gong, X.; Liu, J.; Baskaran, S.; Voise, R. D.; Young, J. S. *Chem. Mater.* **2000**, 12, 1049–1052.

(27) Yang, K.; Zhu, L.; Xing, B. *Environ. Sci. Technol.* **2006**, 40, 1855–1861.

(28) Tomonari, Y.; Murakami, H.; Nakashima, N. *Chem. - A Eur. J.* **2006**, 12, 4027–4034.

(29) Chen, R. J.; Zhang, Y.; Wang, D.; Dai, H. *J. Am. Chem. Soc.* **2001**, 123, 3838–3839.

(30) Chen, J.; Liu, H.; Weimer, W. A.; Halls, M. D.; Waldeck, D. H.; Walker, G. C. *J. Am. Chem. Soc.* **2002**, 124, 9034–9035.

(31) Star, A.; Stoddart, J. F.; Steuerman, D.; Diehl, M.; Boukai, A.; Wong, E. W.; Yang, X.; Chung, S. W.; Choi, H.; Heath, J. R. *Angew. Chemie - Int. Ed.* **2001**, 40, 1721–1725.

(32) Nish, A.; Hwang, J.-Y.; Doig, J.; Nicholas, R. J. *Nat. Nanotechnol.* **2007**, 2, 640–646.

(33) Yim, C. Bin; Dijkgraaf, I.; Merkx, R.; Versluis, C.; Eek, A.; Mulder, G. E.; Rijkers, D. T. S.; Boerman, O. C.; Liskamp, R. M. J. *J. Med. Chem.* **2010**, 53, 3944–3953.

(34) Cheng, F. Y.; Imin, P.; Lazar, S.; Botton, G. A.; de Silveira, G.; Marinov, O.; Deen, J.; Adronov, A. *Macromolecules* **2008**, 41, 9869–9874.

(35) Guo, Z.; Sadler, P. J.; Tsang, S. C. *Adv. Mater.* **1998**, 10, 701–703.

(36) Balavoine, F.; Schultz, P.; Richard, C.; Mallouh, V. V.; Ebbesen, T. W.; Mioskowski, C. *Angew. Chemie - Int. Ed.* **1999**, 38, 1912–1915.

(37) Bradley, K.; Briman, M.; Star, A.; Grüner, G. *Nano Lett.* **2004**, 4, 253–256.

(38) Star, A.; Steuerman, D. W.; Heath, J. R.; Stoddart, J. F. *Angew. Chemie - Int. Ed.* **2002**, 41, 2508–2512.

(39) Zheng, M.; Jagota, A.; Strano, M. S.; Santos, A. P.; Barone, P.; Chou, S. G.; Diner, B. A.; Dresselhaus, M. S.; McLean, R. S.; Onoa, G. B.; et al. *Science* **2003**, 302, 1545–1548.

(40) Zheng, M.; Jagota, A.; Semke, E. D.; Diner, B. A.; McLean, R. S.; Lustig, S. R.; Richardson, R. E.; Tassi, N. G. *Nat. Mater.* **2003**, 2, 338–342.

(41) Heller, D. A.; Jeng, E. S.; Yeung, T.-K.; Martinez, B. M.; Moll, A. E.; Gastala, J. B.; Strano, M. S. *Science* **2006**, 311, 508–511.

(42) Liang, S.; Zhao, Y.; Adronov, A. *J. Am. Chem. Soc.* **2014**, 136, 970–977.

(43) Pochorovski, I.; Wang, H.; Feldblyum, J. I.; Zhang, X.; Antaris, A. L.; Bao, Z. *J. Am. Chem. Soc.* **2015**, 137, 4328–4331.

(44) Lei, T.; Pochorovski, I.; Bao, Z. *Acc. Chem. Res.* **2017**, 50, 1096–1104.

(45) Lei, T.; Chen, X.; Pitner, G.; Wong, H.-S. P.; Bao, Z. *J. Am. Chem. Soc.* **2016**, 138, 802–805.

(46) Toshimitsu, F.; Nakashima, N. *Nat. Commun.* **2014**, 5, 5041. (47) Agard, N. J.; Prescher, J. A.; Bertozzi, C. R. *J. Am. Chem. Soc.* **2004**, 126, 15046–15047.

(48) Jewett, J. C.; Bertozzi, C. R. *Chem. Soc. Rev.* **2010**, 39, 1272. (49) Mbua, N. E.; Guo, J.; Wolfert, M. A.; Steet, R.; Boons, G.-J. *ChemBioChem* **2011**, 12, 1912–1921.

(50) Ning, X.; Guo, J.; Wolfert, M. A.; Boons, G.-J. *Angew. Chemie - Int. Ed.*

2008, 47, 2253–2255.

(51) Beatty, K. E.; Fisk, J. D.; Smart, B. P.; Lu, Y. Y.; Szychowski, J.; Hangauer, M. J.; Baskin, J. M.; Bertozzi, C. R.; Tirrell, D. A. *ChemBioChem* **2010**, 11, 2092–2095.

(52) Yang, H.; Srivastava, P.; Zhang, C.; Lewis, J. C. *ChemBioChem* **2014**, 15, 223–227.

(53) Bernardin, A.; Cazet, A.; Guyon, L.; Delannoy, P.; Vinet, F.; Bonnaffe, D.; Texier, I. *Bioconjug. Chem.* **2010**, 21, 583–588.

(54) Kuzmin, A.; Poloukhtine, A.; Wolfert, M. A.; Popik, V. V. *Bioconjug. Chem.* **2010**, 21, 2076–2085.

(55) Manova, R.; van Beek, T. A.; Zuilhof, H. *Angew. Chemie - Int. Ed.* **2011**, 50, 5428–5430.

(56) Luo, W.; Gobbo, P.; McNitt, C. D.; Sutton, D. A.; Popik, V. V.; Workentin, M. S. *Chem. - A Eur. J.* **2017**, 23, 1052–1059.

(57) Luo, W.; Gobbo, P.; Gunawardene, P. N.; Workentin, M. S. *Langmuir* **2017**, 33, 1908–1913.

(58) Gobbo, P.; Novoa, S.; Biesinger, M. C.; Workentin, M. S. *Chem. Commun.* **2013**, 49, 3982.

(59) Staudinger, H.; Meyer, J. *Helv. Chim. Acta* **1919**, 2, 635–646.

(60) Fong, D.; Bodnaryk, W. J.; Rice, N. A.; Saem, S.; Moran-Mirabal, J. M.; Adronov, A. *Chem. - A Eur. J.* **2016**, 22, 14560–14566.

(61) Chadwick, R. C.; Van Gyzen, S.; Liogier, S.; Adronov, A. *Synth.* **2014**, 46, 669–677.

(62) Dyke, C. A.; Tour, J. M. *J. Am. Chem. Soc.* **2003**, 125, 1156–1157.

(63) Li, H.; Cheng, F.; Duft, A. M.; Adronov, A. *J. Am. Chem. Soc.* **2005**, 127,

14518–14524.

(64) Fong, D.; Adronov, A. *Chem. Sci.* **2017**, 8, 7292-7305.

(65) Strano, M. S.; Dyke, C. A.; Usrey, M. L.; Barone, P. W.; Allen, M. J.; Shan, H.; Kittrell, C.; Hauge, R. H.; Tour, J. M.; Smalley, R. E. *Science* **2003**, 301, 1519–1522.

(66) Tange, M.; Okazaki, T.; Iijima, S. *ACS Appl. Mater. Interfaces* **2012**, 4, 6458–6462.

(67) Dresselhaus, M. S.; Jorio, A.; Hofmann, M.; Dresselhaus, G.; Saito, R. *Nano Lett.* **2010**, 10, 751–758.

(68) Dresselhaus, M. S.; Dresselhaus, G.; Saito, R.; Jorio, A. *Phys. Rep.* **2005**, 409, 47–99.

(69) Doorn, S. K. *J. Nanosci. Nanotechnol.* **2005**, 5, 1023–1034.

(70) Strano, M. S.; Zheng, M.; Jagota, A.; Onoa, G. B.; Heller, D. A.; Barone, P. W.; Usrey, M. L. *Nano Lett.* **2004**, 4, 543–550.

(71) Strano, M. S.; Doorn, S. K.; Haroz, E. H.; Kittrell, C.; Hauge, R. H.; Smalley, R. E. *Nano Lett.* **2003**, 3, 1091–1096.

(72) Weisman, R. B.; Bachilo, S. M. *Nano Lett.* **2003**, 3, 1235–1238.

(73) Larsen, B. A.; Deria, P.; Holt, J. M.; Stanton, I. N.; Heben, M. J.; Therien, M. J.; Blackburn, J. L. *J. Am. Chem. Soc.* **2012**, 134, 12485–12491.

(74) Silvera-Batista, C. A.; Wang, R. K.; Weinberg, P.; Ziegler, K. J. *Phys. Chem. Chem. Phys.* **2010**, 12, 6990.

(75) Choi, J. H.; Strano, M. S. *Appl. Phys. Lett.* **2007**, 90, 223114.

(76) Xia, C.; Advincula, R. C. *Macromolecules* **2001**, 34, 5854–5859.

Chapter 5

Decoration of Polyfluorene-wrapped Carbon Nanotube Thin Films via Strain-Promoted Azide–Alkyne Cycloaddition

This chapter has been reprinted with permission from Polymer Chemistry. Fong, D.; Andrews, G. M.; McNelles, S. A.; Adronov, A. **2018**, *9*, 4460-4467. Copyright (2018) Royal Society of Chemistry.

D. Fong planned the study and synthesized the materials, as well as performed the TGA, Raman, and fluorescence mapping experiments. G. M. Andrews performed the IR spectroscopy and contact angle measurements, and prepared the polymer-SWNT click conjugates. S. A. McNelles provided the strained cyclooctyne derivatives.

Abstract

A generalizable method to decorate carbon nanotubes deposited as a thin film without damaging nanotube optoelectronic properties remains elusive. Here, reactive, noncovalently functionalized polymer–nanotube thin films were prepared using a polyfluorene that is decorated with azide groups in its side chains. The azides allow for Strain-Promoted Azide–Alkyne Cycloaddition to occur between the polymer–nanotube complex and strained cyclooctyne derivatives. It was found that quantitative functionalization of the nanotube thin film occurred efficiently at room temperature, without any catalyst or by-product removal required. This interfacial chemistry resulted in no damage to the nanotube structure or properties, as evidenced by absorption, fluorescence, and Raman spectroscopy. The polymer–nanotube thin films were investigated using thermogravimetric analysis, and it was found that the mass losses upon heating under an inert atmosphere were consistent with complete functionalization of the thin films. Using polyethylene glycol or C_{16} alkyl chains functionalized with a strained cyclooctyne, we modulated the hydrophobicity of the thin film and found that we could prepare Janus nanotube films *via* stepwise functionalization.

5.1 Introduction

In order to take advantage of the exceptional structural,[1–3] mechanical,[4–6] and optoelectronic properties[7–9] of single-walled carbon nanotubes (SWNTs), nanotube exfoliation and dispersion are imperative. However, inter-tube π–π interactions result in insoluble SWNT bundles,[10] and all known commercial SWNT synthetic methods result in a complex mixture of amorphous carbon, leftover metal catalyst particles, as well as both semiconducting and metallic SWNTs.[11–15] To ameliorate these issues, covalent or noncovalent functionalization methods are employed.[16–18] Covalent functionalization involves chemistry directly on the SWNT sidewall, which typically disrupts the extended π-system and destroys the advantageous SWNT properties.[18] Recently, Reich and co-workers reported a covalent functionalization method that preserved SWNT optoelectronic properties, but required elevated temperatures ($60 - 70\,^{\circ}\mathrm{C}$) and lengthy reaction times (2–4 days) to decorate the SWNT surface.[19] Alternatively, noncovalent functionalization involves the formation of supramolecular complexes that do not disrupt the SWNT π-system, which has led to significant interest in this research area.[20–22] For noncovalent functionalization, a dispersant, including surfactants,[23–25] aromatic compounds,[26–28] conjugated polymers,[29–33] proteins,[34–36] polysaccharide–iodine complexes,[37] or deoxyribonucleic acids (DNA),[38–40] is used to coat the SWNT surface. The resulting dispersant–SWNT complex possesses dispersion properties akin to that of dispersant alone. Conjugated polymers are of particular interest, as synthetic control allows for tailored polymer structures. To date, conjugated polymer structure has been primarily modified to achieve the selective dispersion of semiconducting SWNTs (sc-SWNTs),[41] with recent efforts toward developing

polymer backbone structures capable of conformational changes or depolymerization in response to a stimulus.[42–46]

Until recently, little attention has been given to the use of conjugated polymers as a component that can impart reactivity to the polymer–SWNT complex upon supramolecular functionalization. To this end, we have recently prepared a polyfluorene derivative possessing azide groups in the side chains, and then used this polymer to noncovalently functionalize SWNTs.[47,48] The resulting supramolecular complex, which was dispersed in the solution-phase, could then be functionalized using either the Copper-Catalyzed Azide–Alkyne Cycloaddition (CuAAC)[47] or the Strain-Promoted Azide–Alkyne Cycloaddition (SPAAC)[48] without damaging SWNT optoelectronic properties. CuAAC, which was reported concurrently by the groups of Meldal[49] and Fokin/Sharpless[50] in 2002, is an efficient "click" reaction that involves the Cu-catalyzed [3 + 2] cycloaddition between an alkyne and azide to form a triazole ring. Although the reaction is widely accessible due to the ease of alkyne and azide preparation, a recalcitrant issue is the removal of copper in cases where this is required for a given application.[51] SPAAC, meanwhile, was reported in the seminal work by Bertozzi and co-workers in 2004,[52] and takes advantage of ring strain in a cyclooctyne to promote triazole ring formation with an azide in the absence of any catalysts. The reaction occurs rapidly at room temperature and is free of by-products, which has enabled SPAAC to be used extensively in chemical biology,[53–57] as it is bioorthogonal and facile under biological conditions. SPAAC has found less use in materials science to date,[58–62] and with respect to SWNT work, only one other report has been published on its use to produce SWNT nanohybrids.[63]

In this work, we sought to investigate the reactivity of the polymer–SWNT

complex deposited as a thin film. Carbon nanotube thin films have been intensely investigated, with numerous applications including thin film transistors,[64–68] transparent electrodes,[69–73] sensors,[74–78] desalination membranes,[79–81] solar cells,[82] displays,[83] actuators,[84] and a number of others.[85] Facile chemical derivatization of SWNT thin films could thus lead to interesting composite materials tailored to the aforementioned applications. In work by Nakashima and co-workers, SWNT thin films were derivatized with AuNPs using thiol–Au[86] or pyridine–porphyrin[87] coordination bonds. Though this work is intriguing for the preparation of AuNP–SWNT nanohybrids, a generalizable methodology to functionalize SWNT thin films with any small molecule or polymer, while preserving SWNT optoelectronic properties, remains unrealized. In particular, we were interested in investigating the scope of interfacial SWNT thin film reactivity using SPAAC, and in this work we explore spatial control over the properties of the polymer–SWNT thin film, which would otherwise be unattainable using solution-phase functionalization.

5.2 Results and Discussion

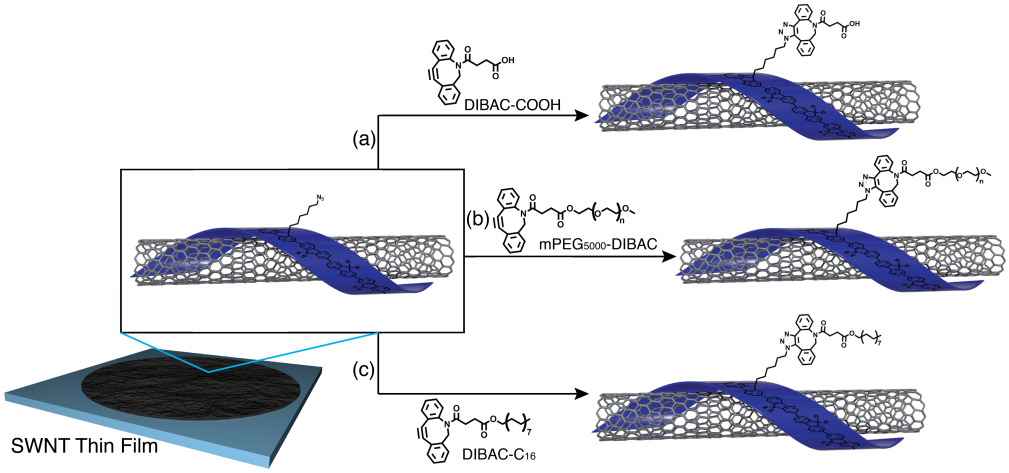
To prepare reactive polymer–SWNT thin films, we first synthesized an azide-containing polyfluorene (**PF-N$_3$**) from commercially-available fluorene according to literature procedures (see Supporting Info for details).[48] As previously reported, the FT-IR spectrum of **PF-N$_3$** contains a peak centered at ∼2090 cm^{-1} upon azidification, which is consistent with the presence of alkyl azide in **PF-N$_3$**. This peak is also visible in the **PF-N$_3$**–SWNT complex and can be used to monitor the progress of SPAAC *via* the disappearance of the azide stretch upon SPAAC functionalization. Using **PF-N$_3$**, we prepared reactive polymer–SWNT complexes

with HiPCO SWNTs following literature procedures.[88] Briefly, a mixture of 15 mg of **PF-N$_3$** and 10 mg of SWNTs in 20 mL of THF was sonicated in a bath sonicator chilled with ice for 2 h. The resulting black suspension was centrifuged at 8346 *g* for 30 min, and the supernatant was carefully removed to isolate the **PF-N$_3$**–SWNT dispersion. The **PF-N$_3$**–SWNT dispersion was stable on the benchtop for at least several months, with no observable flocculation. For initial studies on the reactivity of the **PF-N$_3$**–SWNT thin film, 15 mL of the **PF-N$_3$**–SWNT dispersion was filtered through a 0.2 μm Teflon membrane to obtain the solid polymer–SWNT thin film (total area of ~12.6 cm^2). The thin film thickness measured using optical profilometry was on the order of ~75 mum. Unbound **PF-N$_3$** was removed by washing the thin film with THF until the filtrate did not fluoresce at 365 nm, as determined using a handheld UV lamp.

To explore the reactivity of the **PF-N$_3$**–SWNT thin film, the thin film was soaked in a solution of DIBAC–COOH, which was synthesized according to literature procedures,[89] and the reaction was monitored using IR spectroscopy for the disappearance of the azide peak centred at ~2090 cm^{-1} (Scheme 5.1a and Figure 5.1). Initially, several solvents were screened by cutting a 1 cm^2 sheet of the SWNT thin film, followed by soaking the thin film in a 0.5 mg mL^{-1} solution of DIBAC–COOH (dissolved in either THF, CH_2Cl_2, acetone, or EtOH; see Figure S5.6). IR spectra of the solid thin films were recorded at one-hour intervals, and it was found that by simply soaking the thin film, derivatization was facile, irrespective of the solvent dielectric constant (ϵ = 7.5–25)[90] (Figure 5.1a). Complete functionalization typically occurred within ~3–4 hours under ambient conditions and without stirring. Interestingly, although solvents such as acetone or EtOH are incompatible with the **PF-N$_3$**–SWNT dispersion due to polymer insolubility,

the interfacial functionalization of the solid films circumvents solvent incompatibility issues and allows for smooth conversion to the "clicked" product. This enables cyclooctyne-containing molecules that dissolve poorly in solvents typically used to disperse polymer–SWNT complexes, i.e. THF or toluene, to decorate the polymer–SWNT complex. To further probe the reactivity of the **PF-N$_3$**–SWNT thin film, we prepared a 0.5 mg mL^{-1} solution of DIBAC–COOH in D_2O. Although DIBAC–COOH is insoluble in D_2O alone, it can be solubilized by the addition of six equivalents of K_2CO_3 to form the carboxylate anion, DIBAC–COO$^-$. A sheet of **PF-N$_3$**–SWNT thin film (1 cm^2) was soaked in this alkaline D_2O solution. Interestingly, even after 12 h of soaking in the DIBAC–COO$^-$–D_2O solution, complete conversion of azides was not observed by IR spectroscopy (Figure 5.1b, top). We hypothesized that this result may be due to the hydrophobicity of the pristine **PF-N$_3$**–SWNT thin film, which may impede adequate thin film penetration by the aqueous DIBAC–COO$^-$ solution. To force the aqueous solution into contact with the entire **PF-N$_3$**–SWNT thin film, we placed the thin film on a filtration apparatus and applied vacuum to pull the aqueous DIBAC–COO$^-$ solution directly through the SWNT thin film. We found that the reaction proceeded to complete conversion of azides after passing ~10 mL of the aqueous DIBAC–COO$^-$ solution through the SWNT thin film (Figure 5.1b, bottom). Thus, in spite of the hydrophobicity of pristine **PF-N$_3$**–SWNT thin film, interfacial functionalization by an aqueous solution can be accomplished by forcing thin film percolation *via* vacuum filtration. Lastly, to investigate whether interfacial SPAAC functionalization could be hastened by increasing the concentration of the DIBAC-derivatized molecule, we prepared a 10 mg mL^{-1} solution of DIBAC–COOH in THF and monitored reaction progress with IR spectroscopy. It was found that the reaction

proceeded smoothly within 15 min by simply soaking the **PF-N$_3$**–SWNT thin film in the DIBAC–COOH solution. Thus, if reaction speed is desired and the DIBAC-derivative is abundant, the reaction rate can be substantially increased by simply using a concentrated solution of a DIBAC-derivatized molecule.



SCHEME 5.1: SPAAC functionalization of polymer–SWNT complexes within solid thin films using (a) DIBAC–COOH, (b) mPEG$_{5000}$–DIBAC, and (c) DIBAC–C$_{16}$.

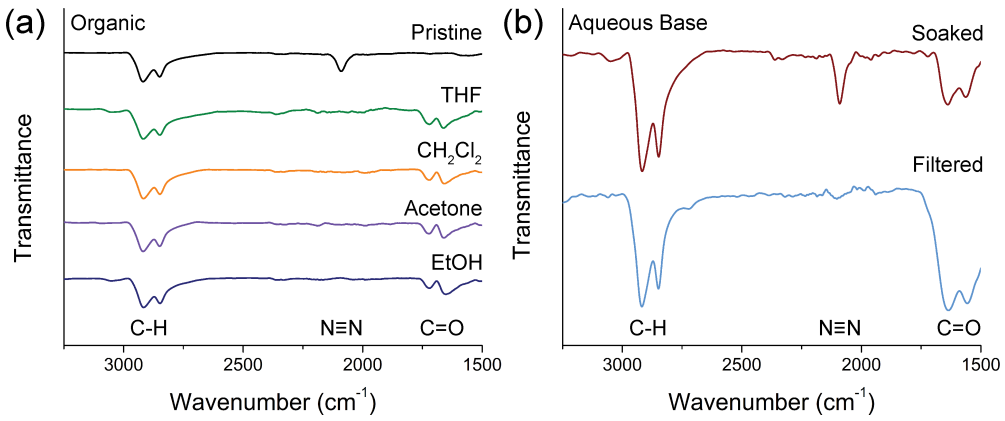


FIGURE 5.1: FT-IR overlay of the **PF-N$_3$**–SWNT thin film after soaking in a 0.5 mg mL^{-1} solution of DIBAC–COOH in various solvents. (a) The pristine thin film (black) was soaked in a solution of DIBAC–COOH dissolved in (i) THF (green), (ii) CH_2Cl_2 (orange), (iii) acetone (purple), or (iv) EtOH (blue). (b) Pristine thin film either soaked (red) or vacuum filtered (light blue) with DIBAC–COOH dissolved in an alkaline aqueous solution.

To further characterize the polymer–SWNT thin film properties, we performed thermogravimetric analysis (TGA) on the **PF-N$_3$** and **PF-N$_3$**–SWNT samples. For the **PF-N$_3$**–SWNT sample, a thin film was prepared by filtering the dispersion (10 mL) through a Teflon membrane, and then removing excess polymer by thorough washing with THF until the filtrate did not fluoresce when irradiated at 365 nm using a hand-held UV lamp. The thin film was then transferred to the TGA crucible for analysis. As the thin film could not be removed from the Teflon membrane in one clean piece, wetting the fragments with MeOH or acetone was found to be necessary to allow for static-free transfer. The samples were heated isothermally under a stream of argon at 100 °C for 15 min to evaporate any residual solvent, followed by heating to 675 °C under an argon atmosphere at a rate of 15 °C min^{-1}. As shown in Figure 5.2, the **PF-N$_3$** sample exhibited a two-step mass loss, with the first step amounting to 6.8% in the 250–325 °C temperature range, followed by a second step amounting to 49.9% in the range of 350–500 °C, for a total mass loss of 56.7%. The first mass loss is consistent with the mass of five nitrogen atoms per repeat unit (see Supporting Info for calculations), which corresponds to thermal azide decomposition that expels $N_{2(g)}$ and forms a reactive nitrene intermediate.[91] The nitrene can subsequently isomerize to an imine or dimerize to form an alkyl azo compound; the latter of which is also thermally unstable and can eliminate another equivalent of $N_{2(g)}$.[92] We speculate that the calculated mass loss of five nitrogen atoms originates from the roughly equal probability of these events occurring (where imine formation would not result in further mass loss, while azo formation would). The second mass loss is consistent with the mass of the remaining solubilizing side chains. For the **PF-N$_3$**–SWNT sample, a total mass loss of 15.4% was observed from ∼150–500 °C and also occurred in two

steps, although these steps were less well-defined than in the polymer-only sample. Given that the mass loss of SWNTs in an inert argon atmosphere is negligible under the conditions used in the TGA experiment, the mass fraction of **PF-N$_3$** ($f_{\mathbf{PF-N_3}}$) can be calculated as:

$$f_{\mathbf{PF-N_3}} = \frac{\varphi_{\mathbf{PF-N_3-SWNT}}}{\varphi_{\mathbf{PF-N_3}}} \tag{5.1}$$

where $\varphi_{\mathbf{PF-N_3}}$ is the mass loss of **PF-N$_3$** and $\varphi_{\mathbf{PF-N_3-SWNT}}$ is the mass loss of the **PF-N$_3$**–SWNT complex. Thus, the $f_{\mathbf{PF-N_3}}$ is 0.27 and the $f_{\mathbf{SWNT}}$ is 0.73 (given that $f_{\mathbf{PF-N_3}} + f_{\mathbf{SWNT}} = 1$). Functionalization of the polymer–SWNT thin film with DIBAC–COOH (MW = 305.33 g mol^{-1}) should increase the side chain mass by ∼187% (see Supporting Info for calculations). To determine whether this is the case, we prepared another **PF-N$_3$**–SWNT sample using the aforementioned procedure, and then functionalized the thin film with DIBAC–COOH in THF. The resulting post-SPAAC sample was washed with THF and then subjected to TGA analysis. As shown in Figure 5.2, the post-SPAAC polymer–SWNT sample again had a two-step mass loss of 27.2%, with 6.1% between 150 and 300 °C, and the remaining 21.1% between 300 and 500 °C. Given that the theoretical increase in side-chain mass after SPAAC is approximately 187%, the expected mass loss within the thin film post-SPAAC would be ∼29%, which closely matches the experimental mass loss observed for the post-SPAAC sample. Thus, the TGA data in tandem with the IR spectra are consistent with the quantitative functionalization of the **PF-N$_3$**–SWNT thin film.

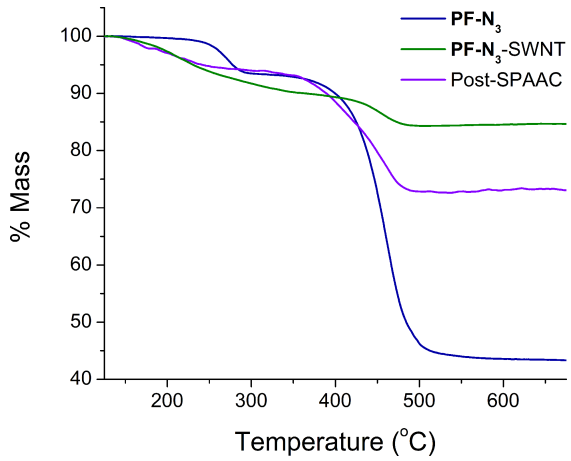


FIGURE 5.2: TGA data showing mass loss upon heating under an argon atmosphere of (i) **PF-N$_3$** (blue), (ii) **PF-N$_3$**–SWNT (green), and (iii) **PF-N$_3$**–SWNT post-SPAAC with DIBAC–COOH (purple).

We proceeded to explore the ability to modulate SWNT surface properties using SPAAC functionalization. To do so, we synthesized monofunctionalized 5 kDa poly(ethylene glycol) monomethyl ether (mPEG$_{5000}$) terminated with DIBAC (mPEG$_{5000}$–DIBAC, Scheme 5.1b) using Steglich esterification with DIBAC–COOH (see Supporting Info for details).[48] For the following experiments, **PF-N$_3$**–SWNT thin film was prepared by filtering 3 mL of dispersion through a 0.2 μm Teflon membrane to prepare a circular thin film with a diameter of 1 cm. Excess polymer was removed by thoroughly washing the thin film with THF until the filtrate did not fluoresce when irradiated at 365 nm. We initially attempted to soak the thin film in a 10 mg mL^{-1} solution of mPEG$_{5000}$–DIBAC in THF or H_2O. After soaking for 12 h under ambient conditions, it was found that only ~50% conversion was achieved for both solutions (see ESI, Figure S5.7). We postulate that the incomplete conversion observed may be due to the decreased ability of larger polymeric molecules to diffuse throughout the **PF-N$_3$**–SWNT thin film, as solvent wettability with the SWNT thin film was irrelevant to conversion percentage. To

circumvent this slow reactivity, we used the vacuum filtration method outlined above with DIBAC–COO^- and found that the reaction proceeded smoothly after ~10 mL of $mPEG_{5000}$–DIBAC solution in THF (10 mg mL^{-1}) was passed through the film. Any unreacted $mPEG_{5000}$–DIBAC was removed by washing the thin film with acetone and CH_2Cl_2. To characterize the surface properties of the **PF-N_3**–$mPEG_{5000}$–SWNT nanohybrid, contact angle measurements were performed. Briefly, 5 μL of Milli-Q water (18.2 MΩ cm^{-1}) was deposited onto the thin film and then allowed to equilibrate for 3 min, followed by contact angle measurements in triplicate (n = 3), with each water droplet being placed at a different location on the SWNT thin film. As shown in Figure 5.3a, the pristine **PF-N_3**–SWNT thin film had a contact angle of 117 ± 1°, which is consistent with a hydrophobic carbonaceous surface. In contrast, the **PF-N_3**–$mPEG_{5000}$–SWNT sample had a contact angle of 73 ± 2°, which is consistent with $mPEG_{5000}$ functionalization (Figure 5.3b). To determine whether the contact angle could be influenced by non-specific adsorption, rather than covalent mPEG linkage, a control experiment was performed where a **PF-N_3**–SWNT thin film was treated with a solution of $mPEG_{5000}$–OH (10 mg mL^{-1} in THF), which cannot undergo a [3 + 2] cycloaddition with the azide moieties in the polymer–SWNT thin film. After washing the **PF-N_3**–SWNT thin film with acetone and CH_2Cl_2, a contact angle of 114 ± 5° was measured, indicating that the $mPEG_{5000}$–OH does not undergo non-specific adsorption to the nanotube surface. In addition to modifying the hydrophilicity of the SWNT thin film, we also sought to derivatize the thin film with a hydrophobic strained cyclooctyne (Scheme 5.1c). To accomplish this, we synthesized DIBAC–C_{16} *via* Steglich esterification of DIBAC–COOH with 1-hexadecanol (see Supporting Info for details). A 5 mg mL^{-1} solution of DIBAC–C_{16} in THF

was prepared and the **PF-N_3**–SWNT thin film was soaked until the reaction was complete, as monitored by IR spectroscopy. The resulting contact angle after functionalization with DIBAC–C_{16} (and washing with acetone and CH_2Cl_2) was 107 ± 3°, which indicated the film hydrophobicity did not change appreciably (Figure 5.3c). In tandem with contact angle measurements, X-ray photoelectron spectroscopy (XPS) analysis was used to examine the elemental composition of the pre- and post-functionalized polymer–SWNT thin films. As shown in Table S5.1, the amount of oxygen increased upon $mPEG_{5000}$ functionalization (from 5.6 to 16%), while the amount of nitrogen and oxygen increased slightly upon functionalization with C_{16}. These changes in elemental composition are consistent with the functionalization of the polymer–SWNT thin films.

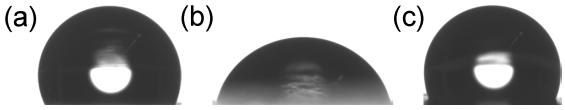


FIGURE 5.3: Modification of **PF-N_3**–SWNT thin film hydrophilicity using strained cyclooctyne derivatization. Photograph of a representative water droplet on the **PF-N_3**–SWNT thin film functionalized with (a) nothing (pristine), (b) $mPEG_{5000}$–DIBAC, or (c) DIBAC–C_{16}. The contact angles are 117 ± 1°, 73 ± 2°, and 107 ± 3°, respectively.

A key strength of our SWNT functionalization methodology in the solution-phase was the preservation of optoelectronic properties of the nanotubes.[48] To determine whether SWNT optoelectronic properties were also preserved when functionalizing **PF-N_3**–SWNT complexes as solid films, we first investigated whether sp^3-C defects were formed *via* Raman spectroscopy. If the SWNT surface is perturbed by chemical functionalization, then an increase in the disorder (D) band, centered at ~1290 cm^{-1}, would be observed and would indicate an increase in the amount of sp^3-hybridized carbon atoms in the SWNT sidewall.[93,94] However, as

shown in Figure 5.4, an increase of the D-band intensity is not observed post-SPAAC in our SWNT sample. This demonstrates that, unlike with covalent functionalization, decoration of SWNT films without introduction of structural defects in the nanotube sidewall is possible if it is performed on the adsorbed conjugated polymer, rather than directly with the SWNT surface. We next interrogated the optoelectronic properties of our SWNT thin films using UV/Vis-NIR spectroscopy (Figure S5.8) and photoluminescence mapping (Figure S5.9). We re-dispersed our pristine and $mPEG_{5000}$–functionalized polymer–SWNT thin films into the solution-phase by sonicating in THF for 1 h and then filtering the polymer–SWNT dispersion through a cotton plug. As shown in Figure S5.8, samples were concentration-matched by dilution until the SWNT absorption peak at ∼1136 nm had an absorption intensity of ∼0.2. It is noteworthy that the absorption features in the UV/Vis-NIR spectrum are preserved upon thin film functionalization. Meanwhile, sc-SWNTs functionalized as a thin film retain their fluorescence when re-dispersed in organic solvent, evidenced by identical fluorescence intensities of all sc-SWNT species in the sample (Figure S5.9). These results give clear evidence that the structural integrity and optical properties of the SWNT scaffold are intact post-functionalization.

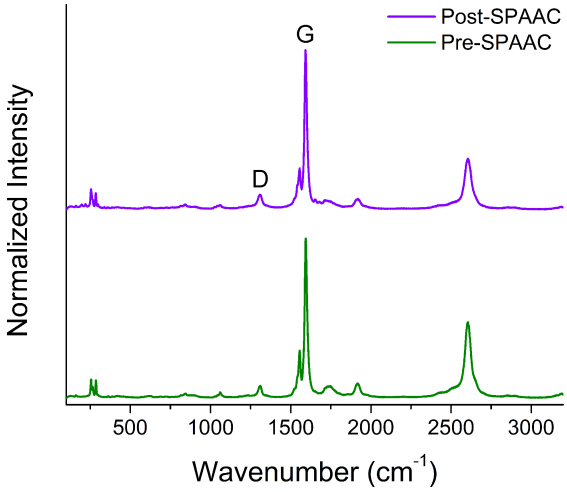


FIGURE 5.4: Raman spectra (λ_{ex} = 633 nm) of **PF-N$_3$**–SWNT dispersions pre-SPAAC (green) and post-SPAAC (purple) with DIBAC–COOH. Spectra were normalized to the G-band at ~1590 cm^{-1} and offset for clarity.

To further characterize the optoelectronic properties of our functionalized thin films, we performed electrical conductivity measurements using the Van der Pauw method.[95] We first prepared square-shaped thin films with dimensions of 0.5 × 0.5 cm for our polymer–SWNT samples by filtering 300 μL of polymer–SWNT dispersion through a Teflon filtration membrane having a 0.2 μm pore diameter, clamped between two solvent-resistant aluminium masks under vacuum. To functionalize the thin films, solutions of strained cyclooctyne in THF (mPEG$_{5000}$–DIBAC or DIBAC–C$_{16}$; 10 mg mL^{-1}, ~300 μL per replicate) were filtered through the thin film. Control samples were also prepared by filtering THF (without the cyclooctyne) through the thin films under identical conditions. The thin films were dried in an oven at 60 °C for 1 h and then resistance was measured by direct contact with four platinum probes placed in the corners of the square-shaped thin film. Voltages from 0 to 250 mV were applied to one pair of contiguous electrodes and the

current was measured on the opposite pair of electrodes (e.g., if the thin film corners were labelled from 1–4 clockwise, the first measurement would apply V_{12} and measure I_{43}). The thin film resistance (R) was calculated from the slope of the resulting I–V curve. The measurements were repeated for all four electrode combinations (i.e., V_{12}, V_{23}, V_{34}, and V_{41}) and the total resistance for the thin film (R_T) was calculated as $R_T = \frac{1}{4}(\frac{V_{12}}{I_{43}} + \frac{V_{23}}{I_{14}} + \frac{V_{12}}{I_{21}} + \frac{V_{41}}{I_{32}})$ (measured in triplicate). The sheet resistance (R_S) was then calculated as $R_S = \frac{\pi \times R_T}{ln2}$. It was found that the R_S of the control thin film was $3.7 \pm 0.5 \times 10^7$ Ω sq^{-1}, and that the R_S of the C_{16}- and mPEG$_{5000}$-functionalized thin films were $7.5 \pm 2.0 \times 10^9$ and $1.0 \pm 0.4 \times 10^{10}$ Ω sq^{-1}, respectively (data are represented graphically in Figure S5.10). The pristine polymer–SWNT thin film sheet resistance is consistent with literature values.[88] The increase in R_S upon functionalization with C_{16} and mPEG$_{5000}$ is consistent with an increase of insulating material surrounding the SWNT surface due to the covalently-bound C_{16} and mPEG$_{5000}$ molecules.

With the ability to modify the surface properties of the **PF-N$_3$**–SWNT thin film, we sought to explore a simple method for spatially-resolved modification of SWNT surface properties. A **PF-N$_3$**–SWNT thin film was again prepared by filtering 3 mL of dispersion through a 0.2 μm Teflon membrane, producing a circular thin film with a diameter of 1 cm that was thoroughly washed with THF to remove excess polymer. To prepare a Janus film that was half hydrophobic and half hydrophilic, we initially attempted to soak half of the **PF-N$_3$**–SWNT thin film in a solution of DIBAC–C_{16} dissolved in CH_2Cl_2, but this resulted in capillary forces drawing the DIBAC–C_{16} solution through the entire partially submerged thin film. To circumvent this, we layered water on top of the CH_2Cl_2 layer to produce a biphasic mixture, which prevented capillary forces from drawing

CH_2Cl_2 beyond the phase boundary (Figure 5.5a). Once the submerged half of the thin film was fully functionalized (within ~6 h), the thin film was placed in a vacuum filtration apparatus and a solution of $mPEG_{5000}$–DIBAC in CH_2Cl_2 (10 mg mL^{-1}) was filtered through the membrane to functionalize the opposite half of the thin film. As shown in Figure 5.5b–d, contact angles of 94 ± 3° (DIBAC–C_{16} functionalized) and 63 ± 2° ($mPEG_{5000}$–DIBAC functionalized) demonstrate that, in a single Janus **PF-N_3**–SWNT thin film, significantly different hydrophilicities were achieved in a spatially-resolved manner, which was accomplished without the use of any masks or specialized equipment. As shown in Table S5.2, XPS analysis again indicates an increase in oxygen content where $mPEG_{5000}$ was used to derivatize the thin film (from 6.1 to 8.5%), in comparison to regions functionalized with C_{16} (Figure S5.11). Although the increase in oxygen signal within this Janus film is not as large as in the separate films described above (likely due to the difference in sample preparation procedure), it is nevertheless consistent with the contact angle results and demonstrates the ability to functionalize a single nanotube film with different species in a spatially defined manner.

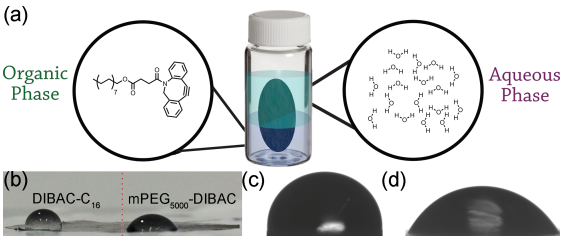


FIGURE 5.5: Preparation of a Janus polymer–SWNT thin film using sequential strained cyclooctyne derivatization. (a) Cartoon representation of Janus thin film functionalization in a biphasic mixture. (b) Photograph (side view) of 5 μL water droplets on the SWNT thin film functionalized with DIBAC–C_{16} (left) and PEG_{5000}–DIBAC (right). The contact angles are 94 ± 3° and 63 ± 2°, respectively. The red dashed line indicates the boundary between hydrophilic (right) and hydrophobic (left) regions. Images (c) and (d) are close-up photographs of representative water droplets on the **PF-N_3**–SWNT thin film functionalized with DIBAC–C_{16} (c) or $mPEG_{5000}$–DIBAC (d).

5.3 Conclusions

Here, we demonstrate that SPAAC can be used to perform interfacial decoration of polymer–SWNT complexes containing azide moieties in the polymer side chains. SPAAC was monitored using IR spectroscopy for the disappearance of the azide stretch at ∼2090 cm^{-1}, and the reaction was found to occur at room temperature, without the addition of any catalysts. Reactive polymer–SWNT complexes could be functionalized with strained cyclooctynes dissolved in a variety of non-polar and polar organic solvents through a simple soaking method. For strained cyclooctynes dissolved in aqueous solution, derivatization could be afforded using vacuum filtration to force the aqueous solution to wet the SWNT thin film. A combination of Raman, UV/Vis-NIR, and fluorescence spectroscopy indicated the preservation of the SWNT structure and properties. TGA indicated that, in tandem with IR spectra, the mass loss pre-SPAAC and post-SPAAC is consistent with complete functionalization of the **PF-N_3**–SWNT thin film. Using $mPEG_{5000}$ or C_{16} alkyl chains derivatized with a strained cyclooctyne, we altered the hydrophilicity of the SWNT thin film. Through sequential functionalization, we could prepare a Janus SWNT thin film that simultaneously contains hydrophilic and hydrophobic regions.

5.4 Supporting Information

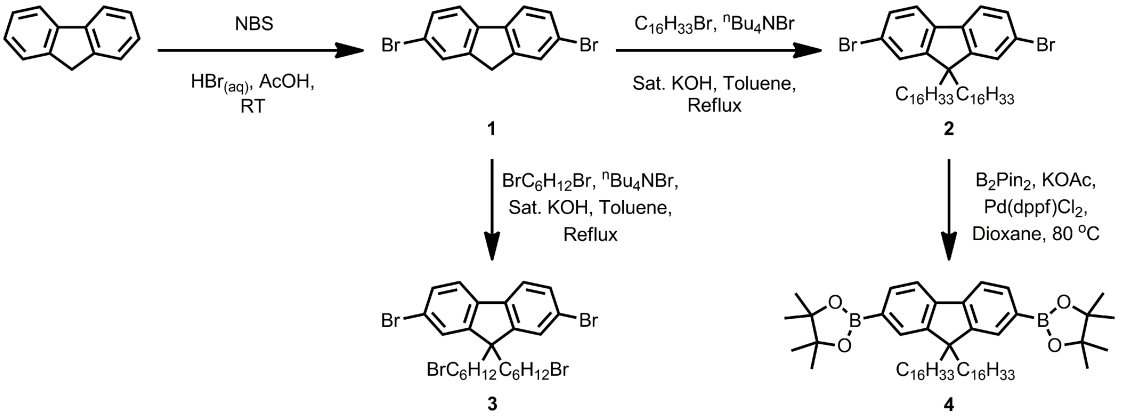
5.4.1 General

Raw HiPCO SWNTs were purchased from NanoIntegris (batch #HR27-104, 10 wt % in anhydrous EtOH) and also used without further purification. Reagents were

purchased from commercial suppliers and used as received. Flash chromatography was performed using an IntelliFlash 280 system from Analogix. Unless otherwise noted, compounds were monitored using a variable wavelength detector at 254 nm. Solvent amounts used for gradient or isocratic elution were reported in column volumes (CV). Columns were prepared in Biotage® SNAP KP-Sil cartridges using 40 – 63 μm silica or 25 – 40 μm silica purchased from Silicycle. NMR was performed on a Bruker Avance 600 MHz or 700 MHz instrument and shift-referenced to the residual solvent resonance. Polymer molecular weights and dispersities were analyzed (relative to polystyrene standards) *via* GPC using a Waters 2695 Separations Module equipped with a Waters 2414 refractive index detector and a Jordi Fluorinated DVB mixed bed column in series with a Jordi Fluorinated DVB 10^5 Å pore size column. THF with 2% acetonitrile was used as the eluent at a flow rate of 2.0 mL/min. Sonication was performed in a Branson Ultrasonic B2800 bath sonicator. Centrifugation of the polymer-SWNT samples was performed using a Beckman Coulter Allegra X-22 centrifuge. Thin film thickness was measured using an optical profilometer (Veeco WYKO NT1100, DYMEK Company Ltd.) in VSI mode. Polymer-SWNT thin films were prepared by filtering the polymer-SWNT dispersion through a Teflon membrane (0.2 μm pore diameter). A straight boundary was prepared between the polymer-SWNT thin film and Teflon membrane by placing a glass slide over half of the polymer-SWNT thin film and using a Kim wipe to remove exposed thin film. The average maximum profile of the ten greatest peak-to-valley separations in the evaluation area, R_z, was used to quantify the thin film thickness. Infrared spectra were recorded using a Thermo Scientific Nicolet 6700 FT-IR spectrometer equipped with a Smart iTX attenuated total reflectance (ATR) sample analyzer. Raman spectra were collected using a Renishaw

InVia Laser Raman spectrometer, with a 500 mW HeNe Renishaw laser (633 nm, 1800 L/mm grating). Laser intensity was set to 1% for the 633 nm excitation wavelength for the polymer-SWNT samples. UV/Vis-NIR spectra were recorded on a Cary 5000 spectrometer in dual beam mode, using matching 10 mm quartz cuvettes. Fluorescence spectra were measured on a Jobin-Yvon SPEX Fluorolog 3.22 equipped with a 450 W Xe arc lamp, digital photon counting photomultiplier, and an InGaAs detector, also using a 10 mm quartz cuvette. Slit widths for both excitation and emission were set to 10 nm band-pass, and correction factor files were applied to account to instrument variations. Photoluminescence maps were obtained at 25 °C, with 5 nm intervals for both the excitation and emission. Thermogravimetric analysis was performed on a Mettler Toledo TGA/DSC 3+, and all measurements were conducted under an argon atmosphere, with sample masses ranging from 0.5 to 1.0 mg. Contact angle measurements were obtained using an Optical Contact Angle (OCA 25) instrument from DataPhysics Instruments (Filderstadt, Germany). Conductivity measurements were recorded using the Model 2450 Interactive Source Meter Instrument (Keithley) with Pt-wire probes. X-ray photoelectron spectroscopy (XPS) survey spectra were collected using a K-Alpha X-ray photoelectron spectrometer system from Thermo Scientific.

5.4.2 Synthetic Procedures



Synthesis of monomers **3** and **4**.

2,7-dibromofluorene (1) (adapted from reference 96)

A round bottom flask equipped with a magnetic stir bar was charged with fluorene (33.2 g, 200 mmol), NBS (89.0 g, 500 mmol) and acetic acid (400 mL). While the mixture was stirring, conc. HBr (10 mL) was slowly added and then the reaction mixture was stirred at RT for 1.5 h. Water (200 mL) was added and the resulting suspension was filtered and washed with water to obtain an orange-white solid. The solid was recrystallized from a 1.5:1 v/v mixture of EtOH:acetone (∼1.8 L total volume), and the mother liquor was recrystallized again from the same solvent mixture (∼1.5 L total volume). The crops were combined to afford **1** (41.2 g, 64%) as a white solid. ^{1}H-NMR (600 MHz; $CDCl_3$): δ 7.67 (d, J = 1.1 Hz, 2H), 7.61 (d, J = 8.1 Hz, 2H), 7.51 (dd, J = 8.1, 1.8 Hz, 2H), 3.88 (s, 2H).

2,7-dibromo-9,9-dihexadecylfluorene (2) (adapted from reference 97)

A round bottom flask equipped with a magnetic stir bar was charged with **1** (2.7 g, 8.3 mmol), 1-bromohexadecane (6.36 g, 20.8 mmol), ^{n}Bu$_4$NBr (537 mg, 1.7 mmol), toluene (16.6 mL), and sat. $KOH_{(aq)}$ (16.6 mL). The reaction mixture was heated

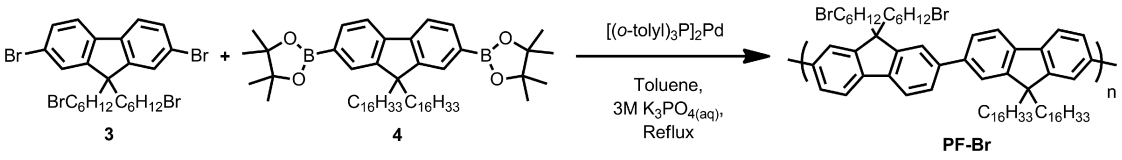
to 60 °C and stirred vigorously for 1 h under a nitrogen atmosphere. The biphasic mixture was allowed to separate and the organic layer was isolated. The aqueous phase was extracted twice with diethyl ether (2 x 20 mL) and the organic extracts were combined and concentrated *in vacuo* to obtain a viscous green oil. The crude product was purified by flash chromatography (100 g column, 100% hexanes over 10 CV) to afford **2** as a white solid (5.19 g, 81%). ^{1}H-NMR (600 MHz; $CDCl_3$): δ 7.51 (d, J = 8.0 Hz, 1H), 7.46-7.43 (m, 2H), 1.92-1.88 (m, 2H), 1.24-1.03 (m, 26H), 0.88 (t, J = 7.0 Hz, 3H), 0.59-0.57 (m, 2H).

2,7-dibromo-9,9-bis(6-bromohexyl)fluorene (3) (adapted from reference 96) A round bottom flask equipped with a magnetic stir bar was charged with **1** (5 g, 15.4 mmol), 1,6-dibromohexane (37.7 g, 154 mmol), toluene (31 mL), and sat. KOH (31 mL). ^{n}Bu_4NBr (1.0 g, 3.1 mmol) was then added and the reaction mixture was heated to 60 °C and stirred vigorously for 1 h under a nitrogen atmosphere. The biphasic mixture was allowed to separate, and the organic layer was isolated. The aqueous phase was extracted twice with diethyl ether (2 x 120 mL) and the organic extracts were combined and concentrated *in vacuo* to obtain a viscous green oil. Excess 1,6-dibromohexane was removed using vacuum distillation (1 mbar, 115 °C) to obtain a viscous yellow oil. The crude mixture was purified by flash chromatography (100 g column, 0 to 20% CH_2Cl_2 in hexanes over 10 CV) to obtain a white solid. TLC analysis of this product indicated that it was composed of two components. Subsequent recrystallization from MeOH (∼250 mL) afforded **3** as a pure white solid (4.4 g, 44%). ^{1}H-NMR (600 MHz; $CDCl_3$): δ 7.53-7.52 (m, 1H), 7.47-7.43 (m, 2H), 3.31-3.28 (t, 2H), 1.94-1.91 (m, 2H), 1.68-1.66 (m, 2H), 1.22-1.19 (m, 2H), 1.10-1.07 (m, 2H), 0.60-0.57 (m, 2H).

2,2'-(9,9-dihexadecylfluorene-2,7-diyl)bis(4,4,5,5-tetramethyl-1,3,2-

dioxaborolane) (4) (adapted from reference 97)

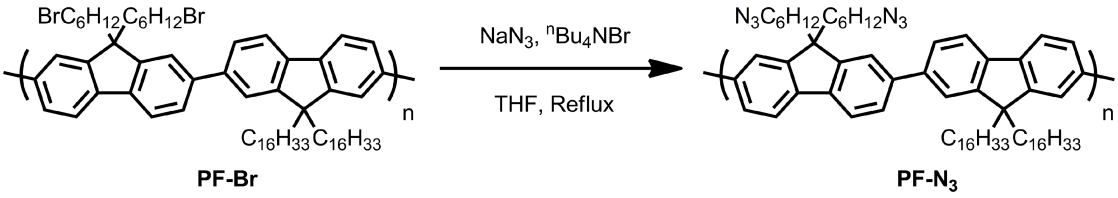
A round bottom flask equipped with a magnetic stir bar was charged with **2** (5.2 g, 6.7 mmol), B_2Pin_2 (3.76 g, 14.8 mmol), KOAc (1.98 g, 20.2 mmol), and dioxane (28 mL). $Pd(dppf)_2Cl_2$ (165 mg, 202 μmol) was added and then the reaction mixture was stirred at 80 °C for 12 h. The reaction mixture was partitioned with water and extracted thrice with Et_2O. The organic extracts were combined and dry loaded onto silica (9.9 g). The crude product was purified by flash chromatography (100 g column, 0 to 70% CH_2Cl_2 in hexanes over 10 CV) to afford **3** as a white solid (4.88 g, 63%). ^{1}H-NMR (600 MHz; $CDCl_3$): δ 7.80 (d, J = 7.5 Hz, 1H), 7.74-7.71 (m, 2H), 2.00-1.97 (m, 2H), 1.39 (s, 12H), 1.24-0.99 (m, 26H), 0.87 (t, J = 7.0 Hz, 3H), 0.55-0.53 (m, 2H).



Poly(dihexadecylfluorene-alt-bis(bromohexyl)fluorene) (PF-Br) (adapted from reference 48)

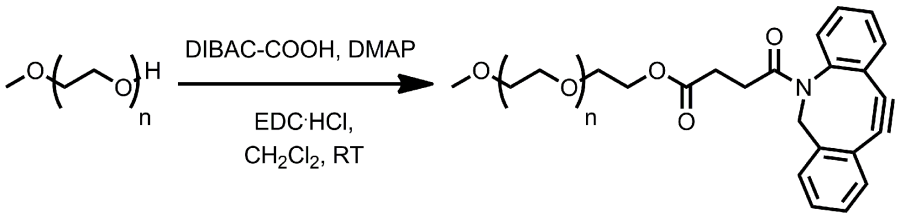
A Schlenk tube equipped with a magnetic stir bar was charged with **3** (447.7 mg, 0.69 mmol), **4** (597 mg, 0.69 mmol), toluene (4.9 mL), and 3M $K_3PO_{4(aq)}$ (4.9 mL). The biphasic mixture was degassed by three freeze-pump-thaw cycles, then, while frozen under liquid nitrogen, $[(o\text{-tol})_3P]_2Pd$ (18 mg, 2.5 μmol) was added under a positive pressure of nitrogen. The Schlenk tube was evacuated and backfilled with nitrogen four times, and the reaction mixture was heated to 80 °C and vigorously stirred for 12 h. The phases were allowed to separate, and the organic layer was isolated and filtered through a single plug of celite and neutral alumina. The plug was thoroughly washed with THF and the flow-through was concentrated *in vacuo*.

The crude polymer was precipitated into MeOH (∼300 mL) and then filtered to afford **PF-Br** as a yellow solid (478 mg, 63%). ^{1}H-NMR (700 MHz; $CDCl_3$): δ 7.85-7.83 (m, 4H), 7.73-7.68 (m, 8H), 3.30 (t, 4H), 2.17-2.11 (m, 4H), 1.72-1.69 (m, 4H), 1.30-1.13 (m, 60H), 0.87 (t, 6H).



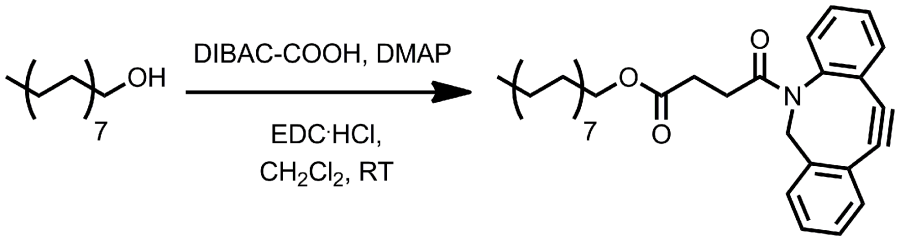
Poly(dihexadecylfluorene-alt-bis(azidohexyl)fluorene) (PF-N_3) (adapted from reference 48)

A round bottom flask equipped with a magnetic stir bar and reflux condenser was charged with **PF-Br** (400 mg, 0.36 mmol), NaN_3 (236 mg, 3.6 mmol), ^{n}Bu$_4$NBr (234 mg, 0.73 mmol), and THF (60 mL) and the reaction mixture was heated to reflux for 12 h. The reaction mixture was filtered through an alumina plug and washed thoroughly with THF, then the solution was concentrated *in vacuo* and precipitated into MeOH (∼200 mL) to afford **PF-N_3** as a yellow solid (328 mg, 86%). ^{1}H-NMR (700 MHz; $CDCl_3$): δ 7.86-7.84 (m, 4H), 7.71-7.68 (m, 8H), 3.15 (t, 4H), 2.21-2.08 (m, 4H), 1.45-1.42 (m, 4H), 1.29-1.14 (m, 60H), 0.87 (t, 6H).



mPEG$_{5000}$-DIBAC (adapted from reference 48). A round bottom flask equipped with a magnetic stir bar was charged with mPEG$_{5000}$-OH (250 mg, 50 μmol), DIBAC-COOH (46 mg, 150 μmol) and 4-dimethylaminopyridine (DMAP; 3 mg,

25 μmol) and CH_2Cl_2 (1 mL). To the solution, *N*-(3-dimethylaminopropyl)-*N*′-ethylcarbodiimide hydrochloride (EDC·HCl) (33 mg, 175 μmol) was added, and the reaction mixture was stirred for 12 h at RT. The reaction mixture was diluted with 5 mL of CH_2Cl_2 and then precipitated into 1:1 Et_2O:hexanes (∼100 mL). The precipitate was collected on a Hirsch funnel, then washed with ice cold ethanol (3 x 20 mL), Et_2O (3 x 20 mL), and dried *in vacuo* to afford **mPEG$_{5000}$-DIBAC** as a fine white powder (246 mg, 93%). ^{1}H NMR (600 MHz; DMSO-d6): δ 7.66 (dd, J = 7.6, 1.2, 1H), 7.62 (d, J = 7.3, 1H), 7.52-7.45 (m, 3H), 7.38 (td, J = 7.4, 1.5, 1H), 7.34 (td, J = 7.4, 1.3, 1H), 7.30 (dd, J = 7.5, 1.2, 1H), 5.03 (d, J = 14.2, 1H), 4.03-3.99 (m, 1H), 3.95-3.91 (m, 1H), 3.51 (s, 1H), 3.24 (s, 3H), 2.67-2.62 (m, 2H), 2.37-2.35 (m, 1H), 2.29 (dt, J = 17.1, 6.4, 1H), 1.81 (dt, J = 16.7, 6.3, 1H).



DIBAC-C$_{16}$ (adapted from reference 48). A round bottom flask equipped with a magnetic stir bar was charged with 1-hexadecanol (0.099 g, 0.404 mmol), DIBAC-COOH (0.130 g, 0.426 mmol), DMAP (0.013 g, 0.106 mmol), and CH_2Cl_2 (1 mL). To the solution, EDC·HCl (0.122 g, 0.639 mmol) was added and then the reaction mixture was stirred for 2 h. The reaction mixture was purified by flash chromatography (25 g column, gradient of 0 to 35% EtOAc in hexanes over 20 CV) to afford DIBAC-C_{16} as a slightly waxy, colourless solid after cooling to −20 °C in a freezer for 2 h (227 mg, 98%). ^{1}H NMR (700 MHz; $CDCl_3$): δ 7.69 (d, J = 7.6, 1H), 7.51-7.50 (m, 1H), 7.42-7.40 (m, 1H), 7.39-7.37 (m, 2H), 7.35 (td, J = 7.5, 1.4,

1H), 7.29 (td, J = 7.5, 0.7, 1H), 7.25 (dd, J = 7.5, 1.1, 1H), 5.17 (d, J = 13.9, 1H), 4.00-3.93 (m, 2H), 3.67 (d, J = 13.9, 1H), 2.73 (ddd, J = 16.7, 8.2, 6.6, 1H), 2.62 (ddd, J = 17.2, 8.2, 6.5, 1H), 2.32 (dt, J = 17.2, 6.3, 1H), 1.95 (dt, J = 16.8, 6.2, 1H), 1.52 (t, J = 6.7, 2H), 1.27 (dd, J = 26.9, 6.1, 26H), 0.88 (t, J = 7.1, 3H). ^{13}C NMR (176 MHz; $CDCl_3$): δ 173.1, 171.8, 151.6, 148.2, 132.4, 129.4, 128.6, 128.39, 128.20, 127.8, 127.2, 125.6, 123.3, 122.8, 115.1, 107.9, 64.8, 55.6, 32.1, 29.84, 29.80, 29.72, 29.67, 29.61, 29.50, 29.39, 28.6, 26.0, 22.8, 14.3. HRMS (ESI) (m/z) for $C_{35}H_{46}NO_3$ $[M+H]^+$ calculated: 530.3629, found: 530.3641.

General SPAAC procedure. PF-N_3-SWNT thin film was prepared by filtering the dispersion through a Teflon membrane with a pore diameter of 0.2 μm. Thin films were washed with THF until the flow-through did not fluoresce at 365 nm, as monitored using a handheld UV lamp. Thin film samples were functionalized by either soaking the thin film in a solution of DIBAC derivative (for organic solvents) or by filtering the DIBAC solution through the thin film using vacuum filtration (for aqueous solvents). Reaction progress was monitored using IR spectroscopy for the disappearance of the polymer azide stretch at ∼2090 cm^{-1}.

TGA Sample Calculation

f is the mass percentage of a given subset of atoms.

Pre-SPAAC:

PF-N_3 repeat unit mass: 1027.60 g · mol^{-1}

N x 5 = 14.01 g · mol^{-1} x 5 = 70.05

$f_{5N} = \frac{70.05}{1027.60} \times 100\% = 6.8\%$ (measured: 6.8%)

Total side chain mass: $[C_{16}H_{33} + C_6H_{12}N_3]$ x 2 = $C_{44}H_{90}N_6$ = 703.40 g · mol^{-1}

Post-SPAAC:

DIBAC-COOH MW: 305.33 g · mol^{-1}

Side chain mass: $C_{44}H_{90}N_6 + \text{DIBAC} - \text{COOH} \times 2 = [703.40 + 305.33]\ \text{g} \cdot \text{mol}^{-1}$ x 2 = 1314.06 $\text{g} \cdot \text{mol}^{-1}$

% side chain mass increase = $\frac{\text{mass(post-SPAAC)}}{\text{mass(pre-SPAAC)}} \times 100\% = \frac{1314.06}{703.40} \times 100\% = 186.8\%$

Note: Mass is of the side chain

Expected mass loss post-SPAAC: Initial observed mass loss (TGA) × side chain mass increase = 15.4% × 1.868 = 28.8% (measured: 27.2%)



FIGURE 5.6: Photograph of the **PF-N$_3$**-SWNT functionalization process. A 1 cm^2 **PF-N$_3$**-SWNT thin film is soaked in a solution of strained cyclooctyne.

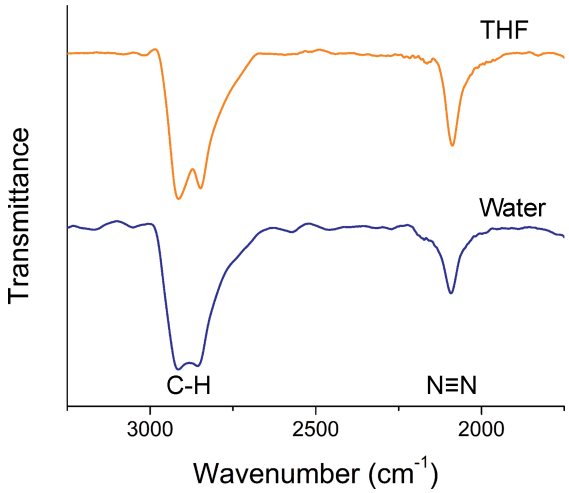


FIGURE 5.7: FT-IR overlay of the **PF-N$_3$**-SWNT thin film soaked in a 0.5 $\text{mg} \cdot \text{mL}^{-1}$ solution of **mPEG$_{5000}$-DIBAC** in THF (orange) or H_2O (blue).

Sample	C (%)	N (%)	O (%)
Pristine	91.04	3.38	5.58
$mPEG_{5000}$-Functionalized	81.83	2.07	16.09
C_{16}-Functionalized	90.10	3.65	6.25

TABLE 5.1: Atomic %s of C, N, and O for **PF-N_3**-SWNT Thin Film Pre- and Post-SPAAC With $mPEG_{5000}$-DIBAC or DIBAC-C_{16}

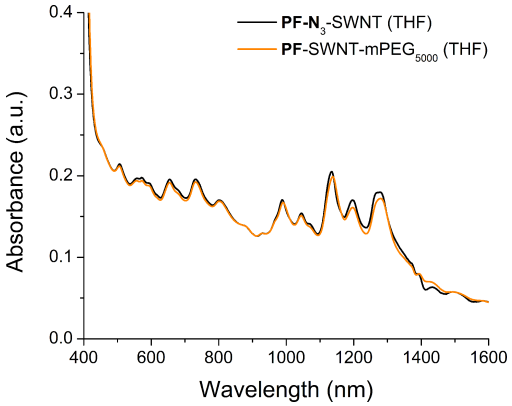


FIGURE 5.8: UV/Vis-NIR spectra of **PF-N_3**-SWNT samples in THF used for PL mapping (i) prior to any functionalization (black), (ii) functionalized with **$mPEG_{5000}$-DIBAC** (orange). The samples were prepared by sonicating the corresponding thin film in THF for 1 h and then filtering the resulting dispersion through a cotton plug.

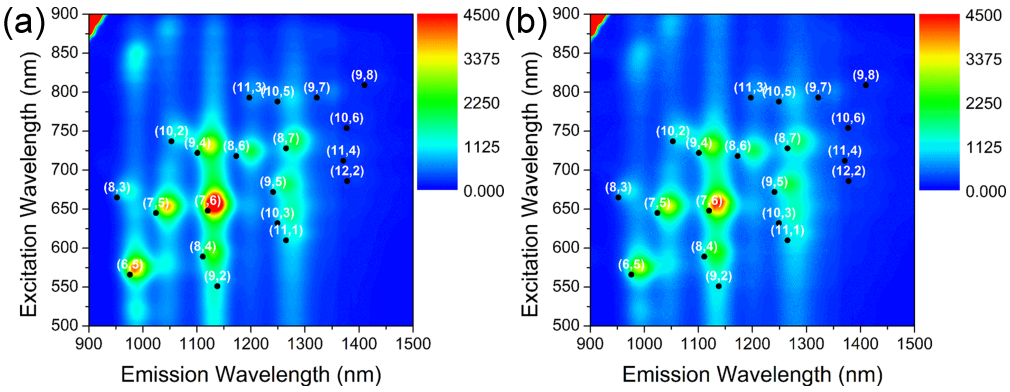


FIGURE 5.9: PL maps of **PF-N_3**-SWNT samples in THF (a) prior to any functionalization, (b) functionalized with **$mPEG_{5000}$-DIBAC**. The samples were prepared by sonicating the corresponding thin film in THF for 1 h and then filtering the resulting dispersion through a cotton plug.

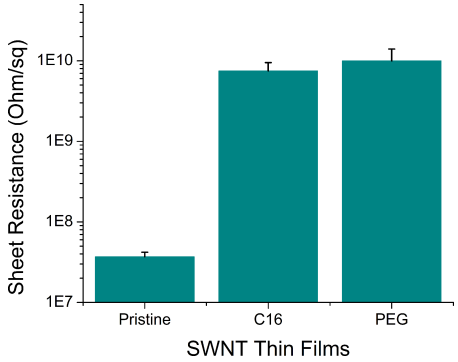


FIGURE 5.10: Bar chart of sheet resistance measurements for (i) pristine, (ii) C_{16}-functionalized, and (iii) $mPEG_{5000}$-functionalized polymer-SWNT thin films.

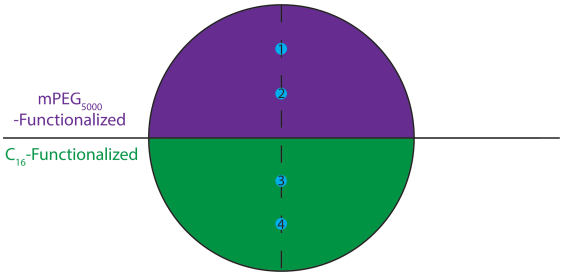


FIGURE 5.11: Idealized cartoon showing the location of XPS measurements made on the Janus polymer-SWNT thin film.

Location	C (%)	N (%)	O (%)
1	88.24	3.26	8.50
2	88.33	2.93	8.74
3	90.25	3.59	6.16
4	90.49	3.42	6.08

TABLE 5.2: Atomic %s of C, N, and O for Janus Polymer-SWNT Thin Film Functionalized With $mPEG_{5000}$-DIBAC or DIBAC-C_{16}

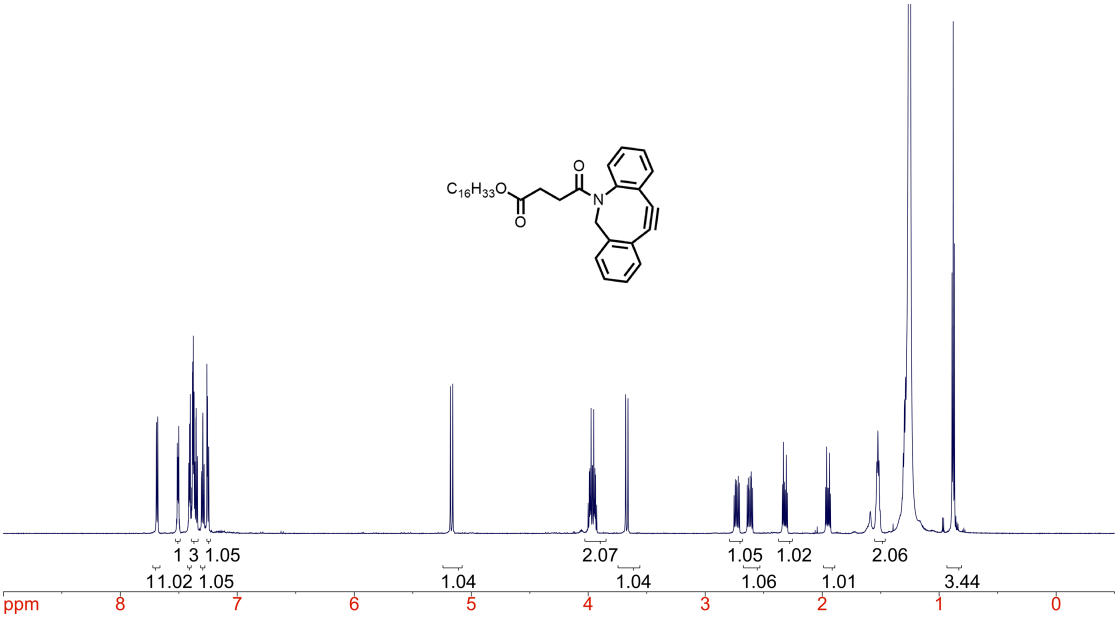


FIGURE 5.12: ^{1}H NMR spectrum of DIBAC-C_{16} in $CDCl_3$.

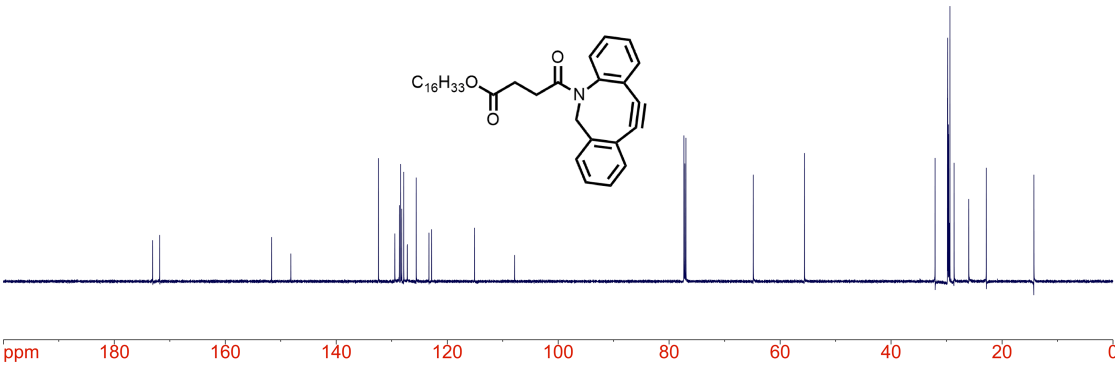


FIGURE 5.13: uDEFT spectrum of DIBAC-C_{16} in $CDCl_3$.

5.5 References

(1) Park, S.; Vosguerichian, M.; Bao, Z. *Nanoscale* **2013**, 5, 1727–1752.

(2) Terrones, M. *Annu. Rev. Mater. Res.* **2003**, 33, 419–501.

(3) Ajayan, P. M. *Chem. Rev.* **1999**, 99, 1787–1800.

(4) Coleman, J. N.; Khan, U.; Blau, W. J.; Gun'ko, Y. K. *Carbon* **2006**, 44, 1624–1652.

(5) Zhang, Q.; Huang, J.-Q.; Qian, W.-Z.; Zhang, Y.-Y.; Wei, F. *Small* **2013**, 9, 1237–1265.

(6) Saito, R.; Dresselhaus, G.; Dresselhaus, M. S. *Physical Properties of Carbon Nanotubes*, vol. 3.; Imperial College Press: London, **2005**.

(7) O'Connell, M. J.; Bachilo, S. M.; Huffman, C. B.; Moore, V. C.; Strano, M. S.; Haroz, E. H.; Rialon, K. L.; Boul, P. J.; Noon, W. H.; Kittrell, C.; et al. *Science* **2002**, 297, 593–596.

(8) Bachilo, S. M.; Strano, M. S.; Kittrell, C.; Hauge, R. H.; Smalley, R. E.; Weisman, R. B. *Science* **2002**, 298, 2361–2366.

(9) Kataura, H.; Kumazawa, Y.; Maniwa, Y.; Umezu, I.; Suzuki, S.; Ohtsuka, Y.; Achiba, Y. *Synth. Met.* **1999**, 103, 2555–2558.

(10) Tasis, D.; Tagmatarchis, N.; Bianco, A.; Prato, M. *Chem. Rev.* **2006**, 106, 1105–1136.

(11) Nikolaev, P.; Bronikowski, M. J.; Bradley, R. K.; Rohmund, F.; Colbert, D. T.; Smith, K. .; Smalley, R. E. *Chem. Phys. Lett.* **1999**, 313, 91–97.

(12) Kong, J.; Cassell, A. M.; Dai, H. *Chem. Phys. Lett.* **1998**, 292, 567–574.

(13) Bernier, P.; Journet, C.; Maser, W. K.; Loiseau, A.; de la Chapelle, M. L.; Lefrant, S.; Deniard, P.; Lee, R.; Fischer, J. E. *Nature* **1997**, 388, 756–758.

(14) Guo, T.; Nikolaev, P.; Thess, A.; Colbert, D. T.; Smalley, R. E. *Chem. Phys. Lett.* **1995**, 243, 49–54.

(15) Kim, K. S.; Cota-Sanchez, G.; Kingston, C. T.; Imris, M.; Simard, B.; Soucy, G. *J. Phys. D. Appl. Phys.* **2007**, 40, 2375–2387.

(16) Hirsch, A. *Angew. Chemie - Int. Ed.* **2002**, 41, 1853–1859.

(17) Britz, D. A.; Khlobystov, A. N. *Chem. Soc. Rev.* **2006**, 35, 637–659.

(18) Campidelli, S.; Klumpp, C.; Bianco, A.; Guldi, D. M.; Prato, M. *J. Phys. Org. Chem.* **2006**, 19, 531–539.

(19) Setaro, A.; Adeli, M.; Glaeske, M.; Przyrembel, D.; Bisswanger, T.; Gordeev, G.; Maschietto, F.; Faghani, A.; Paulus, B.; Weinelt, M.; et al. *Nat. Commun.* **2017**, 8, 14281.

(20) Zhao, Y. L.; Stoddart, J. F. *Acc. Chem. Res.* **2009**, 42, 1161–1171.

(21) Bilalis, P.; Katsigiannopoulos, D.; Avgeropoulos, A.; Sakellariou, G. *RSC Adv.* **2014**, 4, 2911–2934.

(22) Gavrel, G.; Jousselme, B.; Filoramo, A.; Campidelli, S. *Top. Curr. Chem.* **2014**, 348, 95–126.

(23) Islam, M. F.; Rojas, E.; Bergey, D. M.; Johnson, A. T.; Yodh, A. G. *Nano Lett.* **2003**, 3, 269–273.

(24) Moore, V. C.; Strano, M. S.; Haroz, E. H.; Hauge, R. H.; Smalley, R. E.; Schmidt, J.; Talmon, Y. *Nano Lett.* **2003**, 3, 1379–1382.

(25) Gong, X.; Liu, J.; Baskaran, S.; Voise, R. D.; Young, J. S. *Chem. Mater.* **2000**, 12, 1049–1052.

(26) Yang, K.; Zhu, L.; Xing, B. *Environ. Sci. Technol.* **2006**, 40, 1855–1861.

(27) Tomonari, Y.; Murakami, H.; Nakashima, N. *Chem. - A Eur. J.* **2006**, 12, 4027–4034.

(28) Chen, R. J.; Zhang, Y.; Wang, D.; Dai, H. *J. Am. Chem. Soc.* **2001**, 123, 3838–3839.

(29) Chen, J.; Liu, H.; Weimer, W. A.; Halls, M. D.; Waldeck, D. H.; Walker, G. C. *J. Am. Chem. Soc.* **2002**, 124, 9034–9035.

(30) Star, A.; Stoddart, J. F.; Steuerman, D.; Diehl, M.; Boukai, A.; Wong, E.

W.; Yang, X.; Chung, S. W.; Choi, H.; Heath, J. R. *Angew. Chemie - Int. Ed.* **2001**, 40, 1721–1725.

(31) Nish, A.; Hwang, J.-Y.; Doig, J.; Nicholas, R. J. *Nat. Nanotechnol.* **2007**, 2, 640–646.

(32) Yim, C. Bin; Dijkgraaf, I.; Merkx, R.; Versluis, C.; Eek, A.; Mulder, G. E.; Rijkers, D. T. S.; Boerman, O. C.; Liskamp, R. M. J. *J. Med. Chem.* **2010**, 53, 3944–3953.

(33) Cheng, F. Y.; Imin, P.; Lazar, S.; Botton, G. A.; de Silveira, G.; Marinov, O.; Deen, J.; Adronov, A. *Macromolecules* **2008**, 41, 9869–9874.

(34) Guo, Z.; Sadler, P. J.; Tsang, S. C. *Adv. Mater.* **1998**, 10, 701–703.

(35) Balavoine, F.; Schultz, P.; Richard, C.; Mallouh, V. V.; Ebbesen, T. W.; Mioskowski, C. *Angew. Chemie - Int. Ed.* **1999**, 38, 1912–1915.

(36) Bradley, K.; Briman, M.; Star, A.; Grüner, G. *Nano Lett.* **2004**, 4, 253–256.

(37) Star, A.; Steuerman, D. W.; Heath, J. R.; Stoddart, J. F. *Angew. Chemie - Int. Ed.* **2002**, 41, 2508–2512.

(38) Zheng, M.; Jagota, A.; Strano, M. S.; Santos, A. P.; Barone, P.; Chou, S. G.; Diner, B. A.; Dresselhaus, M. S.; McLean, R. S.; Onoa, G. B.; et al. *Science* **2003**, 302, 1545–1548.

(39) Zheng, M.; Jagota, A.; Semke, E. D.; Diner, B. A.; McLean, R. S.; Lustig, S. R.; Richardson, R. E.; Tassi, N. G. *Nat. Mater.* **2003**, 2, 338–342.

(40) Heller, D. A.; Jeng, E. S.; Yeung, T.-K.; Martinez, B. M.; Moll, A. E.; Gastala, J. B.; Strano, M. S. *Science* **2006**, 311, 508–511.

(41) Fong, D.; Adronov, A. *Chem. Sci.* **2017**, 8, 7292–7305.

(42) Liang, S.; Zhao, Y.; Adronov, A. *J. Am. Chem. Soc.* **2014**, 136, 970–977.

(43) Pochorovski, I.; Wang, H.; Feldblyum, J. I.; Zhang, X.; Antaris, A. L.; Bao,

Z. *J. Am. Chem. Soc.* **2015**, 137, 4328–4331.

(44) Lei, T.; Pochorovski, I.; Bao, Z. *Acc. Chem. Res.* **2017**, 50, 1096–1104.

(45) Lei, T.; Chen, X.; Pitner, G.; Wong, H.-S. P.; Bao, Z. *J. Am. Chem. Soc.* **2016**, 138, 802–805.

(46) Toshimitsu, F.; Nakashima, N. *Nat. Commun.* **2014**, 5, 5041.

(47) Fong, D.; Andrews, G.; Adronov, A. *Polym. Chem.* **2018**, 9, 2873–2879.

(48) Fong, D.; Yeung, J.; McNelles, S. A.; Adronov, A. *Macromolecules* **2018**, 51, 755–762.

(49) Tornøe, C. W.; Christensen, C.; Meldal, M. *J. Org. Chem.* **2002**, 67, 3057–3064.

(50) Rostovtsev, V. V.; Green, L. G.; Fokin, V. V.; Sharpless, K. B. *Angew. Chemie - Int. Ed.* **2002**, 41, 2596–2599.

(51) Hein, J. E.; Fokin, V. V. *Chem. Soc. Rev.* **2010**, 39, 1302–1315.

(52) Agard, N. J.; Prescher, J. A.; Bertozzi, C. R. *J. Am. Chem. Soc.* **2004**, 126, 15046–15047.

(53) Jewett, J. C.; Bertozzi, C. R. *Chem. Soc. Rev.* **2010**, 39, 1272.

(54) Mbua, N. E.; Guo, J.; Wolfert, M. A.; Steet, R.; Boons, G.-J. *ChemBioChem* **2011**, 12, 1912–1921.

(55) Ning, X.; Guo, J.; Wolfert, M. A.; Boons, G.-J. *Angew. Chemie - Int. Ed.* **2008**, 47, 2253–2255.

(56) Beatty, K. E.; Fisk, J. D.; Smart, B. P.; Lu, Y. Y.; Szychowski, J.; Hangauer, M. J.; Baskin, J. M.; Bertozzi, C. R.; Tirrell, D. A. *ChemBioChem* **2010**, 11, 2092–2095.

(57) Yang, H.; Srivastava, P.; Zhang, C.; Lewis, J. C. *ChemBioChem* **2014**, 15, 223–227.

(58) Bernardin, A.; Cazet, A.; Guyon, L.; Delannoy, P.; Vinet, F.; Bonnaffe, D.; Texier, I. *Bioconjug. Chem.* **2010**, 21, 583–588.

(59) Kuzmin, A.; Poloukhtine, A.; Wolfert, M. A.; Popik, V. V. *Bioconjug. Chem.* **2010**, 21, 2076–2085.

(60) Manova, R.; van Beek, T. A.; Zuilhof, H. *Angew. Chemie - Int. Ed.* **2011**, 50, 5428–5430.

(61) Luo, W.; Gobbo, P.; McNitt, C. D.; Sutton, D. A.; Popik, V. V.; Workentin, M. S. *Chem. - A Eur. J.* **2017**, 23, 1052–1059.

(62) Luo, W.; Gobbo, P.; Gunawardene, P. N.; Workentin, M. S. *Langmuir* **2017**, 33, 1908–1913.

(63) Gobbo, P.; Novoa, S.; Biesinger, M. C.; Workentin, M. S. *Chem. Commun.* **2013**, 49, 3982.

(64) Cao, Q.; Kim, H. S.; Pimparkar, N.; Kulkarni, J. P.; Wang, C.; Shim, M.; Roy, K.; Alam, M. A.; Rogers, J. A. *Nature* **2008**, 454, 495–500.

(65) Wang, C.; Zhang, J.; Ryu, K.; Badmaev, A.; De Arco, L. G.; Zhou, C. *Nano Lett.* **2009**, 9, 4285–4291.

(66) Yuan, Y.; Giri, G.; Ayzner, A. L.; Zoombelt, A. P.; Mannsfeld, S. C. B.; Chen, J.; Nordlund, D.; Toney, M. F.; Huang, J.; Bao, Z. *Nat. Commun.* **2014**, 5, 3005.

(67) Lau, P. H.; Takei, K.; Wang, C.; Ju, Y.; Kim, J.; Yu, Z.; Takahashi, T.; Cho, G.; Javey, A. *Nano Lett.* **2013**, 13, 3864–3869.

(68) Saran, N.; Parikh, K.; Suh, D.-S.; Muñoz, E.; Kolla, H.; Manohar, S. K. *J. Am. Chem. Soc.* **2004**, 126, 4462–4463.

(69) Wu, Z.; Chen, Z.; Du, X.; Logan, J. M.; Sippel, J.; Nikolou, M.; Kamaras, K.; Reynolds, J. R.; Tanner, D. B.; Hebard, A. F.; et al. *Science* **2004**, 305, 1273–1276.

(70) Zhang, M.; Fang, S.; Zhakidov, A. A.; Lee, S. B.; Aliev, A. E.; Williams, C. D.; Atkinson, K. R.; Baughman, R. H. *Science* **2005**, 309, 1215–1219.

(71) Jackson, R.; Domercq, B.; Jain, R.; Kippelen, B.; Graham, S. *Adv. Funct. Mater.* **2008**, 18, 2548–2554.

(72) Lipomi, D. J.; Vosgueritchian, M.; Tee, B. C.-K.; Hellstrom, S. L.; Lee, J. A.; Fox, C. H.; Bao, Z. *Nat. Nanotechnol.* **2011**, 6, 788–792.

(73) Pasquier, A. Du; Unalan, H. E.; Kanwal, A.; Miller, S.; Chhowalla, M. *Appl. Phys. Lett.* **2005**, 87, 203511.

(74) Yamada, T.; Hayamizu, Y.; Yamamoto, Y.; Yomogida, Y.; Izadi-Najafabadi, A.; Futaba, D. N.; Hata, K. *Nat. Nanotechnol.* **2011**, 6, 296–301.

(75) Li, J.; Lu, Y.; Ye, Q.; Cinke, M.; Han, J.; Meyyappan, M. *Nano Lett.* **2003**, 3, 929–933.

(76) Qi, P.; Vermesh, O.; Grecu, M.; Javey, A.; Wang, Q.; Dai, H.; Peng, S.; Cho, K. J. *Nano Lett.* **2003**, 3, 347–351.

(77) Ghosh, S.; Sood, A. K.; Kumar, N. *Science* **2003**, 299, 1042–1044.

(78) Wang, F.; Gu, H.; Swager, T. M. *J. Am. Chem. Soc.* **2008**, 130, 5392–5393.

(79) Gethard, K.; Sae-Khow, O.; Mitra, S. *ACS Appl. Mater. Interfaces* **2011**, 3, 110–114.

(80) Chan, W.-F.; Chen, H.; Surapathi, A.; Taylor, M. G.; Shao, X.; Marand, E.; Johnson, J. K. *ACS Nano* **2013**, 7, 5308–5319.

(81) Yang, H. Y.; Han, Z. J.; Yu, S. F.; Pey, K. L.; Ostrikov, K.; Karnik, R. *Nat. Commun.* **2013**, 4, 2220.

(82) Guldi, D. M.; Rahman, G. M. A.; Prato, M.; Jux, N.; Qin, S.; Ford, W. *Angew. Chemie - Int. Ed.* **2005**, 44, **2015**–**2018**.

(83) Li, J.; Hu, L.; Wang, L.; Zhou, Y.; Grüner, G.; Marks, T. J. *Nano Lett.* **2006**,

6, 2472–2477.

(84) Yuan, W.; Hu, L.; Yu, Z.; Lam, T.; Biggs, J.; Ha, S. M.; Xi, D.; Chen, B.; Senesky, M. K.; Grüner, G.; et al. *Adv. Mater.* **2008**, 20, 621–625.

(85) Hu, L.; Hecht, D. S.; Gru, G.; Grüner, G. *Chem. Rev.* **2010**, 110, 5790–5844.

(86) Ozawa, H.; Ide, N.; Fujigaya, T.; Niidome, Y.; Nakashima, N. *Chem. - A Eur. J.* **2011**, 17, 13438–13444.

(87) Ozawa, H.; Yi, X.; Fujigaya, T.; Niidome, Y.; Asano, T.; Nakashima, N. *J. Am. Chem. Soc.* **2011**, 133, 14771–14777.

(88) Fong, D.; Bodnaryk, W. J.; Rice, N. A.; Saem, S.; Moran-Mirabal, J. M.; Adronov, A. *Chem. - A Eur. J.* **2016**, 22, 14560–14566.

(89) Chadwick, R. C.; Van Gyzen, S.; Liogier, S.; Adronov, A. *Synth.* **2014**, 46, 669–677.

(90) Vogel, A.; Cook, J. W. *Nature* 1948, 161, 995–995.

(91) L'abbé, G. *Chem. Rev.* **1969**, 69, 345–363.

(92) Seltzer, S. *J. Am. Chem. Soc.* **1963**, 85, 14–18.

(93) Dyke, C. A.; Tour, J. M. *J. Am. Chem. Soc.* **2003**, 125, 1156–1157.

(94) Li, H.; Cheng, F.; Duft, A. M.; Adronov, A. *J. Am. Chem. Soc.* **2005**, 127, 14518–14524.

(95) van der Pauw, L. J. Philips Tech. Rev. **1958**, 20, 220–224.

(96) Xia, C.; Advincula, R. C. *Macromolecules* **2001**, 34, 5854–5859.

(97) D. Fong; A. Adronov, *Macromolecules*, **2017**, 50, 8002–8009.

Chapter 6

Reactive, Aqueous-Dispersible Polyfluorene-Wrapped Carbon Nanotubes Modulated with an Acidochromic Switch via Azide-Alkyne Cycloaddition

This chapter has been reprinted with permission from ACS Applied Polymer Materials. Fong, D.; Yeung, J.; Meichsner, E.; Adronov, A. **2019**, *1*, 797-803. Copyright (2019) American Chemical Society.

D. Fong planned the study, as well as performed the contact angle, Raman, and PL mapping experiments. J. Yeung synthesized the materials, prepared the nanocomposites, and performed the IR and UV/Vis-NIR experiments. Dr. E. Meichsner synthesized the borylated monomer and the D-mannose-alkyne.

Abstract

Decorating hydrophobic carbon nanotube surfaces efficiently in aqueous solution without adversely affecting nanotube optoelectronic properties remains a challenge. In this work, we design a water-soluble polyfluorene derivative that contains azide groups and polyethylene glycol grafts in the side chains. This polyfluorene derivative is used to coat carbon nanotube surfaces, producing a latently-reactive and aqueous-dispersible polymer-nanotube complex. Reaction progress of the aqueous polymer-nanotube dispersion with various polar and non-polar alkyne derivatives is followed using infrared spectroscopy. Decoration of the polymer-nanotube complex with various small molecules or polymers is found to modulate the surface properties of the resulting nanohybrid thin films. Additionally, we develop a vanillin-derived indolinooxazolidine switch that is functionalized with a terminal alkyne and append it to the polymer-nanotube complex. This switch possesses two long-lived states that are interchangeable *via* exposure to acidic or basic conditions. We study the fluorescence emission response of the polymer-nanotube complex using UV/Vis-NIR and fluorescence spectroscopy. The acidochromic switch linked to the polymer-nanotube complex enables control over nanotube emission, while the free switch in solution does not. Photoluminescence mapping reveals a nanotube species-dependent fluorescence quenching response to charge buildup at the nanotube surface.

6.1 Introduction

Our research group has been probing a simple tactic to concurrently decorate single-walled carbon nanotubes (SWNTs) and avoid damage to nanotube properties.[1–5] Substantial efforts have been made to utilize the exceptional optoelectronic,[6–8] structural,[9–11] and mechanical[12–14] properties of SWNTs. However, as-produced SWNT samples are typically insoluble in organic and aqueous solvents due to SWNT bundling.[15] To surpass this issue, covalent or noncovalent functionalization is used.[16–18] Covalent functionalization damages SWNT properties by destroying the sp^2-hybridized SWNT surface,[18] while noncovalent functionalization uses sonication in the presence of a dispersant to form dispersant-SWNT supramolecular complexes, which prevents bundle re-aggregation.[19–21] To this end, surfactants,[22–24] small molecule aromatic compounds,[25–27] biomacromolecules,[28–34] and conjugated polymers[35–39] have been employed. Since conjugated polymers are synthetically facile to modify, significant attention has been garnered in this research area. There has been specific focus on sorting semiconducting SWNTs (sc-SWNTs),[40–42] with efforts made on developing polymers possessing stimulus-triggered depolymerization or conformational changes.[43–47]

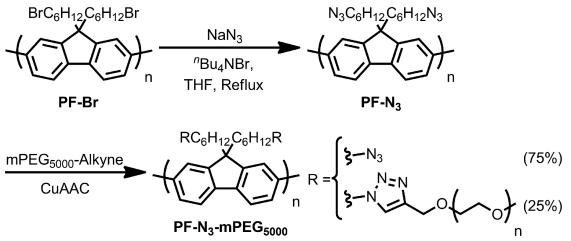
To complement these developments, we have prepared latently-reactive polymer-SWNT complexes with azides in the polymer side chains, which enable SWNT surface decoration using Copper-Catalyzed[1] or Strain-Promoted[2,3] Azide-Alkyne Cycloaddition (CuAAC or SPAAC, respectively). In this work, we sought to expand on the reaction scope for latently-reactive polymer-SWNT complexes. Typically, both conjugated polymers and SWNTs are highly hydrophobic materials. Unless the coupling is performed on a polymer-SWNT thin film,[3] this methodology

is currently limited to coupling partners that are soluble in the non-polar organic solvents. However, SWNT conjugates with polar molecules could unveil interesting biomedical applications in areas such as bioelectronics,[48] drug delivery,[49] or biological imaging.[50] Here, we prepare a water-soluble, latently-reactive polymer-SWNT complex by partially grafting PEG side chains onto the polymer scaffold. The remaining azide groups enable decoration of the resulting polymer-SWNT complex in aqueous solution, which has until now been untenable due to the hydrophobic nature of both the conjugated polymer coating and SWNT surface. We expand the scope of coupling partners to include polar organic molecules such as D-mannose and charged molecules like zwitterionic sulfobetaines. Lastly, we develop a vanillin-derived indolinooxazolidine (IDX) switch that can reversibly interchange between long-lived neutral and charged states. We attach this switch to the polymer-SWNT complex and demonstrate that SWNT emission properties can be influenced by this acidochromic switch. We show that the extent of fluorescence emission quenching is SWNT species-dependent, and that linkage of the switch to the polymer-SWNT complex is necessary for this effect to occur.

6.2 Results and Discussion

To begin our study, we first prepared an azide-containing polyfluorene homopolymer (**PF-N$_3$**). The monomer 2,7-dibromo-9,9-bis(6-bromohexyl)fluorene was prepared according to literature procedures.[2] Borylation of this monomer using Miyaura conditions afforded the diboronic ester coupling partner (Supporting Info, Scheme S6.3). These monomers were polymerized using Suzuki cross-coupling to afford the homopolymer **PF-Br**. Gel permeation chromatography (GPC) analysis on the

PF-Br homopolymer sample revealed an M_n of 16.2 kDa (degree of polymerization of ∼33) and a dispersity (Đ) of 2.33. As shown in Scheme 6.1, the reaction between **PF-Br** and $^{n}Bu_4N(N_3)$ (generated *in situ*) was performed to quantitatively convert **PF-Br** to the homopolymer **PF-N$_3$** (see Supporting Info for details). The polymer samples were characterized by ^{1}H NMR to confirm the presence of alkyl azides (3.15 ppm) in **PF-N$_3$** and the disappearance of alkyl bromides from **PF-Br** (3.31 ppm; see Figure S6.6 in the Supporting Info). IR spectroscopy indicated the presence of alkyl azides (∼2090 cm^{-1}) in **PF-N$_3$** (Supporting Info, Figure S6.7). We next prepared a water-solubilizing side chain, mPEG$_{5000}$-alkyne, by alkylating commercially available mPEG$_{5000}$-OH using NaH and propargyl bromide (see Supporting Info for details). To prepare a water-soluble conjugated polymer with reactive azide moieties, we functionalized **PF-N$_3$** with a substoichiometric amount of mPEG$_{5000}$-alkyne using biphasic CuAAC (0.25 eq of mPEG$_{5000}$-alkyne with respect to azide, resulting in ∼75% azide and ∼25% water-solubilizing mPEG$_{5000}$). The resulting water-soluble conjugated polymer, **PF-N$_3$-mPEG$_{5000}$**, was characterized using ^{1}H NMR spectroscopy. As shown in Figure 6.1, successful coupling was observed from the disappearance of the terminal alkyne proton of mPEG$_{5000}$-alkyne at 2.44 ppm and the appearance of two peaks centred at 4.20 and 4.63 ppm, which corresponds to the methylene groups adjacent to the triazole ring. As well, a new aromatic resonance at 7.47 ppm corresponds to the aromatic proton in the triazole ring. The preservation of residual azide was confirmed by the presence of the resonance at 3.15 ppm, as well as by the azide stretch observed at ∼2090 cm^{-1} in the IR spectrum (Supporting Info, Figure S6.7).



SCHEME 6.1: Synthesis of fluorene-azide-PEG random graft polymer **PF-N$_3$-mPEG$_{5000}$**.

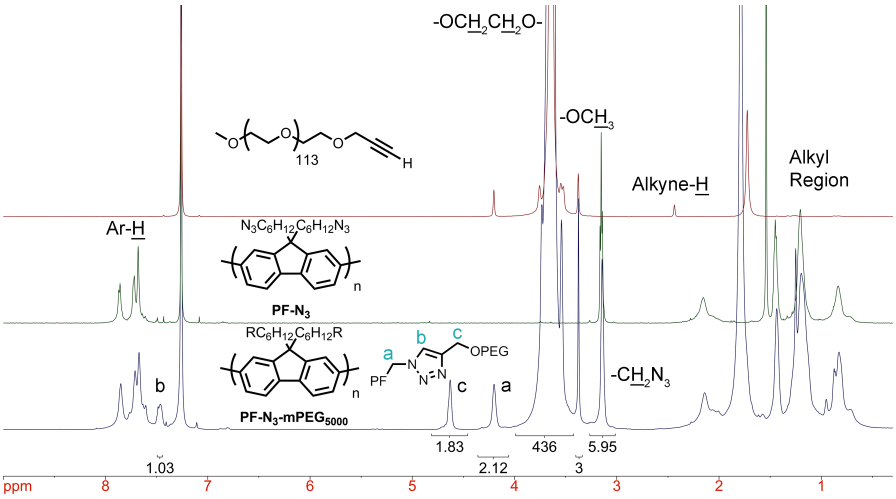


FIGURE 6.1: ^{1}H NMR overlay of mPEG$_{5000}$-alkyne (red), **PF-N$_3$** homopolymer (green), and **PF-N$_3$-mPEG$_{5000}$** (blue) in $CDCl_3$.

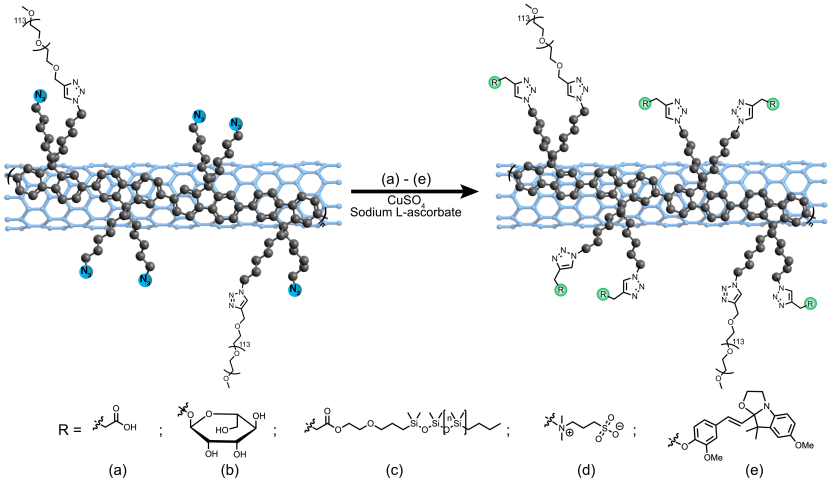
We next prepared **PF-N$_3$-mPEG$_{5000}$**-SWNT complexes with HiPCO SWNTs following modified literature procedures.[51] **PF-N$_3$-mPEG$_{5000}$** (10 mg) and SWNTs (5 mg) in THF (10 mL) were ultrasonicated (∼15 W) at −20 °C (brine/ice bath) for 2 min. The sample was centrifuged for 30 min (8,346 *g*) and the supernatant was isolated to obtain the **PF-N$_3$-mPEG$_{5000}$**-SWNT dispersion. The initial dispersion was prepared in THF as the sonication and centrifugation conditions are milder in less viscous and dense solvents, respectively. To transfer the **PF-N$_3$-mPEG$_{5000}$**-SWNT dispersion from THF to D_2O, 1 volume of the THF dispersion was aliquoted and 2 volumes of D_2O were added. The THF was then removed *in*

vacuo to obtain the aqueous **PF-N$_3$-mPEG$_{5000}$**-SWNT dispersion. D_2O was chosen instead of H_2O as it is transparent in the IR region of the absorption spectrum, enabling SWNT analysis across the full UV/Vis-NIR spectrum. Characterization of the **PF-N$_3$-mPEG$_{5000}$**-SWNT dispersions in THF and D_2O by UV/Vis-NIR spectroscopy indicated well-exfoliated dispersions, as evidenced by the sharp spectral features (Supporting Info, Figure S6.8). The dispersions were stable on the benchtop for at least several months. **PF-N$_3$-mPEG$_{5000}$**-SWNT dispersion reactivity was initially screened using 4-pentynoic acid (Scheme 6.2a). A 200 μL aliquot of the aqueous **PF-N$_3$-mPEG$_{5000}$**-SWNT dispersion was aliquoted to a glass vial, and then D_2O solutions of 4-pentynoic acid (1.1 eq), $CuSO_4{\cdot}5H_2O$ (1 mM), and (+)-sodium L-ascorbate (10 mM) were added for a final reaction volume of 220 μL (see Supporting Information for details). Cu(II) was reduced *in situ* to generate the catalytically active Cu(I) species. Reaction progression under ambient conditions was followed by azide stretch ($\sim$2090 cm^{-1}) disappearance *via* IR spectroscopy. Samples for IR were prepared by filtering an aliquot through a Teflon membrane and washing the sample with dH_2O and THF. As shown in Figure 6.2, the azide stretch ($\sim$2090 cm^{-1}) disappeared upon reaction with 4-pentynoic acid, which occurred within 30 min. Interestingly, the coupling rate was much faster in aqueous solution in comparison to the reaction in organic solvent.[1] We speculate that the generation of catalytically active Cu(I) *in situ* enabled for a stable concentration of active catalyst, allowing for facile conversion at RT. To determine if each reaction component was necessary for a successful reaction, we performed a control experiment where the aforementioned procedure was used, except one component ($CuSO_4$, (+)-sodium L-ascorbate, or 4-pentynoic acid) was replaced with the same volume of D_2O (see Supporting Info for details). The absence of

any of these components results in no disappearance of the azide stretch in the IR spectrum, even after stirring for 16 h at RT (Figure S6.9). Thus, each component is necessary for the [2 + 3] Azide-Alkyne cycloaddition to occur.

With the reaction conditions identified, we turned our attention to investigating the scope of coupling partners (Scheme 6.2b-d). We prepared alkyne-containing derivatives of D-mannose, polydimethylsiloxane (PDMS), and zwitterionic sulfobetaine. α-D-mannose-alkyne was prepared from commercially available D-Mannose pentaacetate *via* Lewis acid-mediated substitution at the anomeric carbon with propargyl alcohol followed by acetate deprotection, as per literature procedures.[52] To prepare $PDMS_{5000}$-alkyne, $PDMS_{5000}$-OH was coupled to 4-pentynoic acid *via* Steglich esterification. Lastly, sulfobetaine-alkyne was prepared by alkylation of commercially available 3-dimethylamino-1-propyne with 1,3-propanesultone. The **PF-N_3-mPEG$_{5000}$**-SWNT complex was reacted with each of these alkyne derivatives and successful coupling was afforded in all cases within 30 min at RT (Figure 6.2). We found that all the "clicked" polymer-SWNT dispersions were stable on the benchtop for at least several months. To characterize the properties of these polymer-SWNT nanohybrids, contact angle measurements were performed on the nanohybrid thin films (see Supporting Info for details). The contact angle for the pristine **PF-N_3-mPEG$_{5000}$**-SWNT thin film was found to be 74 ± 3°, which is consistent with a polymer-SWNT thin film that contains pendant $mPEG_{5000}$ chains (Supporting Info, Figure S6.10).[3] Functionalization with $PDMS_{5000}$-alkyne resulted in a contact angle of 80 ± 5°, which is consistent with the increased hydrophobicity of the PDMS polymer chains. When the polymer-SWNT complex was decorated with polar D-mannose and zwitterionic sulfobetaine, contact angles of 50 ± 1° and 40 ± 4° were measured, respectively. These values are consistent

with the increase in hydrophilicity upon functionalization with polar organic and charged molecules. Overall, these results further support the successful decoration of the water-dispersible polymer-SWNT complex.



SCHEME 6.2: Functionalization of **PF-N$_3$**-mPEG$_{5000}$-SWNT complexes using CuAAC to couple (a) 4-pentynoic acid, (b) D-mannose-alkyne, (c) PDMS$_{5000}$-alkyne, (d) sulfobetaine-alkyne, and (e) IDX-alkyne.

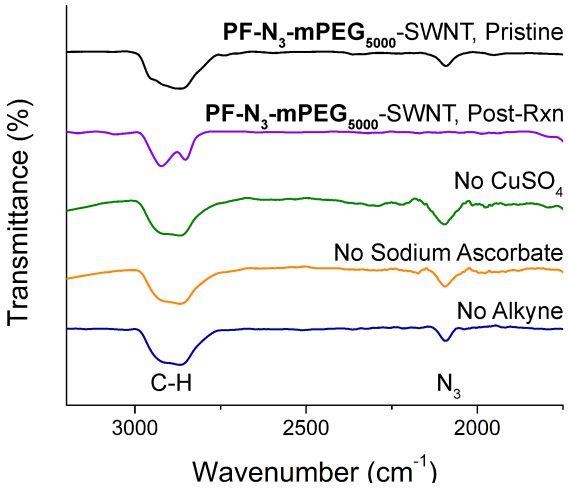


FIGURE 6.2: Functionalization of the **PF-N$_3$**-mPEG$_{5000}$-SWNT complex (black) using CuAAC to couple 4-pentynoic acid (red), D-mannose-alkyne (green), PDMS$_{5000}$-alkyne (blue), and sulfobetaine-alkyne (purple).

To investigate the state of the SWNT sidewall upon functionalization, resonance Raman spectroscopy was performed. Thin films (pre- and post-CuAAC with 4-pentynoic acid) were prepared according to literature procedures.[53] As shown in Figure S6.11, the relative intensity of the disorder (D) band (centered at ~1290 cm^{-1})[54,55] remained unchanged relative to the G band after decoration of the SWNT surface, which indicates preservation of the SWNT sidewall upon functionalization. These results are consistent with other literature reports.[1–3]

Given the preservation of the **PF-N$_3$-mPEG$_{5000}$**-SWNT sidewall and ease of functionalization, we next sought to influence SWNT fluorescence emission by incorporating an acidochromic molecule capable of reversibly forming and removing charge. We proceeded to design an IDX scaffold that contains a terminal alkyne (chemical structure provided in Figure 6.3). These structures are capable of interchangeably switching between long-lived neutral (ring-closed) and charged (ring-opened) states and would thus be able to modulate the charge density along the SWNT sidewall. Electron-donating groups were incorporated into the indole and styrenic rings to red-shift the λ_{max} in the conjugated, charged form beyond 400 nm,[56] which is where the polymer-SWNT complex absorbs. A λ_{max} outside of this range would enable simple monitoring of the switch state by UV-Vis spectroscopy. As shown in Scheme S6.4, commercially available 4-methoxyphenylhydrazine hydrochloride was heated to reflux with 3-methyl-2-butanone in EtOH to prepare a methoxyindole derivative *via* Fischer indole synthesis,[57] followed by *N*-alkylation with 2-bromoethanol. Treatment of this intermediate with KOH followed by extraction with Et_2O afforded an indole derivative with a spirocentre.[58] Separately, vanillin was alkylated with propargyl bromide,[59] which gives the final acidochromic

molecule a reactive handle that enables attachment to the polymer-SWNT complex. Using silica to provide a hydrogen-bonding microenvironment,[58] we dry-loaded the spirocentre-containing indole and alkyne-containing vanillin derivative onto silica from a slurry with CH_2Cl_2 and heated the resulting powder to 100 °C for 15 min to afford the IDX switch (see Supporting Info for details). All attempts to synthesize IDX using solution-based methods failed to produce the desired product. As shown in Figure 6.3a, UV/Vis-NIR spectroscopy was used to interrogate the acidochromic properties of IDX upon the addition of 0 - 1.6 eq of *p*-toluenesulfonic acid (*p*-TSA). Upon titration of IDX with *p*-TSA, the peak at ~300 nm decreased, alongside the concomitant increase in peak intensity at ~450 nm. Gratifyingly, the λ_{max} of IDX was ~450 nm, which is distinguishable from the conjugated polymer absorption. IDX was not found to be emissive (λ_{em} = 800 - 1100 nm) using λ_{ex} = 250 - 750 nm.

We next proceeded to couple IDX to the **PF-N$_3$-mPEG$_{5000}$**-SWNT complex using the aforementioned procedure (see Supporting Info for details) and observed complete conversion by IR within 30 min (Supporting Info, Figure S6.12). With the **PF-PEG$_{5000}$-IDX**-SWNT conjugate in hand, we filtered the aqueous dispersion through a Teflon membrane and washed the sample with dH_2O and THF to remove any unreacted starting material. The resulting thin film was then reconstituted in THF by sonicating for 1 h in an ice-chilled bath sonicator. The **PF-PEG$_{5000}$-IDX**-SWNT conjugate in THF was filtered through a cotton plug and used for the subsequent spectroscopic studies. As shown in Figure 6.3b, UV/Vis-NIR spectra were obtained for the **PF-PEG$_{5000}$-IDX**-SWNT dispersion (i) without additives (pristine), (ii) upon the addition of 1.5 eq of *p*-TSA, and (iii) upon the further addition of 2.0 eq of Et_3N. Intriguingly, the state of IDX

can be easily monitored by the appearance of a new peak centred at ~450 nm, and the ring-opening and ring-closing is controllable by the addition of acid/base, respectively. We found that the polymer-SWNT dispersions were stable upon the addition of acid/base, with no observable flocculation for at least the duration of the subsequent experiments.

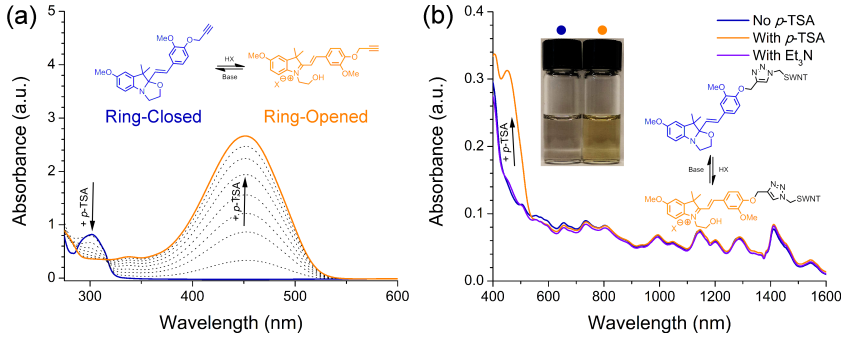


FIGURE 6.3: UV/Vis-NIR spectra in THF of (a) IDX (100 μM) titrated with 0 – 1.6 eq of *p*-TSA (in 0.2 eq increments); and (b) the pristine **PF-PEG$_{5000}$-IDX**-SWNT dispersion (blue trace) followed by the addition of 1.5 eq of *p*-TSA (orange trace) and then the addition of 2.0 eq of Et_3N (purple trace). Polymer-SWNT dispersion photographs are colour-coded accordingly.

We next sought to investigate the emission properties of the **PF-PEG$_{5000}$-IDX**-SWNT conjugate using photoluminescence (PL) mapping. Semiconducting SWNT species were assigned according to literature data.[60] As shown in Figure 6.4a, the most intense PL signal was from the (7,6) species for the pristine **PF-PEG$_{5000}$-IDX**-SWNT conjugate. Upon addition of 1.5 eq of *p*-TSA, fluorescence quenching was observed (Figure 6.4b). Quantification of the fluorescence intensities for a range of SWNT species when the switch is in the neutral (no additive) and charged state (with *p*-TSA) is tabulated in Table S6.1 and shown graphically in Figure 6.5. Interestingly, fluorescence quenching amongst SWNT species is non-uniform, ranging from 10 – 32%. To rule out other possible sources of fluorescence quenching, we performed a control experiment where we obtained a PL map of

the pristine **PF-N$_3$-mPEG$_{5000}$**-SWNT complex, prepared identically to the **PF-PEG$_{5000}$-IDX**-SWNT conjugate, except IDX was omitted from the procedure. As shown in Figure S6.13, the UV/Vis-NIR spectrum of the **PF-N$_3$-mPEG$_{5000}$**-SWNT complex does not change upon addition of *p*-TSA. PL mapping of this dispersion before and after addition of *p*-TSA resulted in minimal changes to fluorescence intensity, indicating that the addition of *p*-TSA alone was not responsible for the change in fluorescence intensities observed (Supporting Info, Figure S6.14 and Table S6.2). We next investigated the reversibility of this system by adding Et_3N to the **PF-PEG$_{5000}$-IDX**-SWNT conjugate post-addition of *p*-TSA. Interestingly, we observed SWNT species-dependent reversibility in fluorescence restoration (Supporting Info, Figures S6.15 and S6.16). Some species, such as (7,5) and (8,4), had minimal fluorescence intensity change upon the addition of base, while some species, such as the (8,6) and (8,7), had almost complete restoration of fluorescence intensity when compared to pre-*p*-TSA addition. The species-dependent fluorescence restoration response is consistent with literature reports.[61] These results may suggest that the isolation of a particular sc-SWNT species [i.e., (8,6) or (8,7)] would be of interest for reversible fluorescence-based SWNT sensors that utilize a charge-sensing mechanism. We next examined whether the linkage between the **PF-N$_3$-mPEG$_{5000}$**-SWNT complex and IDX was necessary to influence the emission properties of the polymer-SWNT complex. To the control sample of **PF-N$_3$-mPEG$_{5000}$**-SWNT complex with *p*-TSA, we added IDX. As shown in Figure S6.13, the addition of IDX to the dispersion results in a new peak centred at ~450 nm, which is consistent with the formation of the ring-opened form of IDX; although there is no linkage between IDX and the polymer-SWNT complex in this sample. PL mapping of this sample indicated no substantial change in the

fluorescence intensities observed (Supporting Info, Figure S6.14). Interestingly, extraneous fluorescence was observed in the bottom-left quadrant of the PL map, despite IDX not being emissive in this region. These data together indicate that attachment of IDX to the polymer-SWNT complex is necessary to modulate the SWNT emission properties.

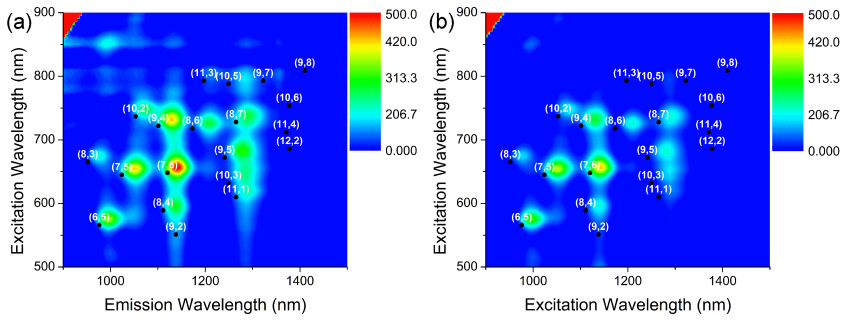


FIGURE 6.4: Photoluminescence maps of the **PF-PEG$_{5000}$-IDX**-SWNT dispersion in THF with (a) no *p*-TSA and (b) 1.5 eq of *p*-TSA. Maps are plotted on the same intensity scale.

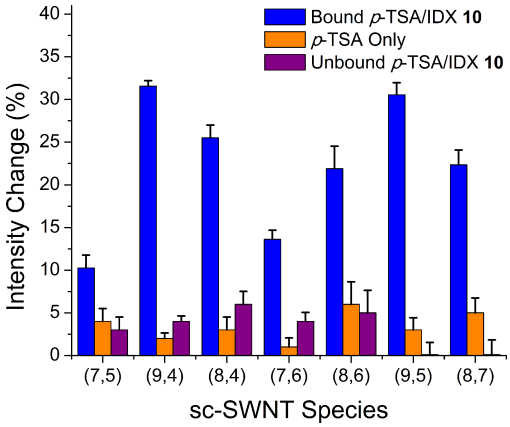


FIGURE 6.5: Graphical representation of non-uniform fluorescence intensity changes for different sc-SWNTs. The experimental condition that includes "clicked" IDX with 1.5 eq *p*-TSA (blue) is compared to the control experiments where only 1.5 eq *p*-TSA is added (orange) and where 1.5 eq *p*-TSA and unbound IDX are added to the polymer-SWNT dispersion (purple). Intensity changes for the control experimental conditions are shown as the absolute value of change. Error bars represent the standard deviation for triplicate measurements (n = 3).

6.3 Conclusions

A water-dispersible polymer-SWNT complex was prepared by partially grafting $mPEG_{5000}$ side chains onto a polyfluorene scaffold using CuAAC, and the presence of $mPEG_{5000}$ and residual azide groups was confirmed by ^1H NMR. Quantitative coupling of polar, zwitterionic, and non-polar molecules to an aqueous-soluble polymer-SWNT complex is achieved using low concentrations of Cu(I) (1 mM) generated *in situ* in D_2O within 30 min under ambient conditions. Successful coupling can be monitored by azide stretch ($\sim$2090 cm^{-1}) disappearance in the polymer-SWNT complex, and control experiments indicate that Cu(II), sodium ascorbate, and alkyne are all necessary for this disappearance to be observed. Coupling of various hydrophobic and hydrophilic small molecules and polymers resulted in changes to the thin film properties of the SWNT nanohybrids, as determined by contact angle measurements. To demonstrate the utility of this efficient coupling chemistry, an acidochromic indolinooxazolidine switch possessing a terminal alkyne was prepared. This vanillin-derived switch enabled the reversible formation of a cationic charge along the polymer-SWNT structure. It was found that the presence of a cationic charge anchored near the SWNT structure results in non-uniform, structure-dependent SWNT fluorescence quenching (10 – 32%), and that linkage of the indolinooxazolidine switch to the polymer-SWNT complex is necessary for this effect to occur. These constructs demonstrate the importance of localizing charge near the polymer-SWNT surface and these results indicate that the enrichment of specific SWNT species may be desirable in the context of a sensing device that detects charged analytes.

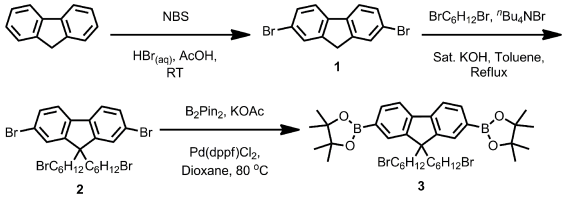
6.4 Supporting Information

6.4.1 General

Raw HiPCO SWNTs were purchased from NanoIntegris (batch #HR27-104, 10 wt % in anhydrous EtOH) and used without further purification. Reagents were purchased from commercial suppliers and used as received. Monomethyl ether PEG_{5000} was purchased from Fluka. Mono-carbinol $PDMS_{5000}$-OH was purchased from Gelest (MRC-C18-100G). Flash chromatography was performed using an IntelliFlash 280 system from Analogix. Unless otherwise noted, compounds were monitored using a variable wavelength detector at 254 nm. Solvent amounts used for gradient or isocratic elution were reported in column volumes (CV). Columns were prepared in Biotage® SNAP KP-Sil cartridges using 40 – 63 μm silica or 25 – 40 μm silica purchased from Silicycle. NMR was performed on a Bruker Avance 600 MHz or 700 MHz instrument and shift-referenced to the residual solvent resonance. High-resolution (HR) electrospray ionization (ESI) MS measurements were carried out on the Micromass/Waters Quattro Ultima (ESI/APCI-LCMS Triple Quadrupole Mass Spectrometer). Polymer molecular weights and dispersities were analyzed (relative to polystyrene standards) *via* GPC using a Waters 2695 Separations Module equipped with a Waters 2414 refractive index detector and a Jordi Fluorinated DVB mixed bed column in series with a Jordi Fluorinated DVB 10^5 Å pore size column. THF with 2% acetonitrile was used as the eluent at a flow rate of 2.0 mL/min. Sonication was performed using a QSonica Q700 ultrasonicator. Centrifugation of the polymer-SWNT samples a Beckman Coulter Allegra X-22 centrifuge. Infrared spectra were recorded using a Thermo Scientific Nicolet 6700 FT-IR spectrometer equipped with a Smart iTX attenuated total reflectance

(ATR) sample analyzer. UV/Vis-NIR spectra were recorded on a Cary 5000 spectrometer in dual beam mode, using matching 10 mm quartz cuvettes. Contact angle measurements were obtained using an Optical Contact Angle (OCA 25) instrument from DataPhysics Instruments (Filderstadt, Germany). Raman spectra were collected using a Renishaw InVia Laser Raman spectrometer, with a 500 mW HeNe Renishaw laser (633 nm, 1800 L/mm grating). Laser intensity was set to 1% for the 633 nm excitation wavelength for the polymer-SWNT samples. Fluorescence spectra were measured on a Jobin-Yvon SPEX Fluorolog 3.22 equipped with a 450 W Xe arc lamp, digital photon counting photomultiplier, and an InGaAs detector, also using a 10 mm quartz cuvette. Slit widths for both excitation and emission were set to 10 nm band-pass, and correction factor files were applied to account for instrument variations. Photoluminescence maps were obtained at 25 °C, with 5 nm intervals for both the excitation and emission.

6.4.2 Synthetic Procedures



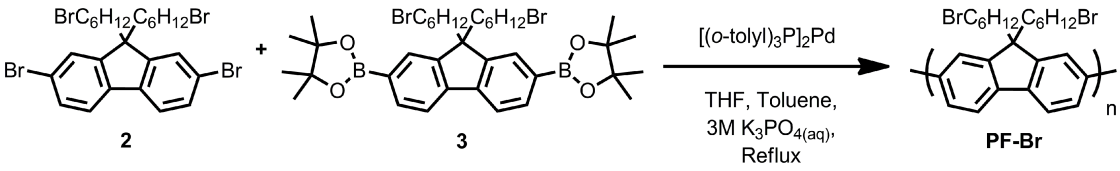
Scheme 6.3: Syntheses of monomers **2** and **3**.

Compounds **1** and **2** were prepared according to literature procedures.[2]

2,2'-(9,9-bis(6-bromohexyl)fluorene-2,7-diyl)bis(4,4,5,5-tetramethyl-1,3,2-dioxaborolane) (3) (adapted from Ref 62)

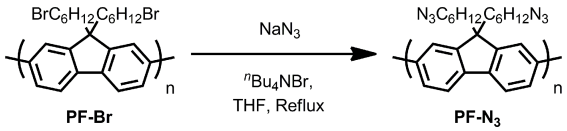
A round bottom flask equipped with a magnetic stir bar was charged with **2** (2.8 g, 4.3 mmol), B_2Pin_2 (2.73 g, 10.8 mmol), KOAc (1.27 g, 12.9 mmol), and dioxane

(42 mL). $Pd(dppf)_2Cl_2$ (95 mg, 129 μmol) was added and the reaction mixture was stirred at 80 °C for 48 h. The reaction mixture was partitioned with water and extracted thrice with CH_2Cl_2. The organic extracts were combined and purified by flash chromatography (100 g column, 30 to 40% CH_2Cl_2 in hexanes over 10 CV, then 40 to 100% CH_2Cl_2 in hexanes over 10 CV) to afford **3** as a colourless solid (1.53 g, 47%). ^{1}H NMR (600 MHz; $CDCl_3$): δ 7.81 (dd, J = 7.5, 1.0 Hz, 2H), 7.73 (m, 4H), 3.25 (t, J = 6.9 Hz, 4H), 2.02-1.99 (m, 4H), 1.64-1.59 (m, 4H), 1.39 (s, 24H), 1.17-1.12 (m, 4H), 1.06-1.01 (m, 4H), 0.57-0.53 (m, 4H).



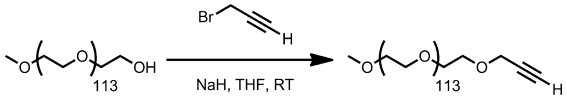
Poly(bis(6-bromohexyl)fluorene) (PF-Br) (Adapted from Ref 1)

A Schlenk tube equipped with a magnetic stir bar was charged with **2** (1.21 g, 1.86 mmol), **3** (1.39 g, 1.86 mmol), THF (6.7 mL), toluene (6.7 mL), and 3M $K_3PO_{4(aq)}$ (13.3 mL). The biphasic mixture was degassed by three freeze-pump-thaw cycles, then, while frozen under liquid nitrogen, $[(o\text{-tol})_3P]_2Pd$ (20 mg, 28.2 μmol) was added under a positive pressure of nitrogen. The Schlenk tube was evacuated and backfilled with nitrogen four times, and the reaction mixture was vigorously stirred at 80 °C for 2 h. The phases were allowed to separate, and the organic layer was isolated and filtered through a single plug of celite and neutral alumina. The plug was thoroughly washed with THF and the filtrate was concentrated *in vacuo*. The crude polymer was precipitated into MeOH (~200 mL) and then filtered to afford **PF-Br** as a yellow solid (1.83 g, quant.). ^{1}H NMR (700 MHz; $CDCl_3$): δ 7.89 (m, 2H), 7.77-7.69 (m, 4H), 3.33 (m, 4H), 2.21-2.15 (m, 4H), 1.73-1.71 (m, 4H), 1.32-1.26 (m, 4H), 1.24-1.18 (m, 4H), 0.88-0.84 (m, 4H).

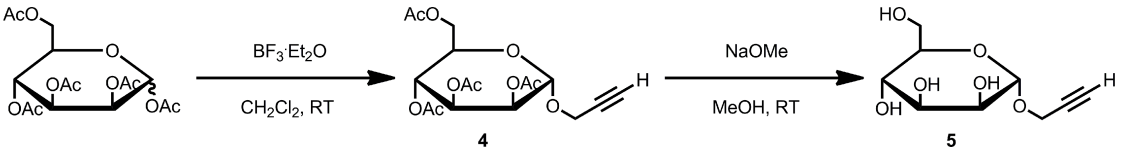


Poly(bis(6-azidohexyl)fluorene) (PF-N_3) (Adapted from Ref 1)

A round bottom flask equipped with a magnetic stir bar and reflux condenser was charged with **PF-Br** (1.50 g, 3.1 mmol), NaN_3 (1.99 g, 30.6 mmol), $^{n}Bu_4NBr$ (1.97 g, 6.1 mmol), and THF (225 mL) and the reaction mixture was heated to reflux for 24 h. The reaction mixture was filtered through an alumina plug and precipitated into MeOH (∼200 mL) to afford **PF-N_3** as a yellow solid (1.08 g, 85%). ^{1}H NMR (700 MHz; $CDCl_3$): δ 7.88-7.85 (m, 2H), 7.73-7.66 (m, 4H), 3.16-3.14 (m, 4H), 2.28-2.11 (m, 4H), 1.46-1.43 (m, 4H), 1.23-1.17 (m, 8H), 0.90-0.78 (m, 4H).

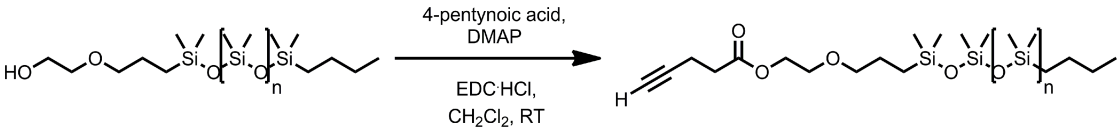


mPEG$_{5000}$-alkyne. A round bottom flask equipped with a magnetic stir bar was charged with mPEG$_{5000}$-OH (5 g, 1.0 mmol), NaH (60 mg, 2.5 mmol), and THF (100 mL). Mild sonication was used to fully dissolve the mPEG$_{5000}$-OH. To the solution propargyl bromide (155 mg, 1.3 mmol) was added, and the reaction mixture was stirred for 24 h at RT. The reaction mixture was precipitated into 1:1 Et_2O:hexanes (∼100 mL), filtered, then washed with Et_2O, ice cold 1% HCl in EtOH, and Et_2O, followed by drying *in vacuo* to afford mPEG$_{5000}$-alkyne as a fine colourless powder (4.62 g, 92%). ^{1}H NMR (700 MHz; $CDCl_3$): δ 4.20 (m, 2H), 3.76-3.51 (m, 463H), 3.38 (s, 3H), 2.44 (m, 1H). ^{13}C NMR (176 MHz; $CDCl_3$): δ 70.7, 59.2, 58.6.

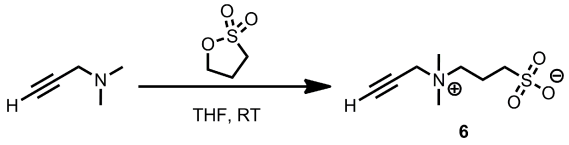


D-mannose-pentaacetate-alkyne (4) (Adapted from Ref 52). A round bottom flask equipped with a magnetic stir bar was charged with D-mannose pentaacetate (1.0 g, 2.56 mmol) and CH_2Cl_2 (25 mL). Under a nitrogen atmosphere, the reaction mixture was cooled to 0 °C and then propargyl alcohol (575 mg, 10.2 mmol) and $BF_3 \cdot Et_2O$ (12.8 mmol) were added dropwise. The reaction mixture was allowed to warm to RT and was stirred for 48 h. The reaction mixture was quenched with sat. $NaHCO_{3(aq)}$ (100 mL) and water (100 mL), then the aqueous phase was extracted thrice with CH_2Cl_2 (3 x 100 mL). The combined organic extracts were concentrated *in vacuo* and purified by silica chromatography (30 to 50% EtOAc in hexanes) to afford **4** as a colourless solid (904 mg, 91%). ^{1}H NMR (600 MHz; $CDCl_3$): δ 5.34 (m, 2H), 5.28 (dt, J = 3.7, 2.0 Hz, 1H), 5.04 (d, J = 1.7 Hz, 1H), 4.31-4.28 (m, 3H), 4.12 (dd, J = 12.3, 2.4 Hz, 1H), 4.04-4.01 (m, 1H), 2.47 (t, J = 2.4 Hz, 1H), 2.17 (s, 3H), 2.11 (s, 3H), 2.04 (s, 3H), 1.99 (s, 3H).

D-mannose-alkyne (5) (Adapted from Ref 52). A round bottom flask equipped with a magnetic stir bar was charged with **4** (200 mg, 0.52 mmol) and anhydrous MeOH (2 mL). Under a nitrogen atmosphere, sodium methanolate (114 mg, 2.12 mmol) was added and the reaction mixture was stirred at RT for 30 min. The reaction mixture was filtered through a plug of Amberlite IRC-50, and the resin was washed with 50/50 MeOH:H_2O (∼50 mL). The filtrate was concentrated *in vacuo* to afford **5** as a colourless solid (113 mg, quant.). ^{1}H NMR (600 MHz; D_2O): δ 5.04 (d, J = 1.7 Hz, 1H), 4.34 (m, 2H), 3.96 (dd, J = 3.5, 1.7 Hz, 1H), 3.91-3.88 (m, 1H), 3.81-3.76 (m, 2H), 3.69-3.67 (m, 2H), 2.92 (t, J = 2.4 Hz, 1H).

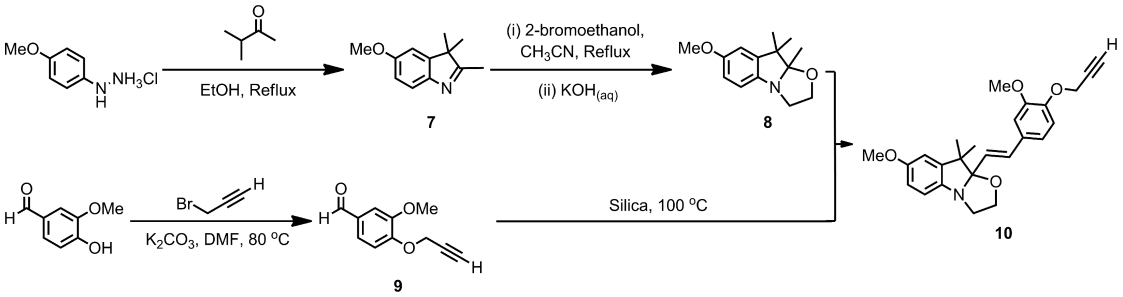


$PDMS_{5000}$-alkyne. A round bottom flask equipped with a magnetic stir bar was charged with mono-carbinol terminated $PDMS_{5000}$-OH (1 g, 0.2 mmol), 4-pentynoic acid (39 mg, 0.4 mmol), DMAP (12 mg, 0.1 mmol), and CH_2Cl_2 (3 mL). To the reaction mixture EDC·HCl (83 mg, 0.2 mmol) was added and the reaction mixture was stirred at RT for 12 h. The reaction mixture was filtered through a silica plug and eluted with 3:5 CH_2Cl_2:hexanes and then the filtrate was concentrated *in vacuo* to afford $PDMS_{5000}$-alkyne as a colourless oil (769 mg, 76%). ^{1}H NMR (700 MHz; $CDCl_3$): δ 4.25 (t, J = 5 Hz, 2H), 3.63 (t, J = 5 Hz, 2H), 3.43 (t, J = 7 Hz, 2H), 2.59 (m, 2H), 2.51 (m, 2H), 1.97 (t, J = 2.6 Hz, 1H), 1.61 (m, 2H), 1.32 (m, 4H), 0.88 (t, J = 7 Hz, 3H), 0.53 (m, 4H), 0.07 (m, 513H). ^{13}C NMR (176 MHz; $CDCl_3$): δ 171.9, 82.6, 74.3, 69.2, 68.6, 64.1, 33.5, 26.5, 25.6, 23.5, 18.1, 14.5, 14.3, 14.0, 1.2.



Sulfobetaine-alkyne 6. A round bottom flask equipped with a magnetic stir bar was charged with 3-dimethylamino-1-propyne (100 mg, 1.2 mmol), 1,3-propane sultone (147 mg, 1.2 mmol), and toluene (900 μL). The reaction mixture was stirred for 12 h at RT. The suspension was vacuum filtered through a Buchner funnel and the resulting colourless solid was washed with MeCN and dried to afford betaine **6** as a colourless solid (155 mg, 63%). ^{1}H NMR (700 MHz; D_2O): δ 4.30 (d, J = 2.5 Hz, 2H), 3.64-3.61 (m, 2H), 3.28 (t, J = 2.5 Hz, 1H), 3.22 (s, 6H), 3.01 (t, J

= 7.2 Hz, 2H), 2.29-2.24 (m, 2H). ^{13}C NMR (176 MHz; D_2O): 81.6, 70.7, 62.3, 54.3, 50.3, 47.1, 18.2. HRMS (ESI^+) (m/z) for $C_8H_{15}NO_3S$ $[M^+H]^+$ calculated: 206.0845, found: 206.0841.



SCHEME 6.4: Synthesis of IDX derivative **10**.

5-methoxy-2,3,3-trimethyl-3*H*-indole (7) (Adapted from Ref 57)

A round bottom flask equipped with a magnetic stir bar and reflux condenser was charged with 4-methoxyphenylhydrazine hydrochloride (1 g, 5.7 mmol), 3-methyl-2-butanone (986 mg, 11.5 mmol), and EtOH (11.5 mL), then heated to reflux for 12 h under a nitrogen atmosphere. The reaction mixture was partitioned between Et_2O and 10% $NaHCO_{3(aq)}$, and the organic layer was extracted. The aqueous layer was washed twice with Et_2O, and then the organic extracts were combined and concentrated *in vacuo*. The crude residue was purified by flash chromatography (25 g column, 10 to 40% EtOAC in hexanes over 15 CV) to afford **7** as a red oil (782 mg, 72%). ^{1}H NMR (600 MHz; $CDCl_3$): δ 7.43 (d, J = 8.3 Hz, 1H), 6.84-6.81 (m, 2H), 3.83 (s, 3H), 2.24 (s, 3H), 1.29 (s, 6H).

7-methoxy-9,9,9a-trimethyl-2,3,9,9a-tetrahydrooxazolo[3,2-*a*]indole (8) (Adapted from Ref 58)

A round bottom flask equipped with a magnetic stir bar and reflux condenser was charged with **7** (780 mg, 4.1 mmol), 2-bromoethanol (772 mg, 6.2 mmol), and CH_3CN (2.0 mL), then heated to reflux for 24 h under a nitrogen atmosphere. The

resulting suspension was cooled to RT, filtered, and the precipitate was washed with Et_2O. The precipitate was suspended in sat. KOH (5 mL) and dH_2O (5 mL) and then stirred vigorously for 15 min at RT. The aqueous layer was washed thrice with Et_2O, and then the organic extracts were combined and concentrated *in vacuo* to afford **8** as a red oil (693 mg, 72%). ^{1}H NMR (600 MHz; $CDCl_3$): δ 6.67 (m, 3H), 3.83 (td, J = 6.8, 2.8 Hz, 1H), 3.77 (s, 3H), 3.66 (ddd, J = 11.1, 6.5, 2.9 Hz, 1H), 3.57-3.48 (m, 2H), 1.41 (s, 3H), 1.37 (s, 3H), 1.17 (s, 3H).

3-methoxy-4-(prop-2-yn-1-yloxy)benzaldehyde (9) (Adapted from Ref 59)
A round bottom flask equipped with a magnetic stir bar was charged with vanillin (500 mg, 3.3 mmol), propargyl bromide (1.47 g, 9.9 mmol), K_2CO_3 (1.36 g, 9.9 mmol), and DMF (2.5 mL). The suspension was vigorously stirred at 80 °C for 3 h. The reaction mixture was partitioned with water and extracted thrice with Et_2O. The organic extracts were combined, dried with anhydrous $MgSO_4$, and then filtered through a cotton plug. The extracts were concentrated *in vacuo* and then purified by flash chromatography (25 g column, 10 to 30% EtOAc in hexanes over 15 CV) to afford **9** as a pale-yellow solid (615 mg, 98%). ^{1}H NMR (600 MHz; $CDCl_3$): δ 9.88 (s, 1H), 7.47 (dd, J = 8.2, 1.9 Hz, 1H), 7.44 (d, J = 1.9 Hz, 1H), 7.15 (d, J = 8.2 Hz, 1H), 4.86 (d, J = 2.4 Hz, 2H), 3.95 (s, 3H), 2.56 (t, J = 2.4 Hz, 1H).

(*E*)-7-methoxy-9a-(3-methoxy-4-(prop-2-yn-1-yloxy)styryl)-9,9-dimethyl-2,3,9,9a-tetrahydrooxazolo[3,2-*a*]indole (10)
A round bottom flask was charged with **8** (46 mg, 197 μmol), **9** (25 mg, 131 μmol), and silica (131 mg). A small amount of CH_2Cl_2 was added to produce a slurry, and then the slurry was concentrated *in vacuo* to produce a yellow-orange powder. The powder was heated in an oil bath to 100 °C for 15 min to produce a red

powder and purified by flash chromatography (10 g column, 30 to 50% EtOAc in hexanes over 15 CV) to afford **10** as a red solid (40 mg, 75%). ^{1}H NMR (700 MHz; $CDCl_3$): δ 7.02 (m, 1H), 7.01 (m, 2H), 6.81 (d, J = 15.9 Hz, 1H), 6.72 (m, 2H), 6.68 (m, 1H), 6.17 (d, J = 15.9 Hz, 1H), 4.78 (d, J = 2.4 Hz, 2H), 3.91 (s, 3H), 3.78-3.74 (m, 1H), 3.65-3.61 (m, 2H), 3.46-3.42 (m, 1H), 2.51 (t, J = 2.4 Hz, 1H), 1.43 (s, 3H), 1.17 (s, 3H). ^{13}C NMR (176 MHz; $CDCl_3$): δ 155.6, 149.9, 146.8, 144.1, 132.0, 124.6, 119.8, 114.5, 112.56, 112.46, 110.7, 109.8, 109.2, 76.0, 63.7, 56.04, 55.92, 50.7, 28.5, 20.4. HRMS (ESI^+) (m/z) for $C_{25}H_{27}NO_4$ $[M^+H]^+$ calculated: 406.2013, found: 406.2028.

CuAAC optimization with 4-pentynoic acid. A glass vial was charged with 200 μL of aqueous **PF-N_3-mPEG$_{5000}$**-SWNT dispersion, then 1.1 equivalents of 4-pentynoic acid (5 μL of a 1.1 mg·mL^{-1} solution in D_2O), $CuSO_4$ (10 μL of a 5.5 mg·mL-1 solution in D_2O), and (+)-sodium L-ascorbate (5 μL of a 87.2 mg·mL^{-1} solution in D_2O) were added for a final reaction volume of 220 μL. Equivalents were calculated by determining the polymer concentration in solution (based on the SWNT dispersion protocol), calculating the mass of polymer present, and then using the molecular weight of the repeat unit (as determined by a weighted average of possible repeat units) to determine the number of moles of azide. The reaction progress was monitored over time by IR spectroscopy. IR samples were prepared by filtering an aliquot of the dispersion through a Teflon membrane with 0.2 μm pore diameter and washing the thin film with THF to remove any unreacted material.

CuAAC control experiments. Using the aforementioned procedure, the D_2O solutions of $CuSO_4$, (+)-sodium L-ascorbate, or 4-pentynoic acid were replaced

with the same volume of D_2O. The control samples were allowed to stir at RT for 16 h prior to IR analysis.

CuAAC with alkyne derivatives. A glass vial was charged with 200 μL of aqueous **PF-N_3-mPEG$_{5000}$**-SWNT dispersion, then 1.1 equivalents of alkyne (5 μL of a 56.2 μM solution in D_2O), $CuSO_4$ (10 μL of a 5.5 mg·mL^{-1} solution in D_2O), and (+)-sodium L-ascorbate (5 μL of a 87.2 mg·mL^{-1} solution in D_2O) were added directly for a final reaction volume of 220 μL. Equivalents were calculated by determining the polymer concentration in solution (based on the SWNT dispersion protocol), calculating the mass of polymer present, and then using the molecular weight of the repeat unit (as determined by a weighted average of possible repeat units) to determine the number of moles of azide. The reaction progress was monitored over time by IR spectroscopy. IR samples were prepared by filtering an aliquot of the dispersion through a Teflon membrane with 0.2 μm pore diameter and washing the thin film with THF to remove any unreacted material.

Contact angle measurements. The contact angle measurements for polymer-SWNT thin films were performed in triplicate (n = 3). Samples were prepared by filtering the polymer-SWNT nanohybrid through a Teflon membrane (0.2 μm pore diameter) upon disappearance of the azide stretch ($\sim$2090 cm^{-1}) by IR and washing the resulting thin film with dH_2O and THF. A 2 μL droplet of Milli-Q water (18.2 MΩ·cm^{-1}) was deposited onto the thin film and then allowed to equilibrate for 3 min. For each replicate, the water droplet was placed at a different location on the thin film.

CuAAC with IDX. The reaction was performed on a 2.0 mL scale of aqueous **PF-N_3-mPEG$_{5000}$**-SWNT dispersion (*vide supra*). Once the reaction was complete by IR, the dispersion was filtered through a Teflon membrane (0.2 μm

pore diameter) and washed thoroughly with dH_2O and THF to remove unreacted material. The resulting **PF-PEG$_{5000}$-IDX**-SWNT thin film was sonicated in 3 mL of THF for 1 h and then filtered through a cotton plug. The dispersion was used for subsequent studies as isolated. Equivalents of *p*-TSA were calculated by determining the moles of azide in the dispersion (*vide supra*). For 1.5 eq of *p*-TSA (425 nmol), 5 μL of a *p*-TSA stock solution in THF (16.2 mg·mL^{-1}) was aliquoted to the dispersion to transform IDX to the ring-opened, charged form. For 2.0 eq of Et_3N (567 nmol), 5 μL of an Et_3N stock solution in THF (11.5 mg·mL^{-1}) was aliquoted to the dispersion to transform IDX from the ring-opened, charged form to the ring-closed, neutral form.

Control experiment with IDX. The aforementioned procedure (*vide supra*) was repeated (including the filtration and washing steps), except IDX was omitted. Workup was identical. The PL maps of (i) pristine dispersion, (ii) dispersion with 1.5 eq of *p*-TSA (an identical 5 μL aliquot was added), and (iii) dispersion with 1.5 eq *p*-TSA and IDX (5 μL aliquot of 40 mg·mL^{-1} solution in THF was added) were obtained.

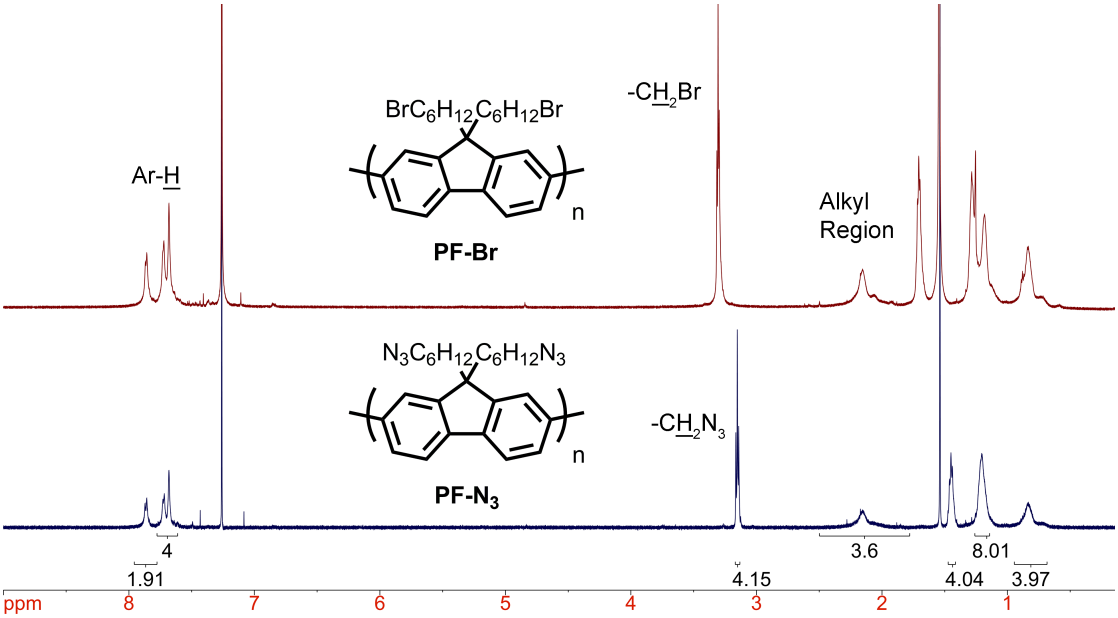


FIGURE 6.6: ^{1}H NMR overlay of **PF-Br** (red) and **PF-N$_3$** (blue) homopolymers in $CDCl_3$.

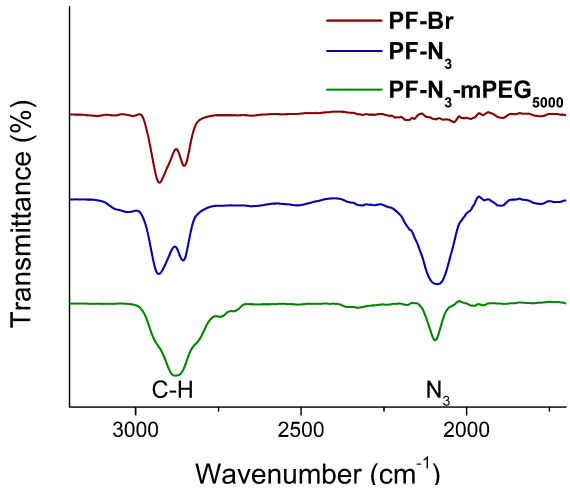


FIGURE 6.7: FT-IR spectra of **PF-Br** homopolymer (red), **PF-N$_3$** homopolymer (blue), and **PF-N$_3$**-mPEG$_{5000}$ (green).

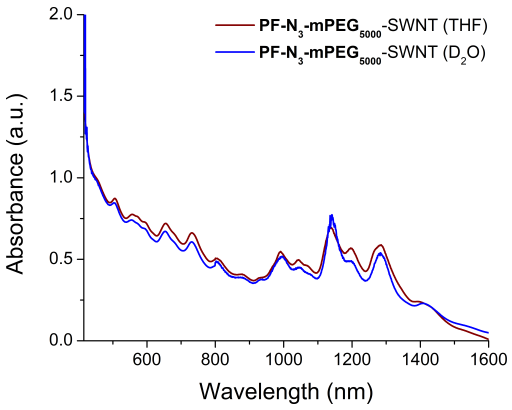


FIGURE 6.8: UV/Vis-NIR spectra of **PF-N$_3$-mPEG$_{5000}$**-SWNT dispersion in THF (red) or D_2O (blue). The pristine THF dispersion was diluted two-fold to match the concentration of the D_2O dispersion.

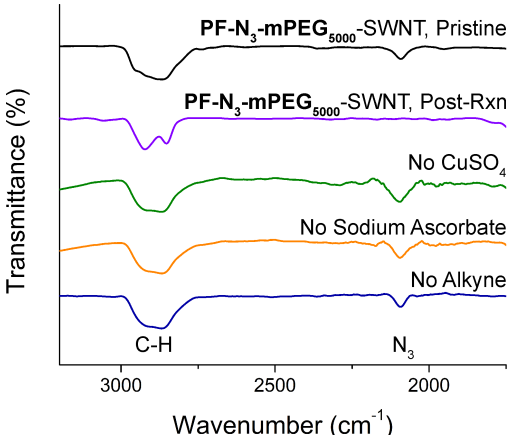


FIGURE 6.9: FT-IR spectra of control experiments where $CuSO_4$ (green), (+)-sodium L-ascorbate (orange), or alkyne, i.e., 4-pentynoic acid (blue) were omitted from the reaction mixture. The control samples were stirred at RT for 16 h prior to obtaining the above IR spectra. The control experiments are juxtaposed with the pristine **PF-N$_3$-mPEG$_{5000}$**-SWNT dispersion (black) and the IR spectrum when the reaction mixture contains all reaction components (purple).

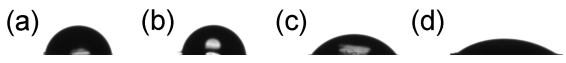


FIGURE 6.10: Photograph of a representative water droplet on the polymer-SWNT thin film functionalized with (a) nothing (pristine), (b) $PDMS_{5000}$-alkyne, (c) D-mannose-alkyne, or (d) zwitterionic sulfobetaine. The contact angles are 74 ± 3°, 80 ± 5°, 50 ± 1°, and 40 ± 4°, respectively.

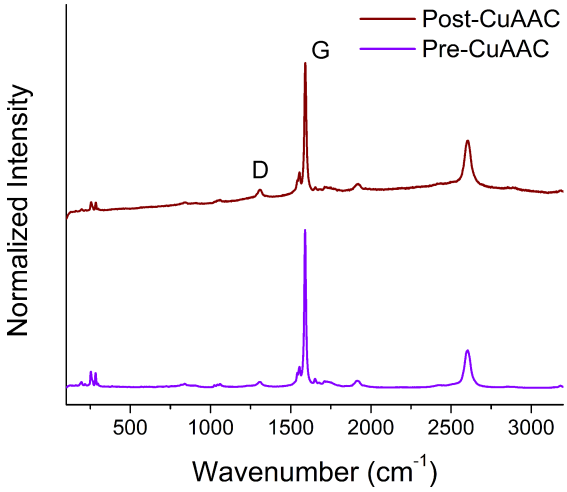


FIGURE 6.11: Raman spectra (λ_{ex} = 633 nm) of **PF-N$_3$-mPEG$_{5000}$**-SWNT dispersions pre- (purple) and post-CuAAC (red) with 4-pentynoic acid. Spectra were normalized to the G-band at ∼1590 cm^{-1} and offset for clarity.

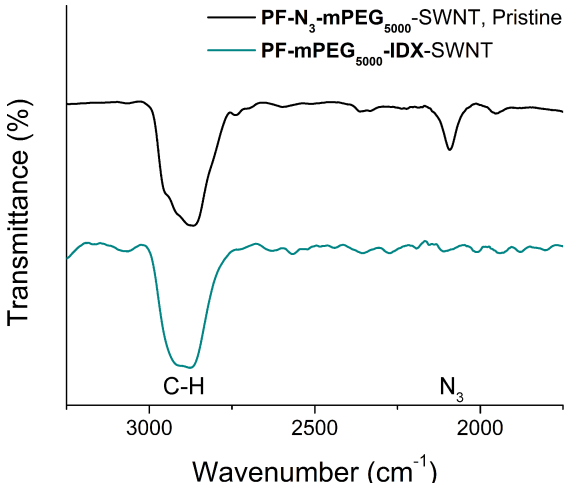


FIGURE 6.12: FT-IR overlay of the CuAAC reaction between **PF-N$_3$-mPEG$_{5000}$**-SWNT and IDX pre- (black) and post-CuAAC (teal). The post-CuAAC IR spectrum was obtained after a reaction time of 30 min.

Species	λ_{ex} (nm)	λ_{em} (nm)	No *p*-TSA
(7,5)	655	1050	426.38
(9,4)	730	1130	413.6
(8,4)	595	1140	292.49
(7,6)	660	1140	479.9
(8,6)	725	1210	284.61
(9,5)	685	1280	313.98
(8,7)	735	1290	278.13
With *p*-TSA	Δ[Intensity]*	With *p*-TSA, Et_3N	Δ[Intensity]*
382.64	-10	382.54	-10
283.03	-32	336.03	-19
217.88	-26	222.05	-24
414.54	-14	424.17	-12
222.31	-22	272.56	-4
218.07	-31	238.66	-24
216	-22	260.86	-6

TABLE 6.1: Fluorescence intensities of sc-SWNT species coated with **PF-mPEG$_{5000}$-IDX** before and after the addition of 1.5 eq of *p*-TSA and 2.0 eq of Et_3N. *Δ[Intensity] was calculated as: $1 - \frac{Intensity\ (no\ p-TSA)}{Intensity\ (Experimental\ Condition) \times 100\%}$.

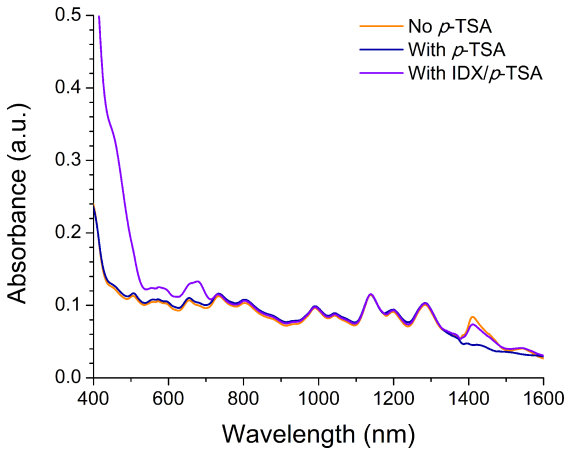


FIGURE 6.13: UV/Vis-NIR spectra of **PF-N$_3$-mPEG$_{5000}$**-SWNT dispersions in THF used for photoluminescence mapping in the control experiment where IDX was not linked to the SWNT surface. Spectra correspond to pristine dispersion (orange trace), dispersion with 1.5 eq *p*-TSA added (blue trace), and dispersion with both 1.5 eq *p*-TSA and 1 eq IDX added (purple trace).

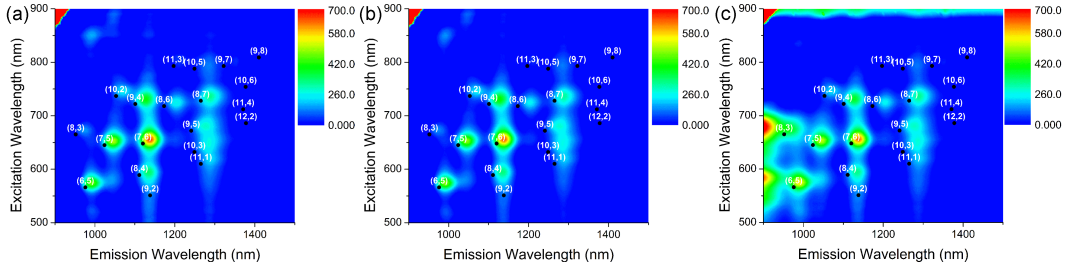


FIGURE 6.14: Photoluminescence maps of control experiment with **PF-N$_3$-mPEG$_{5000}$**-SWNT dispersion in THF with (a) no *p*-TSA, (b) 1.5 eq of *p*-TSA, and (c) 1.5 eq of *p*-TSA and 1 eq of IDX (unbound). Maps are plotted on the same intensity scale.

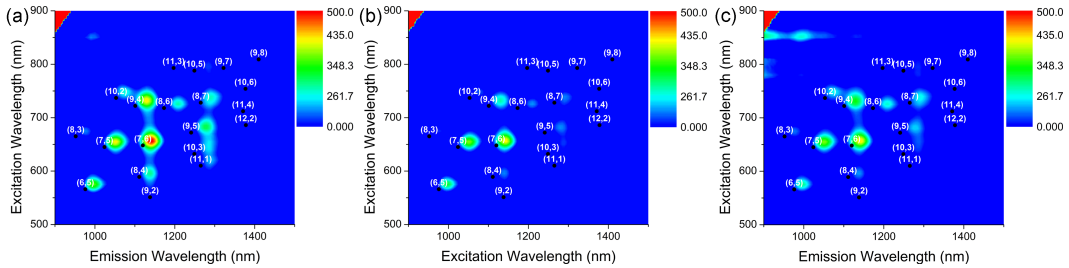


FIGURE 6.15: Photoluminescence maps of the **PF-PEG$_{5000}$-IDX**-SWNT dispersion in THF with (a) no *p*-TSA, (b) 1.5 eq of *p*-TSA, and (c) 1.5 eq of *p*-TSA and 2.0 eq of Et_3N. Maps are plotted on the same intensity scale.

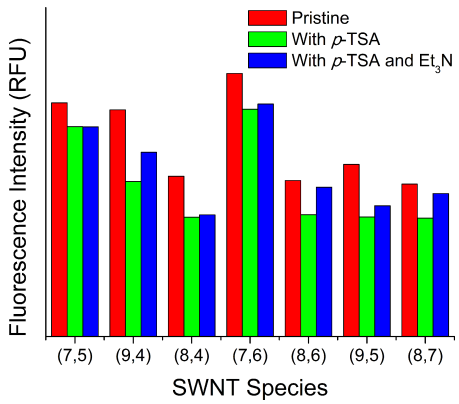


FIGURE 6.16: Graphical representation of fluorescence intensity changes for different sc-SWNTs. The experimental conditions include pristine **PF-PEG$_{5000}$-IDX**-SWNT conjugate (red) followed by the addition of 1.5 eq *p*-TSA (green) and the subsequent addition of 2.0 eq of Et_3N (blue).

Species	λ_{ex} (nm)	λ_{em} (nm)	No *p*-TSA
(7,5)	655	1050	493.2662
(9,4)	730	1130	399.1853
(8,4)	595	1140	335.032
(7,6)	660	1140	635.7377
(8,6)	725	1210	256.4148
(9,5)	685	1280	277.4941
(8,7)	735	1290	320.2069
With *p*-TSA	Δ[Intensity]*	With *p*-TSA, IDX **10**	Δ[Intensity]*
472.8001	-4	508.4712	+3
407.8456	+2	382.532	-4
325.0102	-3	314.768	-6
629.6267	-1	612.3988	-4
241.3379	-6	243.9218	-5
268.5222	-3	278.8159	0
304.722	-5	320.1313	0

TABLE 6.2: Fluorescence Intensities of sc-SWNT Species Coated with **PF-N$_3$**-mPEG$_{5000}$ Before and After the Addition of 1.5 eq of *p*-TSA or 1.5 eq of *p*-TSA and IDX **10**. *Δ[Intensity] was calculated as: $1 - \frac{Intensity\ (no\ p-TSA)}{Intensity\ (Experimental\ Condition) \times 100\%}$.

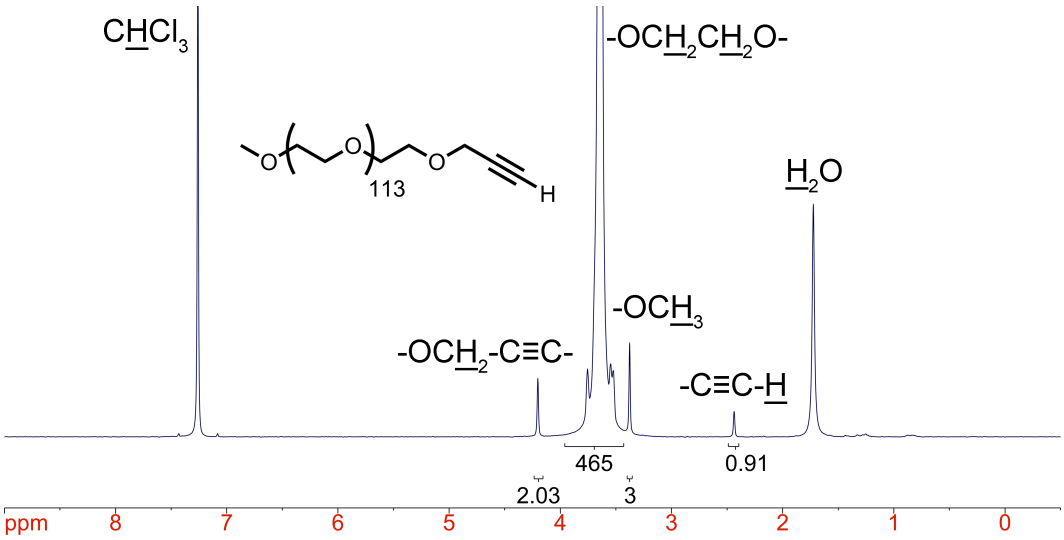


FIGURE 6.17: ^{1}H NMR spectrum of mPEG$_{5000}$-alkyne in $CDCl_3$.

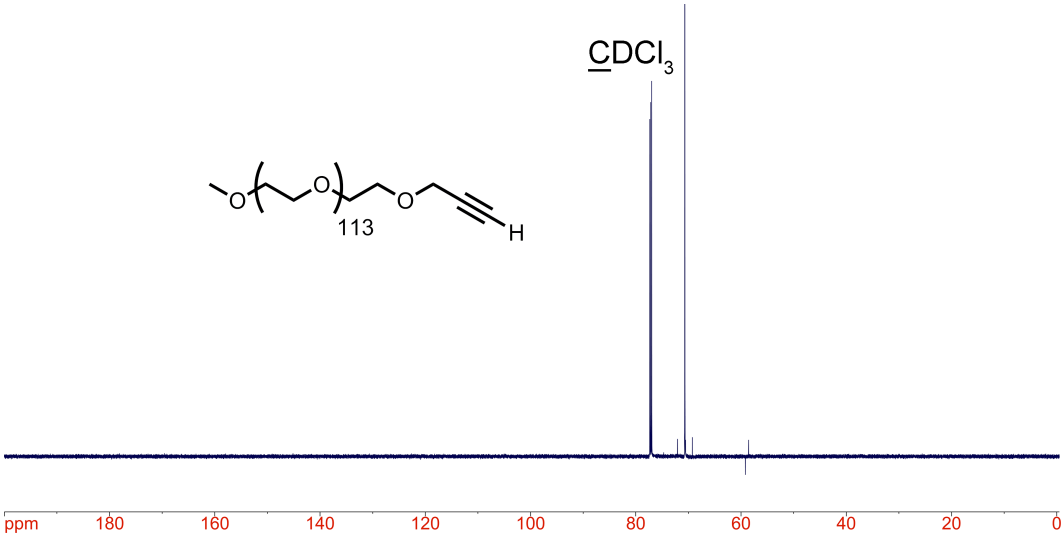


FIGURE 6.18: DEPTq spectrum of $mPEG_{5000}$-alkyne in $CDCl_3$.

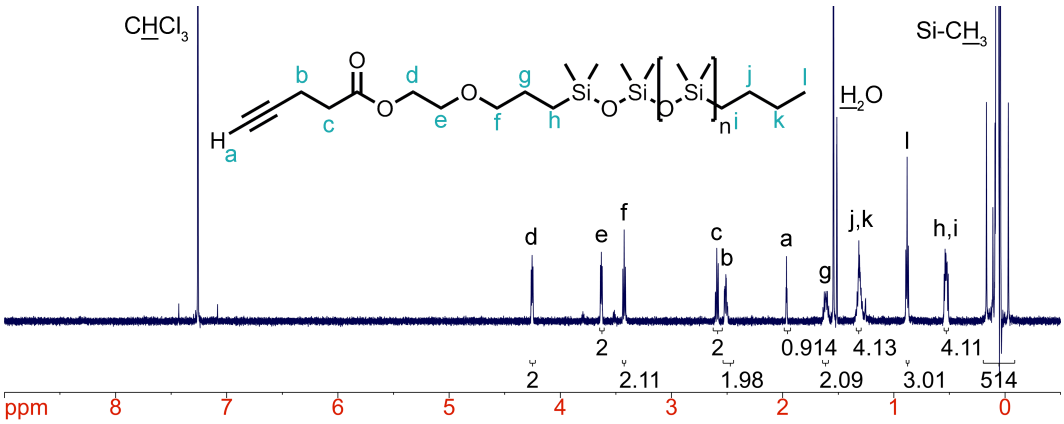


FIGURE 6.19: ^1H NMR spectrum of $PDMS_{5000}$-alkyne in $CDCl_3$.

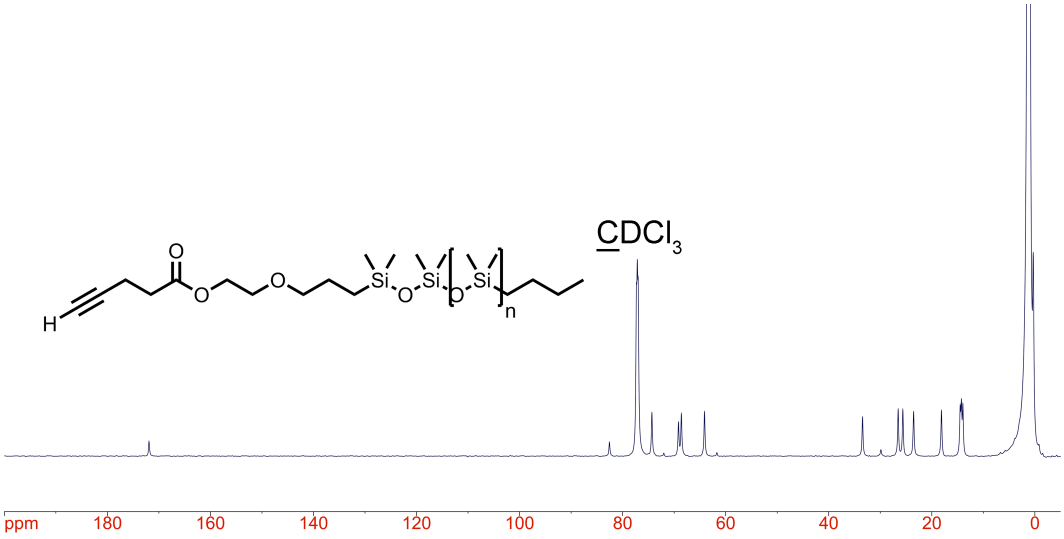


FIGURE 6.20: uDEFT spectrum of $PDMS_{5000}$-alkyne in $CDCl_3$.

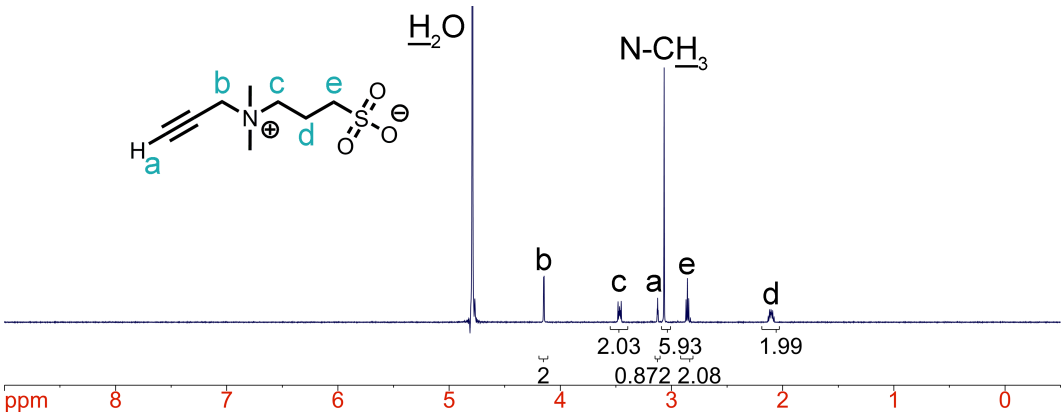


FIGURE 6.21: ^{1}H NMR spectrum of sulfobetaine **6** in D_2O.

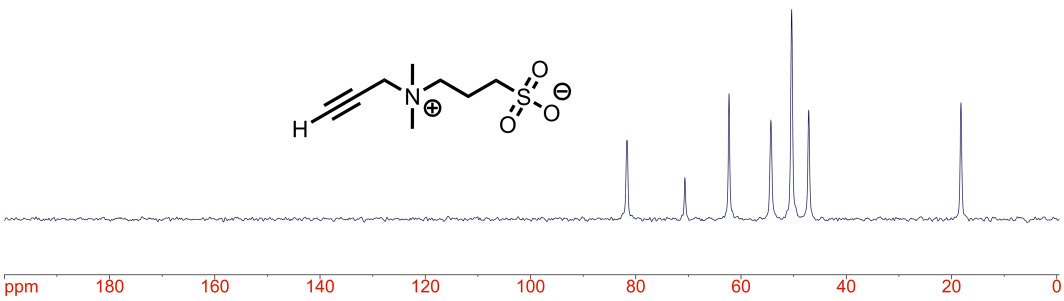


FIGURE 6.22: uDEFT spectrum of sulfobetaine **6** in D_2O.

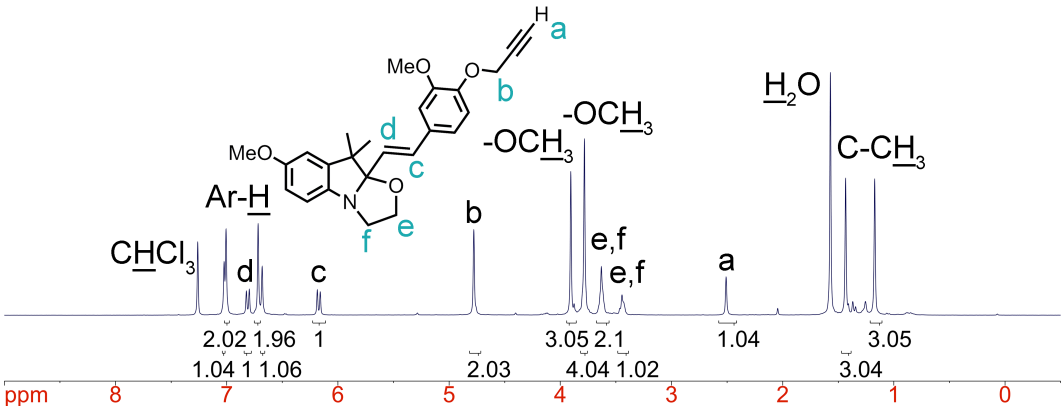


FIGURE 6.23: ^{1}H NMR spectrum of IDX **10** in $CDCl_3$.

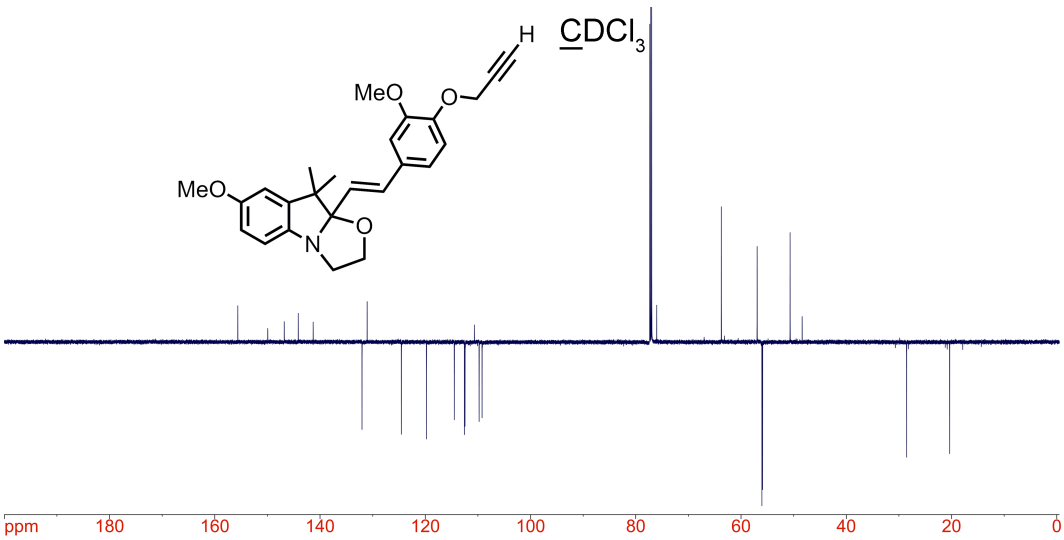


FIGURE 6.24: DEPTq spectrum of IDX **10** in $CDCl_3$.

6.5 References

(1) Fong, D.; Andrews, G.; Adronov, A. *Polym. Chem.* **2018**, 9, 2873–2879.

(2) Fong, D.; Yeung, J.; McNelles, S. A.; Adronov, A. *Macromolecules* **2018**, 51, 755–762.

(3) Fong, D.; Andrews, G. M.; McNelles, S. A.; Adronov, A. *Polym. Chem.* **2018**, 9, 4460–4467.

(4) Fong, D.; Andrews, G. M.; Adronov, A. *J. Polym. Sci. Part A Polym. Chem.* **2018**, 56, 2723–2729.

(5) Shamshoom, C.; Fong, D.; Li, K.; Kardelis, V.; Adronov, A. *ACS Omega* **2018**, 3, 13935–13943.

(6) O'Connell, M. J.; Bachilo, S. M.; Huffman, C. B.; Moore, V. C.; Strano, M. S.; Haroz, E. H.; Rialon, K. L.; Boul, P. J.; Noon, W. H.; Kittrell, C.; Ma, J.; Hauge, R. H.; Weisman, R. B.; Smalley, R. E. *Science* **2002**, 297, 593–596.

(7) Bachilo, S. M.; Strano, M. S.; Kittrell, C.; Hauge, R. H.; Smalley, R. E.; Weisman, R. B. *Science* **2002**, 298, 2361–2366.

(8) Kataura, H.; Kumazawa, Y.; Maniwa, Y.; Umezu, I.; Suzuki, S.; Ohtsuka, Y.; Achiba, Y. *Synth. Met.* **1999**, 103, 2555–2558.

(9) Park, S.; Vosguerichian, M.; Bao, Z. *Nanoscale* **2013**, 5, 1727–1752.

(10) Terrones, M. *Annu. Rev. Mater. Res.* **2003**, 33, 419–501.

(11) Ajayan, P. M. *Chem. Rev.* **1999**, 99, 1787–1800.

(12) Saito, R.; Dresselhaus, G.; Dresselhaus, M. S. *Physical Properties of Carbon Nanotubes*, vol. 3.; Imperial College Press: London, **2005**.

(13) Coleman, J. N.; Khan, U.; Blau, W. J.; Gun'ko, Y. K. *Carbon* **2006**, 44, 1624–1652.

(14) Zhang, Q.; Huang, J.-Q.; Qian, W.-Z.; Zhang, Y.-Y.; Wei, F. *Small* **2013**, 9, 1237–1265.

(15) Tasis, D.; Tagmatarchis, N.; Bianco, A.; Prato, M. *Chem. Rev.* **2006**, 106, 1105–1136.

(16) Hirsch, A. *Angew. Chemie - Int. Ed.* **2002**, 41, 1853–1859.

(17) Britz, D. A.; Khlobystov, A. N. *Chem. Soc. Rev.* **2006**, 35, 637–659.

(18) Campidelli, S.; Klumpp, C.; Bianco, A.; Guldi, D. M.; Prato, M. *J. Phys. Org. Chem.* **2006**, 19, 531–539.

(19) Zhao, Y. L.; Stoddart, J. F. *Acc. Chem. Res.* **2009**, 42, 1161–1171.

(20) Bilalis, P.; Katsigiannopoulos, D.; Avgeropoulos, A.; Sakellariou, G. *RSC Adv.* **2014**, 4, 2911–2934.

(21) Gavrel, G.; Jousselme, B.; Filoramo, A.; Campidelli, S. *Top. Curr. Chem.* **2014**, 348, 95–126.

(22) Islam, M. F.; Rojas, E.; Bergey, D. M.; Johnson, A. T.; Yodh, A. G. *Nano Lett.* **2003**, 3, 269–273.

(23) Moore, V. C.; Strano, M. S.; Haroz, E. H.; Hauge, R. H.; Smalley, R. E.; Schmidt, J.; Talmon, Y. *Nano Lett.* **2003**, 3, 1379–1382.

(24) Gong, X.; Liu, J.; Baskaran, S.; Voise, R. D.; Young, J. S. *Chem. Mater.* **2000**, 12, 1049–1052.

(25) Yang, K.; Zhu, L.; Xing, B. *Environ. Sci. Technol.* **2006**, 40, 1855–1861.

(26) Tomonari, Y.; Murakami, H.; Nakashima, N. *Chem. - A Eur. J.* **2006**, 12, 4027–4034.

(27) Chen, R. J.; Zhang, Y.; Wang, D.; Dai, H. *J. Am. Chem. Soc.* **2001**, 123, 3838–3839.

(28) Guo, Z.; Sadler, P. J.; Tsang, S. C. *Adv. Mater.* **1998**, 10, 701–703.

(29) Balavoine, F.; Schultz, P.; Richard, C.; Mallouh, V. V.; Ebbesen, T. W.; Mioskowski, C. *Angew. Chemie - Int. Ed.* **1999**, 38, 1912–1915.

(30) Bradley, K.; Briman, M.; Star, A.; Grüner, G. *Nano Lett.* **2004**, 4, 253–256.

(31) Star, A.; Steuerman, D. W.; Heath, J. R.; Stoddart, J. F. *Angew. Chemie - Int. Ed.* **2002**, 41, 2508–2512.

(32) Zheng, M.; Jagota, A.; Strano, M. S.; Santos, A. P.; Barone, P.; Chou, S. G.; Diner, B. A.; Dresselhaus, M. S.; McLean, R. S.; Onoa, G. B.; Samsonidze, G. G.; Semke, E. D.; Usrey, M.; Walls, D. J. *Science* **2003**, 302, 1545–1548.

(33) Zheng, M.; Jagota, A.; Semke, E. D.; Diner, B. A.; McLean, R. S.; Lustig, S. R.; Richardson, R. E.; Tassi, N. G. *Nat. Mater.* **2003**, 2, 338–342.

(34) Heller, D. A.; Jeng, E. S.; Yeung, T.-K.; Martinez, B. M.; Moll, A. E.; Gastala, J. B.; Strano, M. S. *Science* **2006**, 311, 508–511.

(35) Chen, J.; Liu, H.; Weimer, W. A.; Halls, M. D.; Waldeck, D. H.; Walker, G. C. *J. Am. Chem. Soc.* **2002**, 124, 9034–9035.

(36) Star, A.; Stoddart, J. F.; Steuerman, D.; Diehl, M.; Boukai, A.; Wong, E. W.; Yang, X.; Chung, S. W.; Choi, H.; Heath, J. R. *Angew. Chemie - Int. Ed.* **2001**, 40, 1721–1725.

(37) Nish, A.; Hwang, J.-Y.; Doig, J.; Nicholas, R. J. *Nat. Nanotechnol.* **2007**, 2, 640–646.

(38) Yim, C. Bin; Dijkgraaf, I.; Merkx, R.; Versluis, C.; Eek, A.; Mulder, G. E.; Rijkers, D. T. S.; Boerman, O. C.; Liskamp, R. M. J. *J. Med. Chem.* **2010**, 53, 3944–3953.

(39) Cheng, F. Y.; Imin, P.; Lazar, S.; Botton, G. A.; de Silveira, G.; Marinov, O.; Deen, J.; Adronov, A. *Macromolecules* **2008**, 41, 9869–9874.

(40) Fong, D.; Adronov, A. *Chem. Sci.* **2017**, 8, 7292–7305.

(41) Wang, H.; Bao, Z. *Nano Today* **2015**, 10, 737–758.

(42) Lefebvre, J.; Ding, J.; Li, Z.; Finnie, P.; Lopinski, G.; Malenfant, P. R. L. *Acc. Chem. Res.* **2017**, 50, 2479–2486.

(43) Lei, T.; Pochorovski, I.; Bao, Z. *Acc. Chem. Res.* **2017**, 50, 1096–1104.

(44) Liang, S.; Zhao, Y.; Adronov, A. *J. Am. Chem. Soc.* **2014**, 136, 970–977.

(45) Pochorovski, I.; Wang, H.; Feldblyum, J. I.; Zhang, X.; Antaris, A. L.; Bao, Z. *J. Am. Chem. Soc.* **2015**, 137, 4328–4331.

(46) Lei, T.; Chen, X.; Pitner, G.; Wong, H.-S. P.; Bao, Z. *J. Am. Chem. Soc.* **2016**, 138, 802–805.

(47) Toshimitsu, F.; Nakashima, N. *Nat. Commun.* **2014**, 5, 5041.

(48) Yang, W.; Thordarson, P.; Gooding, J. J.; Ringer, S. P.; Braet, F. *Nanotechnology* **2007**, 18.

(49) Bianco, A.; Kostarelos, K.; Partidos, C. D.; Prato, M. *Chem. Commun.* **2005**, 571–577.

(50) Liu, Z.; Tabakman, S. M.; Chen, Z.; Dai, H. *Nat. Protoc.* **2009**, 4, 1372–1382.

(51) Fong, D.; Bodnaryk, W. J.; Rice, N. A.; Saem, S.; Moran-Mirabal, J. M.; Adronov, A. *Chem. - A Eur. J.* **2016**, 22, 14560–14566.

(52) Nierengarten, J.-F.; Iehl, J.; Oerthel, V.; Holler, M.; Illescas, B. M.; Muñoz, A.; Martín, N.; Rojo, J.; Sánchez-Navarro, M.; Cecioni, S.; Vidal, S.; Buffet, K.; Durka, M.; Vincent, S. P. *Chem. Commun.* **2010**, 46, 3860.

(53) Fong, D.; Adronov, A. *Macromolecules* **2017**, 50, 8002–8009.

(54) Dyke, C. A.; Tour, J. M. *J. Am. Chem. Soc.* **2003**, 125, 1156–1157.

(55) Li, H.; Cheng, F.; Duft, A. M.; Adronov, A. *J. Am. Chem. Soc.* **2005**, 127, 14518–14524.

(56) Sheng, L.; Li, M.; Zhu, S.; Li, H.; Xi, G.; Li, Y.-G.; Wang, Y.; Li, Q.; Liang,

S.; Zhong, K.; Zhang, S. X.-A. *Nat. Commun.* **2014**, 5, 3044.

(57) Potisek, S. L.; Davis, D. A.; Sottos, N. R.; White, S. R.; Moore, J. S. *J. Am. Chem. Soc.* **2007**, 129, 13808–13809.

(58) Szalóki, G.; Sanguinet, L. *J. Org. Chem.* **2015**, 80, 3949–3956.

(59) Lenhart, J. A.; Ling, X.; Gandhi, R.; Guo, T. L.; Gerk, P. M.; Brunzell, D. H.; Zhang, S. *J. Med. Chem.* **2010**, 53, 6198–6209.

(60) Weisman, R. B.; Bachilo, S. M. *Nano Lett.* **2003**, 3, 1235–1238.

(61) Yum, K.; Ahn, J. H.; McNicholas, T. P.; Barone, P. W.; Mu, B.; Kim, J. H.; Jain, R. M.; Strano, M. S. *ACS Nano* **2012**, 6, 819–830.

(62) Pu, K. Y.; Liu, B. *Macromolecules* **2008**, 41, 6636–6640.

Chapter 7

Visible Light-Mediated Photoclick Functionalization of a Conjugated Polymer Backbone

This chapter has been submitted for publication and is under revision. Manuscript ID: ma-2019-005618. Fong, D.; Lang, A.; Adronov, A. This chapter is included as part of A. Lang's undergraduate thesis document.

D. Fong planned the study, synthesized the initial compounds, performed the initial exploratory experiments, and performed the confocal fluorescence microscopy. A. Lang scaled up the polymer synthesis, performed the HPLC study, the UV-Vis/fluorescence spectroscopy, and prepared the photopatterned silicone composites.

Abstract

Efficient post-polymerization functionalization of conjugated polymer backbones is generally challenging. Here, we report the first example of a conjugated polymer backbone that can be functionalized using visible light. This polymer contains a 9,10-phenanthrenequinone moiety in the conjugated backbone, which reacts with electron-rich vinyl ethers *via* visible light-mediated photoclick chemistry. Synthesis of the 9,10-phenanthrenequinone dibromide monomer requires only a single step from commercially available precursors, and the corresponding polymer can be prepared by Suzuki polycondensation. The second-order rate constant for photoclick functionalization of the resulting conjugated polymer was found to be 2.3 ± 0.2 $M^{-1} \cdot s^{-1}$. The photoclick reaction is insensitive to air and moisture and requires no additional catalysts. The resulting photoclick conjugates were characterized using NMR, UV-Vis, fluorescence, and IR spectroscopy. Photoclick coupling to polyethylene glycol vinyl ether enabled for a dramatic change in polymer solubility and emission properties, while maintaining an identical degree of polymerization and dispersity of the polymer backbone. We demonstrate the first instance of a photopatternable conjugated polymer backbone by incorporating the conjugated polymer into a silicone elastomer and functionalizing it in a spatially-resolved manner.

7.1 Introduction

Conjugated polymers have attracted tremendous attention in the materials and biological sciences for their intriguing optoelectronic properties.[1–4] Many conjugated polymer scaffolds have been investigated, including polythiophene,[5] polyfluorene,[6,7] polycarbazole,[8,9] polyacetylene,[10,11] poly(arylene vinylene),[12] polyphenylene,[13] polypyrrole,[14] and others.[15] This structural diversity, in tandem with post-polymerization modifications such as doping, enables for the tailoring of polymer physical and optoelectronic properties, including solubility, absorption and emission wavelengths, and bandgap (alongside HOMO/LUMO energies).[16–21] Research into the structural diversity of conjugated polymers has flourished in the field of organic electronics, with applications including field-effect transistors (FETs),[22] organic photovoltaics (OPVs),[23,24] light-emitting diodes (LEDs),[25–27] chemical sensors,[28] and magneto-optic materials.[29–32] Recent advances include conjugated polymers containing radicals in both the side chains[33,34] and backbone,[35] the latter of which exhibits ambipolar redox activity and the Faraday effect. Beyond this, conjugated polymers have also been employed as dispersion agents to sort single-walled carbon nanotube (SWNT) species[36–38] or to act as functional SWNT coatings.[39–43] In exploring various conjugated polymer structures, synthetic control over polymer attributes such as the degree of polymerization (DP) and dispersity (Đ) is imperative, as these factors influence polymer properties. Post-polymerization functionalization of the conjugated polymer backbone is necessary to investigate properties in a polymer series with identical DP and Đ.

Several synthetic strategies have been explored to derivatize the conjugated

polymer backbone post-polymerization.[44–46] Our group has published work incorporating strained cyclooctynes into a conjugated polyimine backbone to enable Strain-Promoted Azide-Alkyne Cycloaddition (SPAAC) with various azide derivatives.[44] This work demonstrated that the efficient SPAAC reaction (second order rate constant of 0.031 $M^{-1} \cdot s^{-1}$ in the conjugated polymer backbone) could be used to prepare conjugated graft copolymers with number-average molecular weights (M_n) > 1 M Da. Dichtel and co-workers reported the $Cu(OTf)_2$-catalyzed benzannulation of poly(phenylene ethynylene)s in the presence of excess trifluoroacetic acid (TFA) between the alkyne in the polymer backbone and an *o*-(phenylethynyl)benzaldehyde to prepare poly(phenylene)s.[45] This work allowed access to poly(phenylene) structures that were previously difficult to synthesize. Stevens, Heeney and co-workers reported the quantitative nucleophilic aromatic substitution of an electron-deficient aryl fluoride-containing conjugated polymer with a benzothiadiazole unit using thiols at high temperatures (120 °C).[46] Using this scaffold, multi-functional semiconducting polymer nanoparticles were prepared that simultaneously contained fluorescent dyes and targeting ligands. In each of these cases, either forcing conditions were required to functionalize the conjugated polymer backbone (e.g., elevated temperatures and/or prolonged reaction times)[45,46] or a non-trivial multistep monomer synthesis was required.[44] Evidently, an ideal amalgamation of the efficiency of "click" chemistry with ease of monomer synthesis has remained elusive.

Recently, Zhang and co-workers reported an elegant bioorthogonal photoclick reaction between a 9,10-phenanthrenequinone (PAQ) derivative and electron-rich vinyl ethers mediated by visible light.[47] These authors showed that radical-mediated

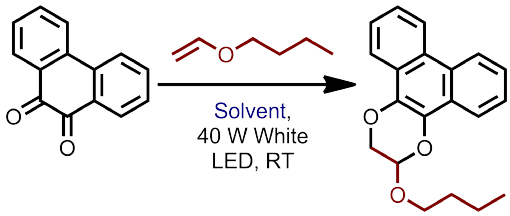
coupling occurred *via* the excitation of PAQ to form a triplet state biradical, followed by addition to an electron-rich vinyl ether and annulation of the resulting biradical intermediate. Intriguingly, this visible light-mediated reaction permitted the bioorthogonal coupling of various fluorescent dyes to proteins in aqueous solution. Building on this efficient chemistry, we report here the synthesis of a PAQ-containing conjugated polymer that can react with electron-rich vinyl ethers upon irradiation with visible light. A radical-mediated coupling to the conjugated polymer backbone enables for the catalyst- and additive-free "click" functionalization of the conjugated polymer backbone under ambient conditions. The synthesis of the required PAQ monomer requires only a single step from commercially available materials, making it easily accessible and enabling its incorporation within a wide array of conjugated polymer scaffolds that are amenable to photoclick functionalization. Moreover, the use of visible light in this reaction allows, for the first time, the spatially-resolved functionalization of a conjugated polymer backbone.

7.2 Results and Discussion

We began our investigation by examining the solvent scope of the visible light-mediated model reaction between commercially available PAQ and butyl vinyl ether (BVE) (Scheme 7.1). The work by Zhang and co-workers showed that a PAQ derivative reacts with electron-rich vinyl ethers upon irradiation with a hand-held white LED.[47] However, these authors only examined 1:1 MeCN/phosphate-buffered saline (PBS) as a reaction medium, as they were particularly interested in bioorthogonal photoclick chemistry. We thus screened for suitable organic solvents that solubilize typical conjugated polymer structures to mediate this photoclick

coupling. A glass vial was charged with PAQ, solvent (MeCN, toluene, CH_2Cl_2, $CHCl_3$, dioxane, or THF), and commercially available BVE (see Supporting Information for details, and Figure S7.5 for the reaction setup). The reaction mixtures were irradiated with white LEDs for 10 min and then analyzed using high performance liquid chromatography (HPLC) (Figure 7.1). We performed the reaction in MeCN as a baseline comparison for reaction efficiency (given that the previous literature report used MeCN successfully as a reaction medium)[47] and found that the reaction proceeded cleanly in MeCN, toluene, and CH_2Cl_2 (>95% conversion by HPLC). Interestingly, ethereal solvents like dioxane and THF resulted in numerous side products, as did $CHCl_3$. There is literature precedent for the light-mediated 1,2-addition of THF or dioxane to PAQ,[48] which is consistent with the appearance of side products in the respective HPLC chromatograms. As well, $CHCl_3$ is known to be unstable to free radicals, as ∼100 ppm of the radical inhibitor amylene is added to improve the shelf-life of commercial samples. The photoclick product, PAQ-BVE, was fully characterized by NMR and IR spectroscopy, as well as mass spectrometry (MS) to confirm its identity. The isolated PAQ-BVE product was also subjected to HPLC analysis to confirm its retention time (red trace in Figure 7.1). In the ^{1}H NMR spectrum of PAQ-BVE, a peak appears at 5.50 ppm, corresponding to the acetal proton (Figure S7.6). Meanwhile, the IR spectrum of the PAQ starting material has a C=O stretch (1672 cm^{-1}), while the PAQ-BVE product only exhibits a styrenic C=C stretch at 1630 cm^{-1} (Figure S7.7). Given this model study, we ascertained that toluene or CH_2Cl_2 were viable solvents for the visible light-mediated photoclick coupling of a conjugated polymer in non-polar organic solution. To examine the full scope of solvent compatibility for this photoclick reaction, we performed additional solvent screening studies with

polar protic solvents (MeOH, EtOH, and ^{i}PrOH), polar aprotic solvents (acetone, EtOAc, DMF, and DMSO), and other non-polar solvents (Et_2O). PAQ was insoluble in hexanes, precluding examination of this solvent. As shown in Figure S7.8, MeOH and EtOAc afforded clean conversion to the product. Interestingly, side products were observed in longer-chain aliphatic alcohols (i.e., EtOH and ^{i}PrOH), as well as several heteroatom-containing solvents (i.e., acetone, DMF, and DMSO). As observed with the other ethereal solvents, Et_2O resulted in side product formation. Overall, a wide variety of non-polar (toluene, CH_2Cl_2), polar aprotic (MeCN, EtOAc), and polar protic (MeOH, water) solvents are suitable for this photoclick reaction.



Scheme 7.1: Small molecule model reaction between PAQ and butyl vinyl ether.

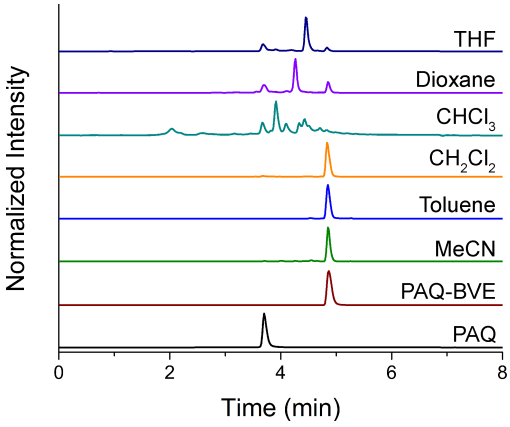
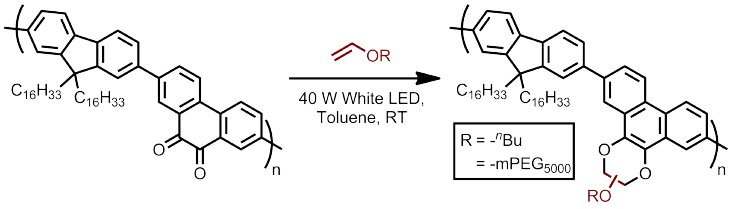


Figure 7.1: HPLC data for the crude reaction mixtures for the photoclick reaction between PAQ and butyl vinyl ether in various organic solvents. The bottom chromatograms correspond to PAQ starting material (black) and the isolated photoclick product PAQ-BVE (red).

With this information in hand, we sought to prepare a PAQ-containing conjugated polymer. A diboronic ester-fluorene monomer containing C_{16} alkyl side chains was synthesized according to literature procedures,[40] and commercially available PAQ was dibrominated using *N*-bromosuccinimide and H_2SO_4.[49] We polymerized these monomers using Suzuki polycondensation to afford **PF-PAQ** as a deep red solid. It was found that leaving the polymerization for 12 h resulted in a polymer with M_n = 4.6 kDa and Đ= 1.80, which contains both oligomeric and short polymer chains, while polymerization for 72 h resulted in a polymer with M_n = 12.2 kDa and Đ= 4.25. As the latter polymer sample was less soluble, we proceeded to use the lower molecular weight sample for subsequent studies. To test the reactivity of **PF-PAQ**, we prepared a stock solution of **PF-PAQ** in toluene (10 mg·mL^{-1}) and then added BVE (1 – 10 eq) to 1 mL of this stock solution. The dark red reaction mixture was stirred at RT under white LED irradiation and turned pale yellow or colourless over the course of 5 – 10 min. (Scheme 7.2; see Supporting Information for details). Solvent was removed *in vacuo*, and the resulting residue was triturated with Et_2O, dried *in vacuo* again, and then the **PF-PAQ-BVE** product was subjected to ^{1}H NMR analysis. As shown in Figure S7.9, reaction progress can be monitored by ^{1}H NMR *via* the appearance of the acetal proton at ∼5.56 ppm, which is consistent with the spectral data for the model compound, PAQ-BVE. As well, the methylene protons adjacent to the oxygen atoms integrate to ∼2:1:1 at 4.45, 4.06, and 3.81 ppm, respectively, which matches both the integrations and chemical shifts observed in the PAQ-BVE model compound (Figure S7.6). An integration of 12:1 aromatic:acetal protons is expected if quantitative conversion occurs, and it was found that at least 3 eq of BVE was required to reach quantitative conversion. Additional characterization

was carried out using IR spectroscopy, where the spectrum of **PF-PAQ** possesses a sharp C=O peak at 1679 cm^{-1}, while the **PF-PAQ-BVE** photoclick product does not possess a peak at this frequency (Figure S7.10).

We next examined the photophysical properties of **PF-PAQ** and its photoclick product, **PF-PAQ-BVE**. To glean insight into the expected photophysical properties of the polymer system, we first explored the properties of the small molecules PAQ and PAQ-BVE (Figure 7.2a). Upon photoclick coupling, the absorption peak for PAQ centred at ∼411 nm disappears in PAQ-BVE. As well, the fluorescence intensity increases substantially in the photoclick product, which is consistent with literature precedent.[47] In the case of the polymer, **PF-PAQ**, the absorption spectrum exhibits a broad shoulder centred at ∼460 nm, which disappears upon photoclick functionalization (Figure 7.2b). Concomitantly, the fluorescence intensity increases significantly in the photoclick product, **PF-PAQ-BVE**, which is consistent with the small molecule system (Figure 7.2b). Interestingly, the fluorescence is substantially redshifted in the polymer system, with a secondary peak centred at ∼530 nm, in addition to the major peak at ∼415 nm. Overall, the photophysical properties of the polymer system are consistent with the properties of the small molecule system, and in tandem with ^{1}H NMR and IR spectroscopy, these results demonstrate that the visible light-mediated photoclick coupling between a PAQ-containing conjugated polymer and an electron-rich vinyl ether is successful in organic solution.



SCHEME 7.2: Visible light-mediated photoclick coupling between **PF-PAQ** and vinyl ether derivatives.

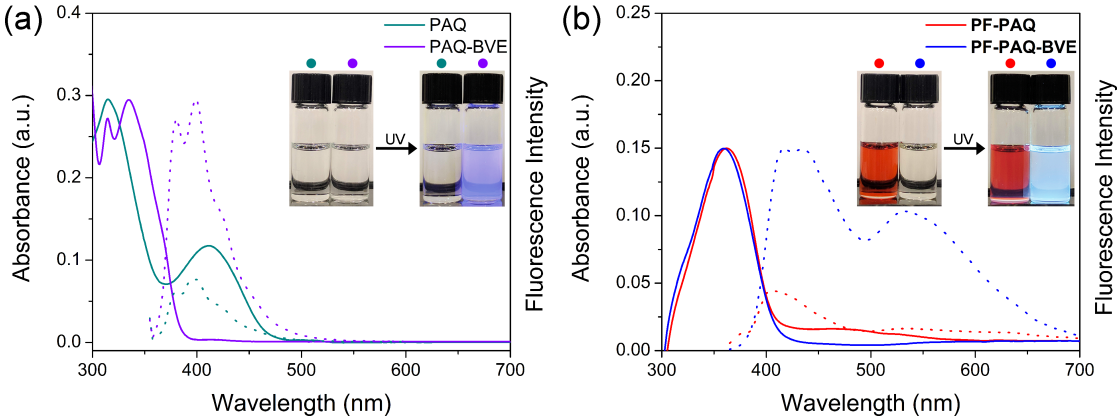


FIGURE 7.2: Photophysical properties in toluene of (a) the small molecule PAQ and its photoclick product, PAQ-BVE, and (b) the polymer **PF-PAQ** and its photoclick product, **PF-PAQ-BVE**. PAQ and PAQ-BVE were excited at λ_{ex} = 350 nm, while **PF-PAQ** and **PF-PAQ-BVE** were excited at λ_{ex} = 360 nm. Solid lines correspond to absorption spectra while dashed lines correspond to emission spectra. Photographs of each compound in toluene are shown prior to and during irradiation with a handheld UV lamp (λ_{ex} = 365 nm). Solutions are colour-coded with the appropriately coloured dot above.

We next explored the reaction kinetics of this photoclick coupling in toluene. Measurement of the molar absorptivities of PAQ ($\epsilon_{411,\text{PAQ}}$) and **PF-PAQ** ($\epsilon_{460,\textbf{PF-PAQ}}$) in toluene revealed values of 2000 ± 24 and 2990 ± 30 $M^{-1}{\cdot}cm^{-1}$, respectively (Figure S7.11). Following literature procedures,[48] we monitored reaction progress in the presence of excess BVE by the decrease in absorbance at 411 nm (PAQ) or 460 nm (**PF-PAQ**) upon irradiation with visible light. For the kinetics experiments, the white LEDs were placed at a distance of 10 cm from the cuvette

containing the reaction mixture, which corresponds to intensities of 120 mW·cm^{-2} (411 nm) for PAQ and 59 mW·cm^{-2} (460 nm) for **PF-PAQ**. Absorbance at 411 nm (PAQ) or 460 nm (**PF-PAQ**) vs irradiation time was measured in triplicate and used to calculate the second order rate constant (Table S7.1). We found that the small molecule second order rate constant was 10.3 ± 0.7 $M^{-1} \cdot s^{-1}$ (Figure S7.12a), which is slightly higher than reported literature values (2.76 $M^{-1} \cdot s^{-1}$).[47] We note that our rate constants were obtained using different solvents (toluene vs 1:1 MeCN:PBS) and PAQ derivatives, and that the light intensity was not reported in the cited manuscript; the combination of which may explain the differences in the reported rate constants. For **PF-PAQ**, the second order rate constant was determined to be 2.3 ± 0.2 $M^{-1} \cdot s^{-1}$ (Figure S7.12b). The decrease in reaction rate of the polymer compared to the small molecule is consistent with literature observations.[45] Remarkably, the reaction rate of **PF-PAQ** with BVE is ∼70-fold faster than the strained cyclooctyne-containing conjugated polyimine derivative we reported (rate constant of 0.031 $M^{-1} \cdot s^{-1}$).

Intrigued by the exceptional reaction kinetics, we next studied the capacity for this photoclick reaction to substantially modify the properties of our conjugated polymer while maintaining a constant DP and Đ. A monomethyl ether polyethylene glycol derivative having a vinyl ether chain end, mPEG$_{5000}$-VE, was synthesized by mesylating mPEG$_{5000}$-OH and then alkylating mPEG$_{5000}$-OMs with ethylene glycol vinyl ether (see Supporting Information for details). Upon photoclick ligation of mPEG$_{5000}$-VE to **PF-PAQ**, we observed dramatic solubility differences. As shown in Figure 7.3a, **PF-PAQ**-mPEG$_{5000}$ exhibited solubility in water, as evidenced by the absorption peak centred at 352 nm in the aqueous UV-Vis spectrum. Meanwhile, **PF-PAQ** alone did not exhibit solubility in water

after prolonged sonication, and $mPEG_{5000}$-VE alone does not absorb in the UV-Vis region. As a control experiment, we sonicated **PF-PAQ** in water with $mPEG_{5000}$-OH present and did not observe any change in polymer solubility. Thus, aqueous solubility is only possible upon the formation of a covalent bond between **PF-PAQ** and $mPEG_{5000}$ *via* the visible light-mediated photoclick coupling. Upon irradiation of the aqueous **PF-PAQ**-$mPEG_{5000}$ solution (λ_{ex} = 360 nm), a single fluorescence peak was observed at 558 nm, which is substantially redshifted compared to the two emission peaks observed for **PF-PAQ-BVE** in toluene (peaks at 415 and 520 nm). Intrigued by this solvatochromism, we examined the absorption and emission properties of **PF-PAQ**-$mPEG_{5000}$ in various solvents (toluene, CH_2Cl_2, THF, EtOAC, acetone, EtOH, MeCN, and water, depicted in Figures 3b and 3c). In all solvents except EtOH and water, absorption spectra were generally very similar, with a λ_{max} at ∼358 nm. Emission maxima of **PF-PAQ**-$mPEG_{5000}$, however, varied significantly (Table S7.2). Among the non-polar solvents, the emission spectrum in CH_2Cl_2 exhibited a single tailing peak centred at ∼438 nm, while emission spectra in toluene and THF possessed three discernible maxima. Interestingly, in MeCN the intensity of the emission peak at ∼558 nm is higher than that of the ∼438 nm peak, while the opposite is true for the other solvents. We speculate that these changes in emission are solvatochromic in nature. Overall, we show that the visible light-mediated photoclick reaction can be utilized to significantly alter the properties of the starting polymer.

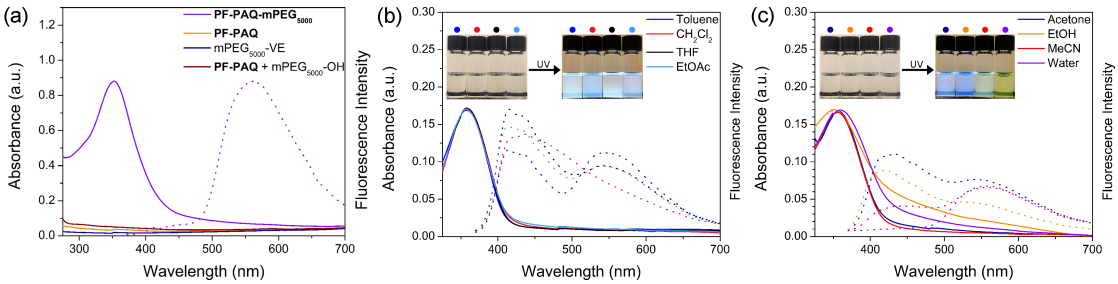


FIGURE 7.3: UV-Vis absorption and fluorescence spectra in water of (a) **PF-PAQ**-mPEG$_{5000}$ (purple), **PF-PAQ** (orange), mPEG$_{5000}$-VE (blue), and **PF-PAQ** in the presence of mPEG$_{5000}$-OH after sonication in water. UV-Vis absorption and fluorescence spectra of **PF-PAQ**-mPEG$_{5000}$ in solvents of varying polarity in (b) and (c). Solid lines correspond to absorption spectra while dashed lines correspond to emission spectra. Photographs of each solution are shown with and without irradiation at λ_{ex} = 365 nm using a handheld UV lamp. Solutions are colour-coded with the appropriately coloured dot above.

Given that this click reaction is driven by visible light, spatial control of the photoclick reaction should be possible. To demonstrate this concept, we embedded **PF-PAQ** into a commercially available two-part silicone elastomer (Scheme S7.3), which was chosen because it can be subsequently swollen in a solution of vinyl ether. To prepare **PF-PAQ-silicone**, we mixed 1 mL of a **PF-PAQ** solution in toluene (10 mg·mL^{-1}) with part A (2.5 g) of the silicone elastomer kit. We then removed the toluene *in vacuo* and added part B (2.5 g). The components were homogenized using a speed mixer and degassed in a vacuum oven at RT, followed by silicone curing in a petri dish at 90 °C for 1 h. The resulting red-coloured **PF-PAQ-silicone** composite (photograph in Figure S7.13a) was cut with a razor blade into smaller pieces and the individual pieces were used for the subsequent experiments. We first examined composite reactivity by immersing a piece in a BVE/toluene solution for 2 min, and then removing the composite from the solution followed by irradiation with white LEDs (see Supporting Information for details). The resulting composite, **PF-PAQ-BVE-silicone**, turned yellow

(photograph in Figure S7.13c) and became strongly emissive, which are attributes that are consistent with **PF-PAQ-BVE** (*vide supra*). As a control experiment, pristine **PF-PAQ-silicone** composite was irradiated with white LEDs, and the resulting composite remained red, which indicates that no reaction occurred in the absence of BVE (photograph in Figure S7.13b). To verify the difference between the irradiated **PF-PAQ-silicone** composites in the absence and presence of BVE, the samples were placed adjacent to each other on a glass slide (Figure S7.13d) and analyzed using confocal fluorescence microscopy. Using brightfield microscopy (Figure S7.13e), both samples are clearly visible in the field of view. When the same area is examined using the confocal fluorescence microscope (Figure S7.13f), only **PF-PAQ-BVE-silicone** is emissive, which is consistent with the properties of the photoclick conjugated polymer. Thus, the coupling reaction is only possible in the presence of both visible light and the vinyl ether coupling partner. To examine the ability to photopattern this material, we prepared a 3D printed mask in the form of a grid with grid line thicknesses of ~500 μm and empty squares with dimensions of ~600 x 600 μm (see Supporting Info for details). We expected that the empty squares would allow for visible light to illuminate the **PF-PAQ-silicone** sample and functionalize the polymer backbone with BVE to form a fluorescent square pattern (Figure 7.4a). After using the 3D printed mask, fluorescent green squares were produced with a resolution of ~500 μm (Figure 7.4b), showing that it is possible to photopattern a conjugated polymer backbone using facile visible light-mediated coupling between a PAQ-containing conjugated polymer and a vinyl ether derivative.

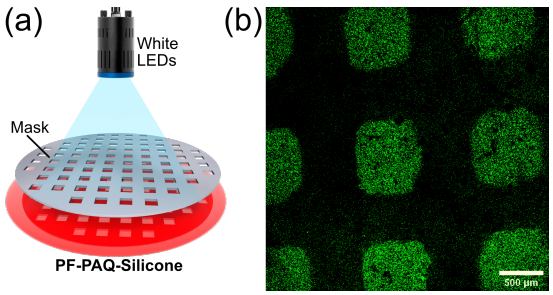


FIGURE 7.4: Cartoon representation of **PF-PAQ-silicone** photopatterning process. (b) A representative confocal fluorescence microscope image of **PF-PAQ-silicone** after soaking the sample in a BVE/toluene solution for 2 min and illuminating with white LEDs while covering with a 3D printed mask.

7.3 Conclusions

We report the first example of a visible light-mediated, photoclickable conjugated polymer backbone. Using HPLC, it was found that a variety of non-polar (toluene, CH_2Cl_2), polar aprotic (MeCN, EtOAc), and polar protic (MeOH) solvents allowed efficient reaction of PAQ with a vinyl ether derivative. Commercially available PAQ was transformed into a suitable monomer in a single bromination step to produce PAQ-Br_2, which was then copolymerized with a fluorene unit to produce **PF-PAQ**. Comparison of the optical properties pre- and post-photoclick revealed that both the small molecule and polymer systems had increased fluorescence intensity upon photoclick functionalization. The second order rate constant of **PF-PAQ** in toluene was 2.3 ± 0.2 $M^{-1} \cdot s^{-1}$, which is an astonishing ∼70-fold faster than that of a strained cyclooctyne-containing conjugated polymer backbone. The solubility and emission properties of the conjugated polymer could be drastically altered by photoclicking with $mPEG_{5000}$-VE to produce a water-soluble conjugated polymer scaffold, while maintaining a constant DP and Đ. Photopatterning of a conjugated polymer backbone embedded in silicone was achieved with ∼500 μm

resolution by using a 3D printed photomask to selectively photoclick only the regions exposed to visible light, as observed using confocal fluorescence microscopy. We envision that this photoclickable PAQ unit will be easily incorporated into various conjugated structures to rapidly explore molecular properties from a single scaffold, and work is now underway in our laboratory to incorporate PAQ into other constructs.

7.4 Supporting Information

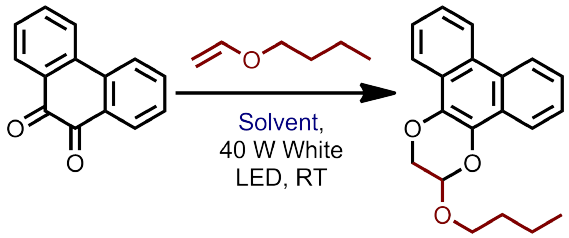
7.4.1 General

Reagents were purchased from commercial suppliers and used as received. Flash chromatography was performed using an IntelliFlash 280 system from Analogix. Unless otherwise noted, compounds were monitored using a variable wavelength detector at 254 nm. Solvent amounts used for gradient or isocratic elution were reported in column volumes (CV). Columns were prepared in Sorbtech EZ Flash MT cartridges using 40 – 63 μm silica or 25 – 40 μm silica purchased from Silicycle. Photochemical reactions were performed using a Kessil A160WE Tuna Blue saltwater aquarium light, and reactions were cooled using an AC Infinity AXIAL 1238 Muffin Fan. Light intensities were measured using a LabMAX-Top equipped with a LM-2 VIS Sensor (Coherent Inc.). NMR was performed on a Bruker Avance 600 MHz or 700 MHz instrument and shift-referenced to the residual solvent resonance. Crude reaction mixtures or products were analyzed *via* HPLC using a Waters 2695 Separations Module equipped with a Waters 2487 dual λ absorbance detector (reactions monitored at 254 nm) and a Phenomenex Luna 3 μ (50 $\times$ 4.6 mm) phenyl-hexyl column. High-resolution (HR) electrospray

ionization (ESI) MS measurements were carried out on the Micromass/Waters Quattro Ultima (ESI/APCI-LCMS Triple Quadrupole Mass Spectrometer). Infrared spectra were recorded using a Thermo Scientific Nicolet 6700 FT-IR spectrometer equipped with a Smart iTX attenuated total reflectance (ATR) sample analyzer. The boronic ester-containing fluorene monomer **1** was synthesized according to literature procedures.[40] Polymer molecular weights and dispersities were analyzed (relative to polystyrene standards) *via* GPC using a Waters 2695 Separations Module equipped with a Waters 2414 refractive index detector and a Jordi Fluorinated DVB mixed bed column in series with a Jordi Fluorinated DVB 10^5 Å pore size column. THF with 2% acetonitrile was used as the eluent at a flow rate of 2.0 mL/min. Sonication was performed using a QSonica Q700 ultrasonicator. UV-Vis spectra were recorded on a Cary 5000 spectrometer in dual beam mode, using matching 10 mm quartz cuvettes. Fluorescence spectra were measured on a Jobin-Yvon SPEX Fluorolog 3.22 equipped with a 450 W Xe arc lamp, digital photon counting photomultiplier, and an InGaAs detector, also using a 10 mm quartz cuvette. Slit widths for both excitation and emission were set to 2 nm band-pass, and correction factor files were applied to account for instrument variations. A commercially available two-part silicone kit (Gelest Optical Encapsulant, PP2-OE41) was used to prepare the polymer-silicone composites. Silicone mixtures were homogenized using a FlackTek Inc. DAC 150 FVZ-K Speed Mixer. 3D printed photomasks were prepared using an Objet 24 3D Printer with a VeroWhite RGD 835 resin (matte finish). Photomasks were made opaque to light by painting over the top face of the photomask using an oil-based fine point black paint marker (Sharpie). Confocal fluorescence microscopy was performed using a Nikon A1 Confocal Eclipse Ti microscope with Nikon A1 plus camera and Nikon

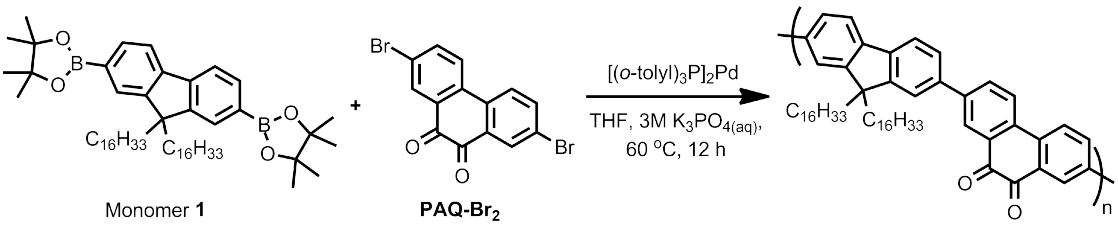
Elements software (4×/0.2 NA objective lens).

7.4.2 Synthetic Procedures



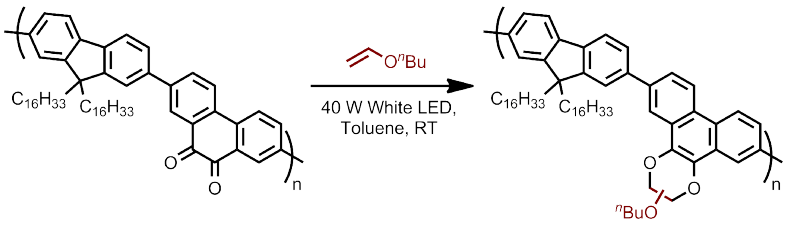
PAQ-BVE solvent screening. A glass vial equipped with a magnetic stir bar was charged with PAQ (10 mg, 48 μmol), solvent (1 mL), and BVE (48 mg, 480 μmol). The reaction mixture was irradiated with white LEDs and stirred at RT for 10 min (apparatus shown in Figure S7.5). The crude reaction mixtures were subjected to HPLC to determine the efficiency of the reaction. For the reaction in toluene, solvent was removed *in vacuo* prior to HPLC analysis as the solvent appeared in the HPLC chromatogram. For the reaction in toluene, the reaction scale was increased to 100 mg of PAQ and the reaction mixture was purified by flash chromatography (12 g silica, 0 to 50% CH_2Cl_2 in hexanes over 10 CV) to afford **PAQ-BVE** as a colourless solid (106 mg, 72% yield). ^{1}H-NMR (700 MHz; $CDCl_3$): δ 8.61 (t, J = 7.0 Hz, 2H), 8.19 (t, J = 8.2 Hz, 2H), 7.62-7.55 (m, 4H), 5.50 (dd, J = 2.5, 1.6 Hz, 1H), 4.43-4.34 (m, 2H), 4.02-3.98 (m, 1H), 3.77 (dt, J = 9.7, 6.7 Hz, 1H), 1.63-1.59 (m, 2H), 1.33 (q, J = 7.5 Hz, 2H), 0.86 (t, J = 7.4 Hz, 3H). ^{13}C NMR (176 MHz; $CDCl_3$): δ 133.4, 130.8, 127.05, 126.87, 126.79, 126.77, 126.5, 126.2, 125.16, 125.05, 122.66, 122.51, 121.1, 120.6, 94.6, 69.1, 66.6, 31.7, 19.3, 13.9. HRMS (ESI$^+$) (m/z) for $C_{20}H_{20}O_3$ $[M+H]^+$ calculated: 309.1485, found: 309.1485.

PAQ-Br$_2$.[49] A round bottom flask equipped with a magnetic stir bar was charged with PAQ (1 g, 4.8 mmol) and conc. H_2SO_4 (24 mL). Upon addition of NBS (1.9 g, 10.6 mmol), the dark green mixture quickly turned dark red. The reaction mixture was stirred at RT for 12 h and then poured onto ice. The resulting dark orange slurry was vacuum filtered and washed with water and MeOH to afford **PAQ-Br$_2$** as an orange solid (1.68 g, 95%). ^{1}H-NMR (600 MHz; $CDCl_3$): δ 8.31 (dd, J = 1.5, 0.8 Hz, 2H), 7.85 (d, J = 1.7 Hz, 4H).



PF-PAQ. A Schlenk tube was charged with a magnetic stir bar and boronic ester monomer **1** (954.0 mg, 1.10 mmol), PAQ-Br$_2$ (402.7 mg, 1.10 mmol), THF (8 mL), and 3M $K_3PO_{4(aq)}$ (8 mL). The biphasic mixture was degassed by three freeze-pump-thaw cycles, then, while frozen under liquid nitrogen, [(*o*-tol)$_3$P]$_2$Pd (18 mg, 2.5 μmol) was added under a positive pressure of nitrogen. The Schlenk tube was evacuated and backfilled with nitrogen three times, and the reaction mixture was heated to 60 °C and vigorously stirred for 12 h. The phases were allowed to separate, and the organic layer was isolated and filtered through a single plug of celite and neutral alumina. The plug was thoroughly washed with THF and the filtrate was concentrated *in vacuo*. The crude polymer was precipitated into MeOH (∼150 mL) and then filtered to afford **PF-PAQ** as a red solid (782 mg, 87%). ^{1}H-NMR (600 MHz; $CDCl_3$): δ 8.58-8.53 (m, 2H), 8.18-8.04 (m, 4H), 7.88-7.85 (m, 2H), 7.75-7.67 (m, 4H), 2.16-2.09 (m, 4H), 1.25-1.09 (m, 48H), 0.85 (m,

10H), 0.76-0.70 (m, 4H). GPC: M_n = 4.6 kDa; Đ = 1.80. The above procedure was repeated on a 100 mg scale of PAQ-Br_2 (0.27 mmol), except the reaction mixture was stirred for 72 h to afford **PF-PAQ** as a dark red solid (132 mg, 60%). GPC: M_n = 12.2 kDa, Đ = 4.25.



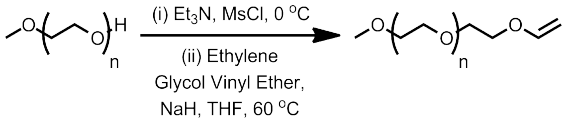
PF-PAQ photoclick reaction with BVE. A glass vial equipped with a magnetic stir bar was charged with **PF-PAQ** (10 mg, 12.2 μmol), BVE (1 – 10 eq, 12.2 – 122 μmol), and toluene (1 mL). The glass vial was irradiated with white LEDs for 30 min at RT, and then solvent was removed *in vacuo*. The crude solid was triturated with Et_2O to remove unreacted BVE and then the polymer was dried *in vacuo* and analyzed by ^{1}H NMR. ^{1}H-NMR (600 MHz; $CDCl_3$): δ 8.74-7.67 (m, 12H), 5.56 (m, 1H), 4.45 (m, 2H), 4.06 (m, 1H), 3.81 (m, 1H), 2.12 (m, 8H), 1.64 (m, 4H), 1.08 (m, 61H).

Determination of second order rate constants. Rate constants were measured following literature procedures.[47] The molar absorptivity in toluene of PAQ (ϵ_{411} = 1996 ± 24 $M^{-1}\cdot cm^{-1}$) and **PF-PAQ** (ϵ_{460} = 2987 ± 30 $M^{-1}\cdot cm^{-1}$) was determined by gravimetrically preparing a serial dilution of the respective compound, then plotting A_{411} or A_{460} vs concentration (converted from molality using $\rho_{toluene}$ = 0.867 $g\cdot mL^{-1}$ and taking molar absorptivity as the slope of the linear regression (n = 3). Reaction mixtures containing PAQ or **PF-PAQ** (∼250 μM) and BVE (∼2.5 mM, 10 eq) were prepared gravimetrically in toluene then irradiated with white LEDs. A_{411} (PAQ) or A_{460} (**PF-PAQ**) was measured in 5 sec intervals

for PAQ and 10 sec intervals for **PF-PAQ**. was plotted vs time (s) to obtain the pseudo-first order rate constant, k_{obs}, as the slope of the linear regression. The second order rate constant, k_2, could then be calculated as:

$$k_2 = \frac{k_{obs}}{[BVE]} \tag{7.1}$$

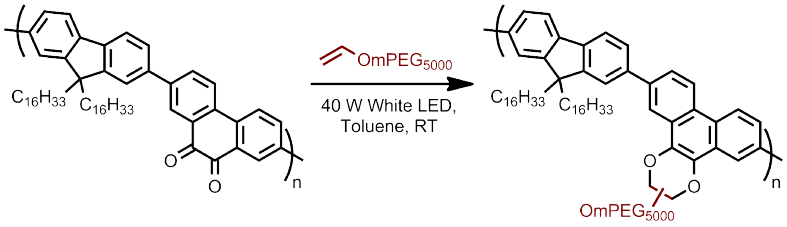
Where [BVE] is the concentration of BVE in M. The data for each trial are tabulated in Table S7.1.



mPEG$_{5000}$-OMs. A glass vial equipped with a magnetic stir bar was charged mPEG$_{5000}$-OH (500 mg, 0.1 mmol), Et_3N (20 mg, 0.2 mmol), and CH_2Cl_2 (1 mL) then cooled to 0 °C. MsCl (57 mg, 0.5 mmol) was added dropwise to the colourless solution, and the reaction mixture was stirred at 0 °C for 2 h. The reaction mixture was filtered through an alumina plug and directly precipitated into Et_2O and vacuum filtered. The crude polymer was used directly in the next reaction.

mPEG$_{5000}$-VE. A glass vial equipped with a magnetic stir bar was charged with mPEG$_{5000}$-OMs (0.1 mmol), ethylene glycol vinyl ether (176 mg, 2 mmol), NaH (60 mg, 2.5 mmol), and THF (0.25 mL). The reaction mixture was heated to 60 °C (melting the mPEG$_{5000}$-OMs to afford a homogenous solution) for 16 h. The resulting viscous orange reaction mixture was filtered through an alumina plug and then precipitated into Et_2O and vacuum filtered to afford mPEG$_{5000}$-VE as a colourless solid (292 mg, 57%). ^{1}H-NMR (700 MHz; $CDCl_3$): δ 6.49 (dd, J = 14.4, 6.8 Hz, ^{1}H), 4.17 (s, ^{1}H), 4.00 (s, ^{1}H), 3.83 (d, J = 24.7 Hz, 4H), 3.64 (s,

^{1}H), 3.38 (s, 3H). ^{13}C NMR (176 MHz; $CDCl_3$): δ 110.1, 86.8, 72.1, 70.87, 70.68, 70.62, 70.60, 69.8, 67.4, 59.2.



PF-PAQ photoclick reaction with mPEG$_{5000}$-VE. A glass vial was charged with **PF-PAQ** (1 mg, 1.2 μmol), mPEG$_{5000}$-VE (31.2 mg, 6.1 μmol), and toluene (1 mL). The glass vial was irradiated with white LEDs for 10 min at RT, and then solvent was removed *in vacuo*. The resulting clicked polymer could not be separated from the mPEG$_{5000}$-VE starting material and was used without purification for the subsequent study. The product was reconstituted in various solvents and interrogated for photophysical properties.

PF-PAQ silicone composites. The preparation process is illustrated in Figure S7.5. **PF-PAQ** (10 mg) was dissolved in toluene (1 mL) and added to part A (2.5 g) of the commercially available silicone elastomer kit. The ingredients were manually mixed together using a small wooden dowel, then toluene was removed *in vacuo* at 90 °C. Part B (2.5 g) of the silicone elastomer kit was added, and the components were homogenized using a speed mixer (3000 *g*, 30 sec). The silicone mixture was poured into a petri dish (circle-shaped with a diameter of 6 cm, for a total area of 28.3 cm^2) and cured at 90 °C for 1 h. The solid silicone elastomer composite was removed from the petri dish and cut into smaller pieces using a razor blade for subsequent experiments.

PF-PAQ silicone composite functionalization. The **PF-PAQ-silicone** composite was soaked in a 50/50 v/v solution of BVE in toluene for 2 min and then removed from the mixture. The silicone composite was then irradiated with white LEDs for 5 min and analyzed using a confocal fluorescence microscope. As a control experiment, the same silicone composite was irradiated in an identical manner (*vide supra*) without soaking in the BVE solution. To functionalize only some of the silicone composite, a 3D printed mask was used to cover specific regions of the silicone composite during irradiation.

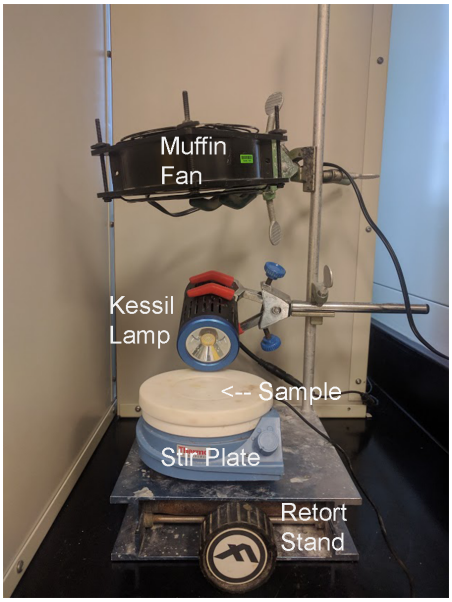


FIGURE 7.5: Photograph of the photochemical reaction setup (reaction sample not shown). The lamp was adjusted accordingly for the specific experiment, and was positioned parallel to the sample during irradiation. A Kessil A160WE Blue Tuna saltwater aquarium light is used to irradiate the sample and an AC Infinity AXIAL 1238 muffin fan is used to keep the reaction mixture from overheating.

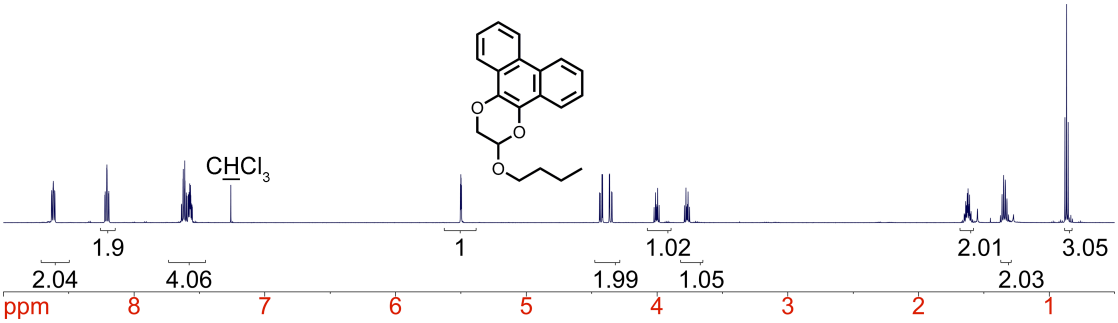


FIGURE 7.6: ^{1}H NMR spectrum of PAQ-BVE.

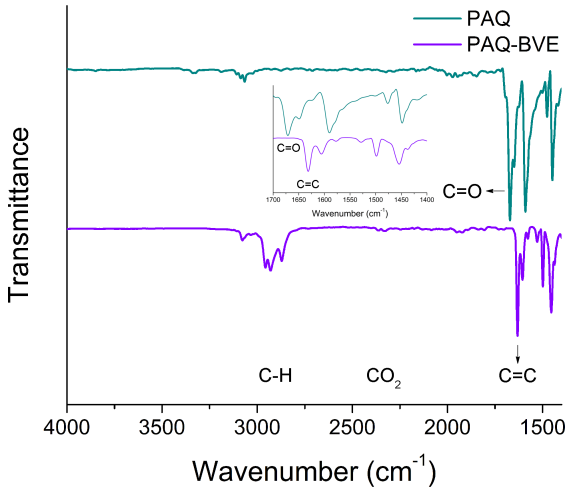


FIGURE 7.7: IR spectra of PAQ (teal) and PAQ-BVE (purple).

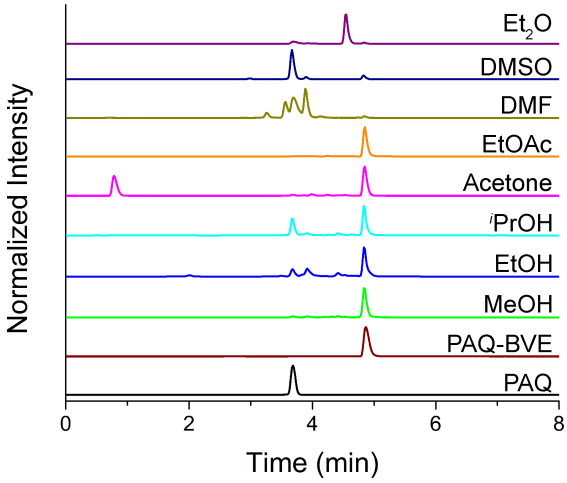


FIGURE 7.8: HPLC traces of the crude reaction mixtures for the photoclick reaction between PAQ and BVE in various solvents. The bottom traces correspond to PAQ starting material (black) and the isolated photoclick product PAQ-BVE (red), respectively.

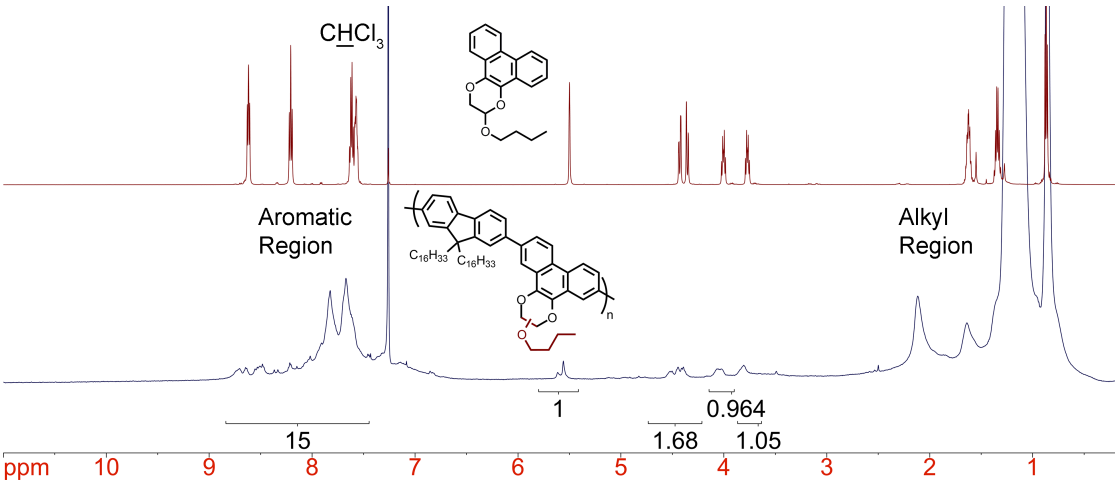


FIGURE 7.9: ^{1}H NMR spectra of **PF-PAQ-BVE** (blue) and PAQ-BVE (red).

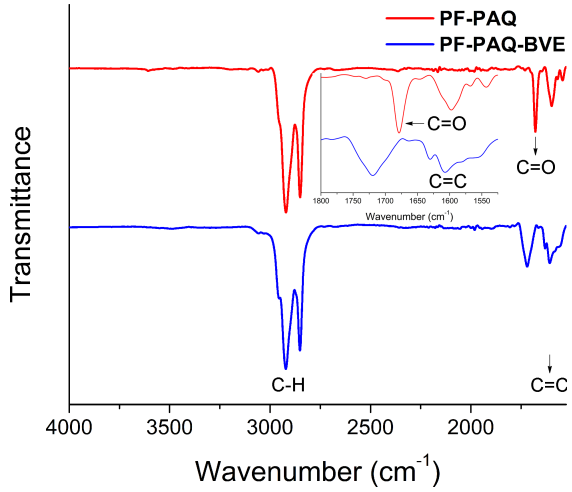


FIGURE 7.10: IR spectra of **PF-PAQ** and **PF-PAQ-BVE**.

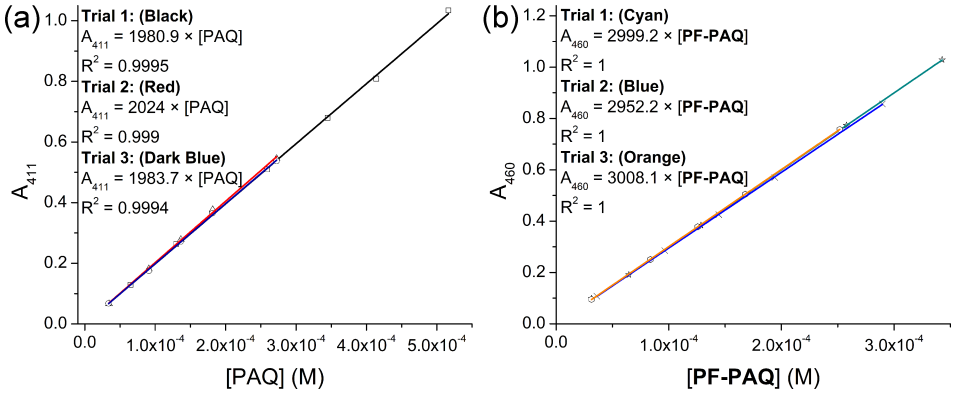


FIGURE 7.11: Plots of absorbance vs concentration (M) in toluene for (a) PAQ and (b) **PF-PAQ**.

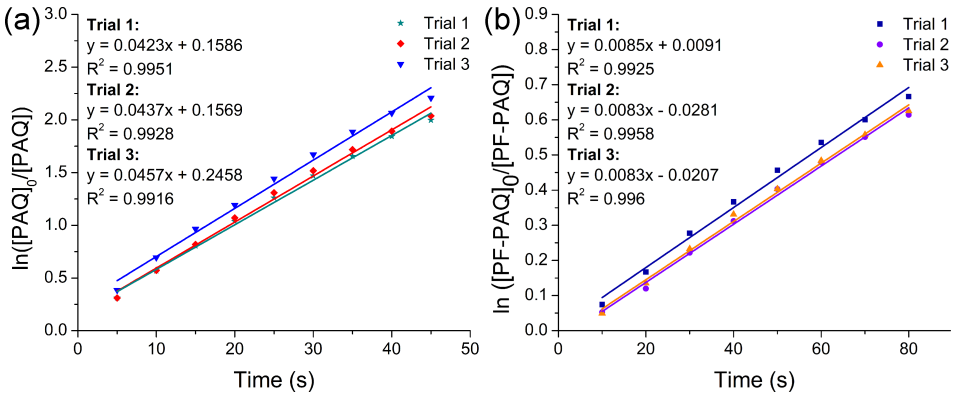


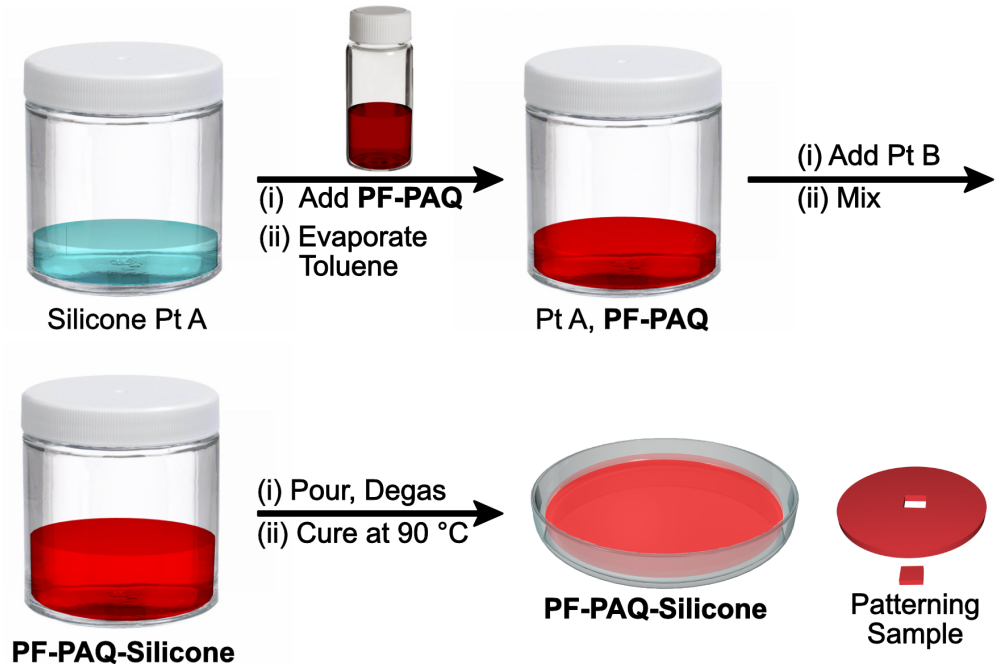
FIGURE 7.12: Plots of $\ln\frac{[PAQ]_0}{[PAQ]}$ or $\ln\frac{[\mathbf{PF-PAQ}]_0}{[\mathbf{PF-PAQ}]}$ vs time (s) for (a) PAQ and (b) **PF-PAQ** (n = 3).

Trial	k_{obs} (s^{-1})	[BVE] (mM)	k_2
PAQ 1	0.0423	3.958	10.69
PAQ 2	0.0437	4.607	9.49
PAQ 3	0.0457	4.280	10.68
PF-PAQ 1	0.0085	3.933	2.16
PF-PAQ 2	0.0083	3.921	2.12
PF-PAQ 3	0.0083	3.271	2.54

TABLE 7.1: Data used to calculate second order rate constants in toluene.

Solvent	Relative Polarity Index	$\lambda_{em,max}$ (nm)
Toluene	2.4	415, 433, 548
CH_2Cl_2	3.1	438
THF	4.0	415, 433, 543
EtOAc	4.4	415, 430, 543
Acetone	5.1	430, 548
EtOH	5.2	418, 540
MeCN	5.8	438, 558
Water	10.2	558

TABLE 7.2: Fluorescence emission peaks of **PF-PAQ-mPEG**$_{5000}$ in various solvents



SCHEME 7.3: Cartoon illustration of the **PF-PAQ-silicone** composite preparation process.

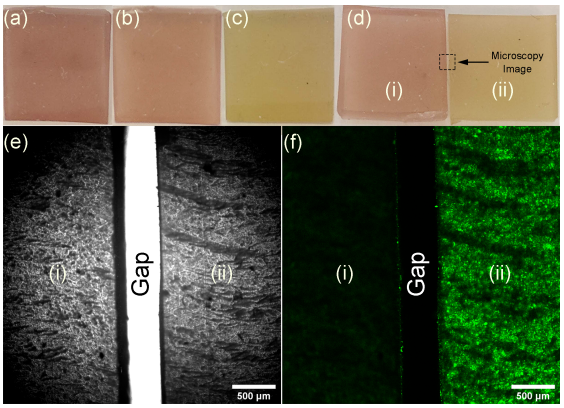


FIGURE 7.13: Photographs of **PF-PAQ-silicone** (a) pre-irradiation and post-irradiation with white LEDs (b) in the absence of BVE and (c) in the presence of BVE. (d) Photograph of the samples used for microscopy post-irradiation with white LEDs (i) without or (ii) with BVE present. Representative (e) brightfield image and (f) confocal fluorescence image of **PF-PAQ-silicone** post-irradiation.

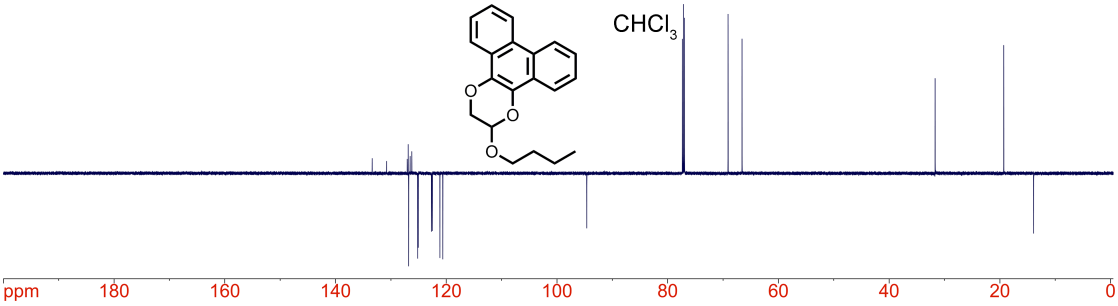


FIGURE 7.14: ^{13}C DEPTq spectrum of PAQ-BVE in $CDCl_3$.

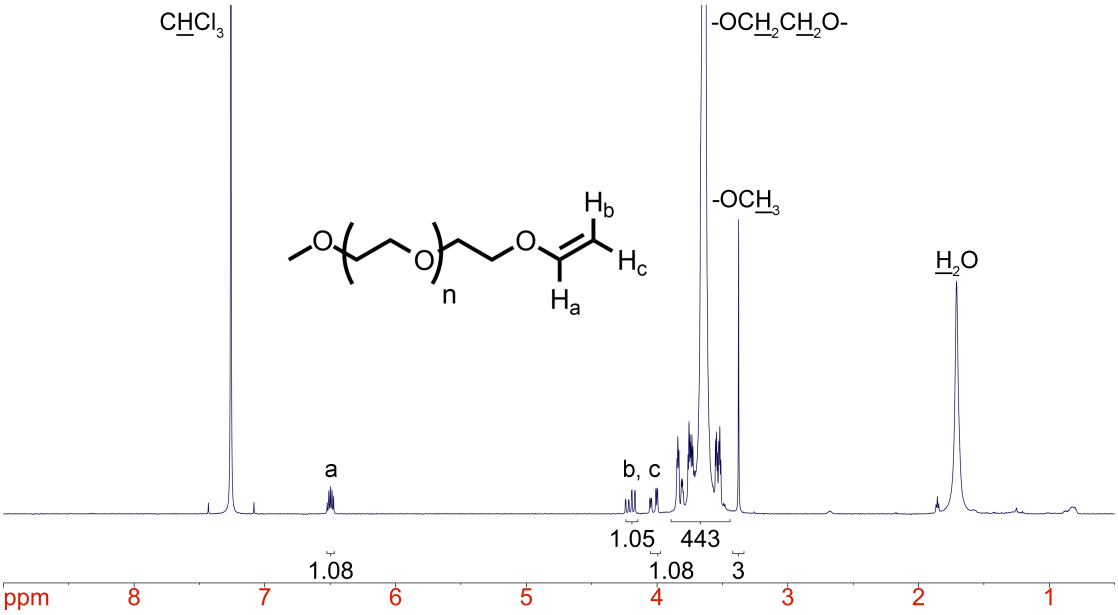


FIGURE 7.15: ^{1}H NMR spectrum of $mPEG_{5000}$-VE in $CDCl_3$.

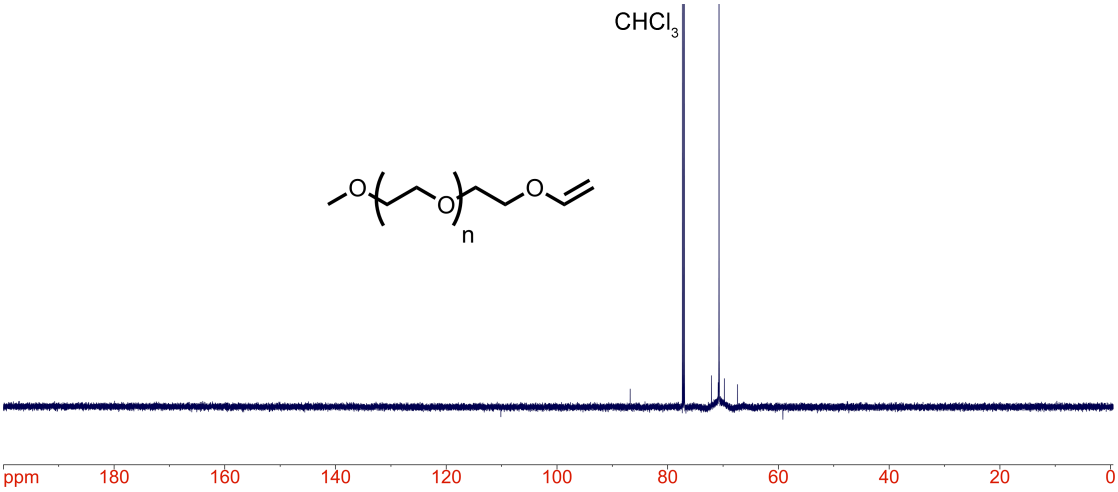


FIGURE 7.16: ^{13}C DEPTq spectrum of mPEG$_{5000}$-VE in $CDCl_3$.

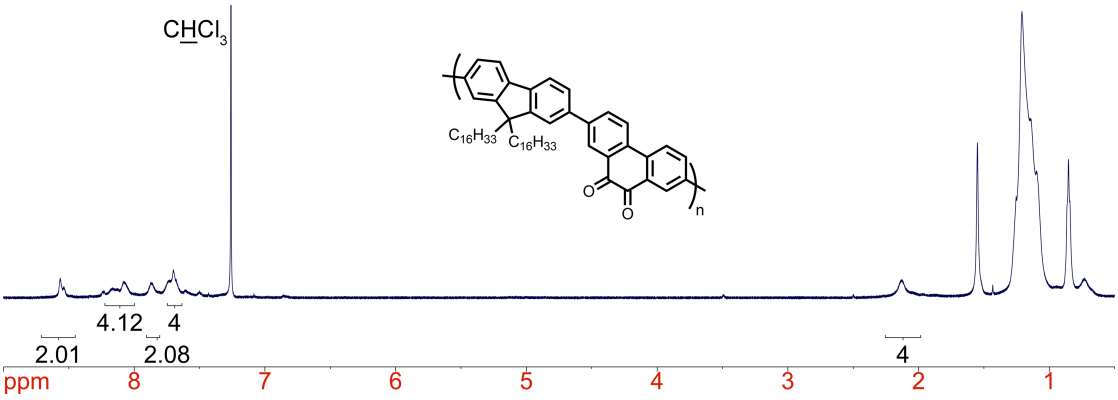


FIGURE 7.17: ^{1}H NMR spectrum of **PF-PAQ** in $CDCl_3$.

7.5 References

(1) Facchetti, A. *Chem. Mater.* **2011**, 23, 733–758.

(2) Skotheim, T.; Reynolds, J. *Conjugated Polymers Processing and Applications*; **2006**.

(3) Thomas, S. W.; Joly, G. D.; Swager, T. M. *Chem. Rev.* **2007**, 107, 1339–1386.

(4) Lv, F.; Qiu, T.; Liu, L.; Ying, J.; Wang, S. *Small* **2016**, 12, 696–705.

(5) Yamamoto, T.; Sanechika, K.; Yamamoto, A. *J. Polym. Sci. Polym. Lett. Ed.* **1980**, 18, 9–12.

(6) Prey, V. V.; Schindlbauer, H.; Cmelka, D. *Die Angew. Makromol. Chemie* **1973**, 28, 137–143.

(7) Leclerc, M. *J. Polym. Sci. Part A Polym. Chem.* **2001**, 39, 2867–2873.

(8) Morin, J. F.; Leclerc, M. *Macromolecules* **2001**, 34, 4680–4682.

(9) Siove, A.; Adès, D.; Chevrot, C.; Froyer, G. *Die Makromol. Chemie* **1989**, 190, 1361–1368.

(10) Chiang, C. K.; Fincher, C. R.; Park, Y. W.; Heeger, A. J.; Shirakawa, H.; Louis, E. J.; Gau, S. C.; MacDiarmid, A. G. *Phys. Rev. Lett.* **1977**, 39, 1098–1101.

(11) Shirakawa, H.; Louis, E. J.; MacDiarmid, A. G.; Chiang, C. K.; Heeger, A. J. J. Chem. Soc. *Chem. Commun.* **1977**, 0, 578–580.

(12) Burroughes, J. H.; Bradley, D. D. C.; Brown, A. R.; Marks, R. N.; Mackay, K.; Friend, R. H.; Burns, P. L.; Holmes, A. B. *Nature* **1990**, 347, 539–541.

(13) Rehahn, M.; Schlüter, A. D.; Wegner, G.; Feast, W. J. *Polymer* **1989**, 30, 1060–1062.

(14) McNeill, R.; Siudak, R.; Wardlaw, J. H.; Weiss, D. E. *Aust. J. Chem.* **1963**, 16, 1056–1075.

(15) Beaujuge, P. M.; Reynolds, J. R. *Chem. Rev.* **2010**, 110, 268–320.

(16) Wang, C.; Dong, H.; Hu, W.; Liu, Y.; Zhu, D. *Chem. Rev.* **2012**, 112, 2208–2267.

(17) Leclerc, M.; Morin, J.-F. *Design and Synthesis of Conjugated Polymers*; Wiley-VCH, **2010**.

(18) Zalar, P.; Henson, Z. B.; Welch, G. C.; Bazan, G. C.; Nguyen, T. Q. *Angew. Chemie - Int. Ed.* **2012**, 51, 7495–7498.

(19) Welch, G. C.; Bazan, G. C. *J. Am. Chem. Soc.* **2011**, 133, 4632–4644.

(20) van Dongen, J. L. J.; Havinga, E. E.; Janssen, R. A. J.; van Haare, J. A. E. H.; Brédas, J.-L.; Cornil, J. *Chem. - A Eur. J.* **2002**, 4, 1509–1522.

(21) Sirringhaus, H.; Brown, P. J.; Friend, R. H.; Nielsen, M. M.; Bechgaard, K.; Langeveld-Voss, B. M. W.; Spiering, a. J. H.; Janssen, R. a. J.; Meijer, E. W.; Herwig, P.; et al. *Nature* **1999**, 401, 685–688.

(22) Sirringhaus, H.; Tessler, N.; Friend, R. H. *Science* **1998**, 280, 1741–1744.

(23) Beaupré, S.; Boudreault, P. L. T.; Leclerc, M. *Adv. Mater.* **2010**, 22, 6–27.

(24) Heeger, A. J. *Chem. Soc. Rev.* **2010**, 39, 2354–2371.

(25) Morin, J. F.; Leclerc, M. *Macromolecules* **2002**, 35, 8413–8417.

(26) Donat-Bouillud, A.; Lévesque, I.; Tao, Y.; D'Iorio, M.; Beaupré, S.; Blondin, P.; Ranger, M.; Bouchard, J.; Leclerc, M. *Chem. Mater.* **2000**, 12, 1931–1936.

(27) Perepichka, I. F.; Perepichka, D. F.; Meng, H.; Wudl, F. *Adv. Mater.* **2005**, 17, 2281–2305.

(28) Tyler McQuade, D.; Pullen, A. E.; Swager, T. M. *Chem. Rev.* **2000**, 100, 2537–2574.

(29) Koeckelberghs, G.; Vangheluw, M.; Van Doorsselaere, K.; Robijns, E.; Persoons, A.; Verbiest, T. *Macromol. Rapid Commun.* **2006**, 27, 1920–1925.

(30) Gangopadhyay, P.; Voorakaranam, R.; Lopez-Santiago, A.; Foerier, S.; Thomas, J.; Norwood, R. A.; Persoons, A.; Peyghambarian, N. *J. Phys. Chem. C* **2008**, 112, 8032–8037.

(31) Araoka, F.; Abe, M.; Yamamoto, T.; Takezoe, H. *Appl. Phys. Express* **2009**, 2, 0115011–0115013.

(32) Wang, P.; Jeon, I.; Lin, Z.; Peeks, M. D.; Savagatrup, S.; Kooi, S. E.; Van Voorhis, T.; Swager, T. M. *J. Am. Chem. Soc.* **2018**, 140, 6501–6508.

(33) Li, F.; Gore, D. N.; Wang, S.; Lutkenhaus, J. L. *Angew. Chemie - Int. Ed.* **2017**, 56, 9856–9859.

(34) Li, F.; Zhang, Y.; Kwon, S. R.; Lutkenhaus, J. L. *ACS Macro Lett.* **2016**, 5, 337–341.

(35) Van Voorhis, T.; Lin, Z.; Peeks, M. D.; Lin, S.; Swager, T. M.; Wang, P. *J. Am. Chem. Soc.* **2018**, 140, 10881–10889.

(36) Fong, D.; Adronov, A. *Chem. Sci.* **2017**, 8, 7292–7305.

(37) Wang, H.; Bao, Z. *Nano Today* **2015**, 10, 737–758.

(38) Samanta, S. K.; Fritsch, M.; Scherf, U.; Gomulya, W.; Bisri, S. Z.; Loi, M. A. *Acc. Chem. Res.* **2014**, 47, 2446–2456.

(39) Fong, D.; Andrews, G.; Adronov, A. *Polym. Chem.* **2018**, 9, 2873–2879.

(40) Fong, D.; Andrews, G. M.; McNelles, S. A.; Adronov, A. *Polym. Chem.* **2018**, 9, 4460–4467.

(41) Shamshoom, C.; Fong, D.; Li, K.; Kardelis, V.; Adronov, A. *ACS Omega* **2018**, 3, 13935–13943.

(42) Fong, D.; Yeung, J.; McNelles, S. A.; Adronov, A. *Macromolecules* **2018**, 51, 755–762.

(43) Fong, D.; Andrews, G. M.; Adronov, A. *J. Polym. Sci. Part A Polym. Chem.* **2018**, 56, 2723–2729.

(44) Kardelis, V.; Chadwick, R. C.; Adronov, A. *Angew. Chemie - Int. Ed.* **2016**, 55, 945–949.

(45) Arslan, H.; Saathoff, J. D. J.; Bunck, D. N. D.; Clancy, P.; Dichtel, W. R. *Angew. Chemie - Int. Ed.* **2012**, 51, 12051–12054.

(46) Creamer, A.; Wood, C. S.; Howes, P. D.; Casey, A.; Cong, S.; Marsh, A. V.; Godin, R.; Panidi, J.; Anthopoulos, T. D.; Burgess, C. H.; et al. *Nat. Commun.*

2018, 9:3237.

(47) Li, J.; Kong, H.; Huang, L.; Cheng, B.; Qin, K.; Zheng, M.; Yan, Z.; Zhang, Y. *J. Am. Chem. Soc.* **2018**, 140, 14542–14546.

(48) Rubin, M. B. *J. Org. Chem.* **1963**, 28, 1949–**1952**.

(49) Liu, W.; Luo, X.; Bao, Y.; Liu, Y. P.; Ning, G. H.; Abdelwahab, I.; Li, L.; Nai, C. T.; Hu, Z. G.; Zhao, D.; et al. *Nat. Chem.* **2017**, 9, 563–570.

Chapter 8

Concluding Remarks

8.1 Scientific Conclusions

Carbon nanotubes are an intriguing allotrope of carbon, with fascinating physical and optoelectronic properties. Research on this allotrope is only in its infancy, with just over a quarter of a century spent trying to understand, purify, and incorporate carbon nanotubes into materials to produce tangible devices. This dissertation is just a very small piece of an increasingly large and complex puzzle. In an attempt to purify and incorporate carbon nanotube samples into devices, conjugated polymers have been an increasingly important dispersant of choice. Conjugated polymers offer the power of organic synthesis for the rational design of polymer properties to impart different properties to the carbon nanotube sample, and to sort carbon nanotube samples to isolate desired carbon nanotube subtypes. Our understanding of structure-selectivity relationships remains in its infancy, and our usage of conjugated polymers as functional dispersants remains underexplored.

In this Thesis, I began by examining the effect of conjugated polymer structure on the selective dispersion of SWNTs. Isolating one variable and testing it in the realm of carbon nanotube science is incredibly difficult, as both the polymer

properties (molecular weight, backbone and side chain structure, helicity, etc.) and dispersion preparation conditions (nanotube batch, polymer:nanotube mass ratio, solvent, temperature, etc.) influence dispersion outcome. Extreme care must be taken to isolate one variable while keeping the other variables identical. More often than not, this is not feasible for both synthetic reasons (limitations in the reproducibility of polymerization conditions and different monomer reactivities) as well as study design limitations (in particular, each research group has their own carbon nanotube samples and dispersion preparation conditions that make it incredibly difficult to make generalizable conclusions).

My first foray into this area was the examination of polymer backbone electronics on dispersion selectivity. In Chapter 2, I attempted to minimize extraneous variables by modifying backbone electronics post-polymerization, which maintains identical DP and dispersity in the polymer series. To do so, I methylated a pyridine-containing conjugated polymer post-polymerization to introduce an electron-withdrawing cationic charge into the polymer backbone. This method minimizes the effects of molecular weight and polymer structure, as both are almost identical pre- and post-methylation. In using methylation, I hoped to minimize changes to the steric bulk along the polymer backbone. DFT calculations indicated that changes to the polymer backbone conformation were minimal upon methylation, while the typical SWNT characterization techniques (UV/Vis-NIR, Raman, and fluorescence spectroscopy, as well as electrical conductivity measurements) indicated that the electron-rich polymer backbone sorted semiconducting SWNTs, while the electron-poor polymer backbone did not. I postulate that incomplete methylation of the polymer backbone (which would otherwise require heating to reflux with neat dimethyl sulfate in a sealed container to obtain full conversion)

may have contributed to incomplete sorting of metallic SWNTs, although this is for now speculation. These results overall suggest that polymer electronics may be an additional variable to consider when designing conjugated polymer structures for carbon nanotube sorting, and that perhaps more insight could be gleaned by examining the reproducibility of this effect in different polymer architectures. The inquisitive reader may note that protonation of the pyridine moiety in the polymer backbone would have produced an even smaller change to the steric environment of the conjugated system – while true, protonation/deprotonation is an equilibrium process, and under the sonication conditions used to prepare the polymer-SWNT complex this results in acid doping of the carbon nanotube surface. Rest assured that this was attempted with a stoichiometric amount of acid vs polymer; the end result is the dispersion of carbon nanotube bundles.

I next examined the assumption that complete polymer backbone conjugation is necessary for the selective dispersion of SWNTs. In Chapter 3, I prepared a series of polymers that contain varying proportions of non-conjugated alkyl linkers (10 - 50%) by incorporating an aryl iodide-containing monomer with an alkyl spacer of variable length (3 - 12 carbon atoms) during the Suzuki polycondensation process. After much screening, I found that semiconducting SWNTs could indeed be sorted using these incompletely conjugated polymers, as judged by UV/Vis-NIR, Raman, and fluorescence spectroscopy. These results demonstrate that more structural diversity is available to the intrepid researcher than initially thought, and that if someone desires the incorporation of non-conjugated linkers into the polymer scaffold, it would still be possible to sort SWNTs afterward and potentially achieve multiple objectives simultaneously.

Following this work, I pivoted to challenging the premise that conjugated polymers were simply a sorting and dispersion vehicle for carbon nanotube samples. I envisioned a system where conjugated polymers could be used as a dispersant that both sorts and imparts reactivity to the polymer-nanotube complex. Furthermore, this methodology would avoid damage to SWNT properties, which cannot be achieved by covalent functionalization methods. To accomplish this, I began by developing a polyfluorene derivative with azide groups in the polymer side chains. In Chapter 4, I used this polymer derivative to coat the carbon nanotube surface, which could then be decorated using efficient SPAAC chemistry with various strained cyclooctyne derivatives. This chemistry could be easily followed by the disappearance of the azide stretch in the IR spectrum, and enabled for the transfer of an identical population of sorted semiconducting SWNTs from toluene to water. This allowed for the study of SWNT emission properties as a function of solvent polarity. Before this, it was essentially impossible to produce a sorted SWNT dispersion that could be dispersed in solvents that were that different in polarity. Furthermore, I showed that SWNT sorting was required *before* polymer-SWNT functionalization, as the "clicked" conjugate could no longer sort SWNTs. Chapter 4 laid the groundwork for a concept where SWNTs could be simultaneously (i) sorted and (ii) decorated to change the inherent properties of the polymer-SWNT complex, while (iii) preserving the optoelectronic properties that make SWNTs an area of fascination to begin with.

In Chapter 5, I expanded on this polymer-SWNT SPAAC chemistry to include polymer-SWNT thin films. Carbon nanotube thin films have been of longstanding interest in the community and are the foundation for numerous applications, most notably being the arena of flexible electronics. I showed that when the conjugated

polymer coating contained azides in the side chains, SWNT thin films could be functionalized simply by soaking in a solvent that contains a strained cyclooctyne derivative. As long as the solvent could wet the thin film, polymer-SWNT thin film decoration was facile and could occur even in solvents that are incompatible with the initial polymer-SWNT dispersion (i.e., polar organic solvents). For aqueous solutions of strained cyclooctyne, thin film wetting issues could be ameliorated by using vacuum filtration to force the aqueous solution through the polymer-SWNT thin film. Given that this chemistry was performed interfacially, sequential functionalization could be used to produce a single "Janus" polymer-SWNT thin film that simultaneously possessed both hydrophobic and hydrophilic regions. This advancement enabled for the decoration of polymer-SWNT surfaces with molecules that are insoluble in the solvent of the initial polymer-SWNT dispersion, as well as for the spatially-resolved functionalization of the polymer-SWNT thin film. A caveat should be noted, however, that there is a limit to the ionic strength of the aqueous solution, as the solution must be able to pass through a hydrophobic Teflon membrane, which is less feasible in buffered solutions or if the molecule of interest is highly charged.

In Chapter 6, I explored the possibility for aqueous solution-phase functionalization of a polymer-SWNT complex. To do this, I developed a polyfluorene derivative that possessed both azide groups (for reactivity) and polyethylene glycol side chains (for water solubility). By using this polymer as the SWNT dispersant, the polymer-SWNT complex could be imparted with both reactivity and aqueous solubility. I demonstrate in this work that polar organic and zwitterionic molecules can be appended to the polymer-SWNT surface, which broadens the capabilities

of reactive polymer-SWNT complexes to include **any** desired molecule. Furthermore, in this work I develop an indolinooxazolidine switch that has two long-lived states, one that is neutrally charged ("ring closed") and one that is charged ("ring opened"). Using this acidochromic switch, I demonstrate that SWNT emission properties can be controlled only if the switch is bound to the polymer-SWNT complex. This work has potential implications in SWNT-based sensors that detect charged analytes, as it demonstrates that the charge must be in close proximity to the SWNT surface in order to have a demonstrable effect on SWNT emission.

Overall, Chapters 4 through 6 demonstrate that the judicious modification of conjugated polymer side chains can enable for the decoration of polymer-SWNT complexes, and even for the modification of dispersability in various media. The underlying goal of this work was to banish the notion that conjugated polymer side chains are simply spectators. I actively pursued rationally-designed side chains to impart desired features into the final polymer-SWNT complex, and have provided the reader with several methods to functionalize polymer-SWNT complexes with a desired molecule of interest.

Lastly, in Chapter 7 I pivot once more to explore a new kind of functional conjugated polymer: One whose backbone structure can be photoclick functionalized using visible light. I incorporate a 9,10-phenanthrenequinone moiety into the conjugated polymer scaffold, which forms a biradical intermediate upon irradiation with visible light. This biradical can then selectively couple to electron rich vinyl ethers, enabling for the formation of a stable covalent bond with rapid reaction kinetics (faster than even that of a conjugated polymer that contains a strained cyclooctyne in its backbone). This exciting chemistry enables for the conjugated polymer properties to be modified while maintaining the same DP and dispersity.

Furthermore, this work provides the first example of a photopatternable conjugated polymer backbone structure. This conjugated polymer structure may be an interesting addition to the reactive polymer-SWNT complex family. Indeed, I hope that in my dissertation I have shown that all components of the conjugated polymer are "up for grabs" in terms of modifying structure to obtain a desired function and outcome.

8.2 General Remarks

In my doctoral work I have shown that undergraduate students can be a valuable asset for getting work done. Moreover, training aspiring scientists how to think about approaching a problem is rewarding, especially after overcoming the inevitable hurdles that come with tackling a real-world chemistry problem. The achievements of my undergraduate trainees are as follows:

Student	Results	Time Spent
G. Andrews	3 publications, 2 cover art features	8 Months
J. Yeung	3 publications	16 Months
A. Lang	2 publications	8 Months

These results could easily be mistaken for those of experienced graduate students, but this is in fact the work output of myself alongside some undergrads. I could have gotten lucky with the three best students in the Department (one exchange student, one chemistry student, and one chemical biology student), but that seems like a dubious claim (my students are quite good, however!) My students were also unable to conjure more time outside of the 24 hours per day and 7 days per week that everyone else has access to.

So what did we do differently?

An important relationship to remember is as follows:

work output = time spent × efficiency of time spent

The implications of this relationship are profound. (i) If no time is put into doing something, it is not possible to accomplish anything. (ii) If time is not efficiently spent, then it does not matter how many hours are put into the activity. (iii) A combination of spending enough time and using time wisely maximizes the work output possible.

In my experience, I have found that people place greater emphasis on spending lots of time on an activity, but spend less time contemplating whether that time is efficiently spent. The real secret behind the success of my undergraduate students is that we carefully allotted our time toward activities that have the best chance of leading us to a tangible result. We do not have a prophetic ability to know what will and will not work, but we certainly tried our best to avoid obviously fruitless paths. If you aim to spend your time on activities with the maximum potential benefit, you will not be disappointed.

My general thought process is as follows: (i) Think of a clear hypothesis that can be tested quickly. (ii) Test the core hypothesis **quickly** (within two weeks) to determine whether the potential manuscript is viable. Do not waste months synthesizing compounds/compound libraries when you do not even know if it will lead to tangible results. (iii) If the hypothesis appears to "hold water" after performing essential control experiments, flesh out the manuscript by thinking in terms of four figures. Each figure in your manuscript is supposed to have a "point": This

will help avoid performing extraneous or pointless experiments. Each "point" supports the overall argument of the manuscript (ideally). (iv) If less lucky, go back to reading the literature to find a better hypothesis and try again.

Overall, the requirements for a "good" undergrad are simple: A student who is (i) hardworking, (ii) careful, (iii) able to learn, and (iv) able to endure the hardship of failure, at least to some extent. As long as a student is willing to show up in the morning day in and day out, I think that one publication per two terms is a reasonable rate of work – with everything else being bonus. And remember, a new graduate student is just an undergrad with a different label – so there is no reason that the undergrad cannot perform as well as a graduate student.

8.3 Recommendations for Future Work

As a general statement, I think greater emphasis should be placed on preparing polymer structures to test specific hypotheses, rather than to simply make something because it can be done. It is exceedingly clear in the natural product literature that making a molecule is typically no longer a real barrier (which indicates how far chemistry has come in the past 50 years). Rather, the real question is what should be made and why, and if a target is valuable enough then the creativity of many scientists can be unleashed to achieve that goal (with enough funding, of course). Serendipity will always play a role in the advancement of human knowledge, but hoping for random chance to be in your favour does not feel very strategic for a community that prides itself on being judicious and thoughtful.

With respect to sorting metallic SWNTs, I would suggest finding a metric (such

as HOMO/LUMO energy levels, or perhaps NMR chemical shifts) and examining if a correlation exists with the relative proportions of semiconducting:metallic SWNTs being sorted. Discovering a metric with a known sorting outcome would greatly improve our molecular understanding of what properties in a dispersant really matter to sort for one SWNT subtype over another.

With respect to reactive polymer-SWNT complexes, the real question is no longer whether it is possible to decorate the carbon nanotube surface without deleteriously affecting optoelectronic properties. The real question is now, "what would we like to decorate the carbon nanotube surface with, and why?" Creativity will be essential moving forward. One could envision, for example, sorting semiconducting SWNTs to produce FETs (or some other organic electronic device) and then clicking on a sensing moiety (e.g., a crown ether) to produce a sensor. Indeed, there is still ongoing work as I move on to the next stage of my career that resembles this general idea. If this basic concept proves fruitful, an additional advancement that would be quite fascinating to explore is the patterning of multiple detection moieties on a single polymer-SWNT thin film. Considering that light is probably the best patterning tool available, and that CuAAC (for instance) can be controlled using visible light, this simple polymer-SWNT chemistry could be used to (i) sort semiconducting SWNTs, (ii) patterning on an array of sensing moieties, and (iii) simultaneously screen for numerous analytes in a complex sample (i.e., multiplex detection).

8.4 Cover Art Gallery

I have been fortunate enough to have had my first-author scientific work featured on the front cover of a peer-reviewed journal four times – interestingly, I almost doubled Prof. Adronov's cover count during my tenure (4 of 9). Below are the cover arts and citations for each of these publications. A special thanks to Scott Laengert for helping with the art for two of these covers.

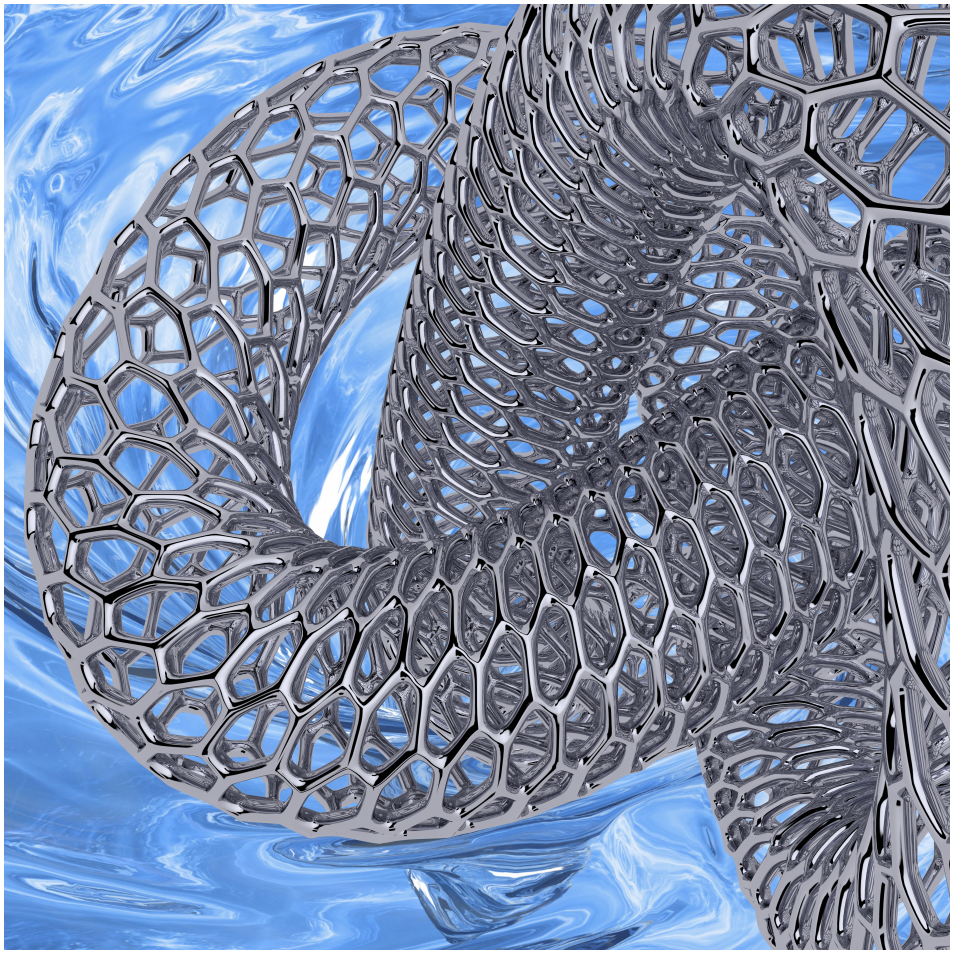


FIGURE 8.1: **Fong, D.**; Bodnaryk, W. J.; Rice, N. A.; Saem, S.; Moran-Mirabal, J. M.; Adronov, A. *Chem. - A Eur. J.* **2016**, *22*, 14560–14566.



FIGURE 8.2: **Fong, D.**; Adronov. A. *Chem. Sci.* **2017**, *8*, 7292-7305.



FIGURE 8.3: **Fong, D.**; Andrews, G.; Adronov, A. *Polym. Chem.* **2018**, *9*, 2873–2879.

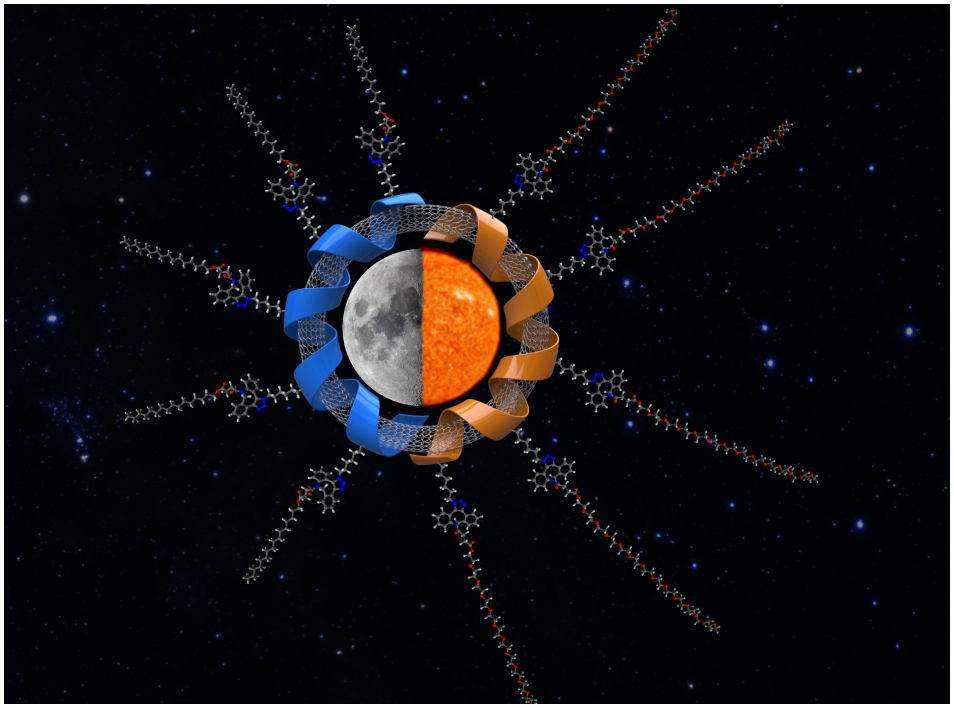


FIGURE 8.4: **Fong, D.**; Andrews, G. M.; McNelles, S. A.; Adronov, A. *Polym. Chem.* **2018**, *9*, 4460–4467.